Dimerization and function within AtbZIPs networks and the role of GBF1 in the crosstalk between stress response and natural senescence

Dissertation

der Mathematisch-Naturwissenschaftlichen Fakultät

der Eberhard Karls Universität Tübingen

zur Erlangung des Grades eines

Doktors der Naturwissenschaften

(Dr. rer. nat.)

vorgelegt von

Carles Marco Llorca

aus València, Spanien

Tübingen

2015

Gedruckt mit Genehmigung der Mathematisch-Naturwissenschaftlichen Fakultät der Eberhard Karls Universität Tübingen.

Tag der mündlichen Qualifikation:	04.02.2016
Dekan:	Prof. Dr. Wolfgang Rosenstiel
1. Berichterstatter:	Prof. Dr. Thomas Lahaye
2. Berichterstatter:	Prof. Dr. Klaus Harter

Danksagung

The production of this thesis was not a straight way, I had to overcome several difficulties, but from them I learnt how important objectivity, integrity, and independent work are in the scientific research. One way or another everything comes to an end, and it is then when all those who helped making possible this work should be acknowledged.

An allererster Stelle möchte ich mich bei Prof. Dr. Ulrike Zentgraf dafür bedanken, dass sie es mir ermöglicht hat, Wissenschaft zu machen. Ebenso gut bei Prof Dr. Klaus Harter und Prof. Dr. Thomas Lahaye für ihre Bereitschaft, sich als Gutachtern zur Verfügung zu stellen

Ein besonderer Dank geht an die ganze Arbeitsgruppe für das tolle Laborklima: Gesine, Jasmin, Justine, Maren, Lena, und Stefan. Dazu gehören auch natürlich die ehemalige Mitgliederinnen Gabi, Ingrid, Kerstin, und Ying, sowie die mehrere Studenten, die ihre Zeit mit uns geteilt haben; vor allem diejenigen die „unter meinem Befehl standen".

Bei der gesamten Abteilung für Allgemeine Genetik bedanke ich mich für ihre Unterstützung bei Fragen oder Problemen, einige Verbrauchsmaterialien, und ein gutes Arbeitsumfeld im Allgemeinen. Besonders hervorzuheben ist Charly, ohne die ich niemals die deutsche Bürokratie schlagen können hätte.

Quiero agradecer al Dr. Kenneth W. Berendzen su accesibilidad, su punto de vista siempre crítico, y en general su buen hacer al frente del servicio de citometría de flujo. Desidero anche ringraziare Caterina Brancato per fornire rottondini senza sosta.

I am very grateful to Prof. Dr. Hans-Peter Piepho and Dr. Waqas Ahmed Malik for the fruitful collaboration we established.

I also thank all members of the MERIT network for the exchange of experiences, and the friendly and collaborative atmosphere they provided.

Agraïsc especialment mon pare no té nas, ma mare és xata, i un germanet que tinc un tros li falta per estimar-me; i a la Mileta per èsser rodoneta i feliç.

This work was supported by the Marie Curie Initial Training Network MERIT, grant agreement, No. 264474.

Sapere aude

Abstract

Environmental response to stress is long known to be able to induce senescence, manifesting the close relationship between the two processes. Yet the interplay between them is poorly understood. At the molecular level, the course of both entails the inhibition of biosynthetic activities and the storage of resources, as well as the activation of catabolic pathways, mobilization of reserves, and production of reactive oxygen species. That metabolic reprogramming is in any case accompanied by a massive change in the transcriptome, revealing the pivotal role played by transcription factors in the regulation of the two processes, and hinting at their function as the potential link connecting stress response and senescence.

The **b**asic region leucine **zip**per (bZIP) family of transcription factors are present in all eukaryotes and control important developmental and physiological processes, which in plants include abiotic and biotic stress responses and leaf senescence. In Arabidopsis, the so called C/S1 network, which includes four bZIPs from the C sub-class and five from the S1 sub-class, is involved in the regulation of the plant energy balance and the allocation of nutrients, with a prominent function in the response to energy deprivation conditions. The induction of natural leaf senescence, in turn, was found to be regulated by another bZIP, namely GBF1, belonging to the G sub-class. An important feature of the bZIPs is that they act as dimers and different monomers can combine, raising the alluring possibility that GBF1 and bZIPs from the C/S1 network could heterodimerize, providing a physical link between the stress response and the senescence processes.

Dimerization is the core of the bZIP function, since different bZIP monomers exhibit distinctive qualities with regard to their transactivation potential and DNA binding specificity. Currently, bZIP heterodimerization is seen as a combinatorial mechanism generating a large variety of dimers with unique properties from a limited set of monomers. However, that assumption has not been systematically addressed and available data usually focus on the study of few dimers, not allowing to verify that hypothesis.

This thesis is committed to the study of the bZIP dimerization and function in Arabidopsis, although it consists of two differentiated parts. The first one investigates about an eventual regulation of the senescence specific activity of GBF1 through heterodimerization, in the context of evaluating the role of that bZIP in the crosstalk between stress response and senescence. Dimerization of GBF1 with members of the C/S1 network was assessed by Bimolecular Fluorescent Complementation (BiFC) assay, identifying bZIP63 as a potential GBF1 interacting partner. The function of the GBF1/bZIP63 heterodimer was subsequently examined in regard to its transactivation capacity and its DNA binding specificity by GUS-based transactivation assay and DNA Protein Interaction-ELISA, respectively. In addition, Arabidopsis lines with altered levels of bZIP63 expression were characterized for senescence-specific phenotypes. Evidence gathered could not support the hypothesis that GBF1 acted as a link connecting the stress response to senescence. On the other hand, data obtained confirmed that bZIP63 is involved in the general development of Arabidopsis plants, although not specifically in the senescence process.

The second part of this work challenged the accepted combinatorial model of bZIP function in Arabidopsis by systematically determining the dimerization and transactivation properties of 16 bZIPs. An interaction matrix analyzing all possible dimers among the 16 bZIPs was generated by BiFC, and the transactivation effect of 47 different bZIP dimer combinations on four promoters known to be targeted by some of those bZIPs was investigated by GUS reporter gene transactivation assays. Results indicated that the 16 bZIPs are organized in three independent interacting networks and that members of the same network exhibited partially redundant transactivation properties, but distinct for each promoter. The extent of the assays and the statistical data treatment performed provided enough perspective to reasonably infer in the organization and function of the Arabidopsis bZIP network: these findings severely limit the possibility that the currently assumed combinatorial model for bZIP function actually happens in Arabidopsis, since bZIP dimers are formed between

monomers which already share similar functions. Accordingly, an alternative model is proposed in which each bZIP network operates as a functional unit, while heterodimerization serves as a mechanism integrating multiple inputs. In addition, *in silico* analyses of the bZIP dimerization motifs suggested the existence of a novel mechanism defining bZIP dimerization specificity based on the differential positioning of certain heptads which play prominent roles in the dimerization process.

Zusammenfassung

Umwelteinflüsse können nicht nur eine Stressantwort auslösen, sondern auch Seneszenz induzieren, was auf eine enge Verbindung dieser beiden Prozesse hindeutet. Jedoch ist ihr Zusammenspiel bisher nur schlecht verstanden. Auf molekularer Ebene beinhaltet der Verlauf beider Prozesse eine Hemmung biosynthetischer Aktivitäten und die Speicherung von Ressourcen, sowie die Aktivierung von Signalwegen des Katabolismus, Mobilisierung von Reserven und Produktion von reaktiven Sauerstoffspezies. Diese Veränderungen im Metabolismus gehen immer einher mit massiven Veränderungen im Transkriptom. Das deutet auf eine zentrale Rolle von Transkriptionsfaktoren in der Regulation beider Prozesse hin, was wiederrum nahelegt, dass sie potentiell ein Bindeglied zwischen Stressantwort und Seneszenz sein können.

Die Familie der **b**asic region leucin **zip**per (bZIP) Transkriptionsfaktoren kommt in allen Eukaryoten vor und ist an der Regulation von wichtigen physiologischen und entwicklungsabhängigen Prozessen beteiligt, wie zum Beispiel bei Pflanzen Antworten auf biotischen und abiotischen Stress sowie Blattseneszenz. In Arabidopsis ist das sogenannte C/S1 Netzwerk, das vier bZIPS der C Subklasse und fünf der S1 Subklasse beinhaltet, an der Regulation des Energiehaushalts und an der Verteilung von Nährstoffen beteiligt. Außerdem hat es eine prominente Funktion in der Antwort auf Nährstoffmangel. Die Einleitung der natürlichen Blattseneszenz wiederrum wird von einem anderen bZIP, GBF1, reguliert, welcher zur G Subklasse gehört. Eine wichtige Eigenschaft der bZIPs ist, dass sie als Dimere agieren und sie verschiedene Kombinationen aus Monomeren bilden. Das untermauert die faszinierende Theorie, dass GBF1 und bZIPs des C/S1 Netzwerks Heterodimere bilden können und dass sie auf diese Weise eine physische Verbindung zwischen Stressantwort und dem Prozess der Seneszenz sein könnten.

Dimerisierung ist der Schlüssel zum Verständnis der bZIP Funktionsweise, denn verschiedene bZIP Monomere zeigen charakteristische Merkmale in Bezug auf ihr Transaktivierungspotential und die Spezifität der DNA-Bindung. bZIP Heterodimerisierung wird als kombinatorischer Mechanismus gesehen, der es ermöglicht, eine begrenzte Menge an Monomeren zu einer großen Vielfalt an Dimeren mit einzigartigen Eigenschaften zu erweitern. Diese Annahme wurde jedoch noch nie systematisch untersucht und die existierenden Studien legen den Fokus überwiegend auf die Untersuchung weniger Dimere – diese Ansätze sind nicht dazu geeignet, die vorher aufgestellte Hypothese zu verifizieren.

Diese Arbeit beschäftigt sich mit der Untersuchung von bZIP Dimerisierung und ihrer Funktion in Arabidopsis. Sie ist in zwei Teile gegliedert, wovon sich der erste mit einer möglichen Regulation der seneszenzspezifischen Aktivität von GBF1 durch Heterodimerisierung beschäftigt. Die Rolle von GBF1 wird im Kontext des Zusammenspiels von Stressantwort und Seneszenz betrachtet. Dimerisierung von GBF1 mit bZIPS des C/S1 Netzwerks wurde mittels eines Bimolecular Fluorescent Complementation (BiFC) Assays untersucht, was bZIP63 als einen Interaktionspartner von GBF1 identifizierte. Transaktivierungspotential und DNA-Bindeverhalten des GBF1/bZIP63 Heterodimers wurden anschließend mit einem GUS-basierten Transaktivierungs-Assay und mit DNA Protein Interaction-ELISA analysiert. Zusätzlich wurden Arabidopsis Linien mit veränderter bZIP63 Expressionsstärke auf seneszenzspezifische Phänotypen untersucht.

Gewonnene Ergebnisse konnten nich unterstützen die Hypothese, dass GBF1 ein Bindeglied zwischen Stressantwort und Seneszenz ist. Andererseits konnte mit den gesammelten Daten bestätigt werden, dass bZIP63 in allgemeine Entwicklungsprozesse von Arabidopsis Pflanzen involviert ist, wenn auch nicht spezifisch in der Seneszenz.

Der zweite Teil dieser Arbeit beschäftigt sich mit dem allgemein akzeptierten Modell der kombinatorischen bZIP Funktion in Arabidopsis. Dimerisierung und Transaktivierungseigenschaften von 16 bZIPs wurden systematisch untersucht. Eine Interaktionsmatrix, die alle möglichen Dimerbildungen dieser 16 bZIPs berücksichtigt, wurde mit BiFC erstellt. Die Transaktivierungseigenschaften von 47 bZIP Dimer Kombinationen auf vier Promotoren, für die bereits bekannt ist, dass sie mit einigen bZIPs interagieren, wurde mittels GUS Reportergen Transaktivierungsassay getestet. Die Ergebnisse deuten darauf hin, dass die 16 bZIPs in drei unabhängig interagierenden Netzwerken organisiert sind und dass bZIPs des selben Netzwerks teilweise redundante Transaktivierungseigenschaften besitzen, jedoch spezifisch für jeden Promoter. Der Umfang dieses Assays und die statistische Auswertung bieten eine ausreichende Grundlage, um fundierte Aussagen über die Organisation und Funktion des Arabidopsis bZIP Netzwerks machen zu können. Die Ergebnisse limitieren stark die bisherige Annahme des kombinatorischen Modells der bZIP Funktionsweise in Arabidopsis, da bZIP Dimere nur von Monomeren gebildet werden, die ähnliche Funktionen haben. Folglich wird ein alternatives Modell vorgeschlagen, in dem jedes bZIP Netzwerk als funktionelle Einheit operiert, während Heterodimerisierung als Mechanismus dient, durch den multiple Input-Signale integriert werden. Außerdem deuten *in silico* Analysen des bZIP Dimerisierungsmotiv auf einen bisher nicht beschriebenen Mechanismus hin, wonach die Spezifität der bZIP Dimerisierung auf der verschiedenen Position bestimmter Heptaden beruht, die eine prominente Rolle im Dimerisierungsprozess spielen.

Table of contents

1 Introduction

Senescence is the final stage in the life cycle of living organisms, which is associated with a decline in the functionality and eventually death. Etymologically the word origins from the Latin word “senescere”, meaning to grow old, and it is commonly seen from the human perspective as a deteriorative aging process. In plants, however, the term senescence has different connotations, suffice it to say that it does not necessarily involve the death of the organism. Plant senescence is not a simply deterioration process, but instead it follows an ordered, highly regulated course which is genetically controlled. Besides, the plant-senescence concept distinguishes between the process at a whole-plant level or at an organ-specific level and, in both cases, senescence can occur at different developmental stages, with variable degrees of severity, and initiated by different causes (Lim et al., 2007; Guiboileau et al., 2010; Thomas, 2013).

The onset of senescence normally occurs under optimal conditions regulated by various factors such as photoperiod, light intensity, or nutrient availability. Nevertheless, senescence is a plastic process, and can be prematurely induced under unfavorable environment or stress conditions as an adaptive response to enhance the chance of survival (Buchanan-Wollaston et al., 2003). Even so, age is the main factor governing senescence (Lim et al., 2007). In fact, it has been observed that senescence cannot be induced before reaching a certain age, what led to the suggestion that certain age-related changes (ARC) must take place before senescence could be initiated (Jing et al., 2005; Jibran et al., 2013).

While the flexibility of the senescence program entails an evolutionary advantage for plants, it has a major impact on the human activity, for premature senescence causes large crop losses decreasing the grain filling and biomass yield and shortening the shelf life of many vegetables and fruits. Abiotic stress is already the main cause of crop losses leading to more than 50% decreases in the yields of most major crop plants, and it will predictably worsen in the current context of climate change (Mittler, 2006; Zentgraf and Hemleben, 2008; Gepstein and Glick, 2013; Danquah et al., 2014). Understanding how the senescence process is regulated is, therefore, of crucial importance, as it will allow the manipulation of the timing of senescence in order to improve the yield and nutritional values of the crops.

1.1 Leaf senescence

The leaf is the plant organ where the photosynthesis is primarily performed, converting the light energy into chemical energy which is stored as carbohydrate molecules. The life cycle of the leaf can be divided in three phases (Wu et al., 2012b). The first stage is defined by an autotroph and sink phase, where the young leaf undergone rapid cell division and expansion by consuming own-generated and imported photoassimilates (Figure 1). In the second stage the leaf behaves as an autotroph and source organ. This mature leaf has a fully developed photosynthetic apparatus and there is net production of photoassimilates, which are stored in the same leaf or exported via phloem. The final stage, the senescence, is characterized by the leaf yellowing due to the loss of the photosynthetic capacity, which results in the loss of autotrophy. In the absence of photosynthesis, the energy production is overtaken by the mitochondria through the respiration of carbon intermediates, and the leaf still behaves as a source, as its content is mobilized to other parts of the plant (Guiboileau et al., 2010).

In monocarpic plants, the released nutrients are relocated to the seeds for the new generation; whereas in polycarpic perennials, they are transferred to growing parts or stored in stem or roots to sustain the initial growth in future seasons. Therefore, leaf senescence represents a savage process of nutrients with an enormous adaptive value, and it is often regarded as a recycling process (Lim et al., 2007). Although

senescence eventually ends in death, that is actively delayed until the nutrients have been remobilized (Buchanan-Wollaston et al., 2003).

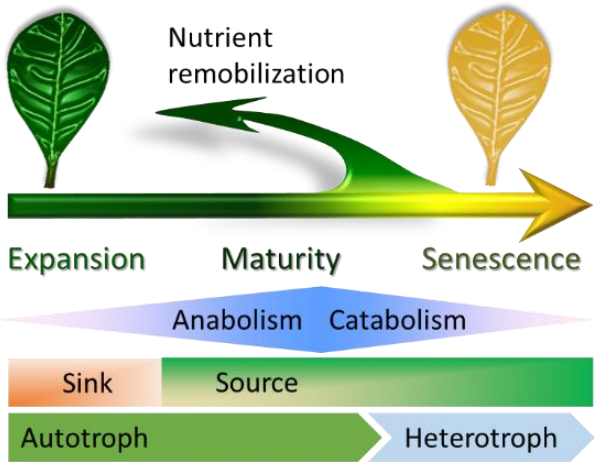

Figure 1. Diagram illustrating the main phases of leaf development. Indicated are the shifts in the metabolism and the nutritional type, as well as the sink-to-source transition.

Leaf senescence is considered as a type of Programmed Cell Death (PCD) because it is genetically programmed, regulated by endogenous factors, requires the ordered activation of a specific series of events, and, ultimately, leads to cell death (Hadfield and Bennett, 1997). However, the categorization of leaf senescence as a PCD turned to be controversial since the observation of regreening in leaves that were already yellowing demonstrated that the senescence process is reversible and it does not obligatory imply cell death (Thomas et al., 2003).

However, some researchers contemplate PCD as a reversible process (Lockshin and Zakeri, 2004), so that the reversibility of the senescence would not make the process incompatible with the PCD definition. Moreover, a physiological role for the regreening has also been questioned, considering the regreening unlikely to happen in natural conditions (van Doorn and Woltering, 2004). Thus, the debate is not closed.

1.1.1 Changes at the cellular level during senescence

Chloroplast breakdown is the first recognizable step in the ordered dismantling of the cellular structures undergoing senescence, and is the cause for the leaf yellowing characteristic of that process. Chloroplast disassembly has a major impact on the cellular metabolism, for it is the primary source of energy in the photosynthetic cells, so that its removal represents a turning point in the cellular energetics. The early chloroplast dismantling is due to the fact that it is the main source of remobilized nutrients, especially of nitrogen, a limiting and essential factor for the plant growth and whose incorporation consumes a substantial amount of energy. The majority of the plant nitrogen is allocated in the leaves during the vegetative growth, and the chloroplasts comprise up to 80% of that nitrogen, mostly of which is in the stroma in the form of ribulose-1,5-bisphosphate carboxylase/oxygenase (RuBisCO) (Ishida et al., 2014).

Chloroplasts are degraded piecemeal, so their content is first budded out in vesicles which are then degraded in the cytoplasm or in the vacuole, and eventually the whole plastids are processed (Figure 2). The stromal content is believed to be first attacked by Reactive Oxygen Species (ROS) produced by thylakoids, resulting in protein fragments which adhere to the chloroplast membrane and are budded out (Avila-Ospina et al., 2014).

The extra-chloroplastic degradation can follow two pathways: an autophagy dependent formation of the so called RuBisCO Containing Bodies (RCB); or an autophagy independent processing by means of the Senescence-Associated Vacuoles (SAV). RBCs are spherical bodies with 0.5 to 1.5 µm in diameter, surrounded by a double membrane, and their interior is similar in composition to the stroma. They contain stromal proteins such as RuBisCO and the chloroplastic Glutamine Synthetase (GS2), but not thylakoid proteins such as light-harvesting chlorophyll a/b protein of photosystem II (LHCII). Conversely, the interior of the SAVs, which are single-membrane lytic vacuoles with 0.5 to 0.8 µm in diameter, is similar to the vacuole. These vesicles contain the senescence-specific acidic cysteine-proteases SAG12, and like the RBCs they contain only stromal proteins and not thylakoid content (Lee et al., 2013; Ishida et al., 2014).

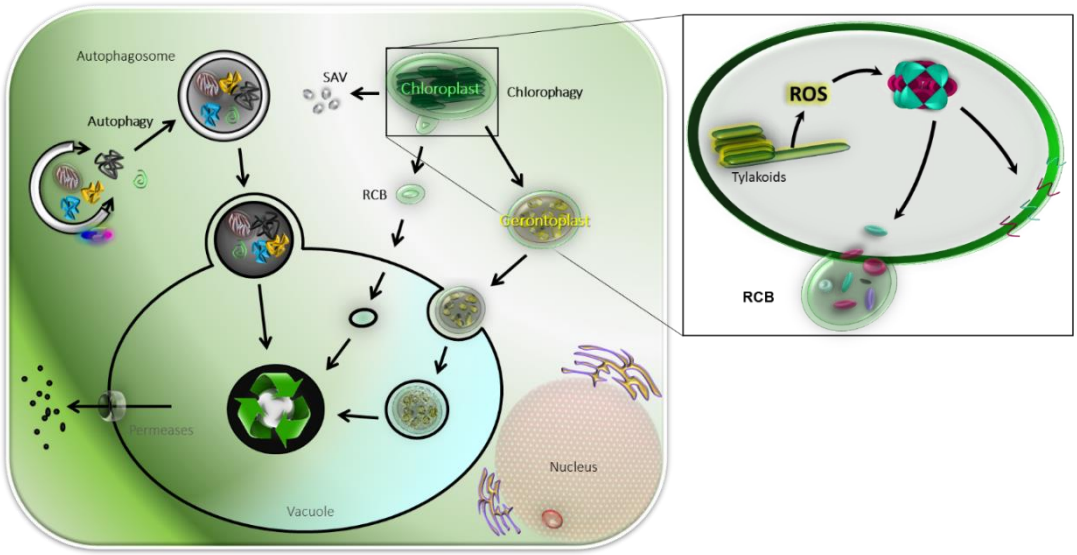

Figure 2. Activated catabolic routes during senescence. Autophagy plays a major role in the recycling of cytoplasmic components. Within the chloroplasts, proteins are attacked by ROS and the resulting fragments attach to the membrane (detailed chloroplast). Extrachloroplastic processing occurs via SAVs and RCBs, and whole chloroplasts are eventually degraded by chlorophagy.

The characteristic leaf yellowing in senescent leaves comes from the thylakoid processing and the subsequent breakdown of the most abundant plant pigment, the chlorophyll. Although, it only represents the 2% of the total nitrogen, chlorophyll removal is required for the remobilization of the chlorophyll-containing apoproteins which represent 20% of the cellular nitrogen, as well as to detoxify its potentially phototoxic effect in order to guarantee the cell functionality (Hörtensteiner, 2006; Hörtensteiner and Kräutler, 2011).

Chlorophyll degradation involves a multi-step pathway called the PAO pathway, for the enzyme that opens the chlorin macrocycle ring in the chlorophyll molecule is the pheophorbide a oxygenase (PAO). This pathway takes place in the stroma and requires the reduction of chlorophyll b to chlorophyll a and the release of the latter from the apoprotein. The final catabolites are colorless, linear tetrapyrroles which are exported to the central vacuole, crossing the membranes by active transport mechanisms (Hörtensteiner, 2013)

As the content of the chloroplasts is consumed, they gradually shrink and transform into gerontoplasts (Parthier, 1988). These accumulate plastoglobuli, which are monolayer particles that contain lipids and proteins derived from the thylakoid dismantling. These vesicles can protrude and emerge into the cytoplasm in order to be recycled (Lundquist et al., 2012). Concomitantly, there is a decrease in the number of chloroplasts due to the autophagy of the whole organelles (Wada et al., 2009).

Peroxisomes are other compartment with an early role in the senescence process. These organelles are single membrane vesicles with 0.1-1.7 µm in diameter, and are in involved in oxidative metabolic processes that generate ROS. At the same time, they contain abundant enzymes for the ROS detoxification such as catalases, superoxide dismutases, and ascorbate peroxidases, thus playing a central role in the ROS balance (Palma et al., 2009). During senescence, the leaf peroxisomes, a specialized type of peroxisomes that perform part of the photorespiration, are transformed into glyoxysomes, which contain enzymes for the β-oxidation of fatty acids and the glyoxylate cycle. This conversion allows the transformation of the thylakoid lipids into sugars, which are used to feed the mitochondria and so compensate the decrease of the photosynthetic activity (del Río et al., 1998).

Mitochondria play an essential role in senescence, for this is an active process that requires energy for catabolic reactions, transport of metabolites, and *de novo* gene expression of degradative enzymes. Accordingly, when the photosynthetic activity decreases, the cell relies on the mitochondria to provide ATP and supply carbon skeletons which are derived from the tricarboxylic acid (TCA) (Keskitalo et al., 2005; Keech et al., 2007). For this reason, mitochondria remain functional until the last stages of senescence. Furthermore, the mitochondria could play an active role in the last stages of senescence inducing the PCD by releasing cytochrome c (Reape et al., 2008).

RNA, especially ribosomal RNA, represents the major pool of phosphate in the cells, which is significantly larger than the following phosphate-containing fractions, the phospholipids and the phosphoesters (Raven, 2012; Veneklaas et al., 2012). As senescence progress, the RNA levels are rapidly reduced in order to mobilize their basic components, and consistently, there is a general decrease in the gene expression (Lim et al., 2007). Conversely, the DNA is maintained until the last stages of senescence, reflecting the requirement of a functional nucleus controlling the senescence process.

1.1.2 Changes in the metabolism during senescence

The purpose of senescence is to recycle the cellular components generated during the vegetative growth, and because of that the cell functionality is maintained until all nutrients have been withdrawal from the cell (Buchanan-Wollaston et al., 2003). Metabolically, the senescence process means a transition from anabolism to catabolism. Carbon and nitrogen assimilation are replaced by an active dismantling of macromolecules and organelles in order to export the catabolites and produce energy in the mitochondria (Guiboileau et al., 2010). This metabolic shift is accompanied by massive changes in the gene expression (Buchanan-Wollaston et al., 2003; Zentgraf et al., 2004; Breeze et al., 2011). The vast majority of the genes are down-regulated in order to decrease the resource usage, especially those related to photosynthesis, photorespiration, and protein synthesis, which decrease sharply with the progress of senescence (Andersson et al., 2004; Lim et al., 2007; Breeze et al., 2011). Conversely, specific genes called **S**enescence-**A**ssociated **G**enes (SAGs) are up-regulated during senescence, which regulate the initiation and progression of the senescence syndrome. These include transcription regulators, hydrolytic enzymes such as proteinases, lipases, and RNases, and proteins involved in nutrient translocation (Gan and Amasino, 1997). The SAGs display distinctive temporal patterns, congruently with the ordered breakdown of the cellular components and the high regulation of each step of the senescence process. Based on their expression profiles, the SAGs are classed into different groups by comparing their expression at three developmental stages (Figure 3): mature green (MG), early senescence (S1), and mid senescence (S2), when yellowing is already visible (Buchanan-Wollaston et al., 2003). Group 1 genes are induced at S1 and their expression is maintained at high level during S2. These include transcription factors, kinases and phosphatases. Group 2 genes exhibit an increase in their expression in S2, and include proteases and cell degrading enzymes. Group 3 genes are expressed at MG and they are down-regulated in S1

and S2. These genes encode RuBisCO and chlorophyll a/b binding proteins among others. Group 4 genes are induced in S1 but their expression drops in S2, and include a vegetative storage protein, a dehydrin-like protein, and transcription factors.

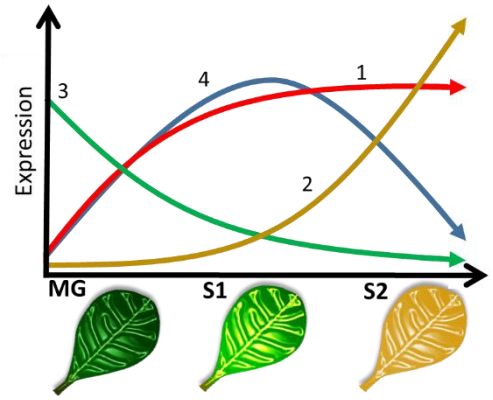

Figure 3. Different temporal patterns of expression of SAGs. The four groups of SAGs according to the classification in Buchanan-Wollaston (2003) are indicated with numbers.

Protein degradation increases in parallel to the decline in the photosynthetic activity, as a consequence of the increment in the cellular proteases. In senescence there is an induction in the expression of many bacterial-derived chloroplastic proteases such as FtsH-, Clp-, and Lon-like proteases (Roberts et al., 2012), which initiate the intra-organelle degradation of the chloroplasts before the formation of RBCs and plastoglobuli. The cysteine protease SAG12 is also strongly induced in senescence leaves and it is located to the SAVs, where it contributes to the degradation of stromal proteins (Otegui et al., 2005).

The majority of the senescence associated proteases are accumulated in the vacuole, hence autophagy plays an important role in the nutrient remobilization during senescence, as it is a major mechanism trafficking proteins to the vacuole (Yamada et al., 2001; Martínez et al., 2007; Müntz, 2007; Roberts et al., 2012). Autophagy is mediated by the formation of autophagosomes, which are double membrane organelles that engulf cytosolic elements and deliver them to the central vacuole (Figure 2), and involves the function of several genes, the so-called **A**u**T**opha**G**y (ATG) genes (Liu and Bassham, 2012; Avila-Ospina et al., 2014). ATG genes are up-regulated in senescence, and many ATG mutants display senescence altered phenotypes (van der Graaff et al., 2006; Phillips et al., 2008; Yoshimoto, 2010; Liu and Bassham, 2012).

In addition to autophagy, the ubiquitin proteasome pathway (UPS), which targets substrates for degradation by the 26S proteasome, is likely to be actively involved in the cytosolic protein breakdown during the senescence, as several proteasome genes such as the polyubiquitin gene SEN3 are up-regulated (Park et al., 1998; Buchanan-Wollaston et al., 2003; Guo et al., 2004), and mutants for proteasome related gene exhibit senescence phenotypes (Woo et al., 2001; Khanna-Chopra, 2012).

Free amino acid levels are high during the leaf expansion due to the active metabolism, but decrease in senescence -in spite of the intensive protein degradation- because they are exported (Soudry et al., 2005; Roy et al., 2013; Avila-Ospina et al., 2014). Consistently there is a concomitant induction of transporters for the export of amino acids and oligopeptides (Guo et al., 2004; van der Graaff et al., 2006).

The content of some amino acids increases during senescence. For instance, the chain branched amino acids isoleucine, valine, and leucine; the aromatic ones tryptophan, tyrosine, and phenylalanine, and diamino acids lysine and arginine (Roy et al., 2013; Watanabe et al., 2013). Those amino acids can be used to provide electrons to the electron transport chain (ETC) in the mitochondria (Araújo et al., 2011), or serve as protective

compounds, such as the accumulation of the osmoprotective proline (Obata and Fernie, 2012; Watanabe et al., 2013). In addition, they can be used as precursors for the synthesis of phenolic compounds, including flavonoids (Strack, 1997). In fact, anthocyanin accumulation occurs during senescence as a protective mechanism against light-induced ROS (Feild et al., 2001).

Together with the increase in the protease activity, there is an induction of enzymes for the amino acid catabolism such as glutamate dehydrogenase, threonine dehydratase, and genes of the branched chain keto-acid dehydrogenase complex (BCKDC) (Buchanan-Wollaston, 1997; Masclaux-Daubresse et al., 2002; Taylor et al., 2004). Deamination of amino acids provides carbon skeletons to be oxidized in the TCA and is accompanied by the release of ammonium. Hence, the ammonium concentration also increases in senescence. The free ammonium is then re-assimilated as glutamine by the action of the cytosolic glutamine synthetase (GS1), which levels are induced in senescence, compensating the decrease of the chloroplastic form (Masclaux et al., 2000). Synthetized glutamine can be exported to the phloem, or can be used as donor of amino groups to aspartate to synthetize asparagine. Accordingly, the expression of *ASPARAGINE SYNTHETHASE 1* (*ASN1*) is induced as well in senescence (Fujiki et al., 2001; Gaufichon et al., 2010). These amino acid conversions cause the increase in the Gln/Glu and Asn/Asp ratios characteristic of the senescent cells (Watanabe et al., 2013), and allow an efficient reutilization of the nitrogen released from the protein breakdown, for glutamine and asparagine are master nitrogen transport forms in the phloem (Buchanan-Wollaston, 1997).

Lipids account for the 5% of the leaf dry weight and up to the 10% of leaf's chemical energy, representing an important reservoir of carbon and energy that can be exploited (Yang and Ohlrogge, 2009). Congruently, there is a decrease in the lipid content during senescence (Watanabe et al., 2013), and an induction of proteins related to lipid catabolism, such as galacto- and phospholipases, acyl hydrolases or lipoxygenases (He and Gan, 2002; Buchanan-Wollaston et al., 2003; Guo et al., 2004; Troncoso-Ponce et al., 2013).

Most of the cellular lipids are forming membranes, from which fatty acids are released by the lipid-degrading activities, and then further catabolized via β-oxidation to provide energy. Thus, enzyme activities involved in the fatty acid oxidation are also induced, e.g. Acyl-CoA oxidases (ACX), ketoacyl thiolases (KAT), and long-chain acyl-CoA synthases (LACS) (Rylott et al., 2001; Yang and Ohlrogge, 2009; Breeze et al., 2011; Troncoso-Ponce et al., 2013). An increase in the triacylglycerol (TAG) content has been also observed during senescence, and it was suggested that the TAGs molecules act as transient storage when the β-oxidation capacity is exceeded (Kaup et al., 2002; Troncoso-Ponce et al., 2013).

Carbohydrate content increases during senescence in spite of the decline of photosynthesis. Metabolites such as mono- and disaccharides, trehalose, or maltose have been reported to raise their concentrations (Masclaux et al., 2000; Jongebloed et al., 2004; Diaz et al., 2005; Watanabe et al., 2013). These sugars are not photosynthesis derived, but they are produced as a product of the starch hydrolysis and the undergoing catabolic reactions. For instance, the acetyl-coA derived from fatty acid oxidation and the degradation of the ketogenic amino acids can be used to synthesize sugars via the glyoxylate cycle and gluconeogenesis; and the expression of enzymes involved in these pathways is induced in senescence (del Río et al., 1998; He and Gan, 2002; Buchanan-Wollaston et al., 2003; Lim et al., 2007).

The cell wall represents another important reservoir of sugars, as it is mainly composed of polysaccharides that can be processed into monomers (Somerville et al., 2004; Chundawat et al., 2011). Cell wall degradation and carbohydrate catabolic activities such as pectinesterase, xylosidase, glucosyl hydrolase, β-glucosidase, or pectate lyase are induced in senescence (Breeze et al., 2011).

Most sugars molecules are consumed by the cell to provide energy or are exported via the many sugar transporters, which are induced in senescence (Quirino et al., 2001; Guo et al., 2004). Other carbohydrate

molecules such as raffinose and galactinol are accumulated in senescence due to their role as osmoportectants or because they act as signaling molecules as trehalose 6-phosphate (T6P) (Watanabe et al., 2013).

RNA content also decreases steadily as the senescence progresses, what is due to the up-regulation of several RNases activities such as the S-like RNases RNS2 in Arabidopsis or SL28 in *Antirrhinum* (Liang et al., 2002; Buchanan-Wollaston et al., 2003; Shane et al., 2014). The released ribonucleotides can be further catabolized or exported, as suggested by the senescence-associated induction of cytidine deaminase, urease, and purine and pyrimidine transporters (Guo et al., 2004).

Ionic compounds are also remobilized in senescence together with the organic molecules. The mineral content of the cell increases along the time being mostly accumulated in the vacuole, in the ETCs of the chloroplasts and mitochondria, and as cofactors for ROS detoxifying enzymes (Diaz et al., 2005; Nouet et al., 2011; Pottier et al., 2014). The remobilization of macro- (Ca, P, S, K and Mg) and micro-nutrients (Fe, Zn, Cu, Ni, Mo, B and Cl) during senescence has been reported for several plant species, including Arabidopsis (Himelblau and Amasino, 2001; Garnett and Graham, 2005; Watanabe et al., 2013; Maillard et al., 2015). Consistently, genes coding for senescence-associated ion-binding proteins and metal transporters are induced, e.g. *COPPER CHAPERONE* (*CCH*) and *RESPONSIVE TO ANTAGONIST1* (*RAN1*) (Himelblau and Amasino, 2001; Guo et al., 2004; van der Graaff et al., 2006; Pottier et al., 2014).

Reactive oxygen species (ROS) accumulate in senescence similarly to other PCD processes. However, the role of the ROS in the PCD is not related to the generation of oxidative damage, but to their function as signaling molecules (Foyer and Noctor, 2005; Gechev et al., 2006; Khanna-Chopra, 2012). The chloroplast is the main source of ROS in the plant cell, as electrons from the photosynthetic ETC can leak from the reduced photosystem I or the ferredoxin to the molecular oxygen (O_2), resulting in the formation of superoxide radicals (O_2^-) (Gechev et al., 2006). Other major sites leading to ROS production are the peroxisomes, in which the oxidation of glycolate and fatty acids releases hydrogen peroxide (H_2O_2), and the mitochondria, where electron leakage also occurs in the respiratory ETC (Figure 4). Besides, extra-cytosolic enzymes such as plasmalemma NAD(P)H oxidases constitute an additional source of ROS (Gechev et al., 2006).

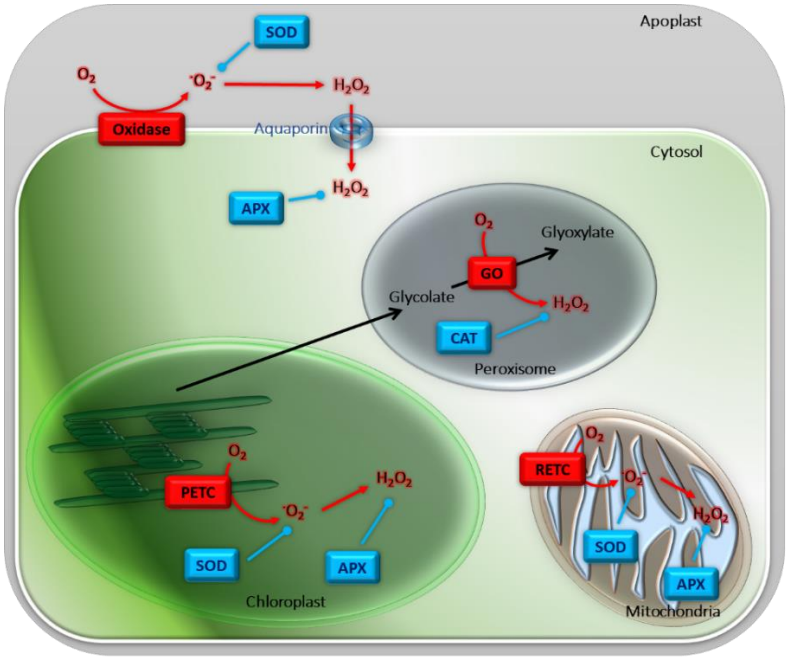

Figure 4. Components involved in the redox balance. Major ROS production sites are photosynthetic and respiratory ETCs (PETC and RETC, respectively), the Glycolate Oxidase (GO) in peroxisomes, and the membrane associated NAD(P)H oxidase. The main enzymatic antioxidant systems scavenging the ROS produced in each site are indicated in blue.

ROS levels are maintained at very low levels (240 µM O_2^- and 0.5 µM H_2O_2 in chloroplasts) in healthy, non-senescence cells due to the action of protective antioxidant systems (Mittler, 2002). ROS detoxification is achieved by enzymatic systems including superoxide dismutase (SOD), ascorbate peroxidase (APX), catalase (CAT), glutathione peroxidase (GPX), and glutathione reductase (GR); as well as by non-enzymatic antioxidants such as ascorbic acid, α-tocopherol, glutathione, or carotenoids. In plants, O_2^- can only be scavenged by the SOD and leads to the formation of H_2O_2, which in turn is catabolized by CAT, APX or other peroxidases (Gechev et al., 2006).

Although oxidative stress accumulates along the plant life (Munné-Bosch and Alegre, 2002), the senescence-associated ROS accumulation results mainly from the reduction in the antioxidant capacity. CAT, APX, and SOD activities decline during senescence, as well as the synthesis and content of ascorbate (Zimmermann and Zentgraf, 2005; Luis et al., 2006; Foyer and Noctor, 2009; Srivalli and Khanna-Chopra, 2009; Smykowski et al., 2010; Khanna-Chopra, 2012). In addition, there is an increase in the ROS production due to the enhanced activity of the peroxisomes and mitochondria, and the activation of enzymes involved in the catabolism of lipids and purines such as lipoxygenases, xanthine oxidase and urate oxidase (Zimmermann and Zentgraf, 2005; Luis et al., 2006; Foyer and Noctor, 2009).

1.1.3 Transcriptional regulation of the leaf senescence

The sequential progression of leaf senescence is achieved by the coordinated regulation of genome-wide gene expression changes in each step, and it is meticulously controlled by multiple regulatory layers involving the combined action of transcription factors, hormones, and metabolites (van der Graaff et al., 2006; Breeze et al., 2011). Given that senescence progression is genetically controlled, the dynamic activation of transcription factors has a central role coordinating the differential gene expression. Transcription factors represent, indeed, a sizable fraction of the identified SAGs, being the plant specific NAC and the WRKY families the major transcription factor groups related to senescence (Guo et al., 2004; Balazadeh et al., 2008; Breeze et al., 2011).

NACs [for **N**AM (No apical meristem), **A**TAF (Arabidopsis transcription activation factor1), **C**UC (cup-shaped cotyledon)] form one of the largest plant transcription factor families, and they are involved in the regulation of stress responses (Jensen et al., 2010). Between 20 to 30 out of the 106 NAC genes are significantly up regulated during senescence in Arabidopsis (Guo et al., 2004; Balazadeh et al., 2008; Breeze et al., 2011; Woo et al., 2013). Several NAC mutants or overexpressing lines exhibit senescence associated phenotypes in Arabidopsis. For instance, mutation in the *NAC-LIKE, ACTIVATED BY APETALA3/PISTILLATA* (*NAP*) gene, which is naturally induced during leaf senescence, results in delayed-senescence phenotype, while its overexpression promotes earlier senescence (Guo and Gan, 2006). ORESARA1 (ORE1, meaning “long living” in Korean) is another NAC transcription factor induced in senescence and acts as a positive regulator of cell death, and loss-of-function *ore1* mutant results in a delayed-senescence phenotype (Kim et al., 2009). Other examples are the JUNGBRUNNEN1 (JUB1) and VASCULAR RELATED NAC-DOMAIN INTERACTING 2 (VNI2) transcription factors, whose overexpression strongly delays senescence, and their knock-down lines exhibit accelerated senescence (Yang et al., 2011; Wu et al., 2012a). Besides Arabidopsis, the involvement of the NAC transcription factors regulating senescence has also been demonstrated in major crops (Uauy et al., 2006; Waters et al., 2009; Zhong et al., 2012; Woo et al., 2013).

WRKYs are a family of zinc-finger transcription factors that are named after the conserved WRKY amino acid sequence in their DNA binding domain, and they are involved in various physiological processes such as stress responses, pathogen defense or development (Llorca et al., 2014; Banerjee and Roychoudhury, 2015). Several of these transcription factors are differentially expressed in senescence (Guo et al., 2004; Balazadeh et al.,

2008; Breeze et al., 2011; Woo et al., 2013), and mutants exhibit senescence related phenotypes. WRKY53 targets several SAGs, including *SAG12*, and it is induced in senescence. Loss-of-function mutants for *WRKY53* display delayed senescence and, conversely, its overexpression accelerates senescence (Hinderhofer and Zentgraf, 2001; Miao et al., 2004). WRKY70 also has been characterized as a negative senescence regulator: it is up-regulated during senescence and mutant plants exhibit accelerated senescence (Ülker et al., 2007). WRKY6 is considered senescence related because it is up-regulated during senescence and targets SAGs such as *SENESCENCE ASSOCIATED PROTEIN1* (*SEN1*) and *SENESCENCE INDUCED RECEPTOR-LIKE KINASE* (SIRK), although *wrky6* mutants do not show altered senescence phenotypes (Robatzek and Somssich, 2002). Moreover, the expression of *WRKY4*, *WRKY7*, *WRKY11*, *WRKY54*, and *WRKY30* is up-regulated during leaf senescence (Balazadeh et al., 2008; Besseau et al., 2012).

Besides NACs and WRKYs, further transcription factor families involved in senescence are the myeloblastosis (MYB), basic region/leucine zipper (bZIP), *APETALA 2*/ethylene response element binding protein (AP2/EREBP), and the auxin response factor (ARF) (Buchanan-Wollaston et al., 2003; Guo et al., 2004; Balazadeh et al., 2008; Breeze et al., 2011).

1.1.4 Hormonal regulation of the leaf senescence

Plant hormones play important roles in development and environmental responses in plants, and they are, as well, central actors controlling the senescence syndrome. All plant hormones are involved in the senescence regulation, either enhancing or retarding the onset or the progression of the process (Figure 5). Congruently, many senescence-related catabolic processes are dependent on functional hormonal pathways (Buchanan-Wollaston et al., 2005), and hormonal levels vary during leaf senescence, so genes involved in their metabolism, perception and signaling are differentially expressed along the process (van der Graaff et al., 2006; Lim et al., 2007; Breeze et al., 2011; Khan et al., 2013; Penfold and Buchanan-Wollaston, 2014).

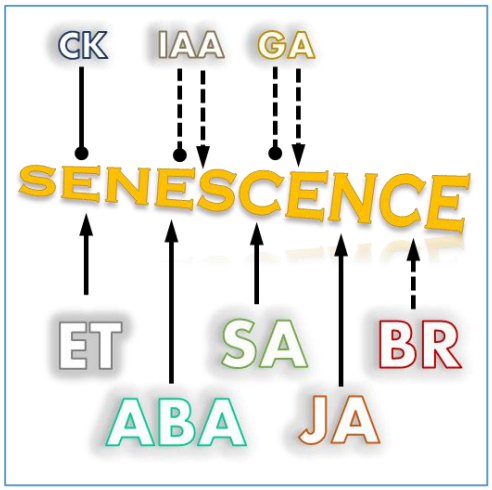

Figure 5. Summary of the effects of the different hormones on the senescence process. Dotted lines indicate effects which are not clear, due to contradictory observations.

Cytokinins (CK) comprise a heterogeneous class of adenine derivatives with isoprenoid or aromatic side chains which were initially found to promote cytokinesis. They regulate plant growth and differentiation and are involved in many developmental processes such as shoot formation, leaf and root differentiation, photomorphogenesis or gravitropism (Jibran et al., 2013; Tarkowská et al., 2014). Endogenous CK levels decline during senescence, along with the expression of genes involved in the CK biosynthesis such as

adenylate isopentenyl-transferase (IPT) or CK synthase; whereas the expression of genes related to CK degradation is increased, e.g. cytokinin oxidase and O-glycosyltransferase (Buchanan-Wollaston et al., 2005; van der Graaff et al., 2006; Lim et al., 2007; Khan et al., 2013). CK were proved to act as potent negative regulators of senescence by driving the expression of the IPT gene (which catalyzes the rate-limiting step in CK biosynthesis) by the *SAG12* promoter (Gan and Amasino, 1995).

The exact mechanism by which CK inhibit senescence is unknown, but there are some clues. For instance, CK induces the expression of extracellular invertase, which hydrolyzes sucrose to hexoses in the process to unload the phloem content into the cell. Thus, the CK decay in senescence will result in lower invertase activity, reducing the phloem unloading characteristic of growing sink tissues (Lara et al., 2004). Similarly, as CK induce catalase and ascorbate peroxidase activities, the CK decrease in senescence is likely related to the loss of the antioxidant system in senescence, (Zavaleta-Mancera et al., 2007). Furthermore, many genes coding for CK-inducible transcription repressors (type A response regulators *ARR4, ARR6, ARR7* and *ARR9*) drop their expression in senescence, suggesting a role for the CK in the transcriptome reprogramming (Buchanan-Wollaston et al., 2005; van der Graaff et al., 2006; Breeze et al., 2011).

Ethylene (ET) is the smallest known plant hormone and it is gaseous under ambient conditions. It regulates processes such as cell division and elongation, abscission, or abiotic stress responses. This hormone is particularly well-known to induce fruit ripening, for what it has been used for thousands of years (Jibran et al., 2013; Tarkowská et al., 2014). Accordingly, ET levels increase during senescence (Ferrante and Francini, 2006; Lim et al., 2007).

ET is synthetized from the methionine and the rate-limiting step is the formation of 1-aminocyclopropane-1-carboxylic acid (ACC) by the ACC synthases. The expression of these enzymes is up-regulated during senescence together with other genes involved in the ET biosynthesis such as ACC oxidases or nitrilases (van der Graaff et al., 2006; Breeze et al., 2011). Moreover, there is an increase in the expression of several components of the ET signal transduction pathway such as ETHYLENE RESPONSE 1 (ETR1), an ET receptor; ETHYLENE-INSENSITIVE 2 (EIN2), an integral membrane protein sharing sequence identity with the natural resistance-associated macrophage protein (NRAMP) family of metal transporters; or EIN3 a transcription factor acting downstream of EIN2 (van der Graaff et al., 2006; Breeze et al., 2011; Li et al., 2013). Mutations in any of those three genes are deficient in ET perception and signaling and exhibit phenotypes with delayed senescence (Oh et al., 1997; Lim et al., 2007; Li et al., 2013). The function of ET in senescence was linked to the NAC transcription factor ORE1, as the expression of *ORE1* is promoted by ET through EIN2, which mediates the down-regulation of the *ORE1* negative regulator micro RNA miR164 (Kim et al., 2009). Besides, ET was found to induce the expression of the senescence-related *WRKY6* (Robatzek and Somssich, 2001).

Auxins are the first discovered phytohormones, they were identified as growth promoters and named after the Greek word for grow, “auxein”. They act in cell division and differentiation, various tropisms, apical dominance, and flowering. Auxins are synthetized from tryptophan and feature an aromatic ring and a carboxylic acid group, and the most abundant and effective auxin compound is the indole acetic acid (IAA) (Jibran et al., 2013; Tarkowská et al., 2014). The role of auxins in senescence is unclear. On the one hand, IAA endogenous levels increase during senescence (Lim et al., 2007; Khan et al., 2013), along with an up-regulation of IAA biosynthetic activities such as tryptophan synthase (TSA1), IAA oxidase (AO1), and nitrilases (NIT1-3); as well as in ARF genes involved in the auxin response such as *MONOPTEROS (ARF5*) and *AUXIN RESPONSE FACTOR 2* (*ARF2*) (van der Graaff et al., 2006; Lim et al., 2007). Besides, the expression of some genes which are positive regulators of senescence is also induced by auxin, e.g. *SENESCENCE-ASSOCIATED RECEPTOR-LIKE KINASE (SARK*) and *SMALL AUXIN UP RNA 36 (SAUR36*) (Xu et al., 2011; Hou et al., 2013).

On the other hand, exogenous IAA delays senescence and represses the expression of some SAGs, among which there is *SAG12* (Noh and Amasino, 1999). Moreover, overexpression of *YUCCA6*, which codes for the

enzyme performing the rate-limiting step of IAA biosynthesis, leads to increased levels of free IAA, and a senescence delay; whereas mutation in *ARF2* leads to delayed leaf senescence phenotypes (Im Kim et al., 2011).

Abscisic acid (ABA) is a terpenoid compound formed by three isoprene units, and it was named after its role in leaf abscission, as it was originally found to be involved in. ABA also regulates seed dormancy and germination, synthesis of storage proteins, stomatal closure, and stress responses against various biotic and abiotic stress (Jibran et al., 2013; Tarkowská et al., 2014). Endogenous ABA levels increase late during senescence with its maximum at the final stage of senescence and, concomitantly, there is an up-regulation of ABA biosynthesis and signaling genes such as *NINE-CIS-EPOXYCAROTENOID DIOXYGENASE 3* (*NCED3*), *ALDEHYDE OXIDASE 3* (*AAO3*), *ABA INSENSITIVE 1* (*ABI1*), *ABI FIVE BINDING PROTEIN* (*AFB1*), *ABA DEFICIENT 2* (*ABA2*) and the *RECEPTOR-LIKE PROTEIN KINASE 1* (*RPK1*) (van der Graaff et al., 2006; Breeze et al., 2011; Lee et al., 2011). The senescence role of ABA derives from the observation that ABA application induces senescence and the expression of SAGs such as *SAG113*, *SEN1*, and *VNI2* (van der Graaff et al., 2006; Yang et al., 2011; Zhang et al., 2012). Moreover, *RPK1* overexpressors are accelerated in senescence, whereas mutant plants are delayed (Lee et al., 2011).

Salicylic acid (SA) is a phenolic compound with long known therapeutic properties. It is named after the Latin name of the willow tree (*Salix*), used to be used as a medicinal plant and from where it was first isolated. SA has a key role in mediating stress responses, particularly in pathogen defense and pathogen-mediated cell-death (Janda and Ruelland, 2014). SA levels rise in senescence when the chlorophyll content start to decline, indicating that SA is involved in the latter part of the senescence program (Lim et al., 2007; Breeze et al., 2011; Khan et al., 2013). SA biosynthesis genes such as *ISOCHORISMATE SYNTHASE 1* (*ICS1*), which codes for a central enzyme in the SA synthesis pathway, are up-regulated at that time, together with SA signaling genes such as *ENHANCED DISEASE SUCEPTIBILITY4* (*EDS4*) (van der Graaff et al., 2006; Breeze et al., 2011).

The function of SA in senescence has been related to the activation of autophagy and the up-regulation of several SAGs such as *SEN1*, *PATHOGENESIS RELATED 1α* (*PR1α*), and *SAG12* (Morris et al., 2000; Buchanan-Wollaston et al., 2005; Schenk et al., 2005; Lim et al., 2007; Ülker et al., 2007; Yoshimoto et al., 2009). Moreover, SA controls the expression of several WRKY transcription factors, e.g. WRKY6, WRKY53, WRKY54, and WRKY70, as well as many AP2-EREBP family members (Robatzek and Somssich, 2001; Miao et al., 2004; Ülker et al., 2007; Breeze et al., 2011; Besseau et al., 2012). Further evidence of the involvement of SA in senescence comes from the observation of delayed senescence phenotypes and decreased SAGs levels in mutants for genes related to SA signaling or biosynthesis such as *NONEXPRESSER OF PR GENES 1* (*NPR1*) and *PHYTOALEXIN DEFICIENT 4* (*PAD4*); as well as in transgenic plants expressing the *Pseudomonas putida* NahG gene, which codes for a salycilate hydrolase that prevents the SA accumulation during senescence (Morris et al., 2000; Lim et al., 2007; Khan et al., 2013).

Jasmonic acid (JA) is an oxylipin compounds derived from the fatty acid α-linolenic acid, a component of chloroplast membranes, and share structural and functional properties with animal prostaglandins. They were first isolated from *Jasminum grandiflorium*, hence their name. JA function in processes such as seed germination, growth inhibition or anthocyanin production, and accumulate in response to various stress (Wasternack and Kombrink, 2009). JA levels accumulate early in senescence, correlated with an up-regulation of genes encoding for JA biosynthesis enzymes such as lipoxygenases (LOX), allene oxide cyclases (AOC), and 12-oxophytodienoate reductase (OPR) (He et al., 2002; van der Graaff et al., 2006; Breeze et al., 2011). Proteins implicated in the JA response are also activated in senescence, including several Jasmonate ZIM-domain (JAZ) transcriptional repressors, the transcription factor MYC2, and the RIBONUCLEASE 1 (RNS1) (van der Graaff et al., 2006; Breeze et al., 2011).

JA promotes the expression of several SAGs such as *SEN1*, *SEN4*, *EARLY RESPONSIVE TO DEHYDRATION 1* (*ERD1*), *SAG21*, *SAG12, CHLOROPHYLLASE 1* (*COR1*), and *WRKY6* (Robatzek and Somssich, 2001; He et al., 2002; Schenk et al., 2005; Jung et al., 2007). Nevertheless, the role of JA in senescence is not yet fully understood since, while external JA application induces senescence, mutants for JA biosynthesis and signaling do not exhibit senescence-related phenotypes, suggesting that JA is not essential for the senescence process (Lim et al., 2007; Jibran et al., 2013; Khan et al., 2013).

Gibberellins (GA) are diterpenoid acids produced by plants and fungi. Indeed, they were first isolated from the fungus *Gibberella fujikuroi* in Japan. GAs induce cell elongation, flowering, germination, and enhance tolerance against various stresses (Jibran et al., 2013; Tarkowská et al., 2014). GA is related to senescence because its levels decline with age, and enzymes involved in its inactivation such as GIBBERELLIN 2-OXIDASE 2 (GA2OX2) increase their expression. However, the role of GA in senescence is unclear, since exogenous GA application has been reported to both delay (van der Graaff et al., 2006; Jibran et al., 2013) and induce senescence (Chen et al., 2014). Moreover, while mutants defective in GA biosynthesis were retarded in senescence (Chen et al., 2014), inhibition of GA biosynthesis with paclobutrazol accelerated the process (Jibran et al., 2013).

Brassinosteorids (BR) are triterpenoids and compose the most recently discovered group of hormones, first isolated from *Brassica napus* pollen in 1979. They regulate developmental processes including shoot and root growth, photo-morphogenesis, seed germination, and stress responses by inducing the antioxidant system (Fariduddin et al., 2014). Exogenous application of BR is able to induce that process, while mutants in genes involved in the BR signaling are delayed in senescence, e.g. *BRASSINOSTEROID INSENSITIVE 1* (*BRI1*). However, no clear transcriptional changes are seen in BR-related genes during senescence (van der Graaff et al., 2006; Jibran et al., 2013).

1.1.5 Metabolic regulation the leaf senescence

ROS play a major role in senescence as signal molecules activating the senescence genetic program (Foyer and Noctor, 2005). Indeed, many SAGs have been found to be ROS-induced, including *METALLOTHIONEIN 1* (*MT1*), *ASPARTIC PROTEINASE A1* (*APA1*), *CHITINASE* (*CHI*), *PR1a*, and *CDF-RELATED GENE RESPONSIVE TO SENESCENCE* (*CRS*) (Navabpour et al., 2003; Cui et al., 2013). Remarkably, ROS also enhance the transcription of several WRKY and NAC genes such as *WRKY53*, *ORESARA1 SISTER1 (ORS1*), *JUB1*, and *NAC WITH TRANSMEMBRANE MOTIF 1-LIKE 4 (NTL4)* (Balazadeh et al., 2008; Balazadeh et al., 2011; Lee et al., 2012; Wu et al., 2012a).

Furthermore, in a reciprocal manner, senescence-associated genes have been found to enhance the ROS production. For instance, the senescence-induced transcription factor NTL4 can promote ROS production by activating the expression of the *RESPIRATORY BURST OXIDASE HOMOLOG D* (RBOHD) and *RESPIRATORY BURST OXIDASE HOMOLOG F* (RBOHF) (Lee et al., 2012); and the senescence-related bZIP transcription factor G-BOX BINDING FACTOR 1 (GBF1) enhances H_2O_2 levels by repressing *CAT2* expression (Smykowski et al., 2010). In rice, WRKY42 is also up-regulated in senescence and represses several ROS-scavenger metallothioneins (Lee et al., 2012; Han et al., 2014).

Further evidences supporting the role ROS in senescence come from mutants with deregulated redox balances such as *ONSET OF LEAF DEATH 1* (*OLD1*), which presents enhanced ROS accumulation and accelerated senescence (Jing et al., 2008). Moreover, plants with artificially reduced H_2O_2 levels by the overexpression of the sensor domain of the *E.coli* OxyR transcription factor were delayed in senescence (Bieker et al., 2012). However, the relationship between ROS and senescence is in other cases ambiguous. For instance, the

mutation of the *VITAMIN C DEFECTIVE 1* (*VTC1*) gene results in no increased ROS levels compared to the wild type, despite exhibiting reduced ascorbate levels, enhanced sensitivity to ROS, and accelerated senescence (Conklin and Barth, 2004). Similarly, the *ore1*, *ore3*, and *ore9* mutants neither exhibit greater levels of antioxidant activities than the wild type, but they are delayed in senescence and present enhanced resistance to ROS (Woo et al., 2004). Therefore, the mechanistic of the ROS signaling in senescence remains unknown, yet some clues point to an intricate crosstalk involving plant hormones. For instance, mutations in the *ARABIDOPSIS A FIFTEEN* (*AAF*) result in delayed senescence and enhance oxidative stress resistance, but this is strictly dependent on a functional *EIN2* gene (Chen et al., 2011). Likewise, the phenotypes of the *atg2* and *atg5* mutants, featuring increased ROS levels and premature senescence, are subject to operative SA signaling pathway (Yoshimoto et al., 2009).

Sugars have a main role as energy and carbon carrier molecules in the metabolism and, additionally, they signal the energy status, regulating important physiological and developmental aspects such as the circadian gene expression in Arabidopsis (Bläsing et al., 2005). As it is explained above, sugar content increases during senescence, and abundant evidences point to a sugar-dependent metabolic regulation of senescence. Sugar accumulation represses photosynthesis, and the majority of senescence-associated genes were found to be sugar inducible (Wingler et al., 2004; Wingler and Roitsch, 2008). Remarkably, hexoses induce the expression of nitrogen remobilization genes such as *NITRATE TRANSPORTER2.5* (*NRT2.5*), *GLUTAMINE SYNTHETASE 1;4* (*GLN1;4*), *SAG12*, *SAG13*, and *PRODUCTION OF ANTHOCYANIN PIGMENT 1* and *2* (*PAP1* and *PAP2*) (Pourtau et al., 2006). Therefore, a senescence-promoting effect has been postulated for sugars.

In agreement, plants with loss-of-function mutations in the *GLUCOSE INSENSITIVE 2-1* (*GIN2-1*) gene -which encodes for a high-sugar sensor hexokinase (HXK)- do not exhibit the senescence-associated accumulation of hexoses, and are delayed in senescence; whereas the overexpression of that gene results in early senescence (Xiao et al., 2000; Moore et al., 2003). In addition, altered levels of Trehalose-6-phosphate (T6P), an important signaling molecule for high carbon availability which is accumulated in senescence, result in delayed or accelerated senescence when those are increased or reduced, respectively (Wingler et al., 2012; Watanabe et al., 2013).

However, the role of sugars in senescence has been a matter of debate, as some researchers found sugars to repress the expression of SAGs such as *SEN1* or *SAG12* (Chung et al., 1997; Noh and Amasino, 1999; van Doorn, 2008). Nevertheless, the studies on the sugar function in senescence are based on different senescence-inducing treatments, so they do not necessary activate the same pathways (van Doorn, 2008; Wingler et al., 2009). Congruously, important differences in the transcriptome were found among different senescence-promoting treatments (Buchanan-Wollaston et al., 2005; Wingler et al., 2009). Besides, the accumulation of sugars alone is not sufficient to trigger senescence, as the senescence-delayed transgenic lines with decreased T6P levels actually accumulate more hexoses than the wild type (Wingler et al., 2012), and sugar accumulation occurs naturally upon certain stress exposures without initiating senescence (Muller et al., 2011; Fernandez et al., 2012).

Based on the observation that the amino acid content decreases in opposition to sugars, the role of the sugar in senescence was proposed to be dependent on the nitrogen content. In this manner, it is the high-sugar/low-nitrogen status which acts as a senescence signal (Guiboileau et al., 2010). This view is consistent with experiments showing that senescence can be induced by sugars combined with low, but not with high nitrogen supply (Pourtau et al., 2004; Wingler et al., 2004; Wingler et al., 2012). Moreover, the so-called correlation control is a well-known method to delay the senescence progression in many plant species, by removing the reproductive organs and so altering the sink-source relationship in the plant, thus the C/N balance (Noodén and Penney, 2001).

1.2 Plant stress

The term stress derives from the Latin “stringere”, to draw tight, and it was instituted in the theory of elasticity in 1823 to refer to the distribution of a force within a material body. Since 1930s the concept has been applied to biology to refer to the unfavorable conditions disturbing the organism homeostasis and hindering the optimal functionality (Keil, 2004; Kranner et al., 2010). Although there are many different kinds of stressors, each and every stress situation involves, by definition, a decline in the metabolic performance, which is accompanied by the activation of protective and compensatory mechanisms in order to restore the physiological balance. Therefore, key aspects of the stress response are conserved in all organisms. A minimal stress response proteome has been found to be evolutionary conserved across species, consisting of circa 300 proteins involved in redox regulation, DNA damage, molecular chaperoning, protein and lipid degradation, energy metabolism, and also including tRNA synthetases for all essential amino acids (Kültz, 2005; Sulmon et al., 2015).

Plants may suffer from different stresses with different consequences for the plant physiology, therefore stress responses are tailored to the specific challenges the plants cope with. For instance, heat stress affects membrane fluidity and induces thermal aggregation of proteins, and plant respond accumulating xanthophylls such as violaxanthin that decrease the membrane fluidity and inducing molecular chaperones such as heat-shock proteins (Bokszczanin et al., 2013). High salinity conditions result in Na^+ accumulation causing severe ion imbalance and inhibiting the uptake of K^+ essential for growth, so tolerance mechanisms involved the activation of the plasma membrane Na^+/H^+ antiporter SALT OVERLY SENESITIVE 1 (SOS1) (Gupta and Huang, 2014). Heavy metals disturb the cellular redox control and inactivate enzymes by displacing cofactors such as Mg^{2+} or binding to sulfhydryl groups, what is counteracted by the biosynthesis of phytochelatins and the modification of the pH of the rhizosphere to precipitate the heavy metals outside of the plant (Hossain et al., 2012). However, in their natural habitats, plants are exposed simultaneously to various stress factors, so that stress responses involve a complicated interplay among different signaling pathways (Ahuja et al., 2010; Kohli et al., 2013; Baxter et al., 2014; Smékalová et al., 2014).

1.2.1 ROS production in stress

Increased ROS levels are a common feature under abiotic stress in plants due to the unbalance between the steady state ROS production and scavenging. Therefore, activation of antioxidant defense mechanisms is a common response under all stress conditions (Murata et al., 2007; Gill and Tuteja, 2010; Maharjan et al., 2014).

ROS cause lipid peroxidation and protein oxidation, affecting membrane structures and enzyme activities. The components of the ETCs are especially vulnerable to oxidative damage and the ETC is impaired by altered membrane fluidity and permeability. Hindering of the electron fluxes under stress results in longer oxidation times of the ETC components, thus, increasing the probability of ROS formation due to electron leakage. In addition, the inhibition of the photosynthetic ETC in plants leads to the activation of the photorespiration, what results in additional ROS production (Kültz, 2005; Murata et al., 2007; Gill and Tuteja, 2010; Sharma et al., 2012; Choudhury et al., 2013). In short, ROS hampering of the photosynthesis leads to amplified ROS generation.

ROS are also known to act as signaling molecules, and under stress there is an initial rapid active ROS generation through various positive feedback mechanisms. For instance, upon Ca^{2+} binding, CALCINEURIN-B LIKE PROTEIN 1 (CBL1) and CALCINEURIN-B LIKE PROTEIN 9 (CBL9) activate the CBL INTERACTING PROTEIN KINASE 26 (CIPK26) which in turn phosphorylates RBOHF, enhancing the ROS production (Baxter et al., 2014;

Mittler and Blumwald, 2015). ROS trigger the opening of Ca^{2+} channels, and RBOHC and RBOHD are Ca^{2+} activated, resulting in a positive feedback. In addition, stress hormones also promote ROS formation in a feedback fashion. ABA induces ROS as stated above, while ROS cause enhance ABA levels by activating its biosynthesis and/or inhibiting its degradation (Mittler and Blumwald, 2015). Similarly, ROS enhance SA biosynthesis, and SA inhibits catalase and ascorbate peroxidase promoting ROS accumulation (Vlot et al., 2009). Besides, ET and BR also induce ROS through the activation of RBOHs, although the precise mechanism remains to be elucidated; while the action of JA remains controversial (Baxter et al., 2014; Xia et al., 2015).

Due to the activation of the antioxidants mechanisms and the existence of negative feedbacks such as the induction of the *CAT1* gene by ABA or the auto-inhibition of the ethylene signaling (Gill and Tuteja, 2010; Vandenbussche et al., 2012; Smékalová et al., 2014), ROS are accumulated transiently, in what is termed oxidative burst (Baxter et al., 2014). That burst of ROS induces transcriptomic changes by triggering signaling cascades or directly modifying the activity of transcription factors (Apel and Hirt, 2004).

1.2.2 Stomata regulation in stress

Stomata are pores in the epidermis of leaves and other aerial parts of the plants, consisting of two guard cells that act as valves maintaining a tradeoff between the CO_2 uptake and the prevention of excessive transpirational water loss. Regulation of the stomatal conductance is considered a main feature of the plant systemic responses to stress (Kohli et al., 2013; Mittler and Blumwald, 2015). Significantly, those hormones which promote the stomatal closure are accumulated during various stresses, whereas those which promote the opening decrease their concentration (Kotak et al., 2007; Nishiyama et al., 2011; Peleg and Blumwald, 2011; Kohli et al., 2013; Santino et al., 2013; Liu et al., 2015). Specifically, ABA, SA, JA, ET, and BR promote stomatal closure, whereas CK and IAA promote the opening. However, the role of each hormone on the stomatal conductance is not fully understood and in some cases there are contradictory results, for instance depending on the concentration assayed (Desikan et al., 2006; Acharya and Assmann, 2009; Peleg and Blumwald, 2011; Daszkowska-Golec and Szarejko, 2013).

Mechanistically, the pore size is controlled by osmotic swelling or shrinking of the guard cells. Aperture results from the expansion of the guard cells driven by an increase in their osmolarity and the subsequent entry of water, whereas closure occurs due to the decrease of the guard cells volume, resulting from a low osmolarity which is compensated by an efflux of water (Acharya and Assmann, 2009; Kollist et al., 2014). Under water deficit conditions induced by drought, cold or high salinity, stomatal closure occurs to prevent dehydration; but because any stress eventually leads to osmotic imbalance, stomatal closure also results from other kinds of stresses such as hypoxia, nutrient deficiency, heat, or pathogen infection (Broadley et al., 2000; Allen and Ort, 2001; Melotto et al., 2008; Rodríguez-Gamir et al., 2011; Macková et al., 2013).

ABA is a key stress hormone accumulated under a variety of stresses such as drought, salinity, cold, heat, heavy metals, and wounding, and its ability to induce stomatal closure has been studied in detail (Larkindale et al., 2005; Tuteja, 2007; Baron et al., 2012; Ashraf and Harris, 2013; Suttle et al., 2013; Danquah et al., 2014; Kim et al., 2014). ABA promotes ion efflux from the guard cells, leading to the loss of water and subsequent cell shrinking, hence, the stomatal closure. This process is achieved through a complicated signaling cascade which is elicited upon ABA binding to the soluble receptors PYRABACTIN RESISTANCE1 (PYR1)/PYR1-LIKE (PYL)/REGULATORY COMPONENTS OF ABA RECEPTORS (RCAR). Then, the activated receptors bind to, and inhibit a group of PROTEIN PHOSPHATASE 2Cs (PP2C) -among which there are ABI1 and ABI2- which are negative regulators of the SUCROSE NON-FERMENTING 1-RELATED PROTEIN KINASE 2 (SNRK2) family members, including SNRK2.2/D, SNRK2.3/I, and OPEN STOMATA 1 (SNRK2.6/E/OST1), therewith allowing the

SNRK2 activation. Activated OST1 activates the plasma membrane-bound NADH oxidases RBOHD and RBOHF, resulting in O_2^- production outside of the cell, which is subsequently converted into H_2O_2 by apoplastic superoxide dismutases. Extracellular H_2O_2 triggers the opening of plasma membrane Ca^{2+} channels leading to an influx of Ca^{2+} into the cytoplasm, which acts as second messenger. Elevation of Ca^{2+} concentration activates S-type (slow) and R-type (rapid) anion channels that release additional Ca^{2+} from internal stores (vacuole and endoplasmic reticulum), and mediate the efflux of Cl^-, $malate^{2-}$, and NO^-_3 from guard cells, causing depolarization of the membrane. That triggers the outflow of K^+ by inactivating the inward-rectifying K^+ channel POTASSIUM CHANNEL IN ARABIDOPSIS THALIANA 1 (KAT1), and activating the outward-rectifying one GATED OUTWARDLY-RECTIFYING K+ CHANNEL (GORK). Besides, SNRK2s also activate SLOW ANION CHANNEL-ASSOCIATED1 (SLAC1) and inactivates KAT1 by phosphorylation, preventing the reentry of ions. Altogether, the loss of anions and K^+ causes the loss of turgor of the guard cells (Macková et al., 2013; Danquah et al., 2014; Mittler and Blumwald, 2015).

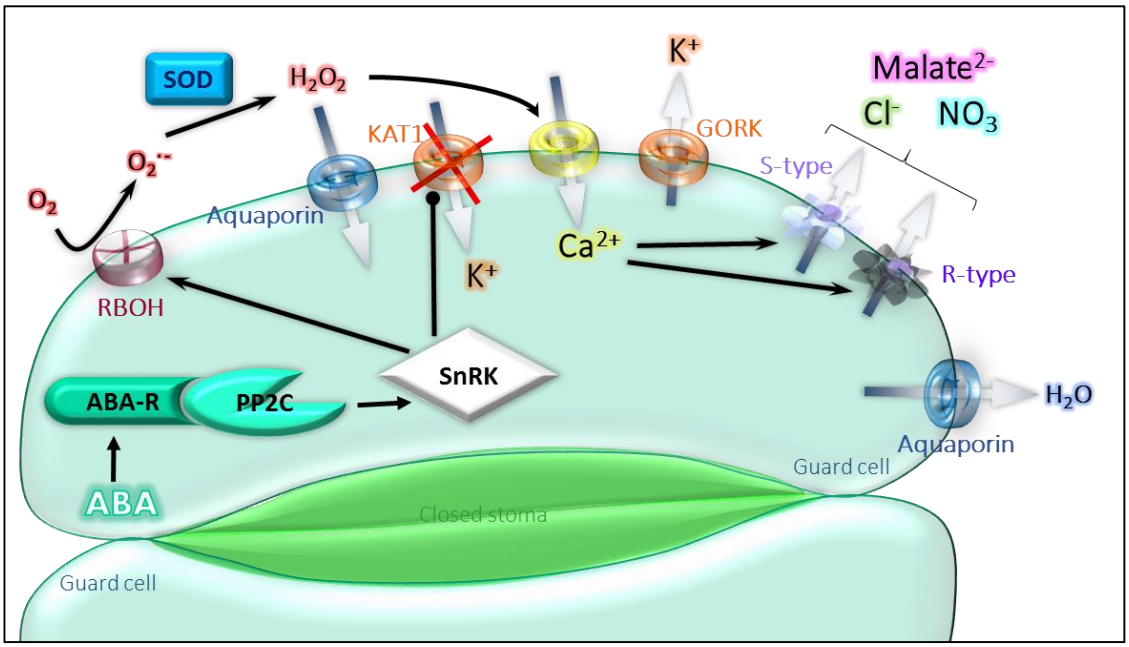

Figure 6. Major elements involved in the closing of stomata. Ion channels, pumps, and transporters are coordinately regulated by the action of ABA and ROS.

1.2.3 The Low Energy Syndrome (LES)

In any organism, stress situations impair normal functions, thus decreasing the energy production. This is especially accrued in plants, as all stresses hamper the photosynthesis process, which is their primary energy source. Photosynthesis perturbation can arise, for example, due to an excess of light inducing photo-damage in the photosystem II, but for most of the stresses it is attributed to the stomatal closure (Kranner et al., 2010; Vass, 2012; Ashraf and Harris, 2013). In addition to the reduced energy production, stress triggers counteracting mechanisms in order to restore the homeostasis and to protect the cell against the damaging effect of toxic species, which involve added energetic costs, directly since many of them rely on the ATP hydrolysis to operate, and indirectly due to the *de novo* biosynthesis of protective components such as chaperones, antioxidant system, or DNA repairing complexes (Kültz, 2005; Duque et al., 2013; Sulmon et al., 2015). Therefore, all stress situations in plants result in important bioenergetic unbalances that trigger

common responses, which have been encompassed under the term Low Energy Syndrome (LES) (Baena-González and Sheen, 2008; Tomé et al., 2014).

One of the earliest responses to stress is the decline in the biosynthetic processes in order to preserve the resources, so that these can be redirected to the maintenance of the homeostasis. In general, there is a dramatic decrease in gene expression, largely due to the regulation of the translation initiation by phosphorylation of the eukaryotic INITIATION FACTOR 2 - subunit α (eIF2α). In plants, the only known eIF2α kinase is GENERAL CONTROL NONREPRESSIBLE 2 (GCN2), which is activated under stress conditions. However, a subset of stress-response genes can bypass the eIF2α phosphorylation-mediated repression of translation by activating alternative mechanism for cap-independent initiation of translation, so that they can be translated. Additionally, there is a down-regulation of the expression of genes coding for several ribosomal proteins and other translation initiation factors such as eIF4α and eIF2γ, which are required for the efficient translation of proteins (Contento et al., 2004; Hey et al., 2010; Munoz and Castellano, 2012; Echevarría-Zomeño et al., 2013).

Along with the translation control there is an immediate cessation of growth. Cell cycle progression depends on the joint action of cyclins (named after the cyclical variation of their concentration along the cell cycle) and CDKs (cyclin dependent kinases). Stress conditions promote the activation of CDK inhibitors and the decrease of the cyclins expression, resulting in a cell cycle arrest at the G1/S and G2/M checkpoints (Kültz, 2005; Kitsios and Doonan, 2011; Komaki and Sugimoto, 2012).

Concurrently with the reduction in the energy consumption, catabolic pathways are activated in order to provide alternative energy sources and reducing equivalents, compensating the loss of photosynthetic activity. Accordingly, there is an increase in activities involved the energy metabolism such as 6-phosphogluconate dehydrogenase (6PGDH) in the pentose phosphate pathway, enolase in the glycolysis, malate synthase and isocitrate lyase in the glyoxylate cycle, as well as citrate synthase and isocitrate dehydrogenase in the TCA cycle (Contento et al., 2004; Kültz, 2005; Tomé et al., 2014).

Extensive protein degradation also occurs in stress, and there is an increase in the expression or in the activation of many components involved in protein catabolism, including the chloroplastic FtsH- and Lon-like proteases, vacuolar proteases such as ALEURAIN-LIKE PROTEASE (AAL, SAG2) and GAMMA VACUOLAR PROCESSING ENZYME (GAMMA-VPE), the autophagy-related proteins ATG8, ATG1, or ATG13, several components of the ubiquitin 26S proteasome system, and enzymes for the amino acid metabolism such as HOMOGENTISATE 1,2-DIOXYGENASE (HGO), LYSINE-KETOGLUTARATE REDUCTASE (LKR), ORNITHINE-AMINOTRANSFERASE (OAT), and BRANCHED CHAIN ALPHA-KETO ACID DEHYDROGENASE (BCKD) (Contento et al., 2004; Kültz, 2005; Baena-González and Sheen, 2008; Lyzenga and Stone, 2011; Akpinar et al., 2012). In addition, hydrolysis of lipids is also activated with a concomitant increase in the expression of several lipases and genes involved in the β-oxidation of fatty acids (Contento et al., 2004).

1.2.4 LES sensing and execution

The metabolic shift resulting from the energy deprivation conditions requires of massive reprogramming of the energy-related transcriptome, involving numerous transcription factors including bZIPs, MYBs, WRKYs, and NACs (Contento et al., 2004; Osuna et al., 2007), and major regulators identified in that process are SNRK1s and TARGET OF RAPAMYCIN (TOR) kinases (Baena-González and Sheen, 2008; Avin-Wittenberg et al., 2012; Tomé et al., 2014).

SnRKs belong to the Sucrose-non-fermenting-1 (Snf1)/AMP-activated protein kinase (AMPK) family of conserved eukaryotic kinases, which are cellular energy sensors and control the energy balance (Hedbacker and Carlson, 2008). Plant SnRKs are divided into three subfamilies: SnRK1 share the highest homology with Snf1 and AMPK, while SNRK2 and SNRK3 are less conserved and are specific to plants. SNRK1s are central regulator of the energy homeostasis, SnRK2s are activated in the ABA response, and SnRK3s are CIPKs which are activated by the Ca^{2+} sensors CBLs (Kulik et al., 2011). SNRK2s and SNRK3s are suggested to be derived from SNRK1s by duplication and, then, diverged creating networks that link stress signaling and metabolic status (Halford and Hey, 2009).

SNRK1 is a heterotrimeric complex in which the activity of the catalytic α-subunit is modulated by the two regulatory β- and γ-subunits. According to the transcriptional profiles of mutants and overexpressing plants for the catalytic α-subunit KIN10, SNRK1 seems to operate as a master regulator in the energy starvation response controlling the transcription of over a thousand genes. Changes in the transcriptome of the KIN10 overexpressor resemble those happening under energy deficiency conditions, and are opposed to the transcriptional profiles obtained with sugar feeding (Baena-González et al., 2007). Plants overexpressing KIN10 show a repression of over 300 genes involved in the biosynthesis of protein, lipid, starch, amino acids, and cell wall; and the induction of other 300 genes related to catabolic pathways, including degradation of proteins, lipids, starch, cell wall and autophagy genes. In addition, KIN10 modifies the expression of a large number of transcription factors, signal transduction pathways, and hormone signaling components (Baena-González and Sheen, 2008). Moreover, SNRK1 also inhibits the function of several proteins related to biosynthetic processes by direct phosphorylation, including 3-HYDROXY-3-METHYLGLUTARYL-COA REDUCTASE (HMGR), SUCROSE PHOSPHATE SYNTHASE (SPS), NITRATE REDUCTASE (NR), TREHALOSE-6-PHOSPHATE SYNTHASE (TPS), FRUCTOSE-2,6-BISPHOSPHATASE (F2KP), as well as the NAC transcription factor ATAF1 (Halford and Hey, 2009; Kleinow et al., 2009).

The activation of SNRK1 requires the phosphorylation of a highly conserved threonine residue in the T-loop by the upstream kinases SNRK1-ACTIVATING KINASE 1 and 2 (SNAK1 and SNAK2). Phosphorylation of that threonine residue occurs under low sugar conditions, whereas in high sugar concentrations it is mostly dephosphorylated by PROTEIN PHOSPHATASE 2As (PP2A), the activity of which is in turn inhibited by ABA (Rodrigues et al., 2013; Crozet et al., 2014). In addition, SNRK1 function is negatively regulated by sugars. Glucose 6-Phosphate (G6P), glucose 1-phosphate (G1P), glucose, sucrose, and T6P have been found to inhibit SNRK1 activity, being the latter much more efficiently and acting with low concentrations (<20μM) (Crozet et al., 2014). T6P is disaccharide found in plants normally in trace amounts, and is accumulated with increasing sucrose levels. Its synthesis results from the transfer of glucose from UDP-glucose to G6P by TPSs, which are widely expressed throughout the plant. T6P removal requires of TREHALOSE-6-PHOSPHATE PHOSPHATASE (TPP) and TREHALASE (TRE), which are both induced under stress (Paul et al., 2008; Ponnu et al., 2011). The inhibitory function of T6P on SNRK1 was observed by artificially inducing T6P accumulation in plants by overexpressing *E.coli* otsA -the bacterial TPS gene- what led to the opposite transcriptional profile to that triggered by the SNRK1 activation. Conversely, plants overexpressing the *E.coli* otsB –the bacterial TPP gene- that had artificially decreased T6P levels, exhibited a similar phenotype to plants overexpressing SNRK1 (Zhang et al., 2009; Wingler et al., 2012). Moreover, trehalose is known to promote the growth arrest on Arabidopsis seedlings (presumably due to the T6P accumulation), and KIN10 overexpressing seedlings are resistant to trehalose treatments (Delatte et al., 2011). Although it is not known how T6P inhibits SNRK1 activity, evidence points to intermediary factors, since it was reported that T6P can inhibit SNRK1 from plant extracts but not from catalytically active purified SNRK1 (Zhang et al., 2009).

TOR is a Ser/Thr protein kinase member of the Phosphoinositide 3-kinase (PI3K)-related kinase family, and it is conserved among all eukaryotes. In mammals and yeast, TOR responds to amino acids, glucose, and growth factors, promoting anabolic processes, cell proliferation and growth; and negatively regulating autophagy and

other catabolic pathways. TOR can form two different functional TOR complexes (TORC1 and TORC2) that contain, in addition to TOR, lethal with sec-13 protein 8 (LST8), and either regulatory associate protein of TOR (RAPTOR) in TORC1, or the rapamycin-insensitive companion of TOR (RICTOR) in TORC2.

In plants, orthologous components for TORC1 have been identified, although the understanding of their function and regulation is still poor due to the embryo lethality of null TOR mutants (Xiong and Sheen, 2012; Tomé et al., 2014; Xiong and Sheen, 2014). The role of plant TOR has been elucidated with Arabidopsis inducible lines, and the discovery of the effectiveness of rapamycin in plants. Most of TOR functions are executed through translational regulation at different levels. TOR controls ribosomal biogenesis through the transcriptional activation of the 45S rRNA by directly binding to its promoter. Accordingly, Arabidopsis *tor* mutants show reduced rRNA levels, whereas TOR overexpression results in increased rRNA expression (Ren et al., 2011; Xiong and Sheen, 2014). Besides, TOR overexpression induces polysome accumulation, enhances the expression of over 100 genes coding for ribosomal proteins and protein biosynthesis (Xiong et al., 2013), and activate key translation regulators such as P70 RIBOSOMAL S6 KINASE (S6K) (Mahfouz et al., 2006; Xiong and Sheen, 2012). At the transcriptional level, TOR regulates broad transcriptional changes, activating anabolic and biosynthetic pathways, cell cycle progression, carbon and nitrogen utilization, and photosynthesis, whereas it negatively regulates the expression of genes related to catabolism, including ATG genes and enzymes of the β-oxidation and the glyoxylate cycle (Xiong et al., 2013; Tomé et al., 2014; Xiong and Sheen, 2014). Consistently, down-regulation of TOR mimics starvation conditions, resulting in growth arrest, constitutive activation of autophagy, accumulation of free amino acids, and the activation of stress related genes (Caldana et al., 2013; Xiong and Sheen, 2014).

It becomes increasingly clear that the conserved TOR and SNRK1 signaling pathways play central and antagonistic roles regulating energy sensing and usage. They are oppositely activated, SNRK1 by low energy and TOR by favorable conditions, and they regulate growth and metabolism in antithetical manners (Robaglia et al., 2012; Lastdrager et al., 2014). Significantly, there is a meaningful negative correlation among those genes whose expression is affected by both SNRK1 and TOR, so that 294 out of 507 genes up-regulated by KIN10 are down-regulated by TOR, while 260 out of 515 genes down-regulated by KIN10 are up-regulated by TOR (Tomé et al., 2014). In addition to the differential regulation of SNRK1 and TOR by the energy conditions, crosstalk between both pathways is suggested based on the inhibitory effect of mammalian AMPK on the TOR function (Smeekens et al., 2010).

bZIP transcription factors also emerge as important mediators of the LES. The five Arabidopsis S1 class bZIPs (bZIP1, bZIP2, bZIP11, bZIP44, and bZIP53) are regulated in abiotic stress responses and have been postulated to be involved in the allocation of energy resources (Weltmeier et al., 2009). Moreover, those five bZIPs carry an upstream ORF which mediates a sucrose-induced repression of translation (SIRT) (Wiese et al., 2005; Baena-González et al., 2007), and bZIP11 was found to regulate the expression of trehalose metabolism genes, altering the T6P levels (Ma et al., 2011). The S1 class bZIPs exhibit synergistic activation in presence of KIN10, being possible downstream effectors of the SNRK1 pathway. Indeed, they directly regulate the expression of *ASN1*, which is activated by the SNRK1 pathway (Baena-González et al., 2007; Tomé et al., 2014).

The S1 group of bZIPs show functional redundancy, so that plants overexpressing bZIP1, bZIP11, and bZIP53 exhibit similar phenotypes, characterized by growth defects, altered amino acid levels and induction of genes involved in catabolic pathways (Baena-González et al., 2007; Sheen, 2014; Tomé et al., 2014). However, those bZIPs seem to operate in conjunction with bZIPs from the C group (bZIP9, bZIP10, bZIP25, and bZIP63), which are also involved in carbohydrate partitioning and stress responses, forming a heterodimerization network (Ehlert et al., 2006). For instance, heterodimers between bZIP53 and bZIP10 synergistically activate the promoter of *PROLINE DEHYDROGENASE* (*PDH*) (Weltmeier et al., 2006). Among the C group, bZIP63 is repressed by glucose, and its activity is activated by SNRK1 (Baena-González et al., 2007; Matiolli et al., 2011; Mair et al., 2015), strengthen a role for those bZIPs in the LES.

1.3 The bZIP family of transcription factors

The **b**asic region/leucine **zip**per (bZIP) proteins are dimeric transcription factors that control important physiological processes in all eukaryotes. In plants, they have undergone a greater expansion, resulting in 75 members in Arabidopsis, 89 in rice, 92 in sorghum, 131 in soybean, and 125 in maize (Shiu et al., 2005; Wei et al., 2012), and they regulate environmental responses such as pathogen defense, abiotic stress signaling, hormone signaling, or energy metabolism; as well as developmental aspects, including flowering, seedling maturation, and senescence (Choi et al., 2000; Abe et al., 2005; Fujita et al., 2005; Baena-González et al., 2007; Alonso et al., 2009; Smykowski et al., 2010; Alves et al., 2013). All members of this family feature the bZIP domain, which normally lies towards the C-terminus of the protein and consists of two elements with different functions disposed along a continuous α-helix: the basic region (BR), coding for a nuclear localization signal (NLS) and responsible for the DNA binding; and the leucine zipper (LZ), a subtype of coiled coil motif which lies downstream of the BR and mediates the dimerization (Figure 7). Besides, the conserved bZIP signature, additional functional motifs and structural features are found specifically in particular members of that family (Schumacher et al., 2000; Jakoby et al., 2002; Miller et al., 2003).

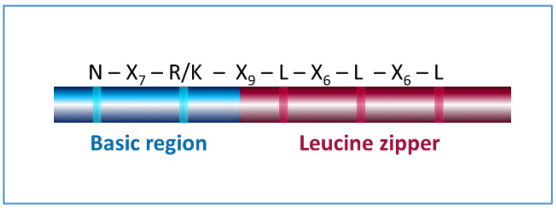

Figure 7. Diagram of the bZIP domain consisting of the basic region and the leucine zipper. The leucine zipper is more variable and can feature different numbers of heptad repetitions.

The bZIP family was sub-classified according to sequence similarities of the different members. In Arabidopsis, 10 bZIP classes were proposed (named A to I, plus S), defined on the basis of the amino acid sequence of the BR and the additional functional domains, aiming to reflect functional similarities among the bZIPs of the same class. Accordingly, class A included bZIPs involved in ABA response, class C members featured an extended leucine zipper, class D were related to defense against pathogens, class E were of unknown function, class G were described to bind to G-box cis-elements present in light-responsive genes, class H were involved in photomorphogenesis, class I were found to carry a substitution of an arginine by lysine in the BR, and class S were smaller and featured a small upstream ORF in their transcripts (Jakoby et al., 2002).

DNA binding takes place through the BR, which is highly conserved and features an invariant N-X7-R motif (N-X7-K in the bZIPs of the I class), and it occurs in the form of bZIP dimers, binding each monomer one half of the cis-element in the DNA. Only few positions of the invariant motif of each BR contact the DNA, what happens along the major groove and all the bases of the cis-element core are contacted (Oliphant et al., 1989; Glover and Harrison, 1995). The DNA sequences recognized by plant bZIPs are preferentially palindromic hexamers featuring an ACGT core. The base positions within these cis-elements are identified with numbers -negatives for the first half of the sequence and positive for the second one- ranging from the two middle positions (i.e. CG) which are both zero. In that manner, four different types of ACGT-based cis-elements are defined based on their nucleotide position +2 as A-box, C-box, G-box, or T-box (Oliphant et al., 1989; Foster et al., 1994).

The BR is highly conserved among all bZIPs, so the DNA binding specificity remains defined by slight variations in the amino acid composition. For instance, members of the CCAAT/enhancer-binding protein (C/EBP) bZIP family in mouse, feature a distinctive valine residue in their BR sequence that discriminates against the

presence of adenine or guanine at the position -3 of the cis-element (Miller et al., 2003). Similarly, a single hydrophobic residue in the BR of Pombe AP-1-like gene 1 (Pap1) from fission yeast and human cAMP-response element binding protein-2 (CREB2) defines their DNA binding specificity, enhancing their interaction with AT-rich DNA sequences (Fujii et al., 2000). However, the manner in which the BR defines the DNA binding specificity in plants is less studied and seems to be rather flexible, since diverse and non-palindromic sequences can also be bound by bZIPs (Jakoby et al., 2002; Ji et al., 2014).

Transactivation activity relies on modules outside of the bZIP domain. Although there are no consensus sequences for the transactivation domains (TAD), available functional analyses describe bZIPs TAD often as fragmented and always located towards the N-terminus of the protein (Heinekamp et al., 2002; Jakoby et al., 2002; Liao et al., 2003; Nishizawa et al., 2003; Friedman et al., 2004; Altarejos and Montminy, 2011; Tang et al., 2012; Matsuo et al., 2014). In Arabidopsis bZIPs, the best studied TAD is the N-terminal proline rich domain (PRD) of the G class of bZIPs, which functions as transcriptional activator in different species (Mermod et al., 1989; Menkens et al., 1995; Sprenger-Haussels and Weisshaar, 2000; Tamai et al., 2002). Nonetheless, PRDs from bZIPs have also been reported to work as repressors in transactivation assays, although that extent is not clear and it was proposed to be a product of squelching (Feldbrügge et al., 1994; Liu et al., 1997; Sprenger-Haussels and Weisshaar, 2000).

Gene expression requires the interplay of numerous proteins including chromatin modifiers, TATA-binding proteins (TBP), or co-activators, and bZIPs have been identified associated to some of these factors. For example, human bZIPs neural retina leucine zipper (NRL) and activating transcription factor 1 (ATF1) recruit TBPs, although the former does it directly and the latter indirectly via the multiprotein bridging factor 1 (MBF1). In yeast, the bZIP General control nonrepressible-4 (Gcn4) gather the Gcn5 histone acetyltransferases (HAT), enhancing histone H3 hyperacetylation that activate the transcription. Similarly, the *Droshophila* FBJ murine osteosarcoma viral oncogene homolog (DFos) activates the transcription by recruiting the Chameau HAT, which promotes H4 acetylation (Kuo et al., 2000; Friedman et al., 2004; Miotto and Struhl, 2006).

Therefore, bZIP transactivation function is normally not achieved by their sole DNA binding, but it results from the cooperation with other elements required for their activation. In Arabidopsis, abundant studies indicate that the binding of bZIPs to their target cis-elements is not sufficient to induce the expression *per se*. For instance, Hy5 binds to the *CHALCONE SYNTHASE* (*CHS*) and *RBCS1a* promoters during light and dark periods indistinguishably, but is only active in the light (Lee et al., 2007). TGACG MOTIF-BINDING FACTOR 2 (TGA2) binds to the promoter of the *PATHOGENESIS-RELATED-1 (PR-1)* gene acting as a repressor, but upon SA treatment it is incorporated with other proteins into an enhanceosome activating the transcription of this gene (Rochon et al., 2006). GBF1 control of Z-box containing promoters was found to require the presence of HEME OXYGENASE 1 (HO1) for optimal activation (Babu Rajendra Prasad et al., 2012). Additionally, particular cellular conditions were found to modulate the function of Arabidopsis bZIP2 and bZIP44, so that they activated the gene transcription driven by the *PDH* promoter under hypo-osmolarity conditions, but not with physiological ion levels (Satoh et al., 2004). Similarly, bZIP53 was found to induce the expression driven by the *ASN1* promoter in the darkness, but not in the light (Dietrich et al., 2011).

Dimerization is a requirement for the DNA binding and, thus, for the bZIP function, since each monomer binds only to one half of the cis-element recognized. Interaction between two bZIPs occurs via their coiled coil motifs, which are α-helices featuring several repetitions of the so-called heptads. Each heptad comprises seven amino acids whose positions are identified with letters from **a** to **g**, and due to the helical conformation, positions **a** and **d** which usually feature hydrophobic residues lie on the opposite side of the helix that positions **b**, **c**, and **f** which usually carry polar amino acids, so resulting in an amphipathic helix. A particular type of coiled coil motifs are the LZs, in which **d** positions are filled with leucines.

The interaction between coiled coil motifs is based on the in interdigitation of the side chains of the residues in the **a** or **d** positions following the knobs-into-holes model proposed by Crick in 1953. That is, each residue from these two positions packs its side chain (knob) into a cavity (hole) formed by the side chains of the four amino acids located on the opposite helix (Crick, 1953; Lupas and Gruber, 2005). This packing depends on the periodical arrange of the equivalent positions (i.e. **a** and **d**) along the interaction interface. However, the α-helix features 3.6 residues per turn, resulting in a phase shift of the heptad positions, so that a twist of about 20° in the helical axis is introduced to maintain a constant periodicity of one heptad every two turns of helix, hence the coiled conformation. Coiled coils can be formed between two or more chains arranged in the same or in opposing directions, but bZIPs interact always in pairs with their helices in parallel (Alber, 1992; Lupas and Gruber, 2005).

The stability of the coiled coil depends primarily on the hydrophobic collapse of the side chains of the amino acids in positions **a** and **d** (Vinson et al., 2002; Lupas and Gruber, 2005). However, this does not depend exclusively on the hydrophobicity of the amino acids in these positions, because the orientations of their side chains (knobs) are different in each position. Residues in **a** positions are oriented so that the vector between their Cα and Cβ atoms lies in parallel to the vector between the Cα atoms of the two residues at the bottom of the hole where it packs, while the vector between the Cα and Cβ residues in **d** positions lies perpendicularly (Figure 8). In other words, the side chains from the **a** positions are directed away from the hydrophobic core, whereas the ones from the **d** positions are directed into it (Harbury et al., 1993).

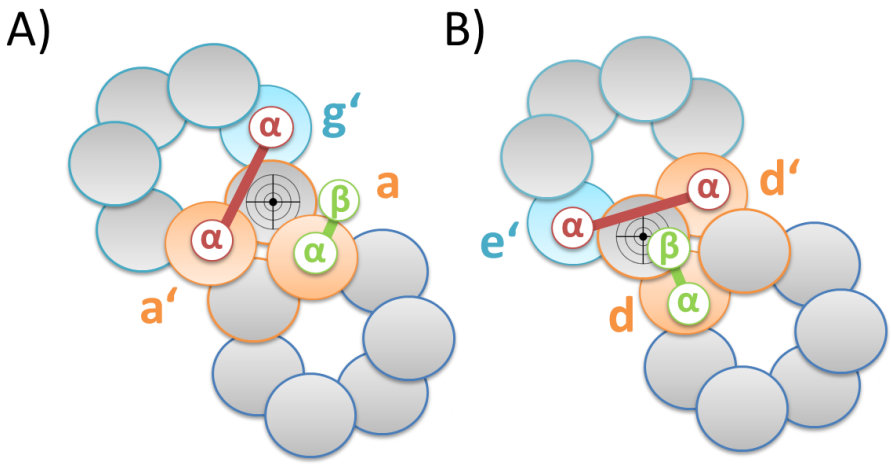

Figure 8. Different types of knobs-into-holes packing in section view. A) Parallel packing of **a** positions. B) Perpendicular packing of **d** positions. Holes are indicated by the bull's eye, and α and β represent the respective carbon atoms of the amino acids in the positions involved in the definition of the packing type, which are indicated by the colored letters. Note that knobs at **a** levels the require a sharp turn from the Cβ to reach the hole, while at **d** levels the Cβ is already oriented towards the hole.

As a result, the distance between the Cβ atoms of residues in **d** positions is smaller, so that the rotamer conformation required by those residues to fit their side chains into the holes is more restricted. Because of that, when **d** positions are occupied by β-branched amino acids (Val, Ile, Thr) they result in interhelical steric clashes between the Cγ2 methyl groups from residues on opposing helices. Conversely, the larger distance between Cβ carbons of residues in **a** positions favors these amino acids, as their bifurcated structure can reach the corresponding hole easier than the unbranched aliphatic residues (Leu, Ala) (Moitra et al., 1997; Wagschal et al., 1999). The calculated stabilizing orders among pairs of non-polar amino acids are Leu, Met, Ile, Phe, Val, and Ala for the **d** positions, and Ile, Val, Leu, Met, Phe, and Ala for the **a** positions (Moitra et al., 1997; Tripet et al., 2000; Acharya et al., 2002; Acharya et al., 2006).

The specificity of the dimerization is mostly defined by residues placed at the **e** and **g** positions. These positions lie crosswise, with **g** positions of one helix facing the **e** positions of the next heptad on the other helix. These are often occupied by charged residues (the acidic Asp and Glu, and the basic Arg and Lys), and depending on whether the **e**-**g** pairs result in same or opposed charges, repulsive or attractive electrostatic forces arise, respectively (Krylov et al., 1994; Arndt et al., 2000) (Figure 9). Interactions resulting in salt bridges formation are further stabilized promoting the dimerization, but repulsive **e**-**g** pairs formation appears to play a stronger role on partner matching, discriminating certain combinations (Vinson et al., 2002). Additionally, amino acids in **a** positions also contribute to the specificity depending on the **a**-**a** pairs formed. Asparagine and isoleucine in that position dramatically favor interactions with monomers carrying the same residue in the **a** position, therefore encouraging homo-interaction. Conversely, charged residues promote the association with monomers that carry a complementarily charged amino acid in the equivalent position, hindering the homo-interaction (Zeng et al., 1997; Wagschal et al., 1999; Arndt et al., 2000; Acharya et al., 2006). Furthermore, electrostatic interactions between **a**-**g** and **d**-**e** positions of opposing helices can also be established, contributing to the partner selection (Glover and Harrison, 1995).

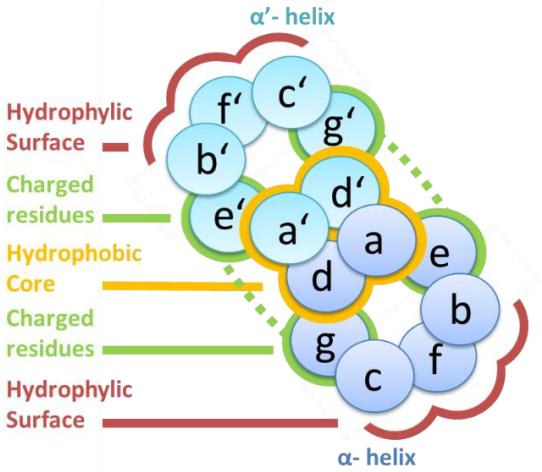

Figure 9. Diagram of the coiled coil interaction in section. The amino acids in positions **a** and **d** configure the hydrophobic core, which is indicated with the yellow halo. Charged residues in positions **e** and **g** generate electrostatic forces, represented by the dashed green lines. The hydrophilic surface is formed by the amino acids in positions **b**, **c**, and **f**. From Llorca et al. 2014.

1.4 Aim of this thesis

Similarities between the senescence syndrome and the stress response are apparent. Both are defined by a full metabolic twist, from a growth-promoting state dominated by anabolic processes to a complete arrest of growth and the activation of catabolic pathways, and result in enhanced ROS production. Congruently, transcriptomic analyses reveal overlapping changes in the gene expression occurring under stress or during senescence; but also important differences, indicating that they have unique singularities and requirements. Stress situations are temporary and therefore they trigger counteracting responses aimed to the recovery of the homeostasis; conversely, senescence represents a no-return situation. This is a fundamental difference between the two processes and it is clearly reflected by the differential management of the antioxidant system, which is deactivated in senescence but enhanced during stress. In agreement, an export of resources has not been described to happen during stress, as the remobilized nutrients in stress are used for the endurance of the cell. Still, in spite of having different purposes, stress conditions can induce senescence, indicating that the two processes are interconnected, although the mechanisms by which such interplay takes places are still poorly understood.

Interestingly, increased resistance to stress is often associated to extended lifespans. This is clearly exemplified by plant lines with altered SNRK1 levels, so that overexpressing lines exhibit longer lifespans, while mutants display early senescence phenotypes (Woo et al., 2004; Crozet et al., 2014). This phenotypic outcome suggests that the stress response can also act blocking the onset of senescence, hinting at the existence of some requirements to be fulfilled in order to permit the transition from the stress response to senescence, in a similar manner to the active prevention of cell death during senescence until full remobilization of nutrients is achieved (Buchanan-Wollaston et al., 2003). Significantly, dark-induced senescence is triggered in individual darkened Arabidopsis leaves, but not in whole darkened plants (Weaver and Amasino, 2001), for a part of the plant can be sacrificed to enhance the chance of survival of the rest, but that is not an option when the plant is affected in its totality. Similarly, the senescence induction by application of the stress-related hormone ET does not occur before the leaves reach a certain age (Jing et al., 2005), indicating that the interplay between stress and senescence is also influenced by the developmental stage.

bZIP transcription factors are known important mediators of physiological responses to environment, including stress situations, and they are involved in controlling developmental processes as well. Previously, the involvement of the Arabidopsis bZIP GBF1 in regulating the onset of senescence was identified in our group. GBF1 was found to down-regulate the *CAT2* expression, resulting in a subsequent increase in the H_2O_2 which acts as a senescence-triggering signal (Smykowski et al., 2010). However, the expression of GBF1 is not up-regulated during senescence, so the down-regulation of the *CAT2* expression by GBF1 is presumed to be regulated post-transcriptionally. Because, bZIPs function as dimers, an alluring possibility is that the GBF1 activity is regulated by the formation of specific heterodimers with other bZIPs. In order to address that possibility, dimerization between GBF1 and bZIPs members of the C and S1 classes, which are involved in the stress response, is examined in this thesis. Among those candidates, bZIP63 arised as a possible GBF1 interacting partner, and so it was investigated in detail. The effect of the GBF1-bZIP63 dimerization was analyzed on the DNA binding and the gene transactivation levels, and phenotypic studies were performed with bZIP63 transgenic lines.

On the second part of this thesis, the relationship between bZIP dimerization and function is analyzed. Because of the distinctive properties of the bZIP monomers, heterodimerization is assumed to operate in a combinatorial manner generating a large variety of dimers with unique properties through specific combination of a limited set of monomers. That premise is challenged by systematically determining the dimerization and transactivation properties of 16 Arabidopsis bZIPs, along with *in silico* analyses of their dimerization motifs.

2 Material and methods

2.1 Work with bacteria

2.1.1 Transformation of chemical competent bacterial cells

100 ng of isolated plasmid were added to 50 µL of chemical competent cells thawed on ice. Samples were incubated 30 minutes on ice and then subjected to a 42 °C heat shock for 1 minute, and placed back on ice for other 5 minutes. 250 µL of LB medium without antibiotics were added to the transformed cells and they were incubated at 37 °C for 1 hour, then spread on a petri dish containing LBA and the appropriate antibodies and incubated overnight at 37 °C.

2.1.2 Bacterial cultures

Bacteria were grown either in liquid LB to maximize the biomass production, or in solidified LBA plates to obtain isolated colonies. Usually, incubations were performed overnight at 37°C, and with vigorous shaking in the case of the liquid cultures; but these parameters were adapted when required. Antibodies were added for selection when required with the final concentrations indicated in Table 1.

Antibiotic	µg/mL
Ampicillin	100
Chloramphenicol	35
Gentamycin	25
Kanamycin	50
Rifampicin	100
Spectinomycin	100

Table 1. Final concentrations of antibiotics used for selection of bacterial cultures.

Different *E.coli*-derived bacterial strains were used depending on the experimental purpose. For cloning and plasmid propagation, DH5α (Taylor et al., 1993) and TOP10 (Invitrogen) strains were used indistinctly; while for protein expression either BL21-SI (Donahue Jr and Bebee, 1999) or BL21 Rosetta-DE3 (Novagen) were selected based on trial and error criteria. The DB3.1 strain (Invitrogen) was used for the propagation of Gateway plasmids.

LB: 1 % Tryptone, 0.5 % Yeast-extract, 1% NaCl. Autoclaved.

LBA: 1 % Tryptone, 0.5 % Yeast-extract, 1% NaCl, 1.5 % agar. Autoclaved.

2.1.3 Vectors

The following vectors were used in this study.

pUC-SPYNE and pUC-SPYCE vectors

The two vectors for the BiFC assay are pUC19 derived and share most of their sequences. In both vectors the protein expression is driven by the CaMV 35S promoter and the nopaline synthetase terminator, and there is an ampicillin resistance gene for clone selection. The differences in the sequences are limited to the peptide tag and the different YFP fragments coded. The two vectors are accordingly designated as pUC-SPYNE and pUC-SPYCE standing for split YFP N-terminal/C-terminal fragment expression (Walter et al., 2004). pUC-SPYNE codes for the first 155 amino acids of the YFP and carries a c-myc tag, while pUC-SPYCE code for the remaining 83 amino acids and a HA tag.

pUC 35S::c-myc

This vector was created ad hoc for this thesis as a modification of the pUC-SPYNE vector to serve as a protein expression vector in plants. The sequence coding for the N-terminal fragment of YFP was deleted by mutagenesis and a stop codon was added after the c-myc tag. The rest of the sequence is identical to the pUC-SPYNE vector.

pENTR/D-TOPO

Commercial vector to generate entry clones for subsequent Gateway cloning reactions (Invitrogen). The plasmid is provided already linearized by the action of the topoisomerase I from *Vaccinia* virus which remains covalently bound to the cleaved ends. PCR products are inserted by TOPO cloning directionally by adding an extra CACC sequence at the 5'end of the forward primer, which combine with a GTGG sequence overhanging from the 3' end of the cleaved vector. The vector codes for a kanamycin resistance gene.

pDONR201

Donor vector to generate entry clones for subsequent Gateway cloning reactions (Invitrogen). The vector codes for a kanamycin resistance gene for bacterial selection, and a chloramphenicol resistance gene for the propagation of the uncloned plasmid.

pH7FWG2 and pK7FWG2

Gateway binary destination vectors for expressing GFP fusion proteins in plants. Expression is driven by a CaMV 35S promoter and terminator and the GFP tag is fused N-terminal respect the cloned protein in the pH7FWG2, and C-terminal in pK7FWG2. Both code for a spectinomycin resistance gene for bacterial selection, and in addition, the former carries a kanamycin resistance gene for plant selection, while the latter carries a hygromycin resistance gene (Karimi et al., 2002).

pDEST15

Commercial Gateway destination vector for bacterial expression of N-terminal-GST tagged proteins (Invitrogen). It includes a T7 promoter for IPTG induction in DE3 cells, a Shine-Dalgarno sequence for ribosomal binding and the initial ATG. The vector codes for an ampicillin resistance gene for bacterial selection, and a chloramphenicol resistance gene for the propagation of the uncloned plasmid.

pDEST17

Commercial Gateway destination vector for bacterial expression of N-terminal-His tagged proteins (Invitrogen). It includes a T7 promoter for IPTG induction in DE3 cells, a Shine-Dalgarno sequence for ribosomal binding and the initial ATG. The vector codes for an ampicillin resistance gene for bacterial selection, and a chloramphenicol resistance gene for the propagation of the uncloned plasmid.

pDEST42

Commercial Gateway destination vector for bacterial expression of C-terminal-His tagged proteins (Invitrogen). It includes a T7 promoter for IPTG induction in DE3 cells, but neither the Shine-Dalgarno sequence nor the initial ATG. The vector codes for an ampicillin resistance gene for bacterial selection, and a chloramphenicol resistance gene for the propagation of the uncloned plasmid.

pBGWFS7

Gateway binary destination vector for the analysis of promoter activity. It codes for a GFP::GUS fusion protein downstream of the recombination site, so that its expression is driven by the promoter cloned. The vectors codes for a spectinomycin resistance gene for bacterial selection and a Basta resistance gene for seedling selection (Karimi et al., 2002).

pTLT

This vector was generated in the Markus Teige's laboratory (University of Vienna). It is a modification of the pGEM-T vector for expressing proteins in plants under the control of a CaMV 35S promoter.

pCB308

Binary vector derived from pBIN19 used for the analysis of promoter activity (Xiang et al., 1999). It carries a polylinker sequence in front of a GUS reporter gene. The vector codes for a kanamycin resistance gene for bacterial selection and a Basta resistance gene for seedling selection.

PMY01

Binary vector for protein overexpression in plants under control of a 35S promoter (Smykowski et al., 2010). The vectors codes for a kanamycin gene for bacterial selection and a Basta resistance gene for seedling selection.

pBT8

This vector was obtained from Dr. Friedrich Schöffl from the University of Tübingen (Li et al., 2010a). It codes for CaMV 35S promoter to express protein in plants. The vector codes for ampicillin resistance.

pET28a

Vector for bacterial expression of proteins double His-tagged at both ends, N- and C-terminus (Novagen). It includes a T7 promoter followed by lac operator, as well as a *lacI* repressor gene for IPTG induction. The vector codes for a kanamycin resistance gene.

pCF203 and pCF205

Vectors derived from pUC19 for protein expression in plants driven by a 35S CaMV promoter. Both vectors code for a spectinomycin resistance gene.

pAC27

Standard cloning vector derived from the pUC119 (Norris et al., 1993). The vector codes for ampicillin resistance.

2.1.4 Plasmid constructs

Clones used during the course of this thesis are indicated in Table *2*.

Nr.	Clone name	Vector	Use	Resistance	Source
860	ASNp::GUS	pBGWFS7	Promoter analysis	Spectinomycin	
971	CAT2p::GUS	pBGWFS7	Promoter analysis	Spectinomycin	
983	LHCB2.4p::GUS	pBGWFS7	Promoter analysis	Spectinomycin	
859	PDHp::GUS	pBGWFS7	Promoter analysis	Spectinomycin	
984	RBCS1ap::GUS	pBGWFS7	Promoter analysis	Spectinomycin	
130	pCAT2::GUS	pCB308	Promoter analysis	Kanamycin	P. Zimmermann
958	AK-GST	pDEST15	Bacterial GST-tag protein expression	Ampicillin	E. Baena-Gonzalez
957	His-KIN10	pET28	Bacterial His-tag protein expression	Ampicillin	E. Baena-Gonzalez
1013	His-bZIP1	pDEST17	Bacterial His-tag protein expression	Ampicillin	
871	His-bZIP2	pDEST17	Bacterial His-tag protein expression	Ampicillin	
1019	His-bZIP9	pDEST17	Bacterial His-tag protein expression	Ampicillin	
1014	His-bZIP10	pDEST17	Bacterial His-tag protein expression	Ampicillin	
870	His-bZIP11	pDEST17	Bacterial His-tag protein expression	Ampicillin	
1001	His-bZIP16	pDEST17	Bacterial His-tag protein expression	Ampicillin	
1015	His-bZIP25	pDEST17	Bacterial His-tag protein expression	Ampicillin	
1016	His-bZIP44	pDEST17	Bacterial His-tag protein expression	Ampicillin	
869	His-bZIP53	pDEST17	Bacterial His-tag protein expression	Ampicillin	
868	His-bZIP63	pDEST17	Bacterial His-tag protein expression	Ampicillin	
1002	His-bZIP68	pDEST17	Bacterial His-tag protein expression	Ampicillin	
864	His-GBF1	pDEST17	Bacterial His-tag protein expression	Ampicillin	
1004	His-GBF2	pDEST17	Bacterial His-tag protein expression	Ampicillin	
1003	His-GBF3	pDEST17	Bacterial His-tag protein expression	Ampicillin	
1018	His-Hy5	pDEST17	Bacterial His-tag protein expression	Ampicillin	
1017	His-HyH	pDEST17	Bacterial His-tag protein expression	Ampicillin	
584	bZIP63-His	pDEST42	Bacterial His-tag protein expression	Ampicillin	A. Smykowski
930	GBF1-His	pDEST42	Bacterial His-tag protein expression	Ampicillin	*
937	GBF1 S11/15/19A-His	pDEST42	Bacterial His-tag protein expression	Ampicillin	*
938	GBF1 S11/15/19D-His	pDEST42	Bacterial His-tag protein expression	Ampicillin	*
2041	GFP-bZIP1	pH7WGF2	Plant GFP-tag protein expression	Spectinomycin	
2039	GFP-bZIP2	pH7WGF2	Plant GFP-tag protein expression	Spectinomycin	
2043	GFP-bZIP9	pH7WGF2	Plant GFP-tag protein expression	Spectinomycin	
272	GFP-bZIP10	pH7WGF2	Plant GFP-tag protein expression	Spectinomycin	
2044	GFP-bZIP11	pH7WGF2	Plant GFP-tag protein expression	Spectinomycin	
2048	GFP-bZIP16	pH7WGF2	Plant GFP-tag protein expression	Spectinomycin	
2040	GFP-bZIP25	pH7WGF2	Plant GFP-tag protein expression	Spectinomycin	
2045	GFP-bZIP44	pH7WGF2	Plant GFP-tag protein expression	Spectinomycin	
848	GFP-bZIP53	pK7FWG2.0	Plant GFP-tag protein expression	Spectinomycin	
849	GFP-bZIP63	pK7FWG2.0	Plant GFP-tag protein expression	Spectinomycin	
2049	GFP-bZIP68	pH7WGF2	Plant GFP-tag protein expression	Spectinomycin	
981	GFP-GBF1	pK7FWG2.0	Plant GFP-tag protein expression	Spectinomycin	
2046	GFP-GBF2	pH7WGF2	Plant GFP-tag protein expression	Spectinomycin	
2047	GFP-GBF3	pH7WGF2	Plant GFP-tag protein expression	Spectinomycin	
2050	GFP-Hy5	pH7WGF2	Plant GFP-tag protein expression	Spectinomycin	
2051	GFP-HyH	pH7WGF2	Plant GFP-tag protein expression	Spectinomycin	
922	bZIP63.2-YFP	pLTL	Plant YFP-tag protein expression	Ampicillin	M. Teige
839	35S::bZIP1	pUC-35Smyc	GUS assay effector	Ampicillin	
877	35S::bZIP2	pUC-35Smyc	GUS assay effector	Ampicillin	
837	35S::bZIP9	pUC-35Smyc	GUS assay effector	Ampicillin	
840	35S::bZIP10	pUC-35Smyc	GUS assay effector	Ampicillin	
836	35S::bZIP11	pUC-35Smyc	GUS assay effector	Ampicillin	
835	35S::bZIP16	pUC-35Smyc	GUS assay effector	Ampicillin	
838	35S::bZIP25	pUC-35Smyc	GUS assay effector	Ampicillin	

834	35S::bZIP44	pUC-35Smyc	GUS assay effector	Ampicillin	
896	35S::bZIP53	pUC-35Smyc	GUS assay effector	Ampicillin	
833	35S::bZIP68	pUC-35Smyc	GUS assay effector	Ampicillin	
895	35S::bZIP63	pUC-35Smyc	GUS assay effector	Ampicillin	
898	35S::GBF1	pUC-35Smyc	GUS assay effector	Ampicillin	
832	35S::GBF2	pUC-35Smyc	GUS assay effector	Ampicillin	
831	35S::GBF3	pUC-35Smyc	GUS assay effector	Ampicillin	
830	35S::HY5	pUC-35Smyc	GUS assay effector	Ampicillin	
829	35S::HYH	pUC-35Smyc	GUS assay effector	Ampicillin	
119	35S::GBF1	pY01	GUS assay effector	Kanamycin	P. Zimmermann
906	bZIP1-SPC	pUC-SPYCE	BiFC	Ampicillin	
903	bZIP2-SPC	pUC-SPYCE	BiFC	Ampicillin	
989	bZIP9-SPC	pUC-SPYCE	BiFC	Ampicillin	
900	bZIP10-SPC	pUC-SPYCE	BiFC	Ampicillin	*
949	bZIP11-SPC	pUC-SPYCE	BiFC	Ampicillin	
982	bZIP16-SPC	pUC-SPYCE	BiFC	Ampicillin	
950	bZIP25-SPC	pUC-SPYCE	BiFC	Ampicillin	
951	bZIP44-SPC	pUC-SPYCE	BiFC	Ampicillin	
901	bZIP53-SPC	pUC-SPYCE	BiFC	Ampicillin	
940	bZIP63-SPC	pUC-SPYCE	BiFC	Ampicillin	*
998	bZIP68-SPC	pUC-SPYCE	BiFC	Ampicillin	*
483	GBF1-SPC	pUC-SPYCE	BiFC	Ampicillin	A. Smykowski
911	GBF1 S11/15/19A–SPC	pUC-SPYCE	BiFC	Ampicillin	
623	GBF1 S11/15/19D–SPC	pUC-SPYCE	BiFC	Ampicillin	A. Smykowski
917	GBF1Leu–SPC	pUC-SPYCE	BiFC	Ampicillin	
913	GBF1-Leu–SPC	pUC-SPYCE	BiFC	Ampicillin	
890	GBF2-SPC	pUC-SPYCE	BiFC	Ampicillin	
978	GBF3-SPC	pUC-SPYCE	BiFC	Ampicillin	
888	HY5-SPC	pUC-SPYCE	BiFC	Ampicillin	
886	HYH-SPC	pUC-SPYCE	BiFC	Ampicillin	
905	bZIP1-SPN	pUC-SPYNE	BiFC	Ampicillin	
904	bZIP2-SPN	pUC-SPYNE	BiFC	Ampicillin	
988	bZIP9-SPN	pUC-SPYNE	BiFC	Ampicillin	
999	bZIP10-SPN	pUC-SPYNE	BiFC	Ampicillin	*
946	bZIP11-SPN	pUC-SPYNE	BiFC	Ampicillin	
977	bZIP16-SPN	pUC-SPYNE	BiFC	Ampicillin	
947	bZIP25-SPN	pUC-SPYNE	BiFC	Ampicillin	
948	bZIP44-SPN	pUC-SPYNE	BiFC	Ampicillin	
902	bZIP53-SPN	pUC-SPYNE	BiFC	Ampicillin	
939	bZIP63-SPN	pUC-SPYNE	BiFC	Ampicillin	*
894	bZIP68-SPN	pUC-SPYNE	BiFC	Ampicillin	*
484	GBF1-SPN	pUC-SPYNE	BiFC	Ampicillin	A. Smykowski
912	GBF1 S11/15/19A–SPN	pUC-SPYNE	BiFC	Ampicillin	
624	GBF1 S11/15/19D–SPN	pUC-SPYNE	BiFC	Ampicillin	A. Smykowski
919	GBF1Leu–SPN	pUC-SPYNE	BiFC	Ampicillin	
914	GBF1–Leu–SPN	pUC-SPYNE	BiFC	Ampicillin	
889	GBF2-SPN	pUC-SPYNE	BiFC	Ampicillin	
578	GBF3-SPN	pUC-SPYNE	BiFC	Ampicillin	
887	HY5-SPN	pUC-SPYNE	BiFC	Ampicillin	
885	HYH-SPN	pUC-SPYNE	BiFC	Ampicillin	
1006	bZIP1	pDONR201	Entry clone	Kanamycin	W. Dröge-Laser
881	bZIP2	TOPO	Entry clone	Kanamycin	
1007	bZIP9	pDONR201	Entry clone	Kanamycin	W. Dröge-Laser
1008	bZIP10	pDONR201	Entry clone	Kanamycin	W. Dröge-Laser
878	bZIP11	TOPO	Entry clone	Kanamycin	
815	bZIP16	TOPO	Entry clone	Kanamycin	
1009	bZIP25	pDONR201	Entry clone	Kanamycin	W. Dröge-Laser
1010	bZIP44	pDONR201	Entry clone	Kanamycin	W. Dröge-Laser
879	bZIP53	TOPO	Entry clone	Kanamycin	
880	bZIP63	TOPO	Entry clone	Kanamycin	
817	bZIP68	TOPO	Entry clone	Kanamycin	
876	GBF1	TOPO	Entry clone	Kanamycin	
819	GBF2	TOPO	Entry clone	Kanamycin	
818	GBF3	TOPO	Entry clone	Kanamycin	
1011	Hy5	pDONR201	Entry clone	Kanamycin	W. Dröge-Laser
1012	HyH	pDONR201	Entry clone	Kanamycin	W. Dröge-Laser
862	pASN	TOPO	Entry clone	Kanamycin	

969	pCAT2	TOPO	Entry clone	Kanamycin	
979	pLHCB2.4	TOPO	Entry clone	Kanamycin	
866	pPDH	TOPO	Entry clone	Kanamycin	
990	pRBCS1a	TOPO	Entry clone	Kanamycin	
-	35S::GFP	Cf203	Plant GFP expression	Spectinomycin	K. Schumacher
974	mCherry-NLS	Cf205	Plant mCherry expression	Spectinomycin	K. W. Berendzen
-	UBQ3::GUS	pAC27	Plant GUS expression	Ampicillin	J. Callis
1177	35S::Luciferase	pBT8	Plant luciferase expression	Ampicillin	F. Schöffl

Table 2. Clones used in this study. The number indicated corresponds to the Zentgraf's laboratory plasmid stock. The last column specifies the source for constructs used, but not generated in this work; and asterisks indicate constructs that were available in the laboratory stock but presented mutations in their sequences, so they were fixed by mutagenesis for this study.

2.1.5 Plasmid DNA isolation

Isolation of plasmids for purposes in which is important to maintain high DNA purity such as sequencing, protoplast transformation, or cloning was performed with commercial kits, including maxi-, midi-, and mini-prep kits manufactured by either PeqLab or Fermentas. In those cases in which the DNA purity is not an issue, such as restriction analysis of clones or plasmid propagation, the plasmids were isolated by alkaline lysis as follows.

4 mL from a 5 mL over-night culture were centrifuged in a table-centrifuge at 8.000 g for 2 minutes. The pellet was resuspended in 250 µL of Solution I by vortexing. Then, 250 µL of Solution II were added and gently mixed by inverting the tubes. After 3 min of incubation time at RT, 350 µL of Solution III were added to the tube, carefully mixed by inversion, and then centrifuged in a table-centrifuge at maximum speed for 5 min at RT. Next, the supernatant was transferred to a new tube and mixed in a 1:1 ratio with ice-cold isopropanol, then centrifuged again at maximum speed for 5 minutes. The supernatant was discarded by inversion and the DNA pellet was washed with 250 µL 70% ethanol and centrifuged again at maximum speed for 5 minutes. After that, ethanol was removed by pipetting and the pellet was air-dried. Finally, the pellet was resuspended in 50 µL of distilled and autoclaved H_2O.

Solution I: 50 mM Glucose, 25 mM Tris-HCl pH 8.0, 10 mM EDTA. Autoclaved. Solution was completed with 10 mg/mL RNase (Ribonuclease A, Roth) just before use.

Solution II: 0.2 M NaOH, 1% SDS. Autoclaved.

Solution III: 3 M Potassium acetate, 11.5 % v/v Acetic acid. Autoclaved.

2.2 Work with plants

2.2.1 Plants growing

Plants were grown at 20-25°C with long day light conditions (16h light/8h dark) and a light intensity of 90-120 µmol s^{-1} m^{-2}. Seeds were usually stratified for 48 hours at 4°C after sowing, and then transferred to the climate chambers. Plants were let grow in room-size climate chambers for genotyping, seed production, or for the generation of new lines (crossing and transformation); but in smaller cabinet climate chambers (Figure 10) for phenotyping purposes, as they ensure more homogeneous and stable conditions. Unless otherwise is stated, all plant lines used in this thesis were *Arabidopsis thaliana* Col-0.

Figure 10. Cabinet climate chamber used for growing plants for phenotypic determination.

2.2.2 RNA extraction, cDNA synthesis, and qPCR

Total RNA extraction was performed with the RNAeasy Plant Mini Kit (Qiagen) from plants grown under long day conditions at 20°C and according to the manufacturer's instructions. 0.5 µg of the extracted RNA were then digested with DNaseI (Fermentas) in a final reaction volume of 20 µL for 30 minutes at 37°C. Then, the enzyme was inactivated by the addition of 2 µL of 50 mM EDTA and incubation at 65°C for 10 minutes.

RNA isolation from seeds was performed following an alternative protocol with the use of organic extractions as previously described (Oñate-Sánchez and Vicente-Carbajosa, 2008). 90 mg of seeds were frozen in a 2 mL Eppendorf tube with liquid nitrogen, then mixed with 550 µL of RNA Extraction buffer and 550 µL of Chloroform and vortexed for 10 sec. Homogenized samples were centrifuged at maximum speed for 3 minutes at RT. The supernatant was transferred to a new 2 mL Eppendorf tube and mixed with 500 µL of water saturated acidic Phenol, then vortexed again thoroughly. Next, 200 µL of Chloroform were added and the mix was centrifuged at maximum speed for 3 minutes at RT. The supernatant was transferred to a new 1.5 mL Eppendorf tube and mixed with 1/3 volume of 8M LiCl solution. After 1 hour of incubation at -20°C, samples were centrifuged at maximum speed for 30 min at 4°C. The supernatant was discarded and the pellet was resuspended in 26 µL of DEPC-treated water and digested with DNaseI (Fermentas) in a final reaction volume of 30 µL for 30 minutes at 37°C. Then, 470 µL of DEPC-treated water were added, along with 250 µL Ethanol and 7 µL of 3M Sodium acetate pH 5.2 solution. Samples were mixed and centrifuged at maximum speed for 10 minutes at 4°C. The supernatant was transferred to a new 1.5 mL Eppendorf tube, and 750 µl Ethanol and 43 µL of 3M Sodium acetate pH 5.2 solution were added and mixed thoroughly. After 1 hour of incubation at -20°C, samples were centrifuged at maximum speed for 20 minutes at 4°C, the supernatant was removed and the pellet washed with 100 µL of 70% Ethanol. The dry pellet was finally resuspended in 20 µL of DEPC-treated water.

The cDNA synthesis was performed with 11 µL of the DNAse-digested RNA extraction using the RevertAid Reverse Transcriptase (Fermentas). First, 1 µL of 100 mM random-hexamer or oligo-dT_{18} primers (Fermentas, in both cases) was added to the RNA extract and incubated for 5 minutes at 65°C. The reaction buffer was then completed by the addition of the remaining components: 4 µL of 5X RT buffer, 2 µL of 10 mM dNTPs, 1 µL of Ribo-Lock (Fermentas), and 1 µL of RevertAid. The reaction was carried out at 42°C for 60 minutes, and then terminated by heating at 70°C for 5 minutes. Finally, the cDNA-containing solution was diluted 1:6 with DEPC-treated water.

The qPCR was performed with iTAQ universal SYBR green supermix (Bio-Rad) in a final volume of 10µl, including 2µl of 1:6 diluted cDNA and the primers at 1µM concentration. Thermocycling conditions used are depicted in Figure 11.

RNA Extraction buffer: 0.4 M LiCl, 0.2 M Tris pH 8.0, 25 mM EDTA, 1% SDS.

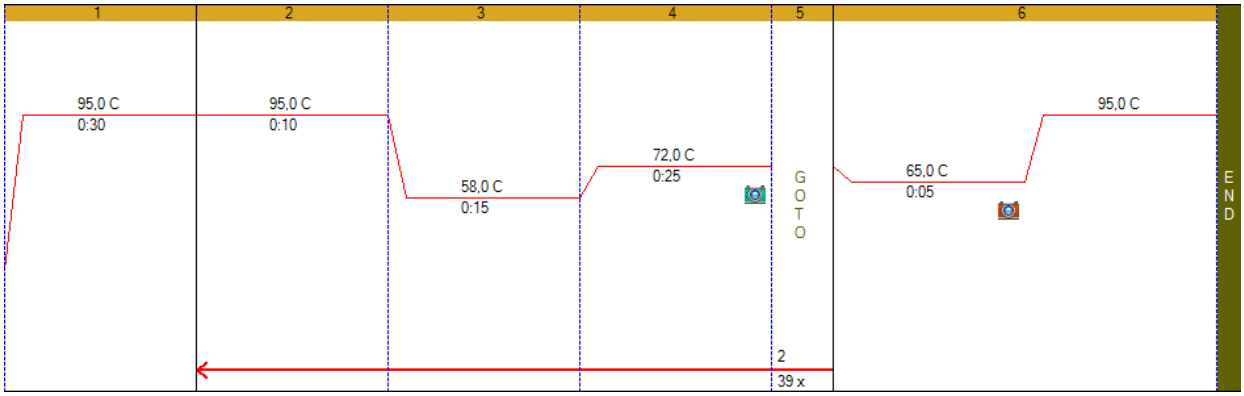

Figure 11. Thermocycling conditions used for the qPCR experiments. Capture from the Bio-Rad CFX Manager 3.1 program.

2.2.3 Genomic DNA extraction from plants

Genomic DNA was extracted from rosette leaves as previously described (Edwards et al., 1991). Leaf material was homogenized with a pestle in a 1.5 mL Eppendorf tube. 400 µL of PCR Extraction buffer were added, the mix was vortexed for 5 seconds, and then centrifuged at maximum speed for 5 minutes at RT. 300 µL of the supernatant were transferred to a new 1.5 µL Eppendorf tube, mixed with the equal volume of ice-cold isopropanol, and centrifuged at maximum speed for 10 minutes at RT. The supernatant was discarded by inversion and the DNA pellet was washed with 70 % Ethanol and centrifuged again. Finally, after the removal of the supernatant, the pellet was left to dry up and then resuspended in 50 µL of TE buffer.

PCR Extraction buffer: 200 mM Tris-HCl pH 7.5, 250 mM NaCl, 25 mM EDTA, 0.5% SDS.

TE buffer: 10 mM Tris pH 8.0, 1 mM EDTA.

2.3 Work with DNA

2.3.1 PCR

Many different PCR settings were used in this work according to the needs and the subsequent purpose of each PCR product. The PCR parameters suggested by the manufacturer were applied by default and adjusted if required, including variations in the template, primers, and DNA concentrations, as well as in the temperature and duration of each PCR step. In some cases, additives such as Mg^{2+} or DMSO were used, and alternative PCR methods such as touch-down or touch-up were applied.

In those cases in which replication fidelity was important, such as gene cloning, Phusion High-Fidelity DNA Polymerase (New England Biolabs) was used. The theoretical primer Tm was calculated on http://tmcalculator.neb.com, and then, a gradient PCR was performed to determine the optimal annealing temperature.

When the purpose of the PCR was to screen for the presence of a certain product or to determine its size, a DNA polymerase without 3'-5' exonuclease proofreading activity was used. Specifically, it was a ready-to-use RedTaq Mastermix 2x (Genaxxon), for which the reaction buffer only required to be completed with the

primers and the DNA template. A gradient PCR was first performed to determine the optimal annealing temperature in this system, starting from the theoretical primer Tm calculated by the provider. This system was proved to be very robust and tolerated a wide range of conditions, so that no modifications of the manufacturer's protocol were needed. Only the extension time was adjusted systematically.

Independently of the system used, PCR products were checked in agarose gels (normally at 1%), and the size of the bands was determined by comparison with a DNA standard (GeneRuler 1Kb Plus, Thermo Scientific).

Phusion Reaction buffer (default): 1X Phusion HF or GC buffer, 200 µM dNTPs mix, 0.5 µM primers, 50 ng genomic DNA or 5 ng of plasmid DNA/ 50 µL reaction, 0.5 µL Phusion polymerase/50 µL reaction.

Phusion thermocycling conditions (default): Initial denaturation at 98°C for 30 seconds. 30 cycles of denaturation at 98 °C for 10 seconds, annealing at the calculated Tm for 15 seconds, and extension at 72 °C for 30 seconds/Kbp of PCR product. Final extension at 72 °C for 5 minutes.

RedTaq Reaction buffer: 1X RedTaq Mastermix, 0.5 µM primers, ca. 5 ng template DNA/20 µL reaction.

RedTaq thermocycling conditions: Initial denaturation at 95°C for 10 minutes. 30 cycles of denaturation at 95 °C for 30 seconds, annealing at 60 °C for 30 seconds, and extension at 72 °C for 1 minute/Kbp of PCR product. Final extension at 72 °C for 10 minutes.

2.3.2 Primers

Primers used in this study are collected in Table 3.

Name	Sequence 5`-3`	Method
bZIP1 Fwd Xba1	GCTCTAGAATGGCAAACGCAGAGAAGAC	Classic cloning
bZIP1 Rev BamHI	CGGGATCCTGTCTTAAAGGACGCCATTG	Classic cloning
bZIP2 Fwd XbaI	GCTCTAGAATGGCGTCATCTAGCAGCAC	Classic cloning
bZIP2 Rev BamHI	CGGGATCCATACATATTGATATCATTAGCC	Classic cloning
bZIP9 Rev SalI	TCCCCCGGGTGGCCAGATGTCTGAGAC	Classic cloning
bZIP9 Fwd XhoI	CCGCTCGAGATGGATAATC ACACAGC	Classic cloning
bZIP10 Rev SalI	TCCCCCGGGGTCCACGCATTTTTTCGG	Classic cloning
bZIP10 Fwd XhoI	CCGCTCGAGATGAACAGTATCTTCTCC	Classic cloning
bZIP11 Rev KpnI	CGGGGTACCATACATTAAAGCATCAGAAG	Classic cloning
bZIP11 Fwd XbaI	TGCTCTAGAATGGAATCGT CGTCGTCGGG	Classic cloning
bZIP16 Fwd BamHI	CGCGGATCCATGGCTAGCA ATGAGATGG	Classic cloning
bZIP16 Rev XhoI	CCGCTCGAGCGTTGAGTCTTTGTATGAATC	Classic cloning
bZIP25 Rev KpnI	CGGGGTACCATGCTTGTGATTCCAATGGG	Classic cloning
bZIP25 Fwd XbaI	TGCTCTAGAATGCACATCG TCTTCTCTGT	Classic cloning
bZIP44 Rev KpnI	CGGGGTACCACAGTTGAAAACATCACCAG	Classic cloning
bZIP44 Fwd XbaI	TGCTCTAGAATGAATAATA AAACTGAAAT	Classic cloning
bZIP53 Fwd XbaI	GCTCTAGAATGGGGTCGTTGCAAATGC	Classic cloning
bZIP53 Rev BamHI	CGGGATCCGCAATCAAACATATCAGC	Classic cloning
bZIP63 Fwd BamHI	CGGGATCCATGGAAAAAGTTTTCTC	Classic cloning
bZIP63 Rev XhoI	CCCTCGAGCTACTGATCCCCAAC	Classic cloning
bZIP68 Fwd BamHI	CGCGGATCCATGGGTAGCA GTGAGATGG	Classic cloning
bZIP68 Rev XhoI	CCGCTCGAGCGCAACATCCTGACGTGTAC	Classic cloning
GBF1 Fwd BamHI	CGCGGATCCATGGGAACGAGCGAAGACAA	Classic cloning
GBF1 Rev KpnI	CGGGGTACCATTTGTTCCTTCACCATC	Classic cloning
GBF2 Rev SmaI	TCCCCCGGGGCTAGCCGCGACAGGATCGG	Classic cloning
GBF2 Fwd XbaI	TGCTCTAGAATGGGTAGCAACGAAGAAGG	Classic cloning
GBF3 Fwd KpnI	GGTACCATGGGAAATAGCAGCGAGG	Classic cloning
GBF3 Rev SmaI	CCCGGGGCCTGCAGCTACTGCTTT	Classic cloning
Hy5 Rev SmaI	TCCCCCGGGAAGGCTTGCATCAGCATTAG	Classic cloning

Hy5 Fwd XbaI	TGCTCTAGAATGCAGGAAC AAGCGACTAG C	Classic cloning
HyH Rev SmaI	TCCCCCGGGGTGATTGTCATCAGTTTTAGG	Classic cloning
HyH Fwd XbaI	TGCTCTAGAATGTCTCTCC AACGACCC	Classic cloning
GBF1-LZ Rev KpnI	GGGGTACCTTGTTCGCATTCGGCCTGCTT	Classic cloning
GBF1+LZ Fwd BamHI	CGGGATCCATGCTTCAACAAAGAGTAGAG	Classic cloning
bZIP2 TOPO REV	TCAATACATATTGATATCATTAGC	GW cloning
bZIP2 TOPO FWD	CACCATGGCGTCATCTAGCAG	GW cloning
bZIP11 TOPO REV	TTAATACATTAAAGCATCAG	GW cloning
bZIP11 TOPO FWD	CACCATGGAATCGTCGTCGTCG	GW cloning
bZIP16 TOPO FWD	CACCATGGCTAGCAATGAGATGG	GW cloning
bZIP16 TOPO REV	TCACGTTGAGTCTTTGTATGAATC	GW cloning
bZIP53 TOPO FWD	CACCATGGGGTCGTTGCAAATGC	GW cloning
bZIP53 TOPO REV	TCAGCAATCAAACATATCAG	GW cloning
bZIP63 TOPO FWD	CACCATGGAAAAAGTTTTCTCC	GW cloning
bZIP63 TOPO REV	CTACTGATCCCCAACGC	GW cloning
bZIP68 TOPO FWD	CACCATGGGTAGCAGTGAGATGG	GW cloning
bZIP68 TOPO REV	TCACGCAACATCCTGACGTGTAC	GW cloning
GBF1 TOPO FWD	CACCATGGGAACGAGCGAAGAC	GW cloning
GBF1 TOPO REV	TTAATTTGTTCCTTCACCATC	GW cloning
GBF2 TOPO FWD	CACCATGGGTAGCAACGAAG	GW cloning
GBF2 TOPO REV	TCAGCTAGCCGCGACAGGATCG	GW cloning
GBF3 TOPO FWD	CACCATGGGAAATAGCAGCGAGG	GW cloning
GBF3 TOPO REV	TCAGCCTGCAGCTACTGC	GW cloning
pASN1 TOPO FWD	CACCGTTATCTGTTTATTTGATAAC	GW cloning
pASN1 TOPO REV	GTTTTTTTTTTGAAGAAAGTG	GW cloning
pCAT2 TOPO Rev	GGTTTGATGAGAAGAGAGC	GW cloning
pCAT2 TOPO FWD	CACCCTTCAGCACATTTTTGAGCCTG	GW cloning
pLHCB TOPO FWD	CACCCTACATATCTCAGGCACGTG	GW cloning
pLHCB TOPO REV	GCTTCTTCTAAACAAGAAC	GW cloning
pPDH TOPO FWD	CACCGGAACTTCTCAAAACAACTG	GW cloning
pPDH TOPO REV	AAAATTCAAAGATTTTGTTTTT	GW cloning
pRBCS1a TOPO FWD	CACCTCCGTGGTCGAGATTGTGTA	GW cloning
pRBCS TOPO REV	TGTTCTTCTTTACTCTTTGTGTGA	GW cloning
Actin qPCR FWD	ACCCGATGGGCAAGTCATCACG	qPCR
Actin qPCR REV	TCCCACAAACGAGGGCTGGA	qPCR
bZIP1 qPCR FWD	CGAAACGGAGAACGCGGGTCTT	qPCR
bZIP1 qPCR REV	TCGTCGACACAATCGCCACCA	qPCR
bZIP2 qPCR FWD	ACCGGAGCTCAAGCTCTTCCGA	qPCR
bZIP2 qPCR REV	ACGCATCCTTGACCTACGTGC	qPCR
bZIP9 qPCR FWD	TCGCCCGCCATTACAGTCCA	qPCR
bZIP9 qPCR REV	TGGCCAGATGTCTGAGACGCA	qPCR
bZIP10 qPCR FWD	TCGCTGCTCCTCCATCCCAA	qPCR
bZIP10 qPCR REV	AGCCATACGGGTTGGCGCTT	qPCR
bZIP11 qPCR FWD	GGCATGTGTTCGAACCCTCTGGT	qPCR
bZIP11 qPCR REV	AGACGCCATGAGAGGCTGGT	qPCR
bZIP16 qPCR FWD	ATCGGCTGTGAGTGCTGGCAT	qPCR
bZIP16 qPCR REV	ATAACCATGAGGCGGCGGCA	qPCR
bZIP25 qPCR FWD	CCGCTAGGCGCTCTAGGAGAAGAA	qPCR
bZIP25 qPCR REV	TCGGCTCTTAATTGGCCTACCTGT	qPCR
bZIP44 qPCR FWD	ATCTGCGAGGAGGTCGAGGATGA	qPCR
bZIP44 qPCR REV	TGACGTAGTGCTGCGTCGTGA	qPCR
bZIP53 qPCR FWD	TTGAGGGCACAGGCTTCGGA	qPCR
bZIP53 qPCR REV	AGGCATCTGCCAAGGGTTCTGC	qPCR
bZIP63 qPCR FWD	ACGGCGTGTGGTGTTTCCGT	qPCR
bZIP63 qPCR REV	TGGCGACAGCAGCACAAGCAA	qPCR
bZIP68 qPCR FWD	TGGTTCTGCTCATGGACCACCC	qPCR
bZIP68 qPCR REV	ACACCTGTAGCCGACACTGGCA	qPCR
GBF1 qPCR FWD	GCCAATCAACAGGAACAGGGTTCA	qPCR
GBF1 qPCR REV	TACCGGCTTCATGGGCACCGAA	qPCR
GBF2 qPCR FWD	TGGGCGTCTCCATCGCCAAT	qPCR

GBF2 qPCR REV	AGGACCTTGTGGTTGTGAGCCC	qPCR
GBF3 qPCR FWD	CGTCAAGTGGTGATACCGGCGT	qPCR
GBF3 qPCR REV	GAAGCCAAGTTTCAGGAGGAACCA	qPCR
Hy5 qPCR FWD	ACCATCAAGCAGCGAGAGGTCA	qPCR
Hy5 qPCR REV	AACTCCGGCACTCGCCGTAT	qPCR
HyH qPCR FWD	TGTTCTAAGCAGCAGCGCCGA	qPCR
HyH qPCR REV	GTTTCTTCCACGGCGGCGTTT	qPCR
Fix GBF1 FWD	GTTCAGGGAACGATGGTGCCTCTCATAGTGATGAAAGTGTCACAG	Plasmid modification
Fix GBF1 REV	CTGTGACACTTTCATCACTATGAGAGGCACCATCGTTCCCTGAAC	Plasmid modification
Fix bZIP63 FWD	CCTGGCGCGCCACTAGTGGATCCGTATGGAGAAAGTTTTCAGCGACGAAG	Plasmid modification
Fix bZIP63 REV	CTTCGTCGCTGAAAACTTTCTCCATACGGATCCACTAGTGGCGCGCCAGG	Plasmid modification
MutDEL N-YFP FWD	TCTTTAAGAGCTCGAATTTCCCCGATCGTTCAAACATTTG	Plasmid modification
MutDEL N-YFP FWD	GGATGGAGCAAAAGTTGATTTCTGAGGAGGATCTTTAAGAG	Plasmid modification
Fix bZIP10 FWD	CTCAGAACGATTCAGCATGGCCGAAAAAATGCGTG	Plasmid modification
Fix bZIP10 REV	CACGCATTTTTTCGGCCATGCTGAATCGTTCTGAG	Plasmid modification
Fix bZIP68 FWD	CTCCGGGGTCTTATCCATATAGTCCCTATGCAATG	Plasmid modification
Fix bZIP68 REV	CATTGCATAGGGACTATATGGATAAGACCCCGGAG	Plasmid modification
MutGBF1 S15A FWD	CAATCTAACCGTGAAGCCGCTAGGCGGTCTAG	Plasmid modification
MutGBF1 S15A REV	CTAGACCGCCTAGCGGCTTCACGGTTAGATTG	Plasmid modification
MutGBF1 S15/19A FWD	GAAGAGGAAACAAGCTAACCGTGAAGCCGC	Plasmid modification
MutGBF1 S15/19A REV	GCGGCTTCACGGTTAGCTTGTTTCCTCTTC	Plasmid modification
MutGBF1 S11/15A FWD	GAAGCCGCTAGGCGGGCTAGATTGCGGAAGCAG	Plasmid modification
MutGBF1 S11/15A REV	CTGCTTCCGCAATCTAGCCCGCCTAGCGGCTTC	Plasmid modification
CAT2 Gbox1 Fwd Biotin	CTCATCACACGTGGAATCC	ELISA
CAT2 Gbox1 Rev	GGATTCCACGTGTGATGAG	ELISA
CAT2 Gbox2 Fwd Biotin	ACAAAGCAGCCACGTCACCCAAGACC	ELISA
CAT2 Gbox2 Rev	GGTCTTGGGTGACGTGGCTGCTTTGT	ELISA
CAT2 Gbox3 Fwd Biotin	ACAGCCCAATGACGTCCTCATTTATT	ELISA
CAT2 Gbox3 Rev	AATAAATGAGGACGTCATTGGGCTGT	ELISA
RBCS1a Gbox1 Fwd Biotin	AATTATCTTCCACGTGGCATTATTC	ELISA
RBCS1a Gbox1 Rev	GGAATAATGCCACGTGGAAGATAAT	ELISA
RBCS1a Gbox2 Fwd Biotin	AGTTTATTTAGACGTGCTAACTTTGT	ELISA
RBCS1a Gbox2 Rev	ACAAAGTTAGCACGTCTAAATAAACT	ELISA
PDH Gbox1 Fwd Biotin	CATAAGGTTTTACGTGCTTCTATAAA	ELISA
PDH Gbox1 Rev	TTTATAGAAGCACGTAAAACCTTATG	ELISA
PDH Gbox2 Fwd Biotin	TAACAGGTAAAACGTGTATGTACATG	ELISA
PDH Gbox2 Rev	CATGTACATACACGTTTTACCTGTTA	ELISA
PDH Gbox3 FwdBiotin	TGCTGTCTCTGACGTCCTTAATTATC	ELISA
PDH Gbox3 Rev	GATAATTAAGGACGTCAGAGACAGCA	ELISA
SALK LBb1.3	ATTTTGCCGATTTCGGAA	SALK
bZIP63 SALK LP	CCTCGAAAAATCCCTTTATGG	SALK
bZIP63 SALK RP	GAGTACCCTTTTCATGGCGAC	SALK
GBF1 SALK LP	TCAGAATCCGATTCCAATCAC	SALK
GBF1 SALK RP	ATGAGAATGCCAATCAACAGG	SALK
GBF1 ex4-Fwd	CCGTACCCAGCAATGTATCC	RT-PCR
GBF1 ex7-Rev	GTCAGCAAGCATCTGTCCAA	RT-PCR
GBF1 ex8-Fwd	TGGTCTTCCCAAGCTGGTGT	RT-PCR
GBF1 ex10-Rev	TTGTTCGCATTCGGCCT	RT-PCR
GBF1 ex11-Rev	CTTTCGACCCAGCAGCATTC	RT-PCR
seq pRBCS1a-800 Fwd	AAATATAGGGGTTTGCATGC	Sequencing
seq pRBCS1a-2000 Rev	CTTGTACCTTTTCCGTTG	Sequencing
seq 35S::MYC REV	CATCGCAAGACCGGCAACAGG	Sequencing
seq AttB1	CAAGTTTGTACAAAAAAGCAGGC	Sequencing
seq AttB2	GACCCAGCTTTCTTGTACAAAGTG	Sequencing
seq pDEST15/17 REV	CCAACTCAGCTTCCTTTCGGGC	Sequencing
seq pDEST17 FWD	GACCACAACGGTTTCCCTCTAG	Sequencing
seq pDEST15 FWD	TTTGCAGGGCTGGCAAC	Sequencing
seq SPN/SPC FWD	ATGCCATCATTGCGATAAAG	Sequencing
seq SPN REV	GTTTACGTCGCCGTCC	Sequencing
seq SPC REV	TGTACAGCTCGTCCATGC	Sequencing

seq M13 FWD	GTAAAACGACGGCCAG	Sequencing
Seq M13 REV	CAGGAAACAGCTATGAC	Sequencing

Table 3. Primers used in this thesis.

2.3.3 Site-directed mutagenesis

This method was used to introduce specific changes in DNA sequences. Reactions were performed with a commercial kit (Quick change II, Agilent) according to the manufacturer's instructions. Primers were designed keeping the mutated bases in the middle of the primer and both primers, forward and reverse, were complementary. The length of the primers was calculated so that they had a Tm>78 °C according to the following formula:

Tm= 81.5 + 0.41 x (% GC) - 675/N - % mismatch

2.3.4 Gene cloning

Two alternative cloning methods were used depending on the vectors available for the different experiments, either the "classic" cloning, based on restriction by endonucleases and subsequent ligation, or the Gateway cloning.

For the classical cloning inserts were obtained by PCR followed by endonuclease restriction or, directly, by restriction from previously cloned plasmids. Vector plasmids were correspondingly digested. Then, digested inserts and vectors were precipitated by adding ice-cold isopropanol in a 1:1 ratio and centrifuging at maximum speed for 5 minutes. Pellets were washed with 70% ethanol and resuspended in 20 µL of distilled and autoclaved H_2O in the case of the inserts, and 50 µL in the case of the plasmids. After determining the DNA concentrations of inserts and vectors with the Nanodrop, a 10 µL ligation reaction was prepared with a 1:5 molar ratio of vector:insert, calculated as:

Insert mass (ng) = 5 x Vector mass (ng) x Insert length (bp) / Vector length (bp)

Ligation reactions were incubated overnight at 4°C, and the day after, bacterial cells were transformed with a volume of the ligation reaction corresponding to approximately 100 ng DNA, and spread on a LBA plate with the corresponding antibiotic.

For the gateway cloning inserts were first cloned into the pENTR/D-TOPO vector and then transferred to the desired destination plasmids. Inserts were produced by PCR, containing the forward primers an additional CACC sequence at their 5' ends. PCR products were then purified by band excision after separation in agarose gel (Gene JET gel extraction kit, Thermo Scientific) and the TOPO cloning reactions were performed downscaling the manufacturer's protocol to a total volume of 2.5 µL with a 1:1 molar ratio of vector:insert, calculated as:

Insert mass (ng) = 10 x Insert length (bp) / 2580

Topo reactions were incubated for 1 hour at RT, and the whole reaction volume was transformed into bacterial cells, subsequently spread on a LBA plate with kanamycin.

Subcloning from Entry clones to pDEST vectors by LR recombination was performed according to the manufacturer's instructions and downscaling the reaction volume to 2 µL. The reaction was carried out for 1 hour at RT, and terminated by addition of Proteinase K. Then, the whole reaction volume was transformed into bacterial cells, which were spread on a LBA plate with the corresponding antibiotic.

The presence of the insert in the colonies was checked performing a colony PCR (using bacterial cells picked from a single colony as template, instead of isolated DNA) or a restriction reaction, and determining the size of the bands in an agarose gel by comparison with a DNA ladder (GeneRuler 1Kb Plus, Thermo Scientific). Samples with the expected pattern of bands were sent to sequencing and for the positive clones, an aliquot of the culture with 15 % v/v Glycerol was flash frozen with liquid nitrogen and stored at -80°C.

2.3.5 Gene accessions

Genes studied in this work are collected in Table 4.

ACT2	AT3G18780	*bZIP2*	AT2G18160	*bZIP9*	AT5G24800	*HyH*	AT3G17609
ASN1	AT3G47340	*bZIP25*	AT3G54620	*CAT2*	AT4G35090	*LHCB2.4*	AT3G27690
bZIP1	AT5G49450	*bZIP44*	AT1G75390	*GBF1*	AT4G36730	*PDH*	AT3G30775
bZIP10	AT4G02640	*bZIP53*	AT3G62420	*GBF2*	AT4G01120	*RBCS1a*	AT1G67090
bZIP11	AT4G34590	*bZIP63*	AT5G28770	*GBF3*	AT2G46270		
bZIP16	AT2G35530	*bZIP68*	AT1G32150	*Hy5*	AT5G11260		

Table 4. Accession numbers of the genes used in this work.

2.4 Work with proteins

2.4.1 Protein expression in bacteria

The expression of recombinant proteins was not performed according to a unique protocol, but the conditions were adapted to each protein. In every case, the bacterial stems used were BL21 derived (either BL21-SI or BL21-Rosetta) and all cultures were grown in LB medium with the appropriate antibody. The following are the common steps of the procedure.

First, a 10 mL pre-culture of fresh transformed cells was grown overnight at 37°C. The day after it was diluted in 100 mL of fresh medium and grown further at 37°C until an OD between 0.5-0.7 was reached. Then, protein expression was induced by adding IPTG to the culture. Optimal IPTG concentration and incubation time and temperature were determined specifically for each protein in an iterative manner. The expression parameters applied in this work ranged as follows: IPTG between 0.1 and 5 mM, temperature between 18 and 37°C, and incubation time between 4 hours and overnight. Default expression conditions initially tried were 1 mM IPTG, 30°C, and 4 hours.

After the induction, cells were harvested by centrifugation at 2500 g for 20 minutes, 4°C. The bacterial pellet was washed with Wash buffer and centrifuged again. The washed pellet was resuspended in the corresponding Lysis buffer and subsequently sonicated on ice with an EpiShear sonicator (Active Motif). Sonication conditions were not fix, because different induction conditions and cultures volumes were used. Usually, 3 to 6 pulses of

< 30% amplitude for 15-30 seconds were applied until the cloudy cell suspension became translucent. The sonicated solution was centrifuged in a table centrifuge at >16.000 g for 1 hour at 4°C. The supernatant was used for further experiments, while the pellet was used to check protein aggregation.

Wash buffer: 10 mM Tris-HCl, 100 mM NaCl, pH 7.5.

2.4.2 His-tagged protein purification

For this protocol, protein was extracted in 20 mL of His Extraction buffer. After sonication and centrifugation, recombinant protein in the supernatant were purified by gravity-flow. The supernatant was passed through a 1.5 mL of TALON metal affinity resin (Clontech) previously equilibrated with 20 mL of His-Extraction buffer. To maximize the binding, the collected flow through was passed again through the column. Then, the column was washed 4 times with 5 mL of Wash buffer 1, and other 4 times with 5 mL of Wash buffer 2. Finally, purified proteins were eluted with 0.75 mL (1 bed volume) of Elution buffer. The purification process was made at RT, but all buffers were kept on ice to prevent protein denaturalization. Aliquots were taken at each step to follow the purification procedure in a protein gel or Western blot.

Extraction buffer: 50 mM Tris pH 7.5, 150 mM NaCl, 5 mM Imidazol, 2.5 mM β-mercaptoethanol.

Wash buffer 1: 50 mM Tris pH 7.5, 150 mM NaCl, 30 mM Imidazol, 2.5 mM β-mercaptoethanol.

Wash buffer 2: 50 mM Tris pH 7.5, 150 mM NaCl, 60 mM Imidazol, 2.5 mM β-mercaptoethanol.

Elution Buffer: 50 mM Tris pH 7.5, 150 mM NaCl, 300 mM Imidazol, 2.5 mM β-mercaptoethanol.

2.4.3 Bradford protein quantification

The protein concentration in solutions was estimated by the Bradford method. 5 µL of the protein extract were diluted in 995 µL of 1x Protein Assay Dye Reagent (Bio-Rad) and incubated for 5 minutes at RT. Then, the absorbance was measured at 595 nm with a T70 UV/VIS spectrophotometer (PG Instruments, Figure 12) and the protein concentration was inferred from a calibration curve generated with measurements of BSA dilutions of known concentration.

Figure 12. The T70 UV/VIS spectrophotometer.

2.4.4 SDS-PAGE

Discontinuous SDS-PAGE was performed to separate proteins by their molecular weight. Gels were polymerized between two 10 x 10 cm glass plates separated by spacer strips and clamped together. The glasses were sealed with 1 mL of the Resolving gel mixture quickly polymerized by adding TEMED to a final concentration of 0.7 % v/v. Then, the Resolving gel mixture was added to the sealed gel chamber and, then, covered with isopropanol to exclude oxygen (which prevents the polymerization) and to create a flat interface between the gels. When the resolving gel was polymerized, the isopropanol was removed by inverting the gel and drying up the remains with filter paper. Finally, the Stacking gel mixture was added, and a comb was inserted on top of it (Figure 13). When the stacking gel was polymerized, the comb was removed and the gel was placed into the electrophoresis chamber and covered with Running buffer.

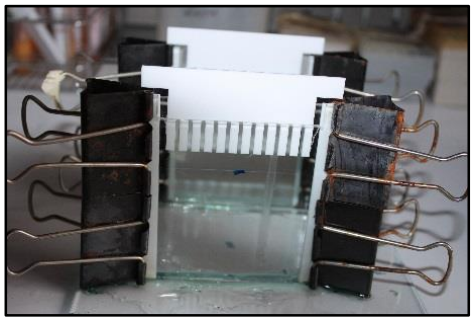

Figure 13. Casted SDS-polyacrylamide gel

Protein samples were mixed with the corresponding volume of 6x Sample buffer and denatured at 95°C for 5 minutes, then loaded into the gel. Along with the protein samples, 5 µL of a protein ladder (PageRuler Prestained, Thermo Scientific) were loaded to identify the approximate MWs of the protein bands. The gel was run at 100V until the blue dye front reached the bottom.

In order to visualize the protein bands after running, the gels were stained with Coomassie dye for at least 1 hour at RT with shaking, and then distained until the protein bands were visible.

Resolving gel mixture: 375 mM tris-HCl pH 8.8, 0.1 % SDS, 12 % acrylamide/bisacrylamide mix (Rotiphorese, Roth), 0.05 % APS, 0.07 % v/v TEMED, H_2O.

Stacking gel mixture: 125 mM tris-HCl pH 6.8, 0.1 % SDS, 4 % acrylamide/bisacrylamide mix (Rotiphorese, Roth), 0.05 % APS, 0.1 % v/v TEMED, H_2O.

6x Sample buffer: 375 mM tris pH 6.8, 0.6 M DTT, 12 % SDS, 60 % v/v glycerol, 0.06 % bromophenol blue.

Running buffer: 25 mM tris, 190 mM glycine, 0.1 % SDS.

Commassie staining solution: 25 % v/v Isopropanol, 65 % v/v Acetic acid, 0.25 % Coomassie Brilliant Blue (R-250).

Commassie distaining solution: 25 % v/v Isopropanol, 65 % v/v Acetic acid.

2.4.5 Western blot

Raw proteins extracts were used for the specific immunodetection of proteins. In the case of bacterial extracts an aliquot of the extract was used, keeping the rest for other experimental purposes. In the case of protoplasts, the protein extracts were performed ad hoc for the Western blot, pooling several transformation reactions together and following the protocol described for the GUS assays.

Proteins were first transferred to a PVDF membrane in a semi dry electroblotting system. 3 pieces of Whatman paper cut to the dimension of the gel and soaked in Towbin buffer were laid on the anode surface of the device. Next, the piece of membrane, soaked in 100 % ethanol, was laid on these, and then the gel previously washed in Towbin buffer. Finally, other 3 pieces of Whatman paper soaked in Towbin buffer were laid on top of the previous layers. The device was closed with the cathode-lid and transfer was carried on at 300 mA for 1 hour.

From this point, not a unique protocol was followed because the antibody dilutions, the composition of the buffers, and the incubation times depended on the antibodies used (Table 5). Usually, the protocol went on as follows. After the transfer, the membrane was washed in Towbin buffer and then blocked in 5 % non-fat milk powder TBS-T for 1 hour at RT with shaking. Then, the membrane was washed 3 times in TBS-T for 5 minutes at RT and incubated with the primary antibody diluted 1:500-1:5000 in 1.5 % non-fat milk powder TBS-T for at least 1 hour at RT or overnight at 4°C, with shaking. Next, the membrane was washed 3 times in TBS-T for 5 minutes at RT and then incubated with the secondary antibody when required, or it was proceeded directly to the detection step in the case of conjugated primary antibodies. The incubation with the conjugated secondary antibody was always performed at RT for 1 hour, and the antibody was usually diluted between 1:7000 and 1:10000 in 1.5 % non-fat milk powder TBS-T. Finally, the membrane was washed 3 times in TBS-T for 5 minutes and a fourth time with TBS. Then, the detection reaction was carried out.

Target	Source	Type	Company
HA-Tag	Mouse	1ary	Cell Signalling
Myc-TAG	Rabbit	1ary	Cell Signalling
Mouse IgG	Goat	AP conjugate	Bio-Rad
Rabbit IgG	Goat	AP conjugate	Jackson IR
His-Tag	Mouse	HRP Conjugate	Qiagen

Table 5. Antibodies used in this work.

Peroxidase-conjugated antibodies were detected by enhanced chemiluminescence (ECL). The working solution containing the peroxidase luminescent substrate was prepared just before using by mixing equal parts of the Peroxide Solution and the Lumino Enhancer Solution (ECL Western Blotting Substrate, Pierce), and the light produced was collected in a photographic film.

Alkaline-phosphatase conjugated antibodies were detected by a chromogenic reaction. The membrane was first equilibrated with the detection buffer for 10 minutes at RT with shaking, and then, incubated in detection buffer containing 2% v/v of NBT/BCIP Stock Solution (Roche), in the dark at RT and without shaking. The reaction was stopped with water when a brown precipitate was observed on the bands where the alkaline-phosphatase was located.

Towbin buffer: 25mM Tris, 192mM Glycine, 20% ethanol.

TBS: 50 mM Tris, 150 mM NaCl, pH 7.5.

TBS-T: 50 mM Tris, 150 mM NaCl, 0.1 % Tween-20, pH 7.5.

Detection buffer: 10 mM NaCl, 10 mM Tris, 5 mM $MgCl_2$, 0.1% Tween-20, pH 9.5.

2.4.6 DPI-ELISA

DNA-protein interactions were characterized by DPI-ELISA (Brand et al., 2010). For this method, His-tagged recombinant proteins (preys) were expressed in bacteria and extracted in Protein binding buffer complemented with proteinase inhibitors. The DNA double strand oligonucleotides (baits) were prepared in advanced by hybridizing the two complementary primers, corresponding to the cis-element to be analyzed. For that, the two primers were diluted in TE buffer to a final concentration of 2 pmol/µL and heated at 95°C for 5 minutes in a thermoblock. The device was then switched off and the dilutions were let cool down inside overnight.

ELISA experiments were carried out in 96 well transparent plates with streptavidin covalently bound to their surface (Immobilizer streptavidin F96 clear, Nunc). First, the biotinylated primers were bound to the streptavidin molecules coating the wells. To each well, 60 µL of the primer mix solution diluted 1:59 in TBS-T were added to each well and the plate was incubated 30 minutes at 37°C with gentle shaking. After that, residual binding spots were blocked with 60 µL of 2.7 % ELISA Blocking Buffer (Roche), incubating the plate for 30 min at RT with shaking. Next, wells were washed 3 times with 80 µL of Protein binding buffer for 10 minutes at RT with shaking prior to the protein binding step. For that, 60 µL of protein extract were added to each well and the plate was incubated at RT for 1 hour with shaking. Usually, 1:50, 1:100, and 1:200 dilutions (in Protein binding buffer) were tested. After the protein binding, wells were washed twice with 80 µL of Qiagen blocking buffer for 10 minutes at RT with shaking. Then, 60 µL of the antibody-containing solution were added to each well and the plate was incubated for 1 hour at RT with shaking. The antibody used was a HRP-conjugated anti-His diluted 1:1500 in Qiagen blocking buffer (Penta-His HRP antibody, Qiagen). After the antibody incubation, the wells were washed 2 times with 80 µL of TBS-T for 10 minutes at RT with shaking, and finally a chromogenic reaction was performed to reveal the presence of bound antibody. For that, wells were incubated with 60 µL of the ODP-solution and incubated in the dark with no shaking until an orange-yellow colored was formed, and the reaction was stopped by the addition of 60 µL of 0.5 M H_2SO_4. Color intensity was measured in a Tecan Sapphire plate reader (Figure 14) at 492 nm using 650 nm as a reference wavelength.

Protein binding buffer: 4 mM Hepes, 100 mM KCl, 0.2% BSA, 8% Glycerol, 5 mM DTT

TE buffer: 10 mM Tris-HCl, 1 mM EDTA, pH 8.0.

Qiagen blocking buffer: 0.5 % Qiagen Blocking reagent in Qiagen Blocking Solution

ODP-solution: 2 % ODP, 0.015 % v/v H_2O_2.

TBS-T: 50 mM Tris, 150 mM NaCl, 0.1 % Tween-20, pH 7.5.

Figure 14. The Tecan Sapphire plate reader used for the absorbance measurements.

2.4.7 *In vitro* kinase assay

In vitro protein phosphorylation was detected by the incorporation of radiolabeled ATP to the phosphorylated protein. Phosphorylable substrate proteins were expressed from pDEST42 vectors, KIN10 was expressed from pET28a and SnAK2 from pDEST15. All proteins were expressed in BL21-Rosetta cells (Novagen) and purified. The kinase assay was performed with 5 µg of purified protein substrates and 1 µg of purified kinases in a final volume of 20 µL in KIN10 Reaction buffer at 30°C for 1 hour. The reaction was then terminated by the addition of 4 µL of SDS-PAGE 6X Sample buffer and boiling the samples at 95°C for 5 minutes. Finally, SDS-PAGE was carried with 10 µL of each sample and the gel was developed by autoradiography.

KIN10 Reaction buffer: 200 mM HEPES pH 7.5, 150 mM $MgCl_2$, 1 mM DTT, 500 µM ATP, and ATP [γ-^{32}P] corresponding to 1 µCi.

2.5 Work with protoplasts

2.5.1 Protoplast isolation from Arabidopsis leaves

Protoplast isolation was performed based on a previous protocol (Sheen, 2002) with modifications. Protoplasts were isolated from 5 week-old plants using mature, fully developed but non-senescence leaves. Shallow cuts were done with a scalpel on the abaxial side of the leaves covering the whole leaf surface, and then they were laid with the cut sided facing down in a Petri dish (5,5cm ⌀) with 10 mL of Enzyme Solution. Enough leaves were prepared to cover the whole surface of the plate. Then, leaves were vacuum infiltrated for 3 hours at RT. The resulting green solution was transferred to a 50 mL Falcon tube and gentle mixed with an equal amount of W5 solution. The diluted protoplasts were filtered through a 200 µM pore nylon cloth into round-bottom tubes, and centrifuged at 80 g for 2 minutes. Most of the supernatant was removed by pipetting, and the remaining volume was washed twice with 10 mL of W5 solution, to be finally resuspended in 10 mL of W5 solution and incubated on ice for 1 hour, keeping the tube in vertical position. Before the ice incubation, an aliquot was taken to count the number of protoplasts in a hemocytometer. After the incubation period protoplasts had precipitated, and the supernatant was pipetted out. The remaining volume was adjusted with MMg Solution to a final concentration of 200,000 cells/mL.

Enzyme solution: 1.25% Cellulase, 0.3 % Macerozyme, 0.4 M Mannitol, 20 mM KCl, 20 mM MES pH 5.7, 10 mM $CaCl_2$. Sterile filtrated, fresh prepared.

MMg solution: 0.5 M Mannitol, 15 mM $MgCl_2$, 4 mM MES pH 5.7. Sterile filtrated, 4 °C.

2.5.2 PEG-mediated transformation of leaf-derived protoplasts

Transformation of green, leaf-derived protoplasts also included modifications respect the previous protocol established (Sheen, 2002). First, up to 20 µg of purified plasmid DNA were pipetted in round–bottom 2 mL micro-centrifuge tubes. Then, 100 µL of the protoplast suspension were gentle added to each tube and mixed by soft tapping. Next, 120 µL of the PEG Solution were slowly incorporated to the protoplasts and gentle mixed. After a 5 minutes incubation at RT, 450 µL of W5 solution were added and mixed by gentle inverting the tubes, which were then centrifuged at 60 g for 1 minute. 650µL of the supernatant were removed, and 450 µL of WI solution were added. The transformed protoplasts were incubate under long day photoperiod.

PEG solution: 40 % PEG 4000, 0.2 M Mannitol, 0.1 M $CaCl_2$. Sterile filtrated.

WI solution: 0.5 M Mannitol, 4 mM MES pH 5.7, 20 mM KCl. Sterile filtrated, 4 °C.

2.5.3 Protoplast isolation from Arabidopsis cell cultures

Protoplasts were generated from a 3-day-old Arabidopsis Col-0 dark-grown cell suspension culture derived from root tissue, maintained by the transformation facility of the ZMBP. 10 mL of the cell culture were centrifuged in round-bottom tubes at 400 g, for 5 min and washed with 10 mL of Cell Wall Digestion buffer without enzymes. Then, the cells were resuspended in 7 mL of Cell Wall Digestion buffer, dispensed into a petri-dish, and incubated for six hours at RT with gentle shaking in the dark. After that, the digested cells were transferred to round-bottom tubes and centrifuged at 100g for 5 min, then washed twice with W5 solution and finally resuspended in 10 mL of W5 solution. One aliquot was taken to determine the concentration, and the rest was kept at 4°C for 30 minutes. Finally, the protoplasts were centrifuged at 100 g for 5 min and the pellet was resuspended in the corresponding volume of MM solution to obtain the required concentration.

Cell Wall Digestion buffer: 1% cellulose, 0.25% macerozym, 8 mM $CaCl_2$, 0.4 M Mannitol, pH 5.5. Sterile filtrated, fresh prepared or frozen at -20 °C.

W5 solution: 154 mM NaCl, 125 mM $CaCl_2$, 5 mM KCl, 5mM Glucose, pH 5.8. Autoclaved.

MM solution: 5 mM MES, 0.4 M Mannitol, pH 6. Autoclaved.

2.5.4 Large-scale PEG-mediated transformation of cultured protoplasts

This type of transformation was carried out in round-bottom tubes and a protoplast solution of $1x10^6$ cells/mL. Up to 20 µg of purified plasmid DNA were added to 250 µl of the protoplast solution. Then, 250 µL of PEG solution were incorporated slowly, gently mixed, and incubated 15 min at RT. Next, 10 mL of W5 solution were added and the tubes were centrifuged at 100 g, 4°C for 5 minutes. The supernatant was removed by pipetting and the pellet was resuspended in 1.6 mL of K3 solution. The transformed protoplasts were incubated in the dark, overnight at 25°C.

PEG solution: 40 % PEG 4000, 0.4 M Mannitol, 0.1 M $Ca(NO_3)_2$, pH 8. Autoclaved and frozen aliquoted at -20°C.

W5 solution: 154 mM NaCl, 125 mM $CaCl_2$, 5 mM KCl, 5mM Glucose, pH 5.8. Autoclaved.

K3 solution: 10 ml macro stock solution (1.5 g $NaH_2PO_4 \bullet H_2O$, 9 g $CaCl_2 \bullet 2\ H_2O$, 25 g KNO_3, 2.5 g NH_4NO_3, 1.34 g $(NH_4)_2SO_4$, 2.5 g $MgSO_4 \bullet 7\ H_2O$, H_2O to 1 liter), 0.1 ml micro stock solution (75 mg KI, 300 mg H_3BO_3, 1 g $MnSO_4 \bullet 7\ H_2O$, • 200 mg $ZnSO_4 \bullet 7\ H_2O$, 25 mg $Na_2MoO_4 \bullet 2\ H_2O$, 2.5 mg $CuSO_4 \bullet 5\ H_2O$, 2.5 mg $CoCl_2 \bullet 6\ H_2O$, H_2O to 100 mL), 0.1 ml vitamins stock solution (100 mg Nicotinacid, 100 mg Pyridoxin•HCl, 1 g Thiamin•HCl, H_2O up to 100 mL), 0.5 ml EDTA stock solution (7.46 g EDTA dissolved in 300 ml H_2O, 5.56 g $Fe(II)SO_4 \bullet 7\ H_2O$ dissolved in 300 ml H_2O, H_2O up to 1 liter), 1 ml Ca-Phosphate stock solution (1.26 g $CaHPO_4 \bullet 2$ H2O dissolved in 200 mL of H_2O, pH 3), 10 mg Myo-Inositol, 25 mg D(+)-Xylose, 13.7 g Sucrose, pH 5.6. Sterile filtrated and frozen at -20°C in 10 ml aliquots.

2.5.5 Small-scale PEG-mediated transformation of cultured protoplasts

Protoplast transformation was carried out in a 96 well round-bottom 2 mL plates (Roth) according to the previously established protocol (Berendzen et al., 2012) using a Liquidator 96 Manual Pipetting system (Mettler Toledo, Figure 15). Cell cultured-derived protoplasts were sieved through a 70 µm filter, centrifuged at 50 g for 5 minutes at RT, and resuspended in MM buffer to adjust the concentration to $4x10^6$ cells/mL. Up to 10 µg of purified plasmid DNA were pipetted into each well with a standard 10 µL pipette. Then, 30 µL of the filtered protoplast suspension were gently dropped on the walls of the wells using a 12-channel 200 µL pipette with cut tips. The protoplasts drops were let fall down to the bottom of the wells by manually spinning the plate, and they were mixed by gently tapping the sides of the plate. Next, 30 µL of the PEG 1500 solution were added directly to the bottom of the wells with the Liquidator 96, mixed by tapping, and incubated at RT for 3 minutes. After that, 30 µL of the MM solution were pipetted to the bottom with the Liquidator 96 and mixed by tapping, followed by the addition of 250 µL of the K3 solution in an analogous manner. Finally, protoplasts were incubated overnight in the dark at RT.

PEG 1500 solution: 40% PEG 1500, 0.2 M Mannitol, 56 mM $Ca(NO_3)_2$, pH 6. Autoclaved and frozen aliquoted at -20°C.

MM solution: 5 mM MES, 0.4 M Mannitol, pH 6. Autoclaved.

K3 solution: 10 ml macro stock solution (1.5 g $NaH_2PO_4 \bullet H_2O$, 9 g $CaCl_2 \bullet 2\ H_2O$, 25 g KNO_3, 2.5 g NH_4NO_3, 1.34 g $(NH_4)_2SO_4$, 2.5 g $MgSO_4 \bullet 7\ H_2O$, H_2O to 1 liter), 0.1 ml micro stock solution (75 mg KI, 300 mg H_3BO_3, 1 g $MnSO_4 \bullet 7\ H_2O$, • 200 mg $ZnSO_4 \bullet 7\ H_2O$, 25 mg $Na_2MoO_4 \bullet 2\ H_2O$, 2.5 mg $CuSO_4 \bullet 5\ H_2O$, 2.5 mg $CoCl_2 \bullet 6\ H_2O$, H_2O to 100 mL), 0.1 ml vitamins stock solution (100 mg Nicotinacid, 100 mg Pyridoxin•HCl, 1 g Thiamin•HCl, H_2O up to 100 mL), 0.5 ml EDTA stock solution (7.46 g EDTA dissolved in 300 ml H_2O, 5.56 g $Fe(II)SO_4 \bullet 7\ H_2O$ dissolved in 300 ml H_2O, H_2O up to 1 liter), 1 ml Ca-Phosphate stock solution (1.26 g $CaHPO_4 \bullet 2$ H2O dissolved in 200 mL of H_2O, pH 3), 10 mg Myo-Inositol, 25 mg D(+)-Xylose, 13.7 g Sucrose, pH 5.6. Sterile filtrated and frozen at -20°C in 10 ml aliquots.

Figure 15. The Liquidator multi-pipetting system.

2.5.6 Protoplast two-Hybrid

Protein-protein interactions determined by this system were cloned in pHBTL-derived vectors and expressed in leaf-derived protoplasts. Protoplasts were transformed according to the protocol for the transformation of leaf-derived protoplasts downscaled to be performed in a 96 well round-bottom plate (Sarstedt) with 30 µL of

protoplasts in each well. Protoplasts were transformed with 2µg of each plasmid: the UAS::firefly luciferase plasmid, the 35S::renilla luciferase plasmid, the BD-fusion protein, and the AD-fusion protein. Transformed protoplasts were incubated overnight under long day conditions (16h/8h light/dark).

The day after, dual luciferase measurements were performed as described (Wehner et al., 2011). The supernatant was removed (protoplasts had precipitated) and then protoplast pellet was resuspended in 50 µL of 1x Passive Lysis Buffer (Promega), mixed by pipetting five times, and incubated on ice for 15 minutes. Then, the 96-well plates were centrifuged at 1000 g for 5 min, and the supernatant was transferred to a new plate. Luciferase measurements were performed with 10 µL of the protein extract and 50 µL of the corresponding Luciferase reagents (Promega) according to the manufacturer's specifications.

2.5.7 GUS assay in 1.5 mL Eppendorf tubes

Protoplasts were transformed, following the large-scale protocol, with 5 µg of each effector construct, 5 µg of the reporter construct, and 0.1 µg of the luciferase construct. The day after, 9 mL of Fall buffer were added slowly to each tube and they were centrifuged at 400 g for 5 min at RT. The supernatant was removed by pipetting and the remaining volume was transferred to a 1.5 mL Eppendorf tube and centrifuged 10 seconds at maximum speed in a table microcentrifuge. The supernatant was removed completely by pipetting and the pellet of protoplasts was dissolved in 100 µL of 1X Protein Extraction buffer. Protoplasts were grinded with a pestle and centrifuged at maximum speed for 10 minutes at 4°C. Then, the supernatant was transferred to a new 1.5 mL tube and kept on ice.

The GUS assay was performed according to previous description (Jefferson, 1987). 1.5 mL Eppendorf tubes were filled with 90 µL of the Assay buffer and heated at 37°C in a thermoblock. Then, 10 µL of the protein extract were added to each tube and mixed by quick vortexing. This was done for each tube independently with 15 seconds of difference between each sample and the next one. Samples were incubated for 30 minutes, and then stopped by adding 900 µL of 0.2 M Na_2CO_3 and quick vortexing. This was done in the same order in which the reactions were initiated, and keeping the 15 seconds time between samples. For each protein extract, three repetitions were performed, accounting for technical replicates. Besides, a blank control was prepared for each sample by adding the 10 µL of the protein extract to a 1.5 µL tube containing the 90 µL of the Assay buffer already mixed with the 900 µL of 0.2 M Na_2CO_3. Fluorescent measurements were performed with and excitation wavelength of 355 nm and measuring the emission at 460 nm in a Tristar LB941 96 well plate reader (Berthold) with a black 96 well flat-bottom plate containing 300 µL of the stopped reaction.

The luciferase assay was performed with 10 µL of the protein extract diluted in 100 µL of Luciferase Assay Reagent (Promega). Immediately after the mixing of the components, Light emission was measured for 10 seconds in the same Tristar LB941 96 well plate reader (Berthold) with a black 96 well flat-bottom plate. No repetitions of the luciferase measurement were performed. A blank measurement was performed using 10 µL of 1X Protein Extraction buffer.

Results were expressed as the quotient between the GUS activity and the light emission measurements, after removing the blank values and averaging the three GUS measurements replicates.

Fall buffer: 0.5 M Mannitol, 15 mM $MgCl_2$, 5 mM MES, pH 6.

1X Protein Extraction buffer: 1X Cell Culture Lysis Buffer (Promega), 1X cOmplete Tablets Proteinase Inhibitor without EDTA (Roche).

Assay buffer: 20 mM Na_2HPO_4, 20mM NaH_2PO_4, 10 mM EDTA, 10 mM β-mercaptoethanol, 0.1 % N-Lauroylsarcosine sodium salt, 0.1 % Triton X-100, 1 mM 4MUG, pH 7.

2.5.8 GUS assay in 96 well

Protoplasts were transformed following the small-scale protocol with 2 µg of the GUS construct, 2 µg of each effector construct, and 0.1 µg of the luciferase construct. The day after, 1.7 mL of Fall buffer were added slowly to each well with the Liquidator 96 and the plates were centrifuged at 400 g for 10 min at RT. The supernatant was pipetted out until approximately 50 µL were left without disturbing the protoplast pellet. The remaining volume (including the pellet) was mixed by pipetting up and down, and 50 µL were transferred to a 96 well 0.2 mL PCR plate containing 50 µL of 2X Protein Extraction buffer in each well, mixed again by pipetting, and incubated on ice for 30 minutes. After the incubation, the plates were centrifuged at 4000 g for 30 minutes at 4°C, and, 50 µL of the supernatant were transferred to a new 96 well 0.2 mL PCR plate and kept on ice.

The GUS assay was performed with 10 µL of the protein extract mixed with 90 µL of the GUS Reaction Buffer in a black 96 well flat-bottom plate. The reaction was incubated at 37°C, being continuously monitored as previously described (Fior et al., 2009) with an excitation wavelength of 355 nm and measuring emission at 460 nm in a 96 well plate reader (Tristar LB941 from Berthold, Figure 16) in black 96 well flat-bottom plates. No technical replicates were performed.

Luciferase activity was quantified for 10 µl of the protein extract in 50 µl of Luciferase Assay Reagent (Promega) and the emitted light was measured for 0.1 seconds. All measurements were done in the same Berthold 96 well plate reader and in black 96 well flat-bottom plates.

Results were expressed as the quotient between the slope calculated for the GUS activity during the 10 and the 30 minutes of reaction and the light emission measurements in the luciferase assay.

Fall buffer: 0.5 M Mannitol, 15 mM $MgCl_2$, 5 mM MES, pH 6.

2X Protein Extraction buffer: 2X Cell Culture Lysis Buffer (Promega), 2X cOmplete Tablets Proteinase Inhibitor without EDTA (Roche).

GUS Reaction buffer: 0.1 mM Tris, 2 mM $MgCl_2$, 2 mM 4-Methylumbelliferyl-β-D-glucuronide (Roth), pH 8.

Figure 16. Berthold plate reader used for fluorescence and luminescence measurements.

2.5.9 BIFC Assay

For the BiFC assay, the coding sequences of the proteins analyzed were cloned into the pSPYNE-35S/pUC-SPYNE and the pSPYCE-35S/pUC-SPYCE plasmids, the former carrying the N-terminal half of the YFP and the latter the C-terminal part (Walter et al., 2004). Assays were carried out in protoplasts transformed with either 10 µg of each plasmid in the large-scale transformation protocol, or 2 µg of each plasmid in the small-scale transformation protocol. Transformed protoplasts were incubated overnight in dark at RT, and analyzed the day after.

Flow cytometric measurements were performed with a MoFLo (2007, Beckman-Coulter, Figure 17). GFP and YFP were excited with a 50 mW 488 nm argon laser and fluorescence emission was detected by two different light channels at 510 – 550 nm and at 565 – 605 nm. Data were subsequently analyzed with FlowJo v10.0.7.

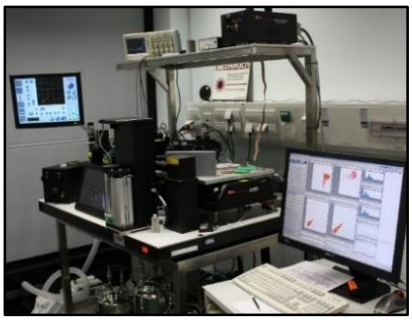

Figure 17. The MoFlo cell sorter used for the flow cytometric analyses.

2.5.10 Statistical data treatment

For the BiFC assay, the fluorescence level for each sample was calculated as the binomial count of the fluorescent events in regard to the total of the events recorded, what was referred as BiFC score. Then, an average BiFC score value was estimated for each combination tested with a generalized linear mixed model framework (GLMM) in SAS (McCullagh and Nelder, 1989). For that, protoplasts counts were treated as binomial random variables conditional on their means, which were modeled using the logit link in Proc GLIMMIX. The model included fixed effects for the fusion conformations on N-terminal fragment of the YFP (SPYCE), C-terminal of the YFP (SPYNE), and their interaction effect; and a random effect for each transformation batch (96 well plate). Besides, a normally distributed random effect was considered for each sample to account for overdispersion. For the fitting of the GLMMs, a pseudo-likelihood method with the variance function $\mu^{1.7}(1-\mu)^{1.7}$ was used, since the typical variance function for binomial distributions (i.e., $\mu(1-\mu)$) did not described appropriately the variability of the data. The hypotheses tests of interest were conducted using the contrast statement within Proc GLIMMIX, and the resulting *p*-values for each hypothesis test were adjusted to maintain the overall 5% Type I error rate using Tukey's adjustment method.

For the GUS assay, linear mixed models were fitted on GUS/LUC ratios for each of the four promoters analyzed. The models included a fixed effect for each bZIP combination and a random effect for each batch of measurements (plate), additionally they considered heterogeneous variance grouped by each bZIP. Hypothesis tests were conducted between each bZIP combination and the reference control, independently for each promoter, and adjusting the *p*-values according to the Dunnett's method for multiple comparisons (Dunnett, 1955).

2.5.11 Confocal microscopy

Both Leica confocal microscopes (CLSM Leica SP2 AOBS or CLSM Leica SP8 AOBS) available at the microscopy service of ZMBP served for images acquisition (Figure 18). Excitation wavelengths used were 488 nm for GFP, 514 nm for YFP, and 561 nm for mCherry. Images capturing and processing was done with the Leica LAS AF software.

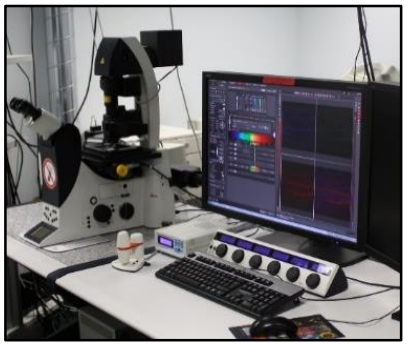

Figure 18. Leica SP8 used for confocal microscopy studies.

3. Results

Part 1: Post-transcriptional regulation of the GBF1 function

During the bolting time of Arabidopsis, there is a decrease in CAT2 activity, resulting in a peak in H_2O_2 that was proposed to serve as a signal to activate the senescence program (Zimmermann et al., 2006). GBF1 was identified as the transcriptional factor causing the repression of *CAT2* expression at the onset of senescence. Concomitantly, Arabidopsis *gbf1* mutant lines displayed neither the *CAT2* down-regulation nor the peak in the H_2O_2, and were described to be delayed in senescence (Smykowski et al., 2010). However, *GBF1* is constitutively expressed (Terzaghi et al., 1997; Jiao et al., 2007), and only a slight increase in its expression during senescence is indicated by the Genevestigator data (Figure 19). Therefore, the senescence-specific activation of GBF1 is expected to happen at the post-transcriptional level. In this part of my thesis I investigated whether the activity of GBF1 is regulated by mechanisms commonly found regulating the bZIP activity such as heterodimerization and phosphorylation.

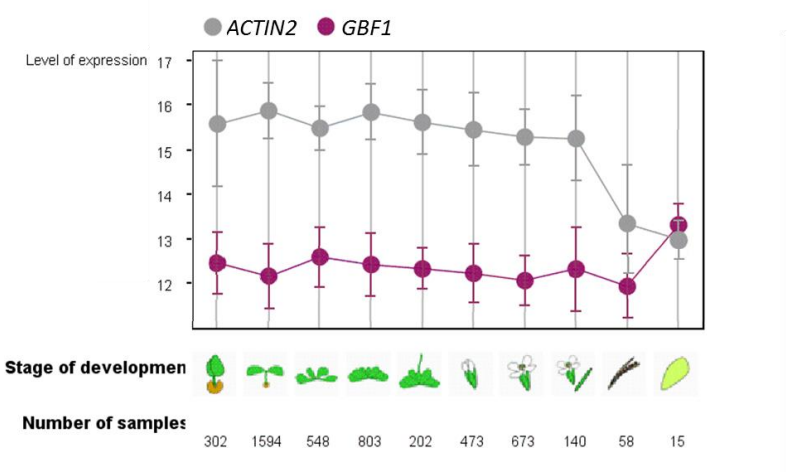

Figure 19. Expression level of *GBF1* and *ACTIN2* at different stages of the development. Data are calculated from Genevestigator. The picture was modified.

3.1 Regulation of GBF1 activity by heterodimerization

Because heterodimerization is considered to be a central mechanism regulating the activity of bZIP transcription factors, this was the first aspect analyzed as a possible mechanism modulating the senescence-specific activation of GBF1. Candidate bZIPs to be studied for interaction with GBF1 were selected based on preliminary data shared by partner research groups belonging to the Marie Curie Initial Training Network within which this work was elaborated (MERIT-ITN). Specifically, bZIP1, bZIP2, bZIP53, and bZIP63 were initially tested, as they were related to the LES, and transgenic lines for those bZIPs exhibited growth alterations.

3.1.1 Interaction between GBF1 and candidate bZIP partners from the C and S1 classes

Heterodimerization between GBF1 and the other four bZIPs was assayed by Bimolecular Fluorescent Complementation (BiFC). In this method for protein-protein interaction detection, proteins in study are expressed *in vivo* fused to a non-fluorescent fragment of a fluorescent protein, and if the studied proteins interact, the two complementary fluorescent fragments are brought close enough to permit the reconstitution of the fluorescent protein (Kerppola, 2008). In other words, if there is interaction, fluorescence can be detected (Figure 20). For this work, I used a split Yellow Fluorescent Protein (YFP)-based system (Walter et al., 2004), and the two resulting fusion proteins conformations were named SPC, the fusions to the C-terminal fragment of YPF, or SPN, the fusions to the N-terminal fragment.

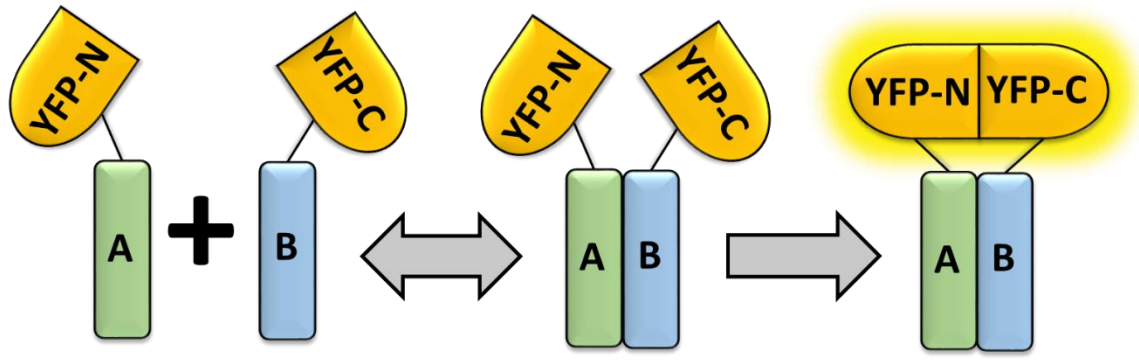

Figure 20. Schematic representation of the BiFC. The re-association of the YFP fragments (YFP-N and YFP-C for the N-terminal fragment and the C-terminal fragment, respectively) is driven by the interaction of the two proteins studied (here A and B). Note that after the reconstitution of the YFP, the BiFC complex remains irreversibly bound.

Although the reconstitution of fluorescent proteins does not require a specific relative orientation of the fusion proteins, particular arrangements of the fusion proteins can result in non-functional proteins which are unable to interact or in topological constraints that preclude the association of the fragments. Therefore, it is advised to test each protein in both fusion conformations (Kerppola, 2008). Accordingly, I tested each bZIP as a SPN- and SPC-fusion, independently.

The BiFC assay was performed in transiently transformed Arabidopsis protoplasts, and fluorescence production was measured by flow cytometric analysis, as it provides a quantitative approach that improves the discrimination of the false positives (Morell et al., 2008; Horstman et al., 2014). For each combination of two bZIPs tested at least three biological replicates were analyzed, each one with a minimum of 30,000 cells screened. Then, a double gating of the acquired flow cytometric data was performed by plotting the results in a two parameters graph. The first gating was based on the logarithmical representation of forward scatter (FSC) versus side scatter (SSC) to identify the viable protoplasts, as often cellular debris have lower FSC, and dead cells higher SSC than living cells. For the second gating, data were plotted as the emitted light measured by the 510 – 550 nm and the 565 – 605 nm channels (also in logarithmic scale), what allows the identification of the YFP fluorescence. Fluorescent cells are defined based on the emergence of a new distinct population in comparison with a negative control (Figure 21).

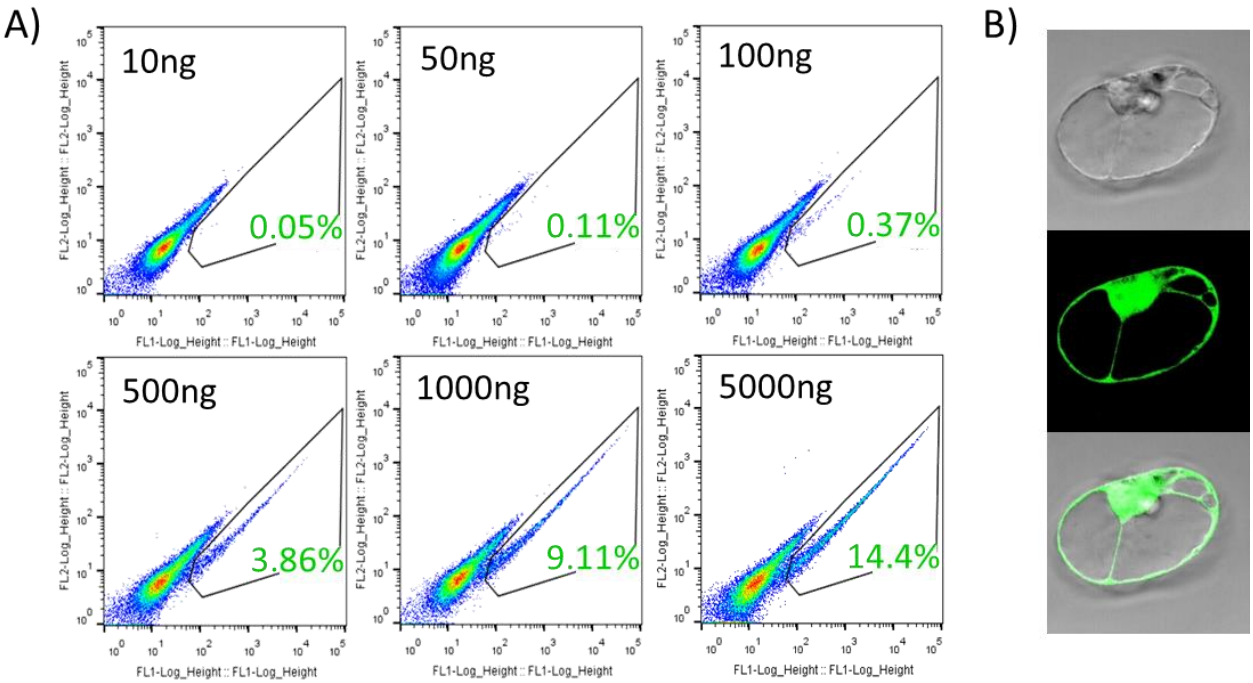

Figure 21. Control protoplasts expressing a GFP under control of a CaMV 35S promoter. A) Flow cytometric outputs displaying how the fluorescent population (framed dots, indicating the percentage respect of the total cells in green digits) increases with the amount of plasmid transformed, which is indicated at the top of each representation. B) Confocal microscopy visualization of transformed protoplasts. From top to bottom the pictures correspond to the transmitted light, the GFP channel, and the merged images.

For those experiments, the GBF1 homodimer was considered as a positive control, since GBF1 homodimer formation was already identified (Schindler et al., 1992a), and combinations with the empty plasmids coding for the fluorescent fragments were used as negative controls. Flow cytometric parameters of interest were the fraction of fluorescent cells (%), the mean fluorescence intensity of the fluorescent fraction, and the product of both, known as Fluorescent Index (FI) (Li et al., 2010b).

The results presented bZIP63 as the only candidate tested that led to clear fluorescence production in combination with GBF1, although that happened only in the bZIP63-SPN fusion conformation (Figure 22). There was an abrupt contrast between the results obtained with the two alternative configurations of bZIP63 (i.e. bZIP63-SPC and bZIP63-SPN), indicating that in one of them the fluorescence production was either enhanced or diminished. It was, however, not possible to distinguish between these two possibilities with the data available. As for the other bZIP candidates tested, they resulted in weak fluorescence production, so that they were considered as negative results.

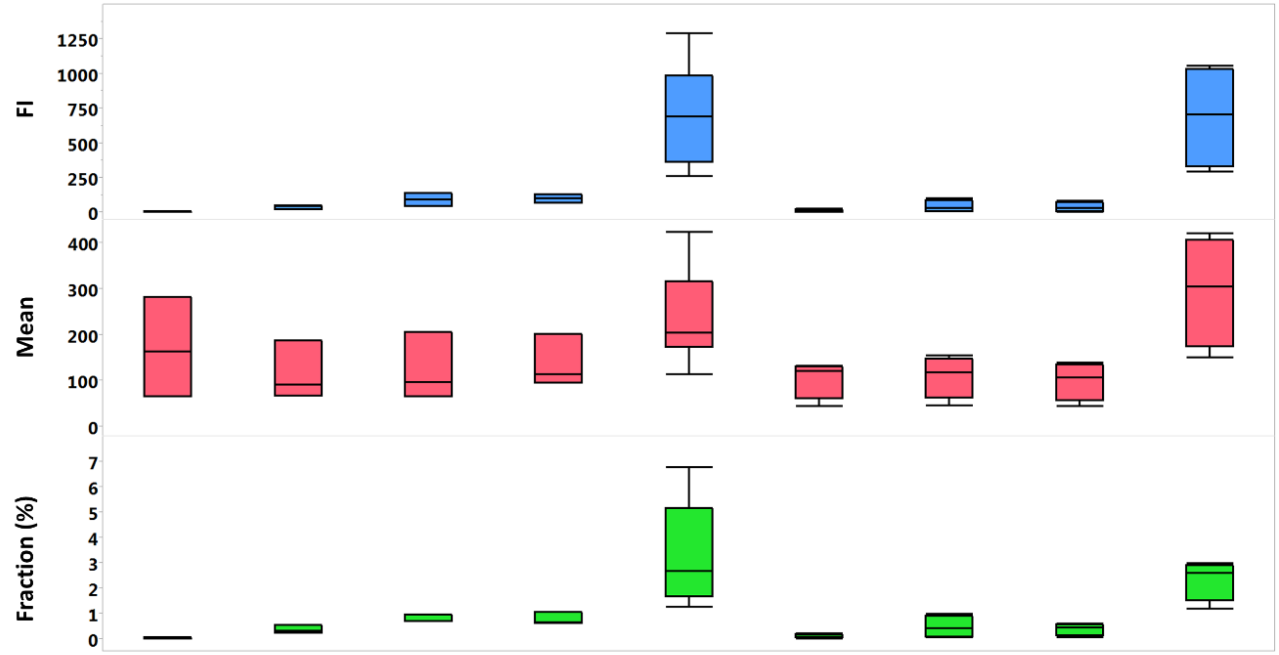

SPN	GBF1	GBF1	GBF1	GBF1	GBF1	bZIP1	bZIP2	bZIP53	bZIP63
SPC	bZIP1	bZIP2	bZIP53	bZIP63	GBF1	GBF1	GBF1	GBF1	GBF1
%	0.01	0.35	0.76	0.76	3.21	0.11	0.45	0.36	2.32
Mean	169.59	114.50	121.87	136.54	232.40	123.74	108.67	99.15	294.89
FI	3.03	36.70	90.66	98.17	676.52	13.34	41.07	36.94	687.10
n	3	3	3	3	12	4	4	4	4

Figure 22. BiFC results for interactions between GBF1 and the candidate dimerization partners. Represented are box plots showing the different parameters analyzed: the fraction of fluorescent cells respect the total population, their mean fluorescent intensity, and the corresponding FI. Calculated average values are indicated below, along with the number of repetitions (n). Only the GBF1 homodimer and the combination of bZIP63-SPN and GBF1-SPC result in apparent fluorescence production.

3.1.2 Confirmation of the GBF1/bZIP63 interaction

In order to exclude that the fluorescence observed in the combinations involving GBF1 and bZIP63 was a product of the self-assembly of the fluorescent fragments, negative controls were performed. GBF1 and bZIP63 split YFP fusion proteins were expressed in protoplasts in combination with the complementary YFP fragment alone (with no bZIP fused) and were analyzed normally. The BiFC measurements performed showed that no self-assembly occurred in any of the two GBF1 fusion proteins, and only a weak, unspecific signal was detected for bZIP63-SPC (Table 6). Therefore, it was confirmed that the strong signals detected in the GBF1 homodimer and GBF1-SPC/bZIP63-SPN combinations were not a product of the self-assembly of the fluorescent fragments, but they were dependent on the presence of the two bZIPs analyzed.

SPN	Emtpy	Emtpy	Emtpy	GBF1	bZIP63
SPC	GBF1	bZIP63	Emtpy	Emtpy	Emtpy
%	0.01	0.24	0	0	0.03
Mean	117.04	286.36	65.17	44.06	105.08
FI	1.17	53.51	0	0	2.94
n	1	2	1	2	2

Table 6. BiFC results for the negative controls. Indicated are the average values for the fluorescent fraction, the mean fluorescence intensity, and the resulting FI, as well as the number of repetitions (n). None combination produces a significant fluorescence signal.

To verify that the observed interactions resulted from the actual dimerization of the bZIPs, this is to say mediated by their LZ motifs, the GBF1 protein was split in two parts at the link between the BR and the LZ motif. The N-terminal fragment (GBF1-NtF) included the first 243 amino acids without the LZ, while the C-terminal fragment (GBF1-CtF) comprised the remaining 73 amino acids including the LZ motif (Figure 23).

Figure 23. GBF1 truncates forms analyzed. The leucine zipper dimerization domain (LZ) is included in GBF1-CtF, but not in GBF1-NtF. BR is the basic domain and PRD is a Proline rich domain located at the N-terminus of GBF1.

When the full length GBF1-SPN was tested with the truncated versions SPC fused, noticeable differences in the measured fluorescence arouse congruently with the role of the LZ in the dimerization. The combination with GBF1-CtF-SPC (which includes the LZ) resulted in a comparable fluorescence production than the native GBF1 homodimer combination, whereas the combination with GBF1-NtF-SPC (with no LZ) led to much lower measurements (Figure 24). However, in the reciprocal combinations (i.e. native GBF1-SPC combined with the truncated versions expressed as SPN fusions), a sharp decrease in the fluorescence occurred for both truncate forms in comparison to the native form, independently of the presence of the LZ motif. Still, the GBF1-CtF truncate resulted in higher fluorescent production than the GBF1-NtF. Therefore, those results suggested that the GBF1 homodimer formation was indeed mediated by the interaction of the leucine zipper motifs, while the decreased fluorescence detected in the GBF1-CtF-SPN/ GBF1-SPC combination was considered to be an artifact product of the truncation.

Regarding the measurements with bZIP63, the reciprocal combinations resulted totally inconsistent. On the one hand, bZIP63-SPN combinations resulted in fluorescence production independently of the presence of the LZ in the GBF1 truncate, yet the combination with GBF1-NtF-SPC (with no LZ) displayed much lower fluorescent than the combination with GBF1-CtF-SPC (with LZ). On the other hand, combinations with bZIP63-SPC led to almost no fluorescence. Therefore, these results failed to provide evidence to confirm that the interaction between GBF1 and bZIP63 was actually mediated by their LZ motifs. Instead, they suggested that either bZIP63-SPN resulted in unspecific fluorescence production or that the GBF1-SPC/bZIP63-SPN interaction was not mediated by the LZ, since the combination with GBF1-NtF-SPC resulted in clearly quantifiable fluorescence in spite of the absence of the LZ motif in that truncate.

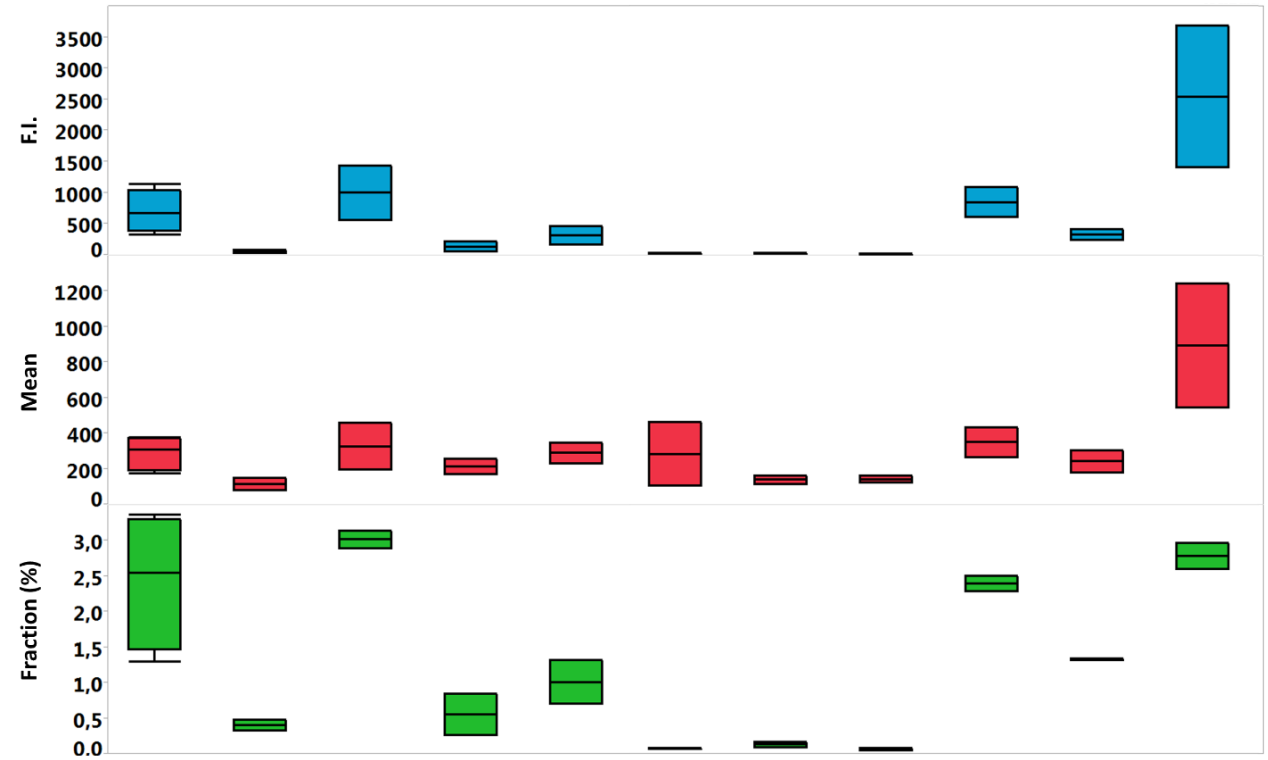

SPN	GBF1	GBF1	GBF1	GBF1-NtF	GBF1-CtF	GBF1	GBF1-NtF	GBF1-CtF	bZIP63	bZIP63	bZIP63
SPC	GBF1	GBF1-NtF	GBF1-CtF	GBF1	GBF1	bZIP63	bZIP63	bZIP63	GBF1	GBF1-NtF	GBF1-CtF
%	2.43	0.39	3.01	0.55	1	0.07	0.12	0.05	2.39	1.32	2.78
Mean	289.54	110.99	323.92	211.09	287.38	282.00	13588	139.64	348.42	240.51	891.33
FI	692.22	46.5	990.85	128.90	306.80	17.97	17.76	7.96	841.97	318.1	2540.94
n	4	2	2	2	2	2	2	2	2	2	2

Figure 24. BiFC results for the GBF1 truncate versions. The LZ dimerization motif was included in the GBF1-CtF truncate, but not in the GBF1-NtF. As previously, the fluorescent fraction, the fluorescence intensity, and the FI are represented in a box plot style and the actual values and the number of repetitions is indicated below.

3.1.3 Subcellular localization of the GBF1 and bZIP63 proteins

Since bZIPs are transcription factors, they must be in the nucleus to exert their function and, therefore, an eventual modulation of the GBF1 activity through dimerization with bZIP63 would be required to happen in the nucleus. In order to evaluate such possibility, the subcellular localization of the BiFC complexes was determined by confocal microscopy. The two positive interactions identified -the GBF1 homodimer and the bZIP63-SPN/GBF1-SPC heterodimer- were found to be nuclear (Figure 25). Significantly, no fluorescent signal was detected in the cytoplasm, indicating that none of those interactions took place outside of the nucleus.

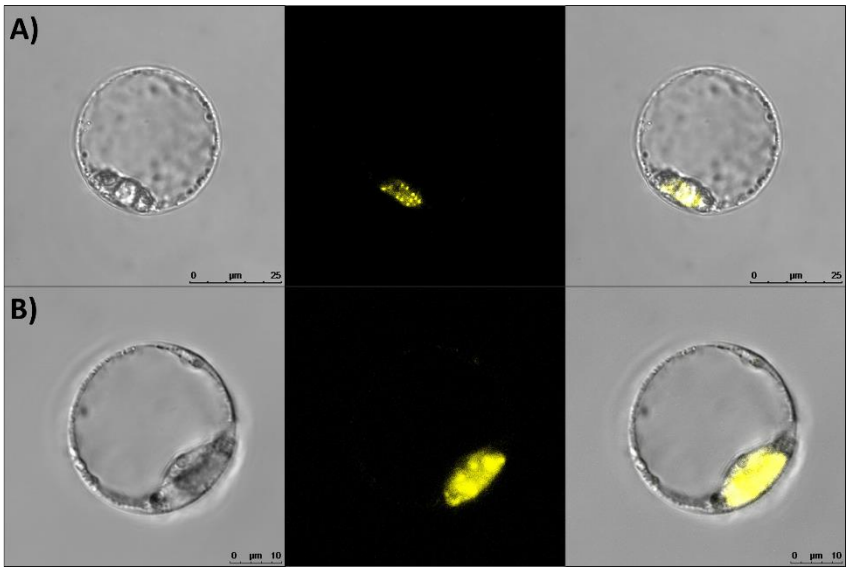

Figure 25. Subcellular localization of the BiFC complexes. A) GBF1-SPN/GBF1-SPC. B) bZIP63-SPN/GBF1-SPC. From left to right, images correspond to: transmitted light, YFP fluorescence, and merged images.

In addition, the observation of the GBF1-SPN/GBF1-SPC sample also revealed that the fluorescence emission was consistently localized in punctate structures, which are known as nuclear speckles. The formation of nuclear speckles in plants has been associated to light signaling (Van Buskirk et al., 2012), and GBF1 function has been related to UV and blue light signaling (Jakoby et al., 2002). Remarkably, the formation of nuclear speckles disappeared in the bZIP63-SPN/GBF1-SPC combination, indicating that they were an exclusive feature of the GBF1 homodimer.

Intriguingly, GBF1 was previously reported to be mostly cytoplasmic (Terzaghi et al., 1997), but, in my observations, the BiFC complex for the GBF1 homodimer appeared exclusively in the nucleus. I considered whether the absence of GBF1 in the cytoplasm could be an artifact due to the formation of the BiFC complex (for instance, it could trap the proteins in the nucleus). In order to rule out that possibility, GBF1 was expressed in protoplasts as a fusion to the full-length GFP, and likewise, bZIP63 was expressed as an YFP fusion, for the bZIP63-YFP construct was already available. For both proteins, I could verify that their localization was exclusively nuclear (Figure 26).

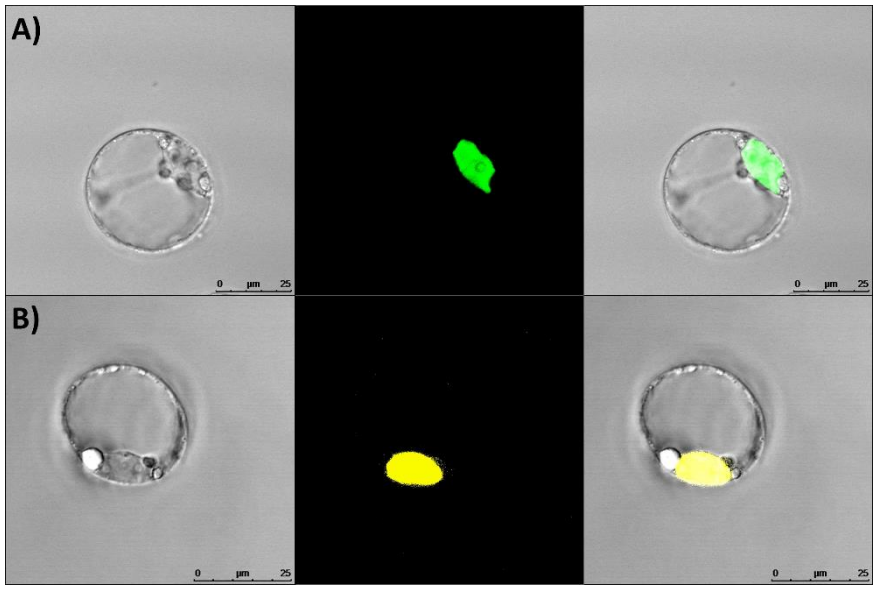

Figure 26. Subcellular localization of full-length fluorescent protein fusions. A) GBF1-GFP B) bZIP63-YFP. From left to right images correspond to: transmitted light, GFP or YFP channel, and merged images.

Still, because the subcellular localization of parsley bZIP G-box binding factors was previously reported to change in response to different light conditions (Harter et al., 1994; Kircher et al., 1999), I considered whether the fact that the protoplasts used in that experiment had been incubated in the dark after the transformation could be the reason for the nuclear localization of GBF1. So, I repeated the observations varying the light conditions. Specifically, protoplasts were incubated in blue (473 ± 10 nm), red (670 ± 10 nm), and far-red (740 ± 10 nm) light conditions after being transformed with the GBF1-GFP construct. For that experiment, an NLS::mCherry protein was co-expressed as a nuclear marker. Once more, fluorescence was confined exclusively to the nucleus in all light conditions tested (Figure 27), indicating that GBF1 localization was not affected by the different light conditions. However, I noticed that the speckle formation was found only in protoplasts incubated under blue light, but not under red and far-red conditions, suggesting that their formation was prevented by the red and far-red conditions. Notwithstanding, these observations were not further confirmed.

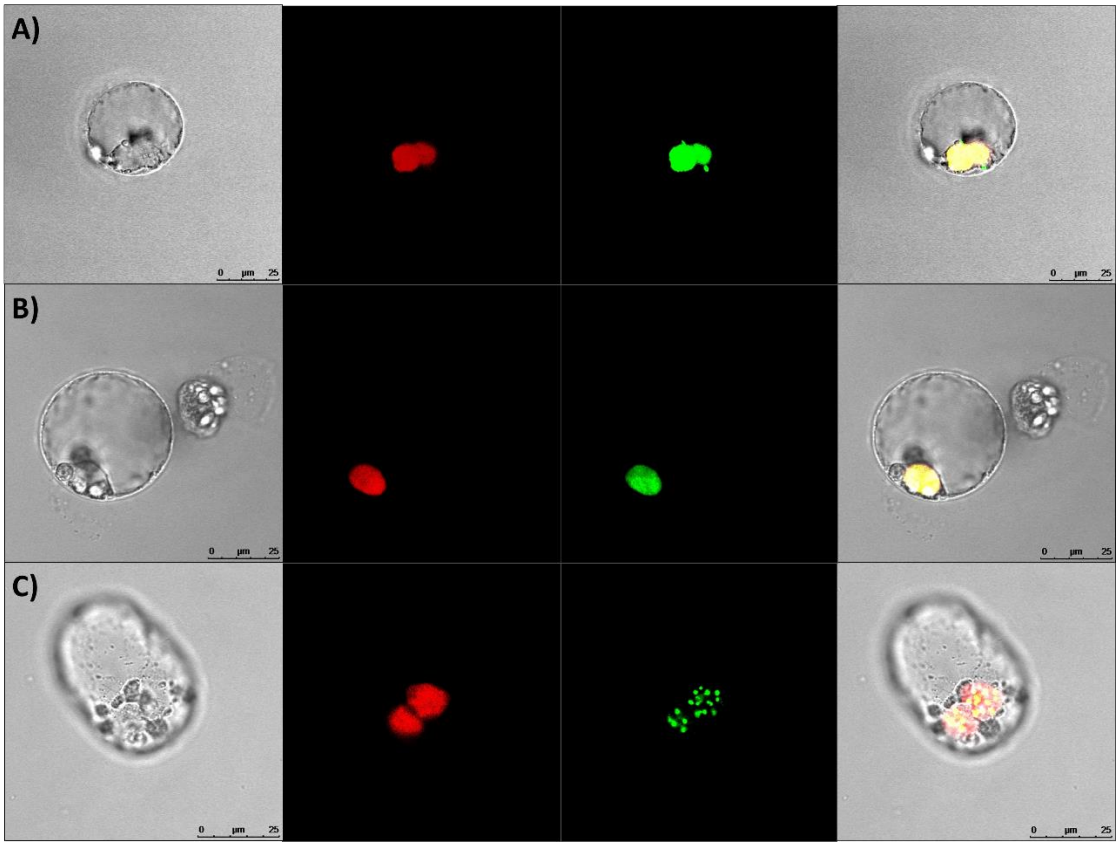

Figure 27. GBF1-GFP localization under different light conditions: A) far red, B) red, and C) blue light. A mCherry-NLS plasmid was co-transformed for nuclear staining. From left to right images correspond to: transmitted light, mCherry signal, GFP signal, and merged images.

Finally, I wanted to exclude the possibility that the different GBF1 localization were due to the different conditions used prior to the protoplast isolation, since the cytoplasmic detection of GBF1 was reported in soybean cells cultured under long day conditions (Terzaghi et al., 1997). The observation was repeated again using protoplasts isolated from green leaves, instead of the usual dark-grown cell culture. Protoplasts were isolated from Arabidopsis leaves of 5-week old plants grown under long-day conditions and maintained under the same light conditions after the transformation. However, neither those conditions stimulated a shift in the fluorescence localization, which was only detected in the nucleus for both proteins, GBF1 and bZIP63 (Figure

28). Thus, I concluded that, in Arabidopsis cells, GBF1 and bZIP63 were exclusively located in the nucleus, in opposition to the previous observations made by Terzaghi et al. in alternative protoplast systems.

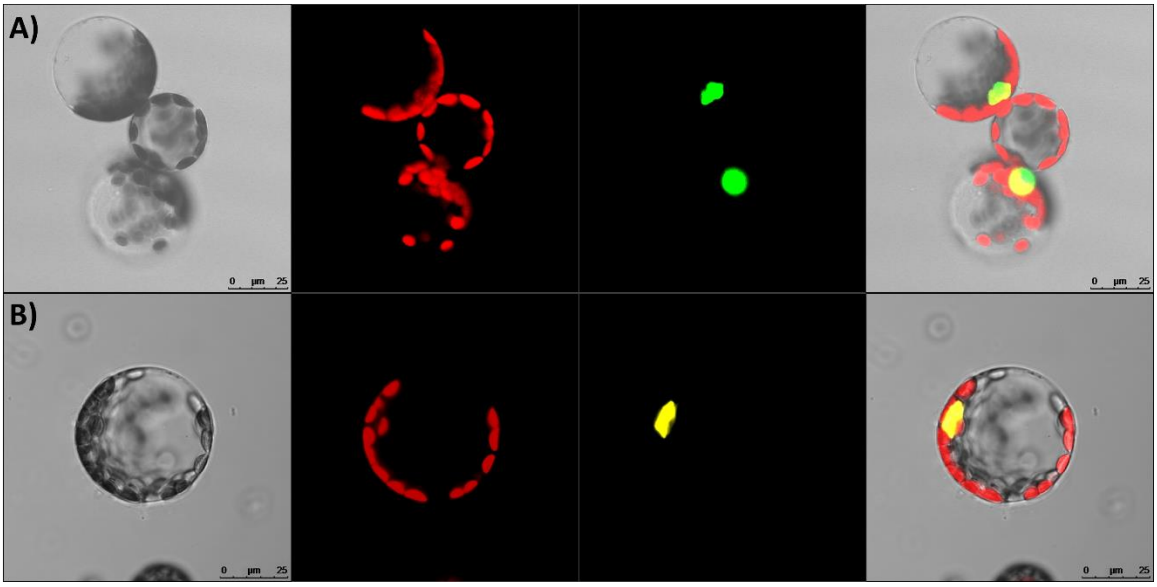

Figure 28. Subcellular localization in leaf-derived protoplasts grown under long-day light conditions. A) and B) GBF1-GFP. C) and D) bZIP63-YFP. From left to right images correspond to: transmitted light, autofluorescence, GFP or YFP channel, and merged images. The GBF1 speckle formation in A) disappears when high fluorescent intensities are used in B), but no speckles are observed for bZIP63-YFP even at low intensities.

3.1.4 Screening for further GBF1 bZIP interacting partners

Further GBF1 interacting bZIP candidates were tested by protoplast two-hybrid (P2H) system, since a partner laboratory of our research network had 57 of the 75 Arabidopsis bZIPs available to be tested in that system. Roughly, the P2H system is based on the yeast GAL4 two-hybrid system but it is carried out in plant protoplasts (Ehlert et al., 2006). The two proteins to be analyzed for interaction are expressed either fused to GAL4 Binding Domain (BD) or to the GAL4 Activation Domain (AD), and the expression of a firefly luciferase reporter gene is driven by the yeast upstream activating sequence (UAS) fused in front of it (Figure 29). Besides, the renilla luciferase protein is co-expressed from a CaMV 35S promoter for normalization.

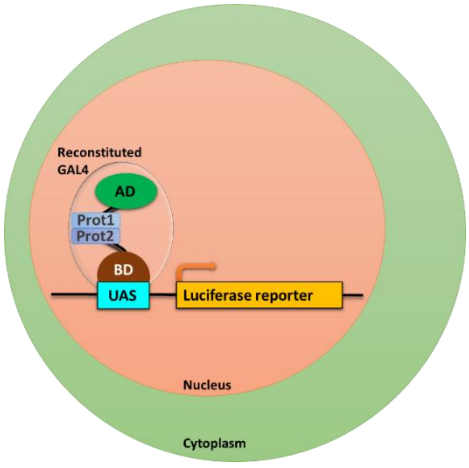

Figure 29. Representation of the P2H system for the analysis of promoter activity. If the two proteins interact (Prot1 and Prot2) the GAL4 transcription factor is reconstituted and promotes the gene expression driven by the presence of the UAS. AD and BD are the GAL4 Activation and DNA binding domains, respectively.

The experiment was performed in the laboratory of Prof. Dr. Dröge-Laser at the University of Würzburg, Germany, and in collaboration with Lorenzo Pedrotti. GBF1 was expressed fused to the BD, and tested for interaction with each of the other 57 bZIPs which were expressed as fusions to the AD. Expression of GBF1-BD alone was tested as control for autoactivation.

Most of the bZIP tested resulted in measurements comparable to the control, meaning that no interaction occurred (Figure 30). Conversely, few of them produced strong signals, evidencing interaction with GBF1. The strongest ones were produced in the combinations with bZIP24-BD and bZIP21-BD, with signal increases of 7.6 and 5.4 fold compared to GBF1-AD alone, respectively. After those two, only bZIP30-BD, bZIP42-BD, and bZIP70-BD exhibited increases greater than 3 fold. These five bZIPs were, thus, the main GBF1 interacting candidates. Nevertheless, those results were striking, for none of the already reported GBF1 interactors resulted in meaningful signals. Specifically, these are bZIP16, bZIP68, bZIP54 (GBF2), bZIP55 (GBF3), bZIP56 (Hy5), bZIP64 (HyH), as well as GBF1 itself (bZIP41) (Schindler et al., 1992a; Shen et al., 2008; Singh et al., 2012). Although, it is known that protein-protein interactions depend on the conditions assayed, and that complementation assays can be influenced by the conformation of the fusion protein, the high number of discrepant results obtained casted doubts on the validity of these results. Hence, no further work was performed with that system, neither were those five interacting candidates validated by other methods.

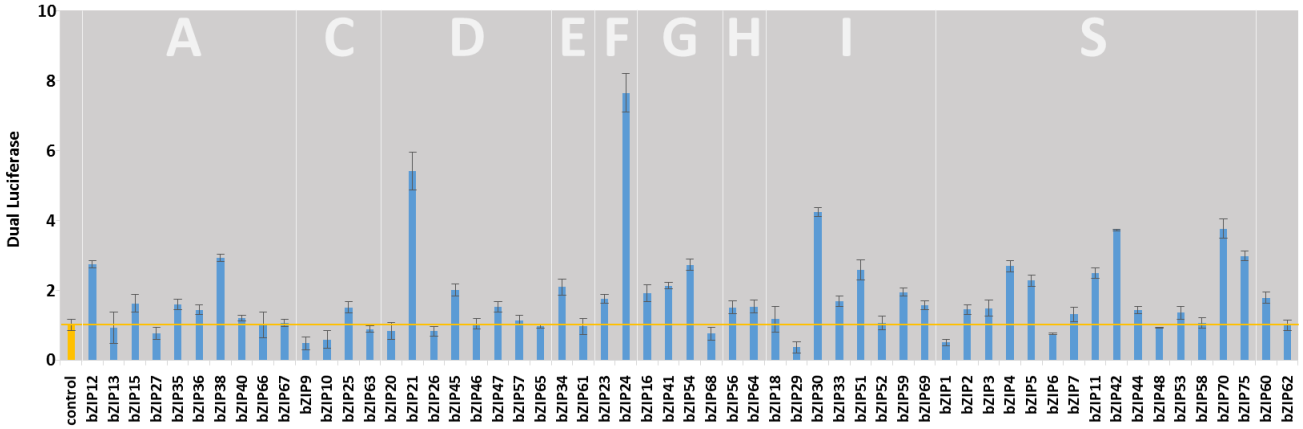

Figure 30. Heterodimerization of GBF1 and other Arabidopsis bZIPS. Values indicate relative dual luciferase measurements averaged for three biological replicates. Error bars are standard deviation. bZIPs are ordered according to their group classification in letters, which are indicated on the top (Jakoby et al., 2002). Yellow bar represents the base line of the autoactivation control.

3.1.5 Effect of bZIP63 on the GBF1 DNA binding activity

Because each bZIP monomer recognizes one half of the cis-element, bZIP dimerization ultimately determines the affinity of the DNA binding (Llorca et al., 2014). Therefore, I examined whether the DNA binding properties of GBF1 were altered in the presence of bZIP63 by performing a **D**NA-**p**rotein **i**nteraction **e**nzyme-**l**inked **i**mmuno**s**orbent **a**ssay (DPI-ELISA). In this method, DNA probes comprising the cis-element under investigation are used as baits, while the candidate DNA interacting proteins are the preys. The DNA probes are biotinylated double stranded oligonucleotides, which are first attached to a streptavidin-coated 96 well plates. The plates are then incubated with crude bacterial extracts containing the recombinant proteins, and in case of interaction the tagged proteins remain bound to the DNA probes after washing. Subsequently, they can be specifically immuno-detected by a HRP-conjugated antibody and their presence exposed by a colorimetric

reaction upon addition of the peroxidase substrate OPD, which is converted in an orange-yellow colored product that can be photometrical measured (Brand et al., 2010) (Figure 31).

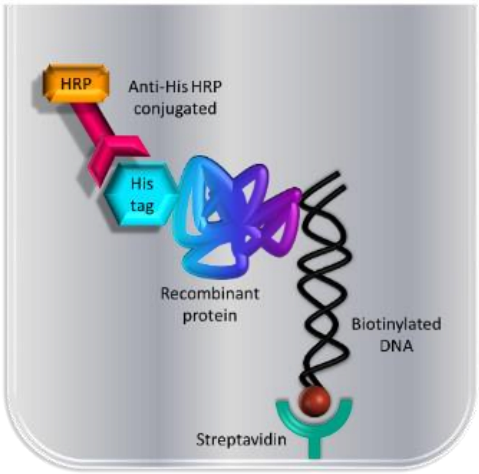

Figure 31. Cartoon representation of the elements involved in the detection of interaction between DNA and protein in the DPI-ELISA.

The cis-elements analyzed were G-boxes present in the promoters of the *RBCS1a* and *CAT2* genes. Specifically, the oligonucleotide probes corresponded to a 19 bp sequence located 940 bp upstream of the *CAT2* gene, and a 25 bp sequence located 69 bp upstream of the *RBCS1a* gene. Both G-box sequences were previously reported to be bound by GBF1 (Schindler et al., 1992a; Smykowski et al., 2010), so they could be used to validate the functionality of the assay.

Recombinant proteins were expressed in *E.coli* BL21-SI cells from the pDEST42 vector as 6xHis-tagged proteins, and crude protein extracts were used for the assay. Different amounts of the GBF1 protein extract were assayed, corresponding to 0.5, 5, 25, 50, and 100 µg of total protein, and different amounts of the DNA oligonucleotides were also tested; specifically, 2, 4, and 10 pmol of DNA probe per well. For each DNA-protein interaction tested, two technical replicates were included in each 96 well plate.

The results confirmed that GBF1 bound to both G-boxes in a concentration dependent manner, although there were pronounced differences in the measurements between the two DNA oligonucleotides. The CAT2 probe led to much weaker signals than the RBCS1a one (Figure 32), suggesting a weaker binding of GBF1 to the *CAT2* G-box sequence. On the other hand, the different DNA amounts tested resulted in only slight differences, meaning that the 2 pmol amount was enough to produce informative results. Regarding the protein amounts, the rule was that the higher the amount, the stronger the signal; but the sample containing 100 µg of protein led to weaker signals than the one containing 50 µg, consistently in all the cases. That was unexpected, as higher protein amounts were not expected to result in an inhibitory effect, but to reach a plateau; and that reduction in the signal was attributed to causes other than the DNA-protein interaction itself.

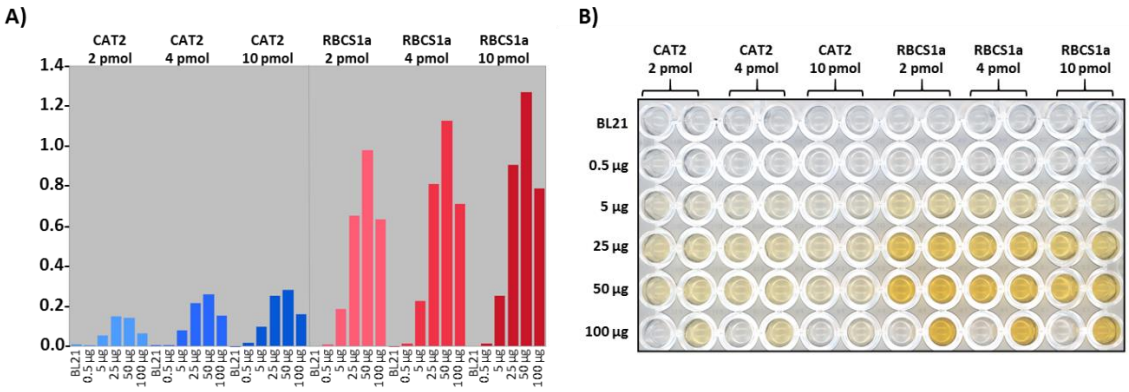

Figure 32. ELISA performed with different amounts of GBF1 protein extract (in µg) and DNA oligonucleotides (in pmol). Untransformed BL21 cells were used as negative control and no replicates were performed for the 100 µg total protein dilution. A) Graph with the measurements of absorbance at 492 nm. Note that no error bars are depicted because only two technical replicates were performed. B) Photograph of the ELISA plate after the reaction.

In order to determine whether the GBF1 DNA binding activity was modified in presence of bZIP63, the DPI-ELISA assay was performed including bZIP63 protein extract. First, the binding of bZIP63 alone was investigated, using the GBF1 protein extract as a positive control and crude protein extract from untransformed cells (BL21) as a negative control. Each extract was tested undiluted and as 1:50, 1:100, and 1:200 dilutions. The GBF1 extract produced a clear binding signal, whereas untransformed BL21 extracts led to no signal (Figure 33), indicating that the experiment worked appropriately. However, the results for the bZIP63 extract did not fit in any of the expected patterns of a positive or a negative interaction, which were clearly represented by the GBF1 (signal dependent on the dilution) and BL21 (flat signal profile) results, respectively. Instead, the undiluted bZIP63 extract produced a strong signal, while the dilutions resulted all negative; and that happened for both DNA probes identically (the difference was the lower values measured for the CAT2 probe). At that time, that strong signal in the undiluted extract was interpreted as an unspecific binding and it was concluded that bZIP63 did not bind to the DNA sequences tested.

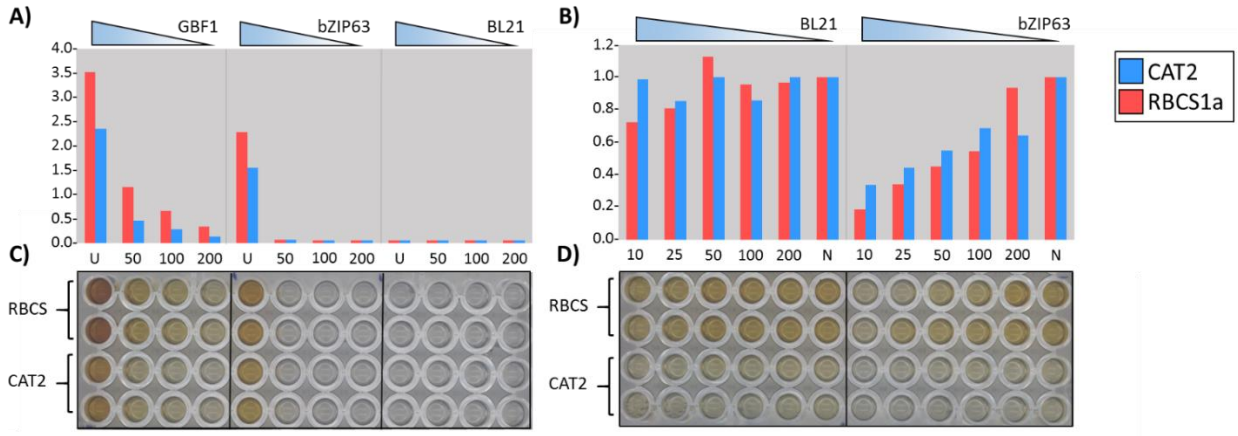

Figure 33. A) DNA binding of single GBF1 and bZIP63 extracts to the G-box sequences. U is undiluted protein extract; 50, 100, and 200 indicate the dilution assayed. Bars indicate absorbance at 492 nm. B) Effect of bZIP63 on the GBF1 G-box binding. 10, 25, 50, 100, and 200 are the dilutions of the bZIP63 protein extract and N means no addition of the bZIP63 protein extract. Bars indicate the absorbance values relative to the "N" sample, independently for each DNA probe. In A) and B) no error bars are depicted because there are only two technical replicates represented. C) and D) are the picture of the plate corresponding to the measurements in A) and B), respectively.

Next, GBF1 and bZIP63 protein extracts were combined together at different proportions in order to uncover any effect of bZIP63 on the GBF1 binding activity. The amount of GBF1 extract was maintained constant, at a 1:50 dilution, and it was combined with different amounts of bZIP63 extract, corresponding to 1:10, 1:25, 1:50, 1:100, and 1:200 dilutions, as well as with no bZIP63 at all. As experimental control, different amounts of the BL21 protein extract were mixed in an identical manner. For that experiment, the results were presented as relative values respect to the measurement obtained for the sample containing only GBF1 extract (without bZIP63), and for each DNA probe independently. Increasing amounts of the bZIP63 protein extract led to decreased absorbance measurements in both DNA probes (Figure 33). Conversely, no clear trend resulted from the addition of the BL21 protein extract, and only a slight decrease in the absorbance appeared at the 1:10 and 1:25 dilutions. Therefore, assumed that bZIP63 did not bind to the DNA probes alone, the decrease in the absorbance by the addition of the bZIP63 extract suggested that bZIP63 prevented the GBF1 binding to the two G-boxes tested.

In order to confirm those results, the experiments were repeated several times, and as expected, single GBF1 protein extracts regularly led to strong signals in a concentration dependent manner, and untransformed BL21 extracts were always negative. However, the bZIP63 protein extracts resulted in inconsistent results, so that they sometimes produced signals and sometimes they did not. Moreover, when the GBF1 and bZIP63 extracts were combined, they resulted in reduced, enhanced, or unchanged signals in regard to the GBF1 extract alone, indistinctly. Therefore, although initially it was considered that bZIP63 prevented GBF1 binding to both G-boxes tested, that conclusion was eventually called into question due to the lack of replicability. Remarkably, while GBF1 protein could be expressed satisfactorily in bacteria, bZIP63 was poorly expressed. Besides, Western blot analysis of the bZIP63 protein extracts showed a smaller band than expected or, alternatively, several bands; but in any case a single band with the theoretical size. Those observations hinted at an inadequate expression of the bZIP63 recombinant protein affecting its activity (Bondos and Bicknell, 2003) as a possible explanation for the experimental variability. As a result of that variability, the ELISA experiments could only conclude with confidence that the GBF1 crude extract resulted in binding signal, and that the untransformed BL21 cells did not, while the binding of bZIP63 and its effect on the GBF1 binding activity were inconclusive.

3.1.6 Effect of bZIP63 on the transcriptional activity of GBF1

In order to determine whether the transcriptional activity of GBF1 could be modified by bZIP63, a gene transactivation assay based on a GUS reporter gene was performed. The transcriptional effects of GBF1, bZIP63, and the combination of both were tested on two promoters reported to be targeted by GBF1, *RBCS1a* and *CAT2* (Smykowski et al., 2010; Singh et al., 2012). For that purpose, the coding sequences of the *GBF1* and *bZIP63* genes were cloned in a pUC 35S::c-myc vector to be expressed as c-myc-tagged protein effectors, and the *RBCS1a* and *CAT2* promoters were cloned upstream of a GUS reporter gene in a pBGWFS7 vector, comprising 1.5 Kbp upstream of the gene start and the 5'UTR. Since both genes were reported to be expressed in roots (Bueso et al., 2007; Sawchuk et al., 2008) in agreement with Genevestigator data (Figure 34 A), I proceeded with the experiments in the usual root-derived cultured protoplasts system. Protoplasts were transformed according to the large-scale protocol with one of the promoter::GUS constructs and either one or two of the constructs for the expression of effector proteins. Besides, a pBT8 vector coding for firefly luciferase gene under the control of a CaMV 35S promoter was co-transformed for normalization purposes. The uncloned pUC 35S::c-myc vector was used as control for basal expression. The assays were performed as previously described (Jefferson, 1987) in 1.5 mL Eppendorf tubes.

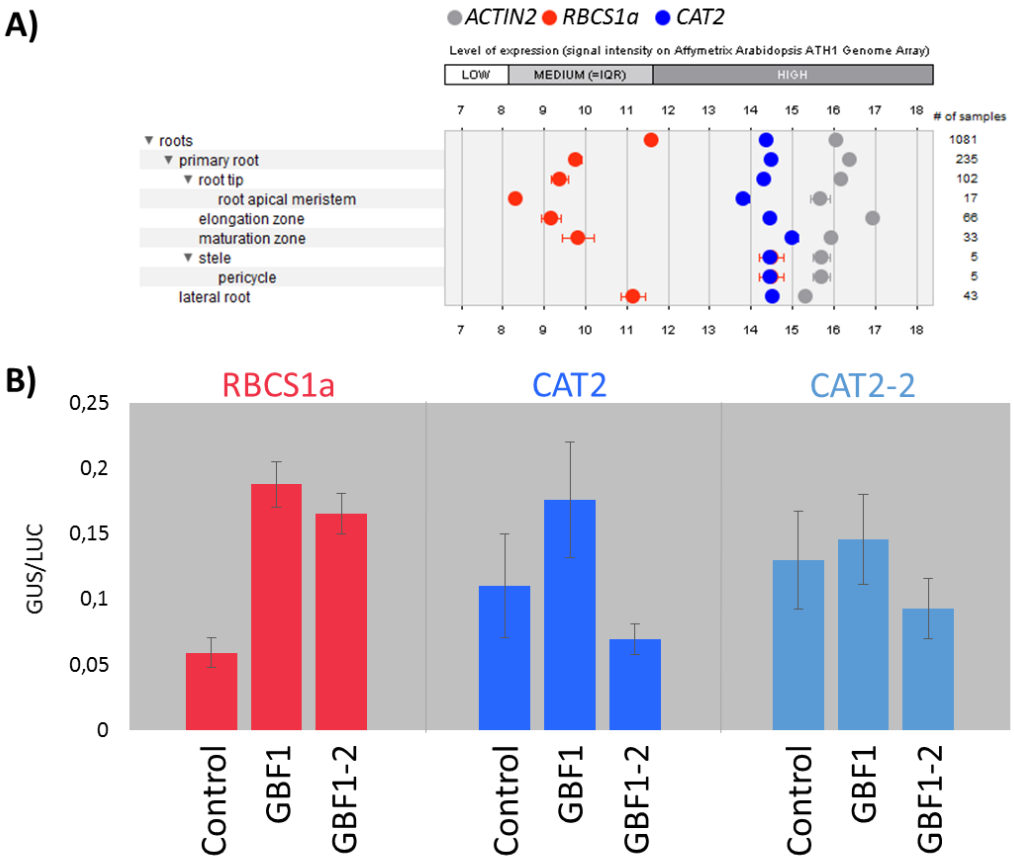

Figure 34. A) Genevestigator data showing the expression levels of *ACTIN2*, *RBCS1a*, and *CAT2* genes in root tissues of wild type plants in log2 scale. The picture was modified. B) GUS assay including the original constructs used for the description of the *CAT2* down-regulation by GBF1: CAT2-2 stands for the CAT2::GUS in pCB308, and GBF1-2 for the GBF1-pY01 construct. Results represent the average of three biological replicates and error bars are standard deviation.

In my experiments I could not reproduce the conspicuous down-regulatory effect of GBF1 on both promoters previously reported (Smykowski et al., 2010; Singh et al., 2012). Because of that, the experiments were repeated several times aiming to replicate the results described for GBF1. Variations in the amounts of the plasmids transformed and alternative systems such as leaf-derived green protoplasts or assays in 96-well plates were tried, but the absence of effect was robust. Yet, the GUS assay performed well with a pAC27 plasmid for GUS expression driven by the POLYUBIQUITIN 3 promoter (UBQ3::GUS) included as a control (Norris et al., 1993), so the functionality of the assay was out of doubt.

Given that the repression of *CAT2* by GBF1 was identified in our same laboratory but using different plasmid vectors, I also enquired whether the different vectors could account for those differences. Therefore, I assayed the same constructs used originally. Specifically, the *CAT2*::GUS construct was based on the pCB308 vector and included 1.4 Kbp of the upstream sequence and the 5'UTR, and GBF1 was cloned into the PY01 vector (Smykowski et al., 2010). However, the *CAT2* promoter construct still resulted in no clear changes in the expression of the reporter gene (Figure 33 B). As for the *RBCS1a* promoter, its expression even increased when GBF1 was co-expressed from any of the two effector plasmids (either pUC 35S::myc or PY01). Hence, I could conclude that under the conditions tested GBF1 did not show any effect on the *CAT2* expression, and instead, it was likely to act as an activator of the *RBCS1a* expression.

3.1.7 Phenotypic characterization of Arabidopsis lines with altered bZIP63 levels

GBF1 was identified as a regulator of the onset of senescence and, concomitantly, Arabidopsis *gbf1* mutant lines exhibited a marked delay in senescence (Smykowski et al., 2010). Therefore, in order to investigate whether bZIP63 was involved in the senescence-specific regulation of GBF1, Arabidopsis lines with altered bZIP63 levels were phenotypically characterized for senescence. Specifically, the lines analyzed were a homozygous T-DNA insertion line (SALK_006531) and two lines overexpressing bZIP63::GFP fusion proteins mediated by a CaMV 35S promoter. The overexpressing lines were provided by Prof. Dr. Wolfgang Dröge-Laser from the University of Würzburg, Germany, labeled as L1.1.1, and L14.2.1, and in this work they were referred as bZIP63 OX-2, and bZIP63 OX-3, respectively. Those three lines were characterized together with a wild type Arabidopsis Col-0 line as control for normal development, and the *gbf1* mutant line (SALK_144534) as a control for delayed senescence.

Seeds from the same line were first sown on a medium-size pot and stratified at 4°C for 48 hours. About 10 days after, seedlings were transferred to smaller, individual pots and growth under long-day conditions. Senescence-specific phenotypic determination was performed at different time points, consisting in the categorization of rosette leaves according to their color in green, green/yellow, yellow, and brown; and the determination of the chlorophyll content of leaves Nr. 3, 7, and 10 with an atLEAF+ chlorophyll meter. Besides, pictures were taken showing the rosette leaves ordered according to the leaf-age. The sampling for the phenotypic characterization usually comprises four or five plants per line, which are selected not randomly, but aiming to be representative of each line. However, I considered that an important subjective component was present in that pre-selection of plants, as well as in the categorization of leaves by color, therefore I carried out my phenotypic analysis as blind assays in order to avoid the possibility of incurring in experimenter bias. In such manner, pots were identified with a code (different codes were used in successive experiments) and the different plant lines were randomly mixed in the same tray. The identity of the lines was only revealed after all data were gathered at the end of the experiment.

Results showed that both bZIP63 overexpressing lines were delayed in senescence according to their lower number of yellow or brown leaves in comparison to the wild type at any time point, and congruently, their chlorophyll content was higher (Figure 35). On the other hand, neither *bzip63* nor *gbf1* mutant lines exhibited altered senescence phenotypes compared to the wild type line. The absence of the senescence delayed phenotype in the *gbf1* line was unexpected, but robust over further repetitions.

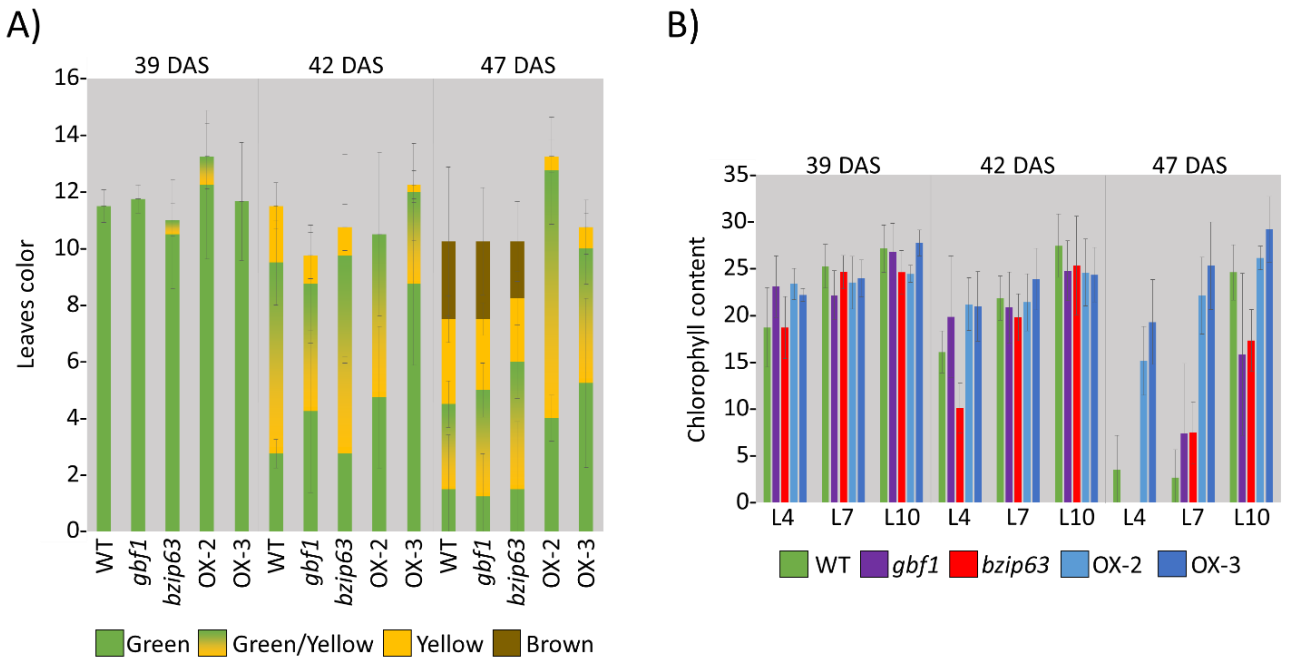

Figure 35. Senescence phenotypes of Arabidopsis lines with altered bZIP63 expression. Wild type (WT), *gbf1 mutant (gbf1), bzip63* mutant (*bzip63*), bZIP63 OX-2 (OX-2), bZIP63 OX-3 (OX-3). Charts represent the average of four plants randomly selected. Error bars are standard deviation. A) Number of leaves categorized by colors. B) Chlorophyll content measured with an atLEAF+ chlorophyll meter (no units). Measurements were performed in leaf Nr.4 (L4), Nr.7 (L7), and Nr.10 (L10).

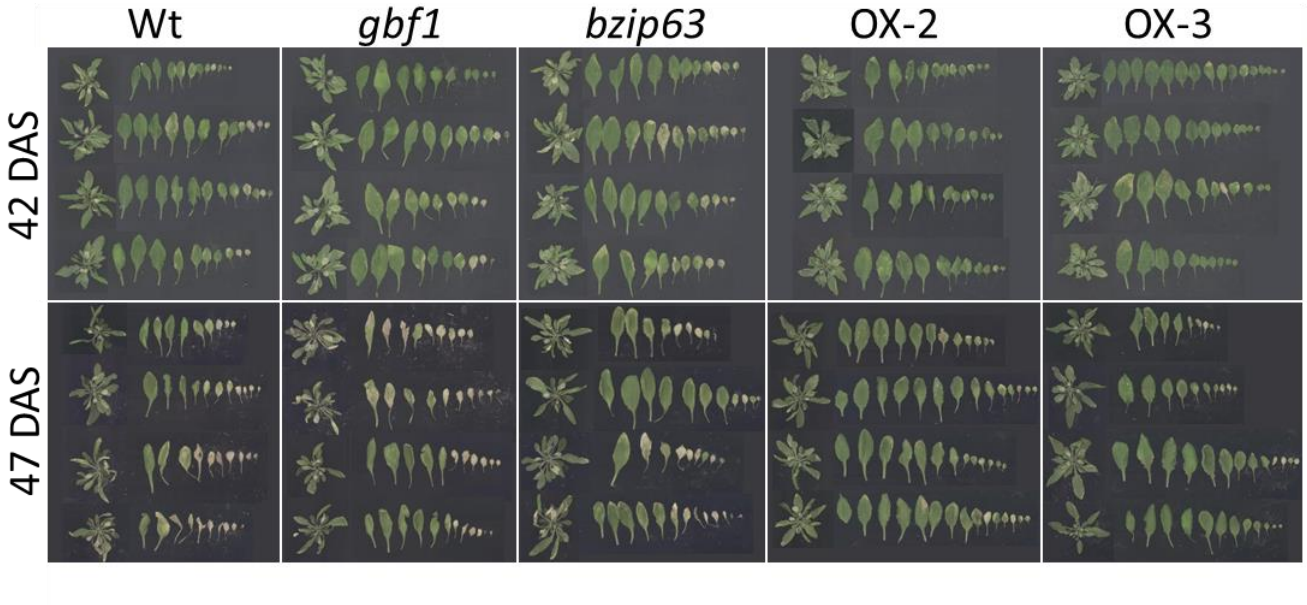

Figure 36. Rosette leaves ordered by leaf age, from young (left) to old (right). All four plants used to generate the results in Figure 35 are here depicted in order to reflect the variability

3.1.8 Continuous phenotype determination of Arabidopsis lines with altered bZIP63 levels

Because the phenotype characterization was based on data gathered at certain time points, the results were no informative in regard to the progression of senescence. As they were, it could not be discriminated whether the bZIP63 OX-2 and bZIP63 OX-3 plants were actually delayed in senescence or they underwent a general delay in the development; and indeed the bZIP63 overexpressing lines exhibited a low germination rate that suggested that something else than senescence was altered. Therefore, I decided to perform an alternative phenotyping approach, in order to track changes in the development of the plants all along their lifetimes. Plants were monitored every few days, determining for each one, the rosette maximum radius, the height, the number of green leaves, and the number of leaves which already started yellowing. That last parameter was intended to reflect the yellowing emergence, so it included leaves with any degree of yellowing, from the tiniest yellow spot to fully yellow or brown leaves. Besides, a daily observation was performed in order to note the time when the first bud, the first opened flower, the first silique, and the first shattered silique appeared. Finally, the progression of senescence was also assessed by determining the day in which all rosette leaves showed at least 50% of their surface yellow or brown (RY50), and when they were completely yellow or brown (RY100).

The experiment was conducted as a blind assay, being each pot identified with a unique number. Plants were grown under long day conditions at 25°C, and monitoring 36 plants per line. The results revealed great homogeneity among the five lines in most of the parameters analyzed (Figure 38), in contrast to the marked differences seen in the discontinuous phenotyping results.

The rosette maximum diameter expanded identically in all lines. Shoot growth was slower in the bZIP63 overexpressing lines but it was maintained longer (48 DAS median) than the other lines (41 DAS median), hence these plants were taller in the end.

Bud emergence occurred with a median of 25 DAS for all lines, yet a slightly delay in bZIP63 OX-2 and bZIP63 OX-3 and advance in *gbf1* and *bzip63* was recognizable. However, bud emergence was noted inaccurately, because it coincided with two days in which no measurements were performed, so that the noted differences were likely to be more pronounced. Flower opening in bZIP63 OX-2 and bZIP63 OX-3 lines took place with a median of 29 DAS, delayed respect the rest of the lines (26 DAS median). Flower opening annotation was not detailed for the same reason as bud emergence, but the graphic representation of this parameter suggested that *gbf1* and *bzip63* lines were actually accelerated respect the wild type.

First siliques were observed in the wild type with a median of 29 DAS, one day earlier in *gbf1* and *bzip63*, and two days later in the bZIP63 overexpressors. Shattered siliques in *gbf1* and *bzip63* lines appeared with a median two days earlier than the wild type, consistent with their earlier emergence, while in bZIP63 OX-2 and bZIP63 OX-3 lines were observed with the same timing as the wild type (44 DAS median), meaning that these lines spent less time for the silique maturation. An interesting remark given their lower germination rates.

Leaf production was slightly delayed in *gbf1*, bZIP63 OX-2, and bZIP63 OX-3 lines respect to the wild type. Notwithstanding, the bZIP63 overexpressors sustained new leaf production for longer time (28 DAS median), catching up with the wild type; whereas the *gbf1* line stopped the production at the same time as the wild type (22 DAS median), hence it ended up with less leaves. First yellowing signs were detected with a median of 23 DAS affecting only few leaves in all lines, and further leaves were not affected until ca. 34 DAS, meaning that that yellowing was not related to the process of natural senescence in which further leaves are steady affected by yellowing (Figure 37). In fact, before those first few leaves showed yellowing signs, an unscheduled short period of water deficit occurred, which could have triggered stress-induced senescence of the oldest

leaves. Still, it is remarkable that bZIP63 OX-2 and bZIP63 OX-3 lines exhibited a less number of leaves affected by that initial yellowing.

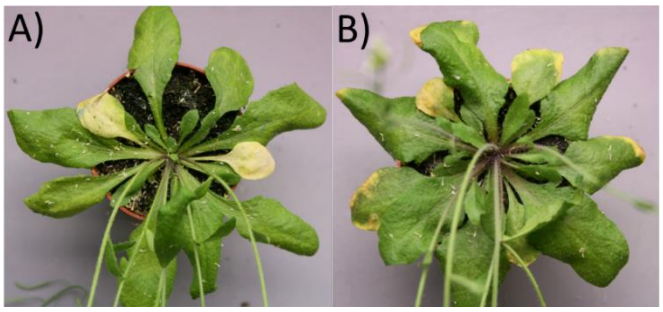

Figure 37. A) Stress induced senescence in older leaves. B) Yellowing at the leaf tips in the bZIP63 overexpressing lines.

The senescence-related steady appearance of yellowing signs in further leaves started at 31 DAS in bZIP63 OX-2 and bZIP63 OX-3 lines, earlier than in the other lines in which it took place with a median of 37 DAS. However, the rate of yellowing emergence in further leaves slowed down from 42-44 DAS, so that the time point when all rosette leaves were affected was strongly delayed in the bZIP63 OX-2 and bZIP63 OX-3 lines (medians of 55 DAS and 60 DAS, respectively) in comparison to the other lines (48 DAS median).

Furthermore, the bZIP63 overexpressing lines were also delayed in the RY50 and RY100 values, meaning that the yellow spots expanded slower in those lines. Indeed, that delay was much more pronounced taking into account that at the end of the experiment (66 DAS), most of the plants from those lines had not reached yet the RY100 and the RY50 time points. This is to say, the RY50 and RY100 values calculated for the bZIP63 OX-2 and bZIP63 OX-3 lines were actually underestimations. Specifically, 88 % of the bZIP63 OX-2 plants and 66 % of the bZIP63 OX-3 plants accounted for the calculation of the RY50, and only 33 % and 16 % for the RY100, respectively. For these two lines, most of the leaves annotated as showing yellowing signs actually exhibited only yellowing at their tips, and further expansion was severely retarded (Figure 38).

To sum up, these results indicated that bZIP63 OX-2 and bZIP63 OX-3 plants exhibited a general delay in development, instead of a senescence-specific retardation. The onset of senescence was not delayed, but it was the progression what was strongly affected. On the other hand, neither *gbf1* nor *bzip63* displayed recognizable alterations in their senescence phenotypes, and instead, they appeared to be rather early flowering.

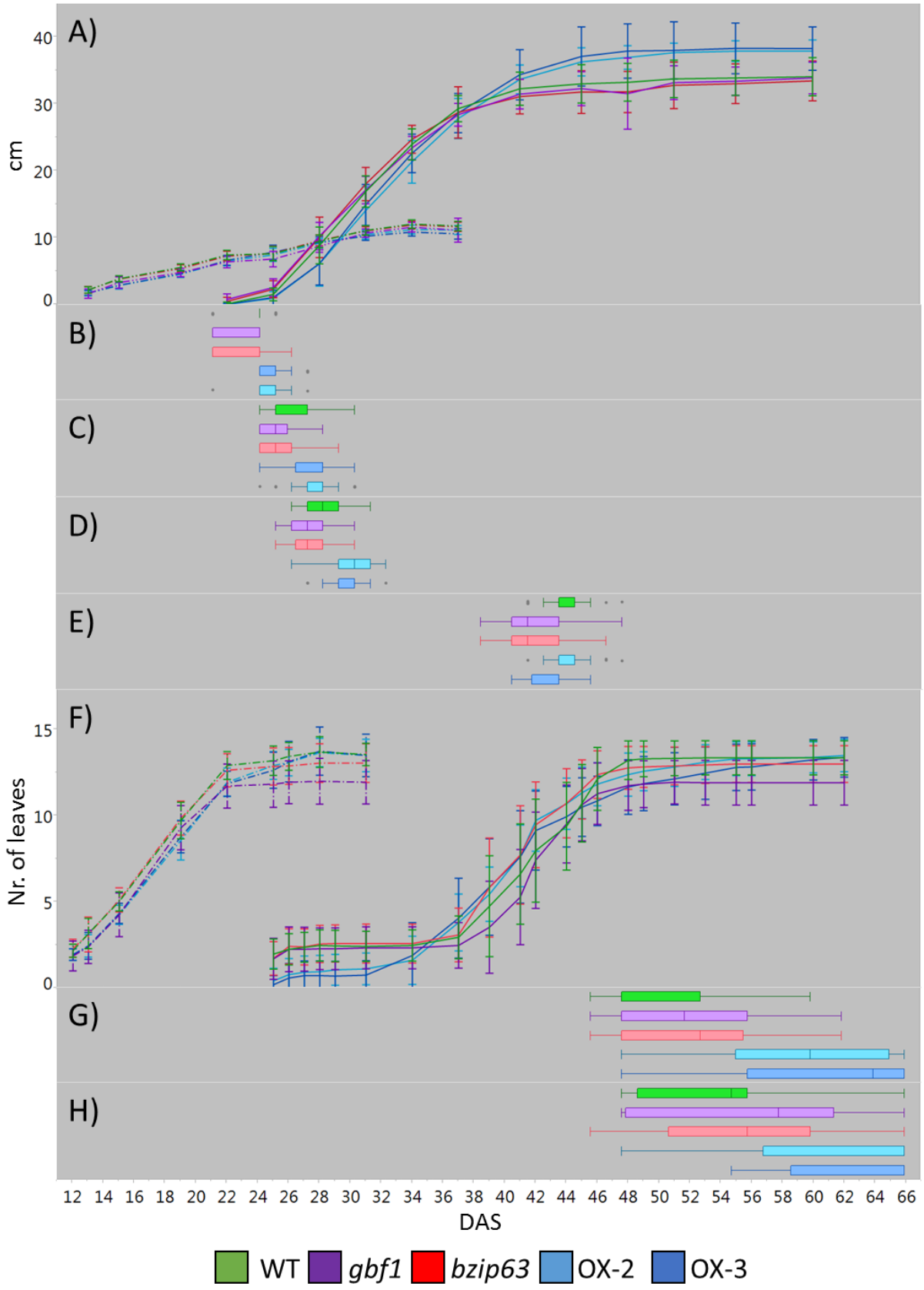

Figure 38. Continuous phenotyping of Arabidopsis lines with altered bZIP63 expression. Wild type (WT), *gbf1 mutant (gbf1), bzip63* mutant (*bzip63*), bZIP63 OX-2 (OX-2), bZIP63 OX-3 (OX-3). A) Rosette radius in dotted lines and height in continuous lines. Represented are averages and standard deviation. B) First bud appearance. C) First opened flower. D) First silique appearance. E) First silique shattered. F) Number of green in dotted lines and number of leaves with yellowing in continuous lines. Represented are averages and standard deviation. G) RY50 values. H) RY100 values.

In order to provide an integrative overview of the data and ease the assessment of similarities and differences among the five Arabidopsis lines analyzed, a principal component analysis (PCA) was performed with the cooperation of Dr. Justine Bresson. For that purpose, data from the four parameters which were continuously monitored -height (H), diameter (D), number of green leaves (G), and number of leaves which started yellowing (Y)- were used to fit sigmoid curves describing their expansion in each line. Fitting was performed in R 3.0.2 (R Development Core Team) based on the SigmoidalFitting.R script from the Phenopsis database (http://bioweb.supagro.inra.fr/phenopsis/), modeled as $Y \sim A / (1 + e^{-((t - X0) / B)})$. Where A is the final value of the variable (the sigmoid curve plateau), B is the duration of the maximum expansion rate, t is the time, and X0 is the inflexion point of the curve. The PCA analysis included the maximum slope (Rmax), the inflexion point (IP), and the final value (A) of the calculated curves were used, and the six parameters - first bud, first opened flower, first silique, first silique shattered, RY50, and RY100- represented by a single measurement (Figure 39 A).

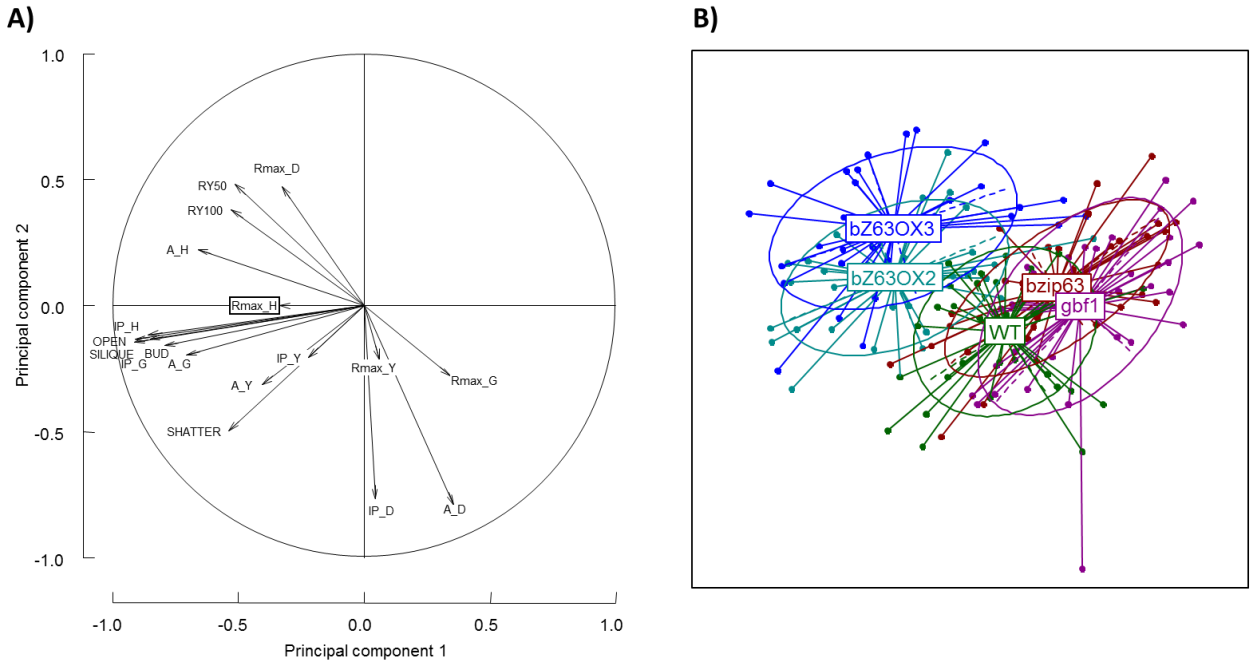

Figure 39. A) Representation of the variables included in the PCA. Only the first two axes are showed. B) Projection of individual plants. For each line, the center of gravity and the inertia ellipse are represented. Ellipses are centered on the mean and their sizes represent 1.5 standard deviations of the axes coordinates, while the slopes of the large axes are given by the covariances.

First, second, and third principal component (PC) explained 34.5 %, 13.9 %, and 10.5% of the total variance, respectively (Figure 40). PC1 was mainly contributed by flower opening time, silique emergence, height IP, and the IP for the leaves emergence, which are all traits related to a mature state of development. PC2, was primarily correlated with the A and IP diameter values, describing the rosette expansion. PC3 was related to the final number of leaves, represented by the A values of the number of green leaves and the number of yellowing leaves.

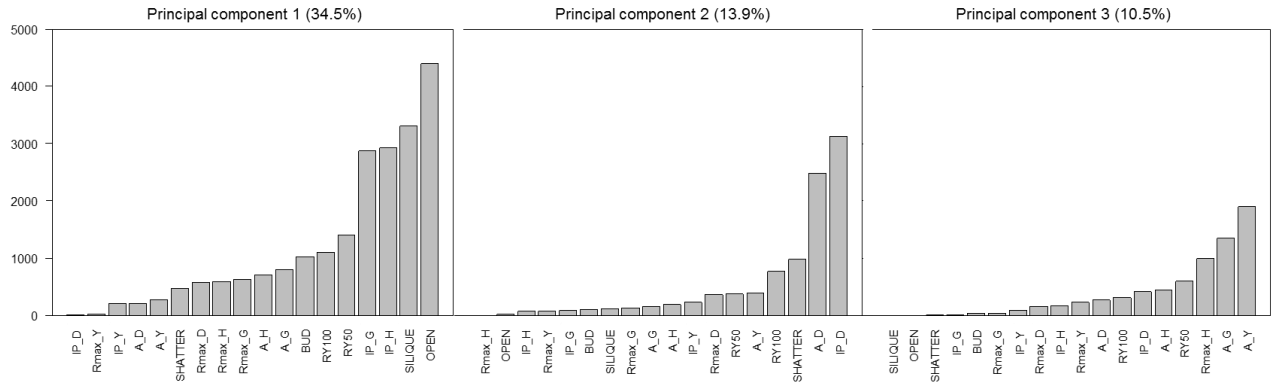

Figure 40. Loadings of the variables on the three firsts principal components of the PCA.

Projection of individuals (Figure 39 B) revealed significant differences between the wild type and the three bZIP63 lines (P<0.001 for the overexpresors and P<0.01 for the mutant, ANOVA on PC coordinates), but not between the wild type and the *gbf1* line. Along the PC1, the bZIP63 overexpressing lines were separated from the wild type in the opposite direction than the *gbf1* and *bzip63* lines, indicating that that those lines featured antagonistic developmental phenotype. Interestingly, all lines resulted separated from the wild type in the same direction on PC2, which was mainly described by the rosette expansion, suggesting that the diameter data were more informative than it could have been expected from the highly similar profiles of all lines in Figure 38. Indeed, the detailed observation of the curves representing the rosette expansion revealed that WT, *gbf1*, and *bzip63* showed a pronounced decrease in their expansion rates between 23 and 25 DAS, while both bZIP63 overexpressing lines continued to grow normally (Figure 41). Remarkably, that impasse in the rosette expansion approximately coincided with the emergence of the first yellowing signs, meaning that both events could be related.

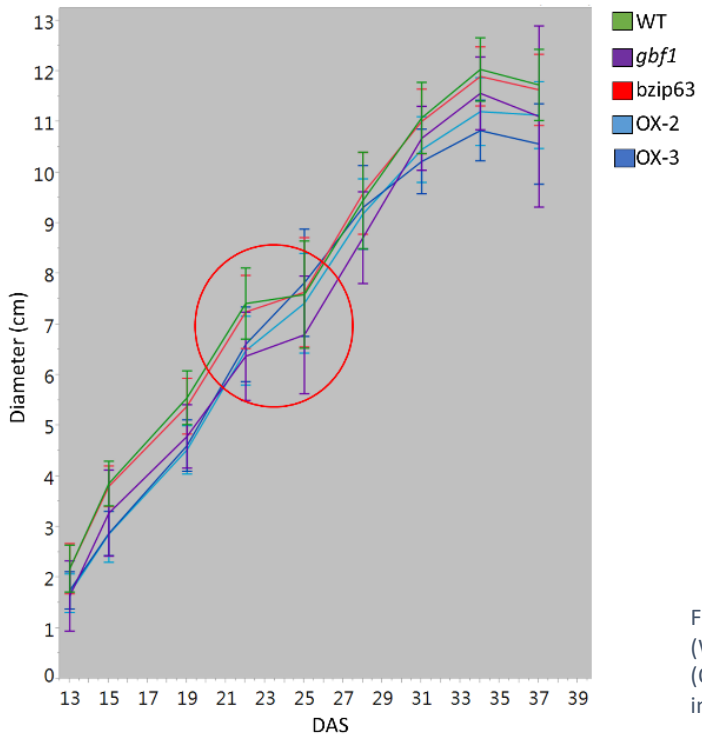

Figure 41. Rosette diameter expansion in detail. Wild type (WT), *gbf1 mutant (gbf1), bzip63* mutant (*bzip63*), bZIP63 OX-2 (OX-2), bZIP63 OX-3 (OX-3). The red circle indicates the change in the pattern.

3.1.9 Screening for senescence phenotypes among mutant lines for LES related genes

The identification of new candidates potentially interacting with GBF1 was also addressed by searching for mutants with altered senescence phenotypes among Arabidopsis transgenic lines with altered levels of LES related genes. Those included most of the bZIPs of the C/S1 network and the catalytic SnRK1 α-subunits KIN10 and KIN11. In that case, because of the elevated number of lines to be analyzed (26) a shorter version of the senescence-specific phenotype determination based on single time points was performed. Specifically, only the color of the leaves and the time of flowering were annotated. The experiment was performed with the collaboration of Stefan Bieker and Prof. Dr. Ulrike Zengraf as a blind assay with 25 plants per line. The identity of the lines was revealed after the experiment according to Table 7.

Nr.	Line	Ecotype
1	kin11-1	Ws
2	kin11-2	Ws
3	kin10	Col-0
4	gbf1	Col-0
5	Wild type	Col-0
6	bzip1	Col-0
7	bzip53	Col-0
8	bzip53/bzip1	Col-0
9	bzip25	Col-0
10	bzip10/bzip25	Col-0

Nr.	Line	Ecotype
11	bzip10/bzip53	Col-0
12	bzip10/bzip25/bzip53	Col-0
13	bzip1/bzip10/bzip25/bzip53	Col-0
14	bzip9	Col-0
15	bzip1/bzip9/bzip53/bzip63	Col-0
16	bzip10	Col-0
17	bzip63	Col-0
18	bzip2/bzip11/bzip44	Col-0
19	35S::bZIP9-GFP	Col-0
20	35S::bZIP25-GFP	Col-0

Nr.	Line	Ecotype
20	35S::bZIP25-GFP	Col-0
21	bzip9/bzip25	Col-0
22	35S::bZIP63-GFP	Col-0
23	Wild type	Ws
24	35S::bZIP10-HA	Col-0
25	35S::bZIP10	Col-0
26	35S::bZIP25	Col-0

Table 7. Identity of the lines analyzed. Note that two different Arabidopsis backgrounds were used.

At 46 DAS, lines 4, 9 and 21 (*gbf1*, *bzip25*, and *bzip9/bzip25*, respectively) showed accelerated signs of yellowing compare to the rest (Figure 42 A). At 54 DAS, the line 22, which corresponded to the bZIP63 OX-2 analyzed above, displayed a conspicuous delay in senescence. Conversely, lines 4, 11, 17, 21 (*gbf1*, *bzip10/bzip53*, *bzip63*, *bzip9/bzip25*, respectively) were accelerated. Line 23, the Wassilewskija (Ws) wild type, was also accelerated compared to the Col-0 wild type line, while senescenc signs were milder in the kin11 mutant lines in Ws background (lines 1 and 2), thus meaning that these two lines were actually delayed. At 60 DAS, the most senescent lines were the 3, 4, 11, and 12 (*kin10*, *gbf1*, *bzip10/bzip53*, *bzip10/bzip25/bzip53*, respectively). On the contrary, lines 10, 19, 22, and 26 (*bzip10/bzip25*, 35S::bZIP9::GFP, 35S::bZIP63::GFP, and 35S::bZIP25::GFP, respectively) were the less senescent.

Regarding the bolting time (Figure 42 B), over 50% of plants from lines 1, 4, 9, 11, and 23 (*kin11-1*, *gbf1*, *bzip25*, *bzip10/bzip53*, and Ws wild type, respectively) had bolted at 32 DAS, earlier than the Col-0 wild type (line 5) for which most of the plants bolted at 34 DAS. Both kin11 mutants in Ws background mutant lines bolted slightly delayed in regard to the Ws wild type, and that was more pronounced for line 2 (*kin11-2*). On the other hand, a significant fraction of the plants from lines 8, 12, 16, 22, 25, and 26 (*bzip53/bzip1*, *bzip10/bzip25/bzip53*, *bzip10*, 35S::bZIP63::GFP, 35S::bZIP10, 35S::bZIP25) bolted at 36 DAS.

According to those data, only lines 4, 11 and 22 (*gbf1, bzip10/bzip53* and 35S::bZIP63::GFP) were consistent in their phenotypes all along the development. The former two were accelerated in senescence and bolting, and the latter was delayed in both parameters. For the rest of the lines, the results were more difficult to interpret, since knock-out lines for multiple bZIPs behaved distinctly depending on the bZIP genes lesioned, probably due to the complex interrelation among those genes. For instance, line 11 (*bzip10/bzip53*) was accelerated in senescence and bolting almost in all time points, but line 12 and line 13, which were also *bZIP10* and *bZIP53* defective (*bzip10/bzip25/bzip53* and *bzip1/bzip10/bzip25/bzip53*, respectively), did not exhibit any obvious altered phenotypes at any time point; even more line 12 bolted with delay. Thus, that experiment failed to provide new bZIP candidates linking LES and senescence. However, it confirmed the delay and the advance in

the development of the bZIP63 overexpressing line and the *gbf1* mutant line, respectively, in an independent manner to my previous observations, since plants were characterized without my participation.

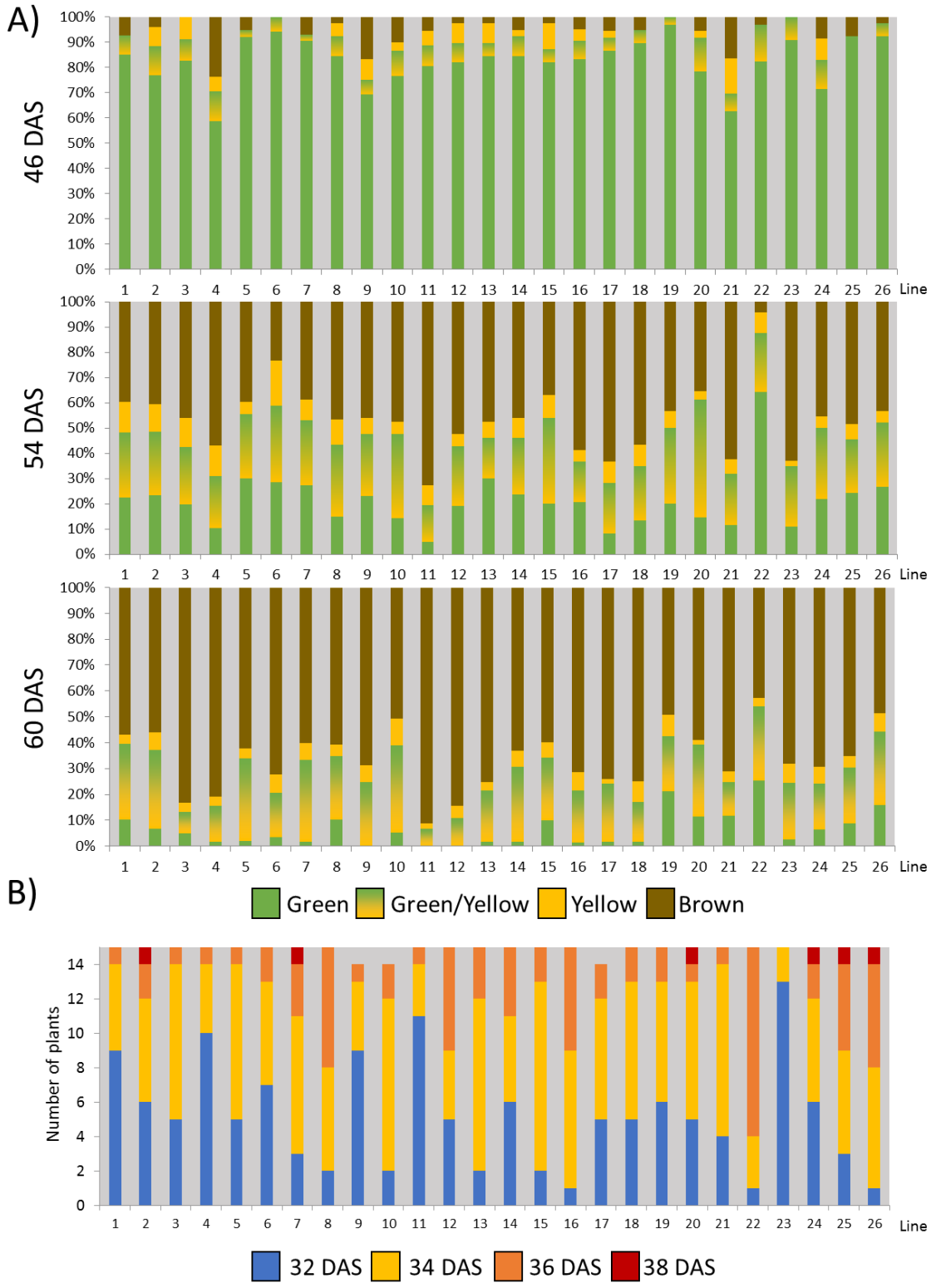

Figure 42. Phenotypic screening of the 24 transgenic lines. Line 5 and line 23 are Col-0 and Ws wild type lines, respectively. A) Leaves categorization by colors. Bars represent the average of five plants for each time point. Results are represented in percentage and without error bars in order to ease the recognition of trends. B) Bolting time. Bars indicate the number of plants with flowers at the days of observation indicated. Values are absolute numbers. n=15, and n=14 for lines 9, 10, and 17.

3.1.10 Authentication of the *gbf1* mutant line

The absence of the expected delayed-senescence phenotype in the *gbf1* mutant line was striking but robust, since the phenotype for that line was several times characterized with consistent results. I could exclude the possibility that the seeds could have been contaminated, because the genotypes of the *gbf1* line were determined during the construction of a double mutant *gbf1*/*bzip63* line. The presence of the T-DNA insert was confirmed to be homozygous in both lines (i.e. *gbf1* and *bzip63*) by PCR using SALK T-DNA primers (Figure 43). In addition, the PCR products generated with the T-DNA primers were sequenced, so that the precise location of the insert was determined. Those were located in the nucleotide position 2149 of *GBF1*, corresponding to the ninth exon, and in the nucleotide position 23 of *bZIP63*, corresponding to the 5'UTR.

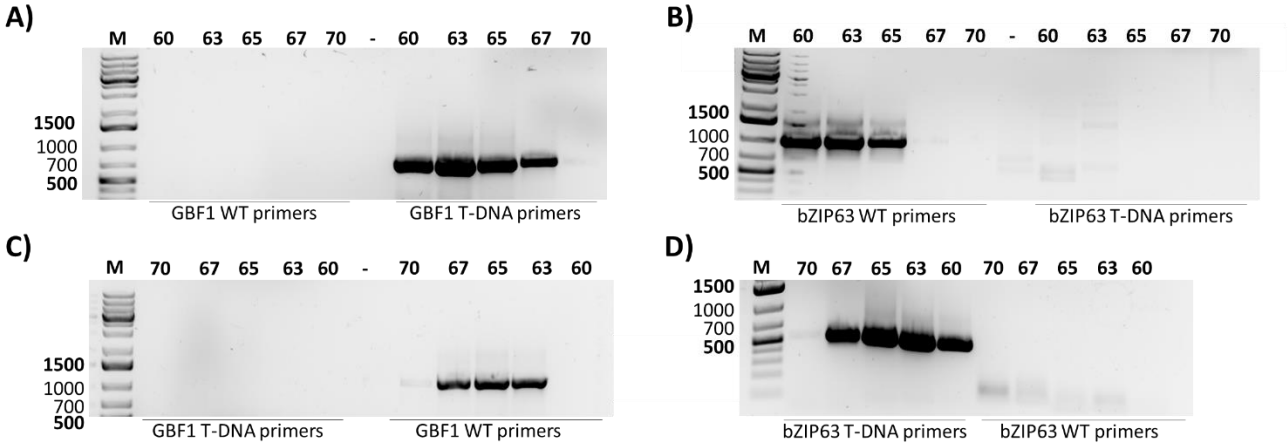

Figure 43. Checkout of the T-DNA insertions in the *gbf1* and *bzip63* lines. PCR was made with an annealing temperature gradient between 60 and 70 °C, as indicated above the gels. M is the DNA ladder, and the band sizes are indicated in bp units. WT primer pairs are the Left (LP) and Right (RP) genomic primers of the corresponding gene, which in the wild type gene versions produce an amplicon of 1139 bp from *GBF1* and 994 bp from the *bZIP63*; T-DNA primer pairs combine the Left border T-DNA primer (Lb1.3) with the corresponding RP and result in a product of 400-700 bp. PCRs in A) and B) were performed with genomic DNA from *gbf1* plants, in C) and D) genomic DNA from *bzip63* plants was used. Notice that pictures in C) and D) are reverse oriented respect the ones in A) and B).

I also verified that the GBF1 expression was still knocked out in the *gbf1* line. I performed a RT-PCR with three alternative primer pairs, which bound to different positions of the gene (Figure 44). The first one amplified from exon 4 to exon 7 -before the T-DNA insertion- and congruently, a band could be seen in both lines, mutant and wild type. The PCR products for other two primer pairs included the exon 9 -where the T-DNA insertion is located-: one pair amplified from exon 8 to exon 10 and the other until exon 11. Both primer pairs resulted in no product when the *gbf1* cDNA was used as template, but could amplify well when the wild type cDNA was used, indicating that the expression of GBF1 was completely knocked out, in agreement with previous works (Smykowski et al., 2010). Thus, those results could confirm that the *GBF1* expression was abolished in the *gbf1* line.

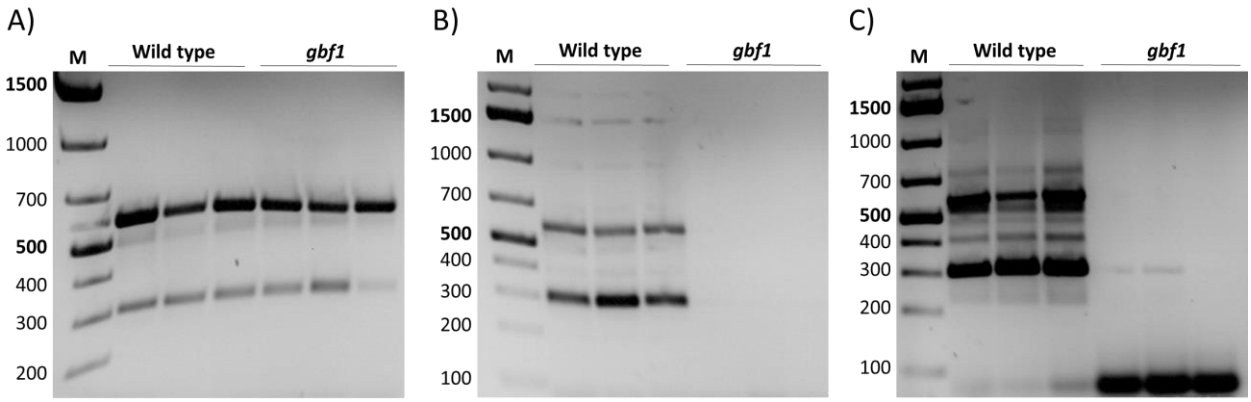

Figure 44. GBF1 knockout verification by PCR from cDNA. M is the DNA ladder, and the band sizes are indicated in bp units. Three different *gbf1* and wild type plants were tested. A) Primers amplifying between exon 4 and exon 7, before the T-DNA insertion. B) Primers amplifying between exon 8 and exon 10. C) Primers amplifying between exon 8 and exon 11. Note that multiple bands appear in the gel, as no DNase was used during the cDNA synthesis. All primer pairs were designed to amplify 300 bp of the cDNA, so that the upper bands correspond to the genomic DNA.

3.2 Regulation of GBF1 activity by phosphorylation

Phosphorylation is a common mechanism regulating the activity of bZIPs at different levels, including DNA binding level, transcriptional activation, turnover, or subcellular localization (Djamei et al., 2007; Kirchler et al., 2010; Sirichandra et al., 2010; Kawamoto et al., 2015). Particularly, GBF1 DNA binding activity was found to be stimulated by phosphorylation by casein kinase II (CKII) from broccoli (Klimczak et al., 1992). Therefore, I also researched whether GBF1 activation in senescence could be regulated by phosphorylation.

3.2.1 GBF1 is not a substrate for SnRK1

Although GBF1 does not bear the SnRK1 consensus target sequence (Huang and Huber, 2001), phosphorylation by KIN10 was still analyzed since that kinase plays a central role in the LES and the overexpression of the catalytic SnRK1 α-subunit KIN10 results in a delayed senescence phenotype (Baena-González et al., 2007). An *in vitro* kinase assay was performed in the laboratory of Dr. Baena-Gonzalez at the Instituto Gulbenkian de Ciência in Lisbon, Portugal, and in collaboration with Mattia Adamo. Purified GBF1 recombinant protein was tested as phosphorylate substrate for KIN10 in presence of radiolabeled ATP, and a protein fragment containing the first 173 amino acids of ABF2 (ABRE-binding factor 2) was included as a positive control for KIN10 (Rodrigues et al., 2013). The functionality of the kinases was verified by the strong phosphorylation of ABF2 by KIN10 (Figure *45*, lane 2), as well as by the KIN10 phosphorylation by SnAK2 and the SnAK2 auto-phosphorylation, which were observable in all samples in which both proteins were present in agreement with previous reports (Crozet et al., 2010). However, no radioactive band was detected for GBF1 (Figure 45, lane 5), confirming that GBF1 was not a KIN10 target.

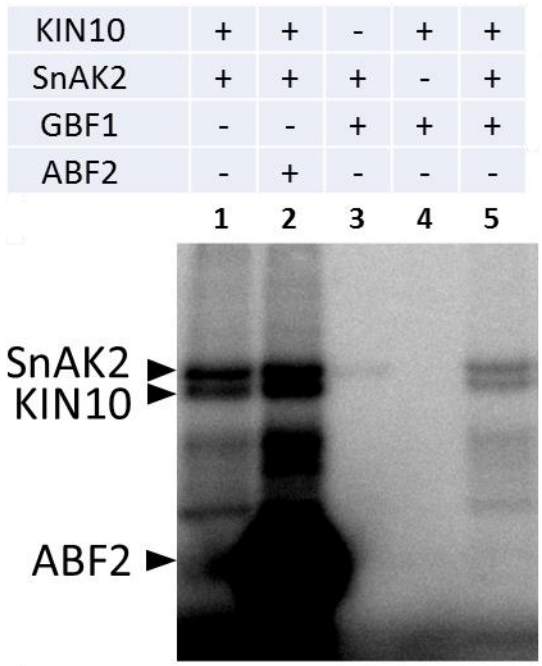

Figure 45. Autoradiography of the *in vitro* kinase assay. Combinations of kinases and substrates were performed according to the table above. Theoretical MWs of the substrate proteins are 37.1 KDa for GBF1, 22 KDa for ABF2, 55 KDa for KIN10, and 63 KDa for SnAK2.

3.2.2 Impact of the phosphorylation mimicry on the GBF1 DNA binding capability

A previous report indicated that bZIP63 was phosphorylated by a calcium-dependent kinase, and experiments with mutated versions of bZIP63 in which three conserved serine residues of its BR were substituted by aspartate residues resulted in a dramatic decrease in the DNA binding capability of that bZIP (Kirchler et al., 2010). Because GBF1 also features those three same serine residues, which are located in positions 11, 15, and 19 of the basic region (Figure 46 A), I investigated whether the GBF1 DNA binding activity could be regulated similarly to bZIP63 through the phosphorylation of those three serines.

The three serine residues in GBF1 were mutated to either aspartate (to mimic the phosphorylated state) or to alanine (to mimic the unphosphorylated state) by site-directed mutagenesis, and they were referred as 3A and 3D, respectively. The GBF1 mutated proteins were expressed in bacteria, and their DNA binding activity was assayed by DPI-ELISA as described above. Both DNA probes, RBCS1a and CAT2, were tested along with their corresponding mutated versions in which the G-box sequence core (ACGT) was substituted by CATG.

As expected, the wild type version of GBF1 bound strongly to both DNA probes in a concentration dependent manner (Figure 46 B), and almost no binding occurred to the probes containing the mutated G-box sequences, confirming the specificity of the GBF1 interaction. As for the mutated versions of GBF1, both led to much weaker signals than the native GBF1, despite showing similar protein levels in Western blot (Figure 46 C). Those results indicated that the mutation of these residues affected the DNA binding in a manner unrelated to the phosphorylation mimicry.

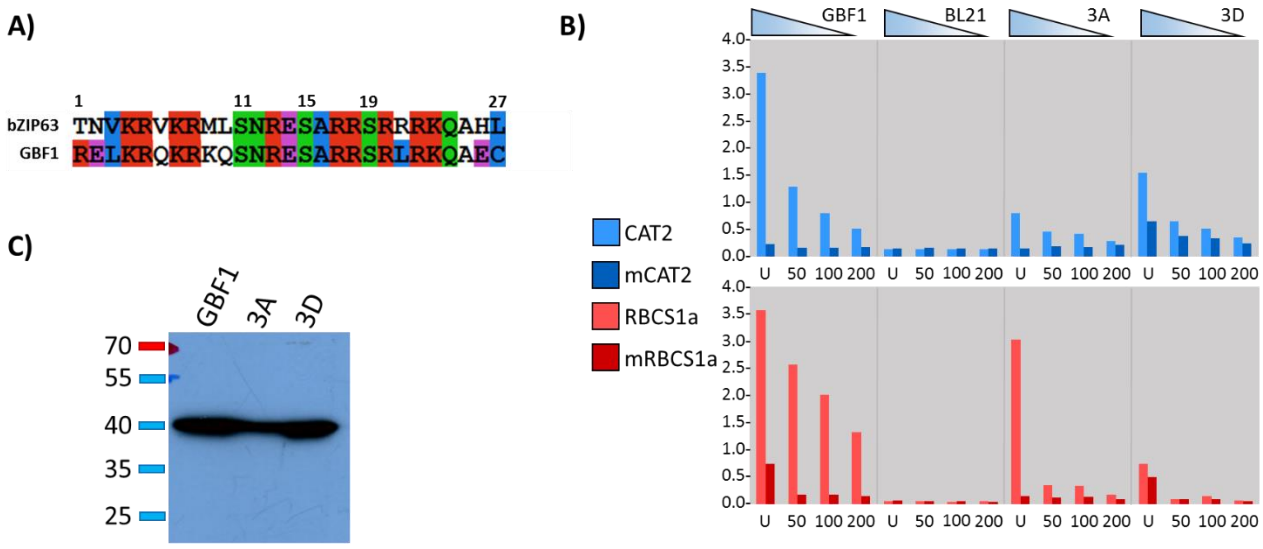

Figure 46. ELISA with GBF1 phosphorylation mimicry mutants. A) Basic domain of GBF1 and bZIP63 representing the three serines mutated in positions 11, 15, and 19. Amino acids sequences were aligned with Clustal X and were colored according to the default settings. B) Absorbance measurements at 492 nm. GBF1 mutant versions with the three serines mutated to alanine are indicated as 3A and to aspartate as 3D. U is undiluted protein extract; 50, 100, and 200 indicate the different protein dilutions assayed. Blue and red bars are the measurements for the CAT2 and the RBCS1a DNA probes, respectively. No error bars are depicted as only two technical replicates are represented. C) Western blot of the protein extracts used for the ELISA. Detection was performed with the penta-His HRP conjugated antibody. On the left it is indicated the dyed bands of the protein ladder and their MW in KDa. GBF1 MW is 37.1 KDa.

3.2.3 Effect of phosphorylation mimicry on the GBF1 dimerization

Dimerization between bZIPs is postulated to be coupled to their folding, and the BR of some bZIPs has been reported to be unstructured in the absence of DNA (Mason and Arndt, 2004; Yoon et al., 2006; Seldeen et al., 2008). Therefore, I examined whether the dimer formation was affected in the GBF1 mutated versions carrying the aforementioned serine substitutions in the BR. Dimerization was evaluated by BiFC as above, investigating the homodimer formation of each GBF1 version. The results showed that GBF1 mutant with alanine substitutions produced similar fluorescent levels than the native version, while much weaker signals were measured in the mutant with aspartate substitutions (Figure 47). Thus, those results indicated that aspartate but not alanine substitutions interfered with the dimerization.

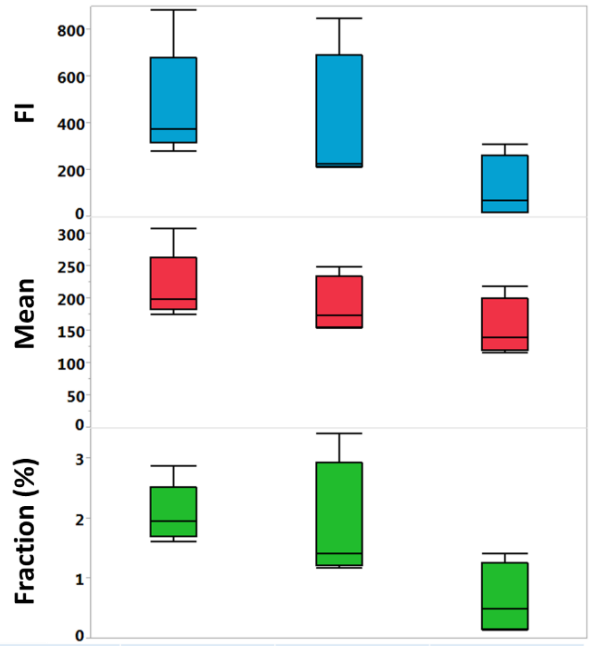

SPN	GBF1	GBF1 3A	GBF1 3D
SPC	GBF1	GBF1 3A	GBF1 3D
%	2.08	1.86	0.63
Mean	218.35	188.77	153.04
FI	474.45	379.71	117.52
n	5	4	4

Figure 47. BiFC with GBF1 phosphorylation mimicry mutants. Represented are box plots showing the fraction of fluorescent cells respect the total population, the mean fluorescent intensity, and the FI. Values are indicated below, together with the number of repetitions (n).

Part 2: Networks of bZIPs: from interaction to function

Given that the bZIP active form is the dimer and different bZIP monomers possess distinctive DNA-binding affinities and transactivation capabilities, bZIP heterodimerization is assumed to operate as a combinatorial mechanism, generating a large diversity of dimers with unique properties by specifically combining a limited set of monomers. However, even though this is presumed to be central feature of the bZIP function, studies confirming this assumption are rare. In this part of my thesis, I challenged the functionality of the bZIP combinatorial mechanism in Arabidopsis by systematically analyzing the relationship between dimerization and function of 16 bZIPs. These belong to different groups according to the Jakoby classification, which is based on the sequence of the BR and other functional domains (Jakoby et al., 2002). Specifically, they are bZIP9, bZIP10, bZIP25, and bZIP63 from the C group, GBF1, GBF2, GBF3, bZIP16, and bZIP68 from the G group, Hy5 and HyH from the H group, and bZIP1, bZIP2, bZIP11, bZIP44, and bZIP53 from the S1 group. Because of the many bZIPs investigated, when dealing with a whole bZIP group I will refer to it with the group defining letter used as a prefix to the "bZIP" acronym (e.g. C-bZIPs or G-bZIPs), and so avoid mentioning each particular bZIP.

According to the literature, the C- and S1-bZIPs dimerize between each other forming an interacting network, and are involved in responses to abiotic stress conditions such as high salt or darkness, carbohydrate homeostasis, and seed development (Ehlert et al., 2006; Hanson et al., 2008; Alonso et al., 2009; Kang et al., 2010; Dietrich et al., 2011; Tomé et al., 2014). On the other hand, G- and H-bZIPs participate in physiologically related processes, such as light signaling and seed development (Shen et al., 2007; Hsieh et al., 2012; Singh et al., 2012; Iglesias-Fernandez et al., 2014). Therefore, it could be suspected that interactions between some of these bZIPs occur, modulating their function. Based on that and on the previous work with GBF1 and S1-bZIPs, those 16 bZIPs were selected for the present study, which has been published in PLOS one.

3.3 Analysis of the dimerization between the 16 bZIP proteins

Analyzing the interaction of a high number of bZIPs represented a challenging task, as the number of possible combinations to be analyzed increases exponentially with the number of monomers studied. Therefore, although I used roughly the same BiFC method as it is explained in the first part, important modifications of the protocol were required. First, protoplast transformations were made in 96-well plates according to the small-scale transformation protocol. Second, in the subsequent flow cytometric analyses, only the fraction of fluorescent counts respect to the total living cells was taken into account. That was decided in order not to neglect weak interactions, as calculating the FI helps discriminating true signals from the background, but it disfavors the identification of weak signals. Third, fluorescence production was determined following a statistical approach by fitting a generalized linear mixed model on the entire dataset in order to estimate an averaged BiFC score for each bZIP combination. That was referred as the BiFC score.

The experimental part of this work was performed with the collaboration of Dr. Kenneth W. Berendzen and Stefan Mahn, while data were processed by or with the assistance of Dr. Waqas Ahmed Malik and Dr. Hans-Peter Piepho from the University of Hohenheim, Germany.

3.3.1 Generation and testing of a dimerization matrix for 16 bZIP proteins

BiFC assays were performed following a double design, so that the analysis of the 16 bZIPs, each one tested in both fusion conformations, resulted in a 16x16 matrix, representing the 120 reciprocal bZIP combinations plus the 16 homodimers (Figure 48). Because each combination of two bZIPs was tested twice (either as SPN or as SPC fusions), the reciprocity between the results generated from equivalent pairs of bZIPs was evaluated in order to substantiate the data. Amongst the 120 comparisons tested only eight resulted significantly different, this is to say, in those cases the two fusion conformations led to different results (Figure 48).

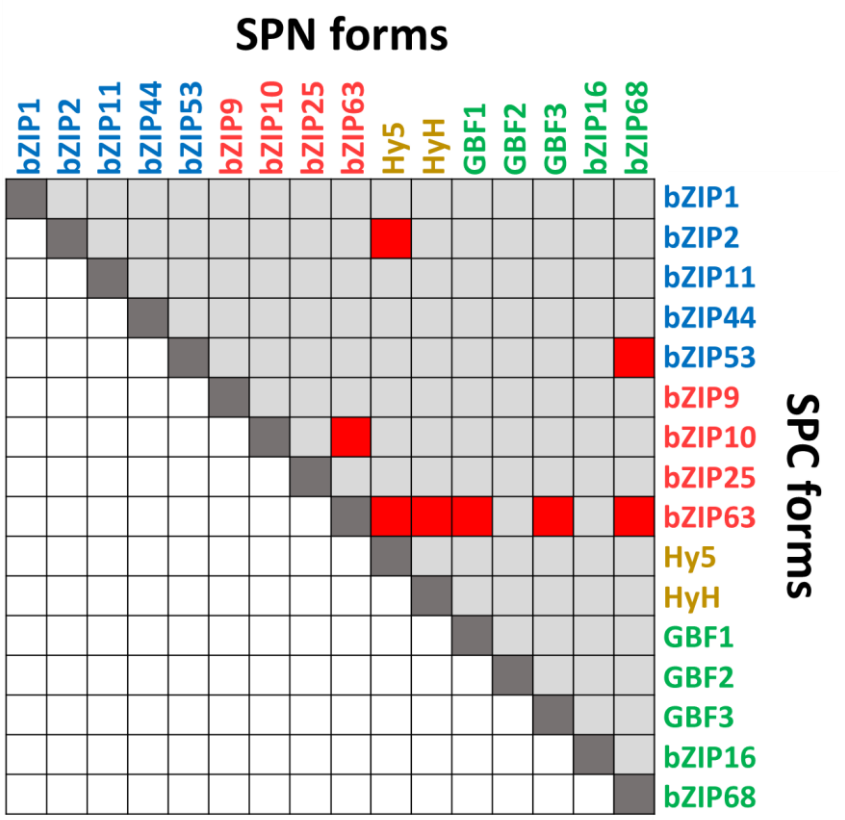

Figure 48. Reciprocal matrix with the 256 combinations tested. Each bZIP pair was tested in the two fusion conformation represented by the white and light grey squares, with the exception of the homodimers, in dark grey. The different colors indicate the bZIP groups: blue are S1-bZIPs, red are C-bZIPs, yellow are H-bZIPs, and green are G-bZIPs. Red squares on the upper side of the matrix indicate those pair comparisons between reciprocal bZIP combinations which resulted significant.

Notwithstanding, the inspection of those eight discordant results showed that six of them affected the protein bZIP63. To explain why bZIP63 concentrated so many disparate measurements, I compared the means for each row and for each column, which are known are marginal means. The most striking difference arose between the bZIP63-SPN column in comparison to the rest of rows and columns, indicating that the measurements involving bZIP63-SPN were inconsistent with the rest of the dataset (Table 8). That outcome hinted at that particular arrangement of the fluorescent protein fragments either enhancing the fluorescence production or easing the split YFP reconstitution.

Level	bZIP63-SPN	GBF3-SPC	GBF1-SPC	GBF1-SPN	bZIP16-SPN	GBF2-SPC	Hy5-SPC	bZIP16-SPC	bZIP63-SPC	GBF3-SPN	Hy5-SPN	bZIP1-SPN	HyH-SPC	bZIP68-SPC	bZIP68-SPN	GBF2-SPN	bZIP2-SPC	bZIP53-SPC	HyH-SPN	bZIP1-SPC	bZIP2-SPN	bZIP10-SPC	bZIP53-SPN	bZIP25-SPN	bZIP25-SPC	bZIP11-SPC	bZIP10-SPN	bZIP44-SPN	bZIP11-SPN	bZIP44-SPC	bZIP9-SPC	bZIP9-SPN
Group	A																															
		B	B	B	B	B	B	B	B	B	B	B	B	B	B	B	B	B	B	B	B	B	B									
			C	C	C	C	C	C	C	C	C	C	C	C	C	C	C	C	C	C	C	C	C	C	C								
							D	D	D	D	D	D	D	D	D	D	D	D	D	D	D	D	D	D	D	D	D	D					
								E	E	E	E	E	E	E	E	E	E	E	E	E	E	E	E	E	E	E	E	E	E				
									F	F	F	F	F	F	F	F	F	F	F	F	F	F	F	F	F	F	F	F	F	F			
											G	G	G	G	G	G	G	G	G	G	G	G	G	G	G	G	G	G	G	G	G	G	G

Table 8. Connecting Letters Report comparing the means of all the measurements for each bZIP in the two fusion conformations. Levels not connected by a common letter are significantly different (α=0.05). From Llorca et.al, 2015.

In order to determine if the anomalous bZIP63-SPN values altered the pattern of interaction or just the intensity of the fluorescence, I calculated the similarity between the interaction profiles obtained for with the two fusion conformations of bZIP63. The Pearson's correlation coefficient indicated that both profiles were positively correlated in a significant manner (Figure 49). That meant that the disparate BiFC scores measured were caused by an enhanced fluorescence production, without modifying the relative proportions calculated for each bZIP combination. In that manner, I could confirm the reciprocity of the bZIP63 measurements. Still, the bZIP63-SPN measurements were excluded for comparison purposes in further analyses because of their different range.

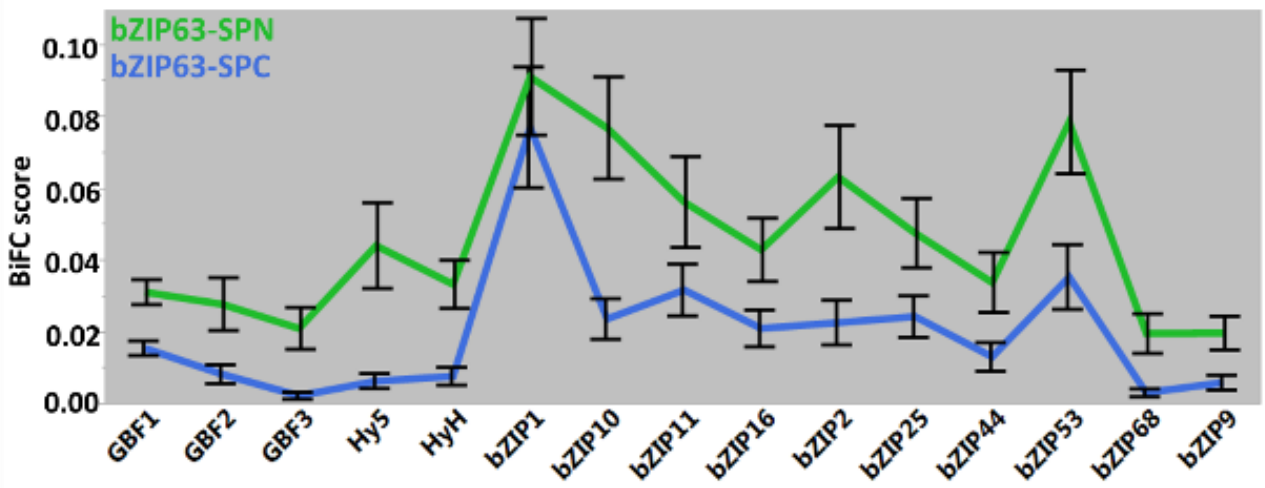

Figure 49. Comparison of the interaction profiles of bZIP63-SPN (green) and bZIP63-SPC (blue) along the different bZIP partners tested. Represented are the BiFC score means and their standard errors. Pearson's correlation coefficient calculated was R=0.835 and p-value <0.001.

3.3.2 Clustering of the dimerization matrix

Then, to better explore the data and uncover similarities among the interaction patterns of the 16 bZIPs, the matrix with the calculated BiFC scores was represented as a heat map. The rows and columns were arranged by hierarchical clustering independently for each fusion conformations (i.e. for rows and for columns), resulting in equivalent outcomes (Figure 50). The main discrepancy between the outcome for rows and columns was the positioning of bZIP63 due to the discordant values of bZIP63-SPN mentioned above, which formed a distinct single-leafed clade in the column (SPN) clustering. Even so, bZIP63 was still grouped with the C- and S1-bZIPs in both outcomes.

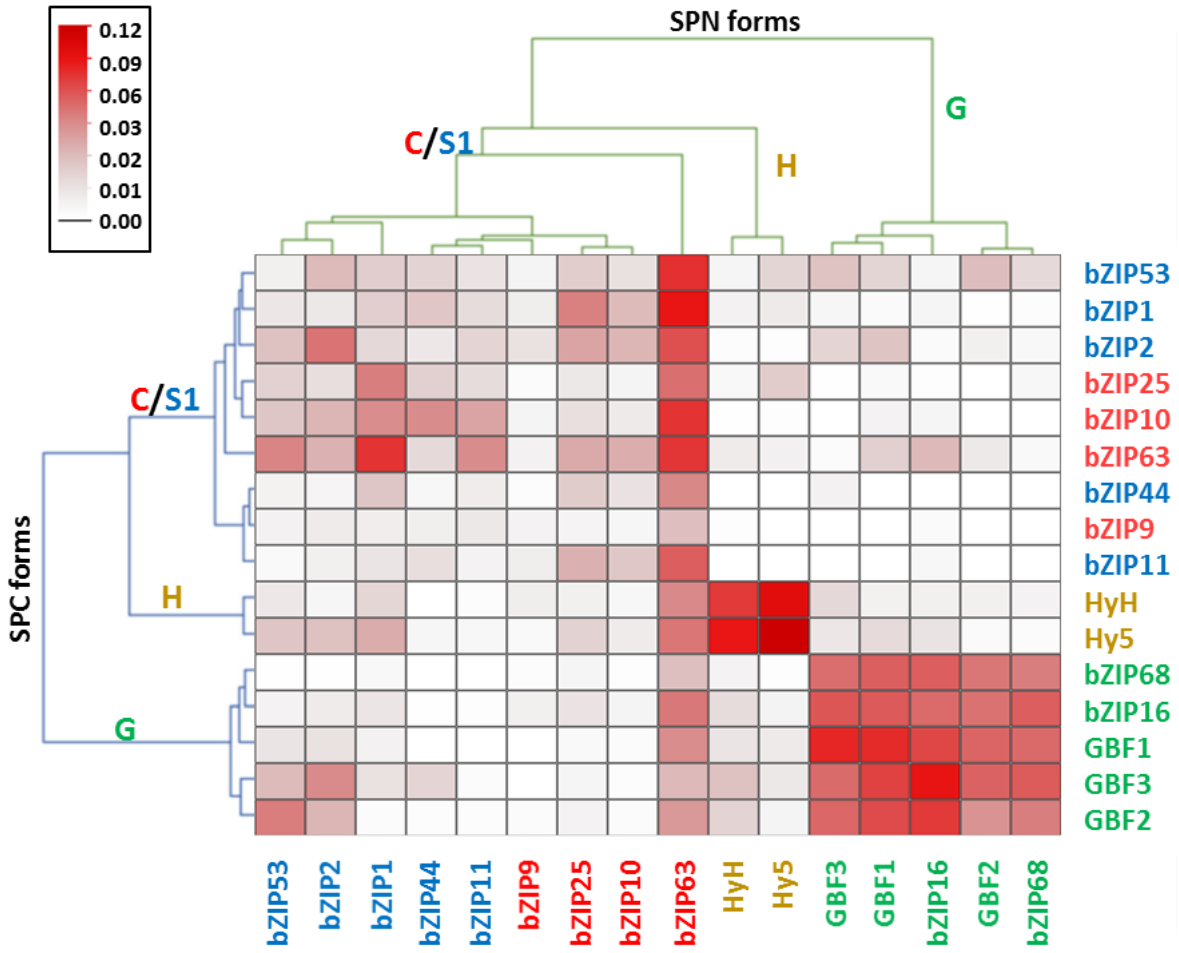

Figure 50. Clustered heat map. The clustering was performed independently for the SPN and the SPC conformations resulting in three main clusters that correlate to the different bZIP groups in the Jakoby classification, which are indicated by their group defining letter. The increasing intensity of the red color corresponds to the higher BiFC scores, according to the color scale. From Llorca et.al, 2015.

Three main clusters were formed: the first one included the G-bZIPs, the second one the H-bZIPs, while the third one comprised the C- and S1-bZIPs together. The G-bZIPs were the most divergent, as judged by the linkage distance. Congruently, the heat map displayed a sharp contrast in the coloring intensity of the homotypic dimers (between two G-bZIPs) and the heterotypic ones (formed by one G-bZIPs and a bZIP from

another group). A similar pattern was obtained for the H-bZIPs, with a clear contradistinction between the homotypic and the heterotypic dimers.

Overall, the C and S1-bZIPs displayed profiles with low BiFC scores in general. Even so, an increase in the signal of the heterotypic interactions (between one C-bZIP and one S1-bZIP) was recognizable (Figure 51). The highest BiFC scores calculated for the C-bZIPs resulted in their combinations with the S1-bZIPs, and vice versa, the S1-bZIPs led to their highest values when interacting with the C-bZIPs. In other words, the profiles for these two classes of bZIPs (i.e. C and S1) complemented each other's, in spite of forming a same dendogram clade.

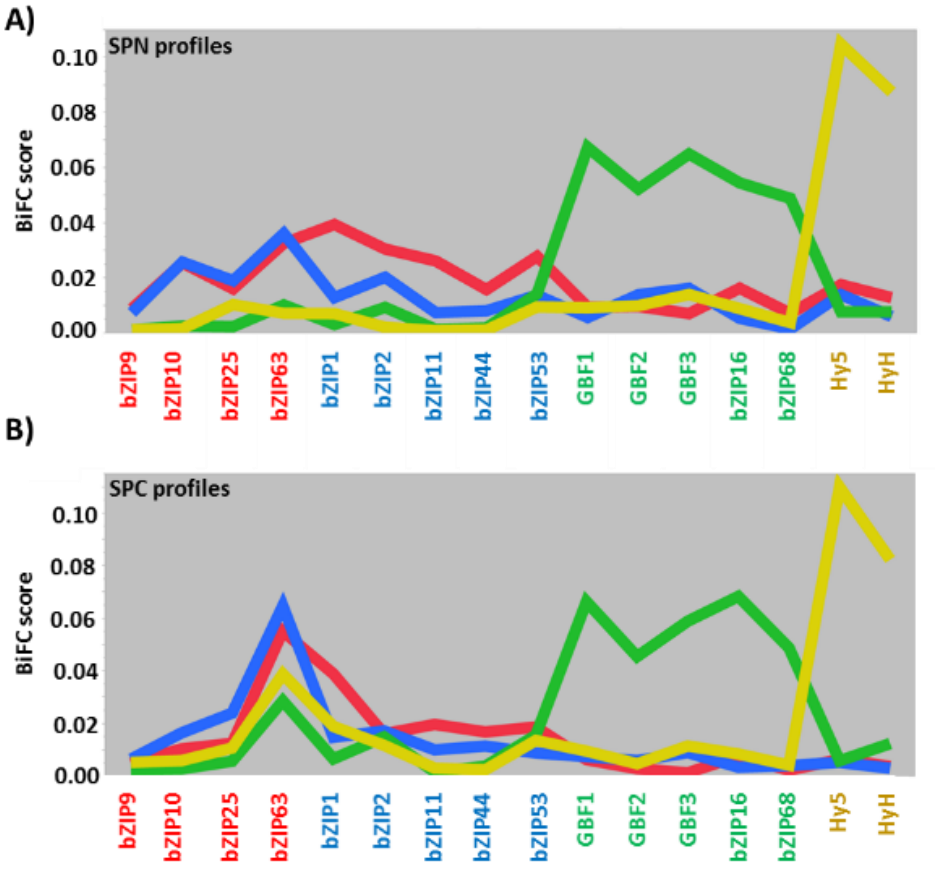

Figure 51. Interaction profiles of the 16 bZIPs. Represented are the BiFC score means for an entire group according to their classification: blue are S1-bZIPs, red are C-bZIPs, yellow are H-bZIPs, and green are G-bZIPs. A) Column profiles of the SPN fusion conformations. B) Row profiles of the SPC fusion conformations. From Llorca et.al, 2015.

Altogether, the BiFC assay uncovered an interesting viewpoint on bZIP function, for the analysis of the dimerization arranged the bZIPs almost in the same manner as in the Jakoby classification. This is a remarkable fact since that classification is not based on the sequence of the dimerization motif (the LZ), but on the sequence of the DNA-binding motif , as well as other functional domains (Jakoby et al., 2002). Therefore, those results suggested that a given pattern of dimerization is associated to certain functional features.

3.3.3 Analysis of the dimerization strength

Protein-fragment Complementation Assays (PFCA), such as BiFC, can provide information about the relative affinities of the interactions if they are analyzed quantitatively. In these methods, the measured signal is positively scalar to the amount of reporter protein reconstituted, and that in turn, relies on the strength of the interaction (Kerppola, 2008; Morell et al., 2008; Gehl et al., 2011; Li et al., 2011; Wang and Carnegie, 2013). According to that, the analysis of the interaction matrix revealed pronounced differences amongst the estimated BiFC scores, suggesting that different bZIP dimers were formed with distinctive interaction strengths.

In order to assess that possibility, I examined the expression levels achieved by the different fusion proteins in the transiently transformed protoplasts, to determine whether the different bZIPs were expressed at the same level (Figure 52). Western blot results showed that the protein amounts detected for the 16 bZIPs were differing, although they were mostly coinciding between the two conformations of each bZIP (SPN and SPC fusions), substantiating each other. Besides, protein levels resulted quite homogeneous among bZIPs belonging to the same group (the H- and S1-bZIPs led to bulky protein bands, while the C- and G-bZIPs produced weak bands), suggesting that they were specific for each bZIP group.

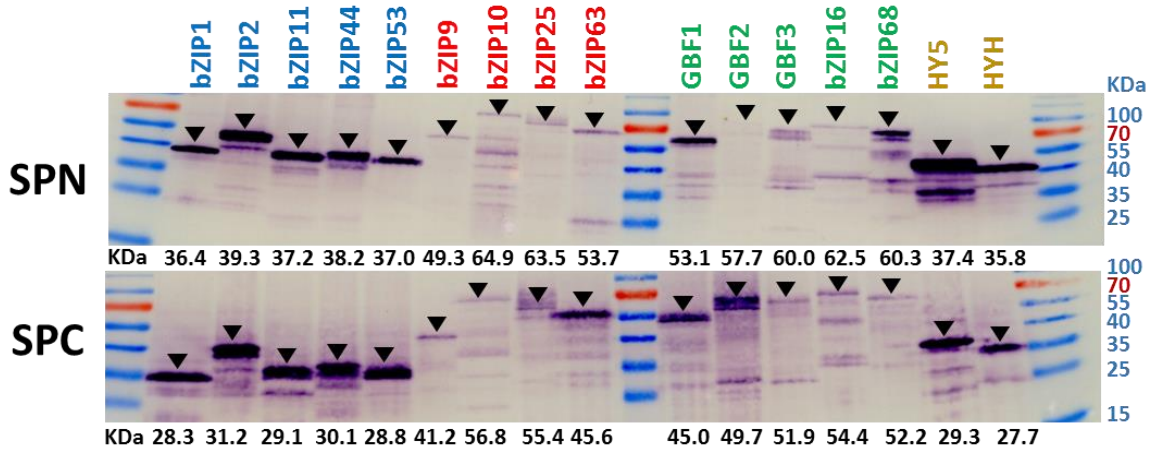

Figure 52. Western blot of protein extracts from protoplasts. For each sample 7 µg of total protein were loaded after pooling together protoplasts from four different transformations (small scale). The top membrane (SPN) was incubated with anti-Myc, and the bottom one (SPC) with anti-HA. The bands with the expected sizes are indicated with arrows. Notice that bZIPs migrate with a greater apparent MW than calculated, as it has been reported before (Yoon et al., 2006). From Llorca et.al, 2015.

Those variations in the detected proteins did not correlate with the differences in the BiFC scores. For instance, the G-bZIPs produced very high BiFC scores but they resulted in weak protein bands and, conversely, the S1-bZIPs resulted in low BiFC scores but huge amounts of detected protein. Moreover, each bZIP led to distinctive signal strengths as the dimerizing partners alternated, so that the differences in the BiFC scores could not be attributed to unequal expression of the fusion proteins. Therefore, I assumed that the BiFC scores were a distinctive feature of each bZIP pair tested and they could be used to compare the affinity of the interactions.

Then, I established the groups to be compared according to the interaction profiles outlined in Figure 51, and excluding the values from bZIP63-SPN combinations. The first group included homotypic dimers between G-bZIPs, and the second one between H-bZIPs, while three more groups were formed for the C- and S1-bZIPs:

two comprising only the homotypic dimers of each bZIP class (either C-bZIPs, or S1-bZIPs), and a third one with the heterotypic heterodimers (Figure 53 A). Finally, the rest of combinations were used to set an additional "catchall" group.

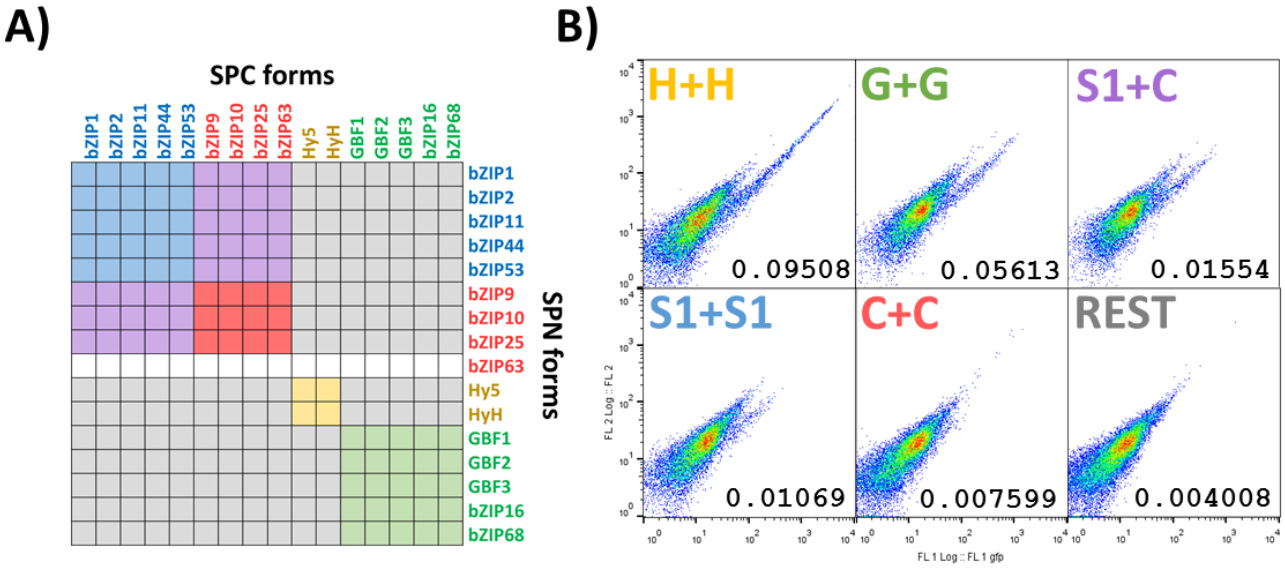

Figure 53. A) Scheme of matrix division into the groups to be compared. Elements of the table with the common color belong to the same group. Blue are homotypic combinations of S1-bZIPs, red are homotypic combinations of C-bZIPs, purple are heterodimers between C- and S1-bZIPs, yellow are homotypic combinations of H-bZIPs, green are homotypic combinations of G-bZIPs, light grey are the rest of combinations. Notice that bZIP63-SPN values were not used, they are indicated in dark grey. B) Flow cytometry outputs representative for each of the six groups and their adjusted BiFC score means. Figures and caption are from Llorca et.al, 2015, modified.

A mean BiFC score was calculated for each of the six groups (Figure 53 B) and they were compared statistically, resulting all groups significantly different from the others (Figure 53). The highest means were calculated for the groups comprising the homotypic dimers for H- and G-bZIPs, in agreement with their outstanding coloring in the heat map. These were followed by the heterotypic heterodimers between C- and S1-bZIPs, the homotypic S1-bZIP dimers, and the homotypic C-bZIP dimers; and that precise order was in agreement with the quantitative results presented by a previous report (Ehlert et al., 2006), substantiating the use of the BiFC scores for estimating the dimerization strength made here. Finally, the catchall group resulted in the lowest BiFC mean, in agreement with the fact that most of the negative interactions fell into that group. Therefore, those results indicated that homotypic dimers for C- and H-bZIPs are much more stable than any dimer formed between the C- and/or S1-bZIPs, and verified the preferential heterotypic heterodimerization between C- and S1-bZIPs previously described (Ehlert et al., 2006; Kang et al., 2010)

Comparison	Estimate	Standard Error	Adj P
H-G	0.5692	0.1106	<.0001
H-S1C	18.954	0.1287	<.0001
H-S1	22.750	0.1340	<.0001
H-C	26.189	0.1506	<.0001
H-catch	32.624	0.1086	<.0001
G-S1C	13.261	0.08236	<.0001
G-S1	17.058	0.09067	<.0001
G-C	20.497	0.1131	<.0001
G-catch	26.932	0.05274	<.0001
S1C-S1	0.2850	0.07586	0.0002
S1C-C	0.7236	0.1005	<.0001
S1C-catch	13.670	0.07308	<.0001
S1-C	0.3439	0.1065	0.0025
S1-catch	0.9874	0.08224	<.0001
C-catch	0.6434	0.1063	<.0001

Table 9. Comparison of the groups BIFC scores (only the group-defining letter are indicated). The groups were tested using the Estimate statement of Proc Glimmix. The resulting p-values were adjusted using the Scheffé method (Scheffe, 1953). Notice that estimates values are on logit scale.

3.3.4 Establishment of a dimerization map for the 16 bZIPs studied

To provide a graphic representation of the data, I generated a map of the interactions taking place among the 16 bZIPs. A criterion was established delimiting which combinations were positive and which negative on the basis of the group means represented in Figure 53 B, and aiming to reflect the variability of the data as well as the reciprocity between the two alternative conformations of the protein fusion. The cutoff BiFC score was set up to a value of 0.01, and the whole standard error interval was required to be above that threshold for each pair of equivalent results in order for a combination to be considered as a positive interaction (Table 10). Naturally, the reciprocity criterion was not applied to the homodimers, as they cannot be tested in alternative conformations; and neither to the bZIP63 combinations as the values involving bZIP63-SPN were excluded.

Ex.	SPN	SPC	Mean	St. Error	MSEMI	MSEMI>0.01	Interaction
1	bZIP2	bZIP10	0,02216	0,005839	0,016321	Yes	Yes
	bZIP10	bZIP2	0,02226	0,006059	0,016201	Yes	
2	bZIP1	Hy5	0,02417	0,006492	0,017678	Yes	No
	Hy5	bZIP1	0,008389	0,002579	0,00581	No	
3	bZIP25	GBF1	0,003345	0,001437	0,001908	No	No
	GBF1	bZIP25	0,003241	0,001138	0,002103	No	

Table 10. Three examples of the definition of interaction. Example 1 is considered as interaction, whereas examples 2 and 3 are not. SPN and SPC indicate which bZIP is fused to each YFP fragment. MSEMI stands for minimum standard error interval, calculated as mean-SEM.

In total, 43 bZIP pairs were considered as interacting out of the 136 different bZIP combinations tested, and their representation illustrated three main networks (Figure 54). The largest one was the already identified C/S1 network (Ehlert et al., 2006; Kang et al., 2010), in which heterotypic dimers were preferentially established, hence, more abundant. However, the outcome presented here identified less dimers formed within that network than in the other studies. These discrepancies are likely to result, to a great extent, from the different criteria followed in order to consider a result as a positive interaction. In this work, unlike the others, the absence of reciprocity was taken as a discriminating criterion for interaction, thus making it more conservative. Still, it was remarkable that the three independently determined C/S1 networks shared

coincidences such as identifying bZIP9 and bZIP63 as the bZIPs establishing the less and the most interactions, respectively.

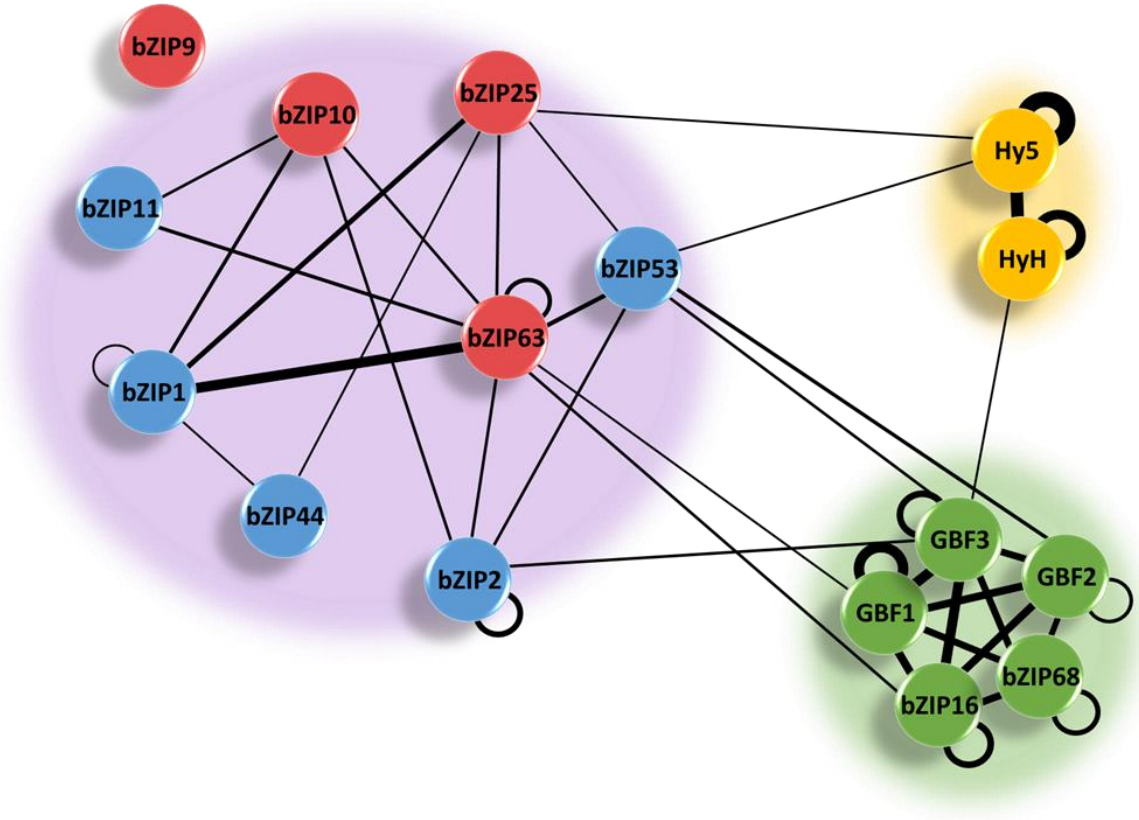

Figure 54 . Interaction map of the 16 bZIPs based on a cutoff of 0.01. The width of the connecting lines is proportional to the BiFC score mean for the two bZIPs connected, relative to the Hy5 homodimer (which exhibited the highest BiFC score). From Llorca et al., 2015.

The other two networks depicted consisted of only homotypic dimers, either of G-bZIPs or H-bZIPs, therefore they were named the G and the H networks, respectively. Members within these two networks could dimerize with themselves with an absolute lack of specificity, consistent with other observations (Schindler et al., 1992a; Holm et al., 2002; Shen et al., 2008; Shaikhali et al., 2012). Beyond those three networks, there was a substantial lack of interactions and only few sporadic dimers were identified interconnecting the different networks.

3.4 Bioinformatic dissection of the LZs sequences

In silico prediction of bZIP proteins is based on the identification of the bZIP signature as a whole, including the BR and the LZ domains (Riechmann et al., 2000; Jakoby et al., 2002; Deppmann et al., 2004). However, because the BR is highly conserved, it could have a higher impact than the LZ in the bZIP annotation process, so that singularities in the LZ could have been overlooked. The LZ motifs of the 16 bZIPs analyzed in this work were previously predicted to be different in length: the C- and S1-bZIPs LZs were calculated to be longer, with

up to 10 heptad repetitions, while the G- and H-bZIPs would feature short LZs with 5 and 4 heptads respectively (Jakoby et al., 2002; Deppmann et al., 2004; Deppmann et al., 2006). Because the G and H network dimers (with shorter LZs) resulted in conspicuously higher BiFC scores than C/S1 network dimers (with longer LZs), I enquired whether the differential lengths of the LZs could be the reason for the different affinities of the bZIP dimers. Therefore, I analyzed *in silico* different aspects of the LZs of the 16 bZIPs in order to asses such possibility.

3.4.1 Motif prediction

First, I estimated the probability of coiled coil and LZ formation in order to verify previous predictions. For that purpose, I made use of two different prediction programs, 2ZIP and COILS programs (Lupas et al., 1991; Bornberg-Bauer et al., 1998). As expected, the coils program computed coiled coil motifs in all bZIP sequences, spanning not only the previously predicted LZ regions but also entering into the BRs (Figure 55). Remarkably, the coiled coil motifs estimated for the LZ regions of the G- and H-bZIPs were clearly defined for all window sizes analyzed, while in the C- and S1-bZIPS predictions for smaller window sizes resulted in worse defined profiles, with areas of lower coiled coil probability, and defining a depression around the center of the LZ sequences. Therefore, the COILS predictions revealed that the different bZIPs presented particularities in their LZs, and those were consistent among the members of the same interaction network. Indeed, they correlated with the differences in the interaction strength, for bZIPs with well-defined coiled coil predicted motifs exhibited the higher BiFC scores (i.e. C- and H-bZIPs), whereas bZIPs with less confident predictions displayed lower BiFC scores (i.e. C- and S1-bZIPs).

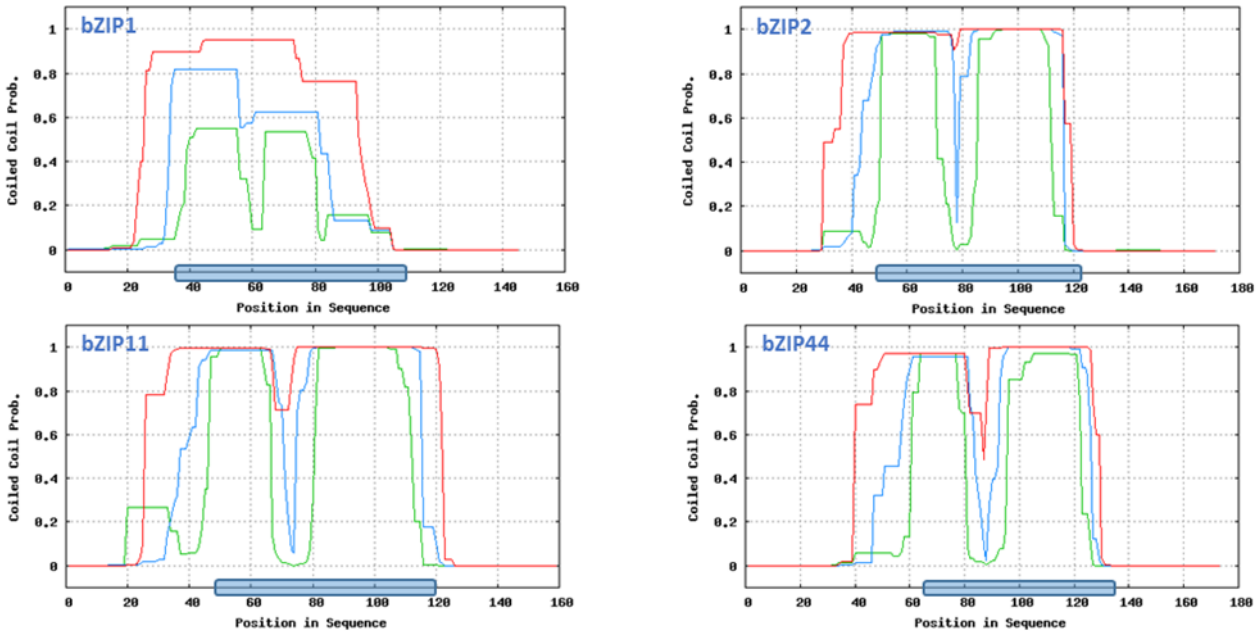

Figure 55. (This and following page). COILS outputs indicating the probability of each residue to for a coiled coil. Green, blue, and red lines indicate a window prediction of 14, 21, or 28 residues respectively. The blue bar at the bottom represents the region corresponding to the previously predicted LZs, starting from the heptad 0 and spanning for 10 heptads in the C- and S1-bZIPs, 7 heptads in the G-bZIPs, and 5 heptads in the H-bZIPs. From Llorca et al., 2015.

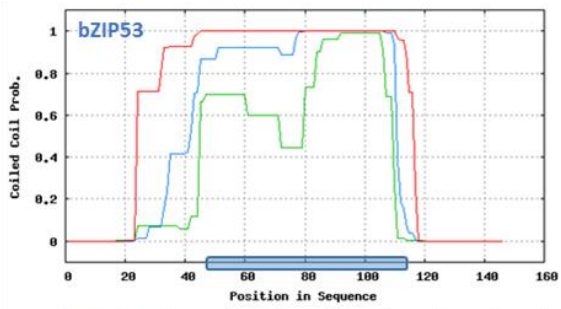
bZIP53
Coiled Coil Prob.
Position in Sequence

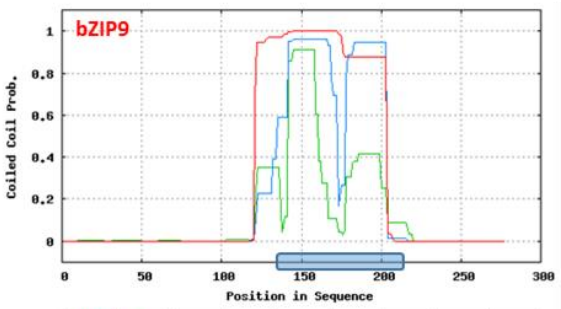
bZIP9
Coiled Coil Prob.
Position in Sequence

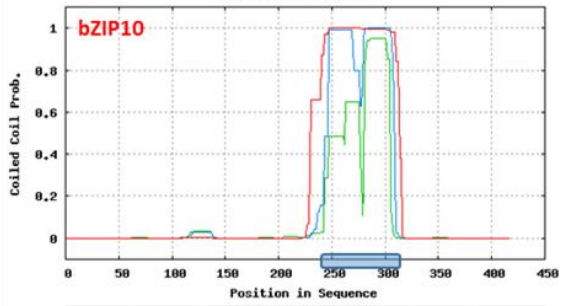
bZIP10
Coiled Coil Prob.
Position in Sequence

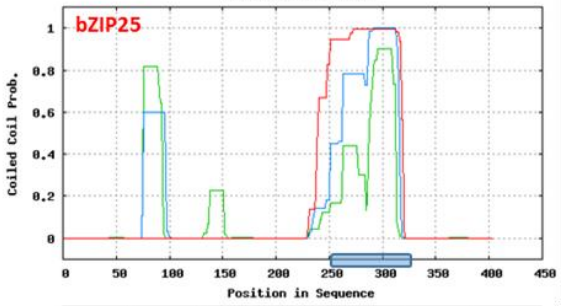
bZIP25
Coiled Coil Prob.
Position in Sequence

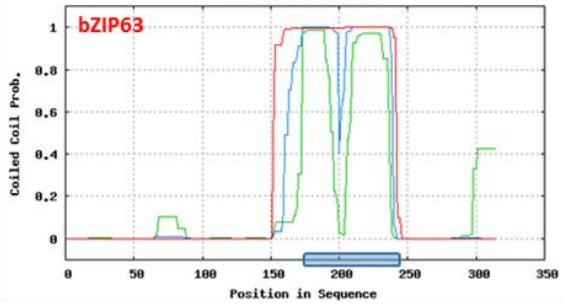
bZIP63
Coiled Coil Prob.
Position in Sequence

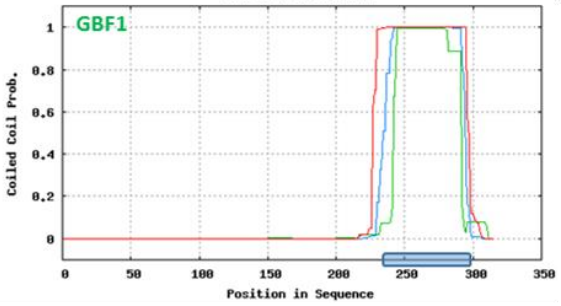
GBF1
Coiled Coil Prob.
Position in Sequence

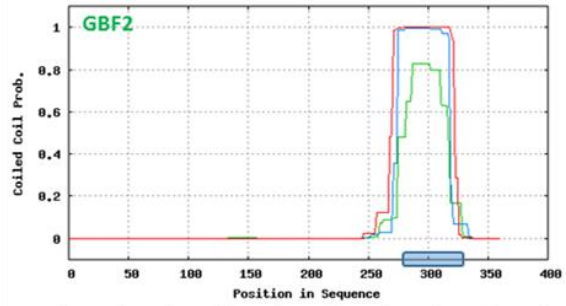
GBF2
Coiled Coil Prob.
Position in Sequence

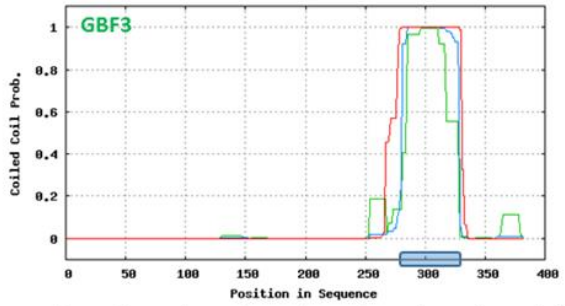
GBF3
Coiled Coil Prob.
Position in Sequence

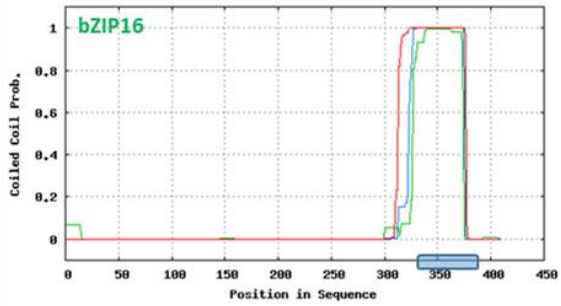
bZIP16
Coiled Coil Prob.
Position in Sequence

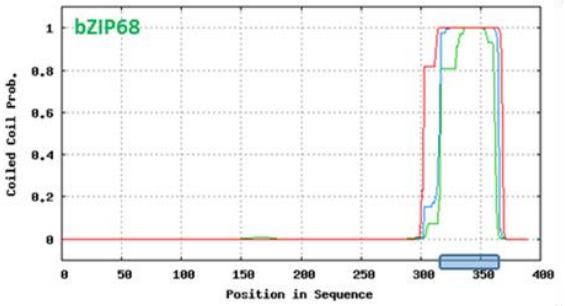
bZIP68
Coiled Coil Prob.
Position in Sequence

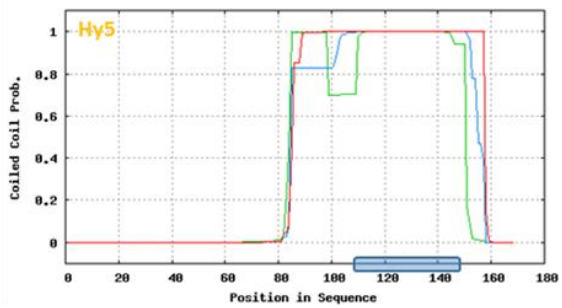
Hy5
Coiled Coil Prob.
Position in Sequence

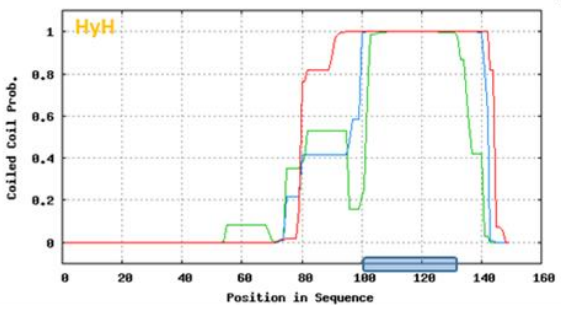
HyH
Coiled Coil Prob.
Position in Sequence

Predictions with the 2ZIP program were even more astonishing, since the LZs sequences in the C- and S1-bZIPs were indeed not predicted to form such motifs. Only for bZIP11 a short LZ motif was predicted between heptads four and seven (Figure 56). Still, 2ZIP predicted coiled coil motifs for all the C- and S1-bZIPs, but those did not span along all the LZ sequence. The longest predicted coiled coils were those of bZIP63 and bZIP53, with eight heptads, whereas the shorter one was calculated for bZIP9, with only three repeats; an intriguing remark, recalling that bZIP63 established the most interactions in the BiFC assay, while bZIP9 established none. Also very interesting was the fact that two separated coiled coil motifs were computed for bZIP25, bZIP44, bZIP2, and bZIP11, suggesting that these bZIPs either carry a bipartite interacting motif or can establish alternate conformations of the coiled coil motif. Besides, for bZIP1 and, especially, bZIP9 the predicted coiled coils were much shorter than in the other C- or S1-bZIPs. Those unexpected results revealed a greater heterogeneity in the bZIP dimerization motif than had been anticipated, and even questioned the classification as LZs (though not the coiled coil) of the so far so assumed sequences in the C- and S1-bZIPs. Therefore, those sequences were from there on referred more generally as coiled coil only.

		H0	H1	H2	H3	H4	H5	H6	H7	H8	H9
		abcdefg	abcdefg	abcdefg	abcdefg	abcdefg	abcdefg	abcdefg	abcdefg	abcdefg	abcdefg
bZIP1	CCCCCCC	CCCCCCC	CCCCCCC	CCCCCCC	CCCCCCC	CCCCCCC	CCCCCCC	-------	-------	-------	-------
bZIP2	CCCCCCC	CCCCCCC	CCCCCCC	CCCCCCC	-------	CCCCCCC	CCCCCCC	CCCCCCC	CCCCCCC	CCCCCCC	-------
bZIP11	CCCCCCC	CCCCCCC	CCCCCCC	-------	-------	CCCLZLZ	LZLZLZL	ZLZLZLZ	LZLZCCC	CCCCCCC	CCCCCCC
bZIP44	CCCCCCC	CCCCCCC	CCCCCCC	-------	-------	CCCCCCC	CCCCCCC	CCCCCCC	CCCCCCC	CCCCCCC	-------
bZIP53	CCCCCCC	CCCCCCC	CCCCCCC	CCCCCCC	CCCCCCC	CCCCCCC	CCCCCCC	CCCCCCC	CCCCCCC	CCCCCCC	-------
bZIP9	CCCCCCC	CCCCCCC	CCCCCCC	CCCCCCC	CCCCCCC	-------	-------	-------	-------	-------	-------
bZIP10	CCCCCCC	CCCCCCC	CCCCCCC	CCCCCCC	CCCCCCC	CCCCCCC	CCCCCCC	CCCCCCC	CCCCCCC	CCCCCCC	-------
bZIP25	CCCCCCC	CCCCCCC	CCCCCCC	CCCCCCC	-------	CCCCCCC	CCCCCCC	CCCCCCC	CCCCCCC	CCCCCCC	-------
bZIP63	CCCCCCC	CCCCCCC	CCCCCCC	CCCCCCC	CCCCCCC	CCCCCCC	CCCCCCC	CCCCCCC	CCCCCCC	CCCCCCC	-------
GBF1	CCCCCCC	CCCLZLZ	LZLZLZL	ZLZLZLZ	LZLZLZL	ZLZLZLZ	LZLZLZL	ZLZLCCC	-------	-------	------
GBF2	-------	CCCLZLZ	LZLZLZL	ZLZLZLZ	LZLZLZL	ZLZLZLZ	LZLZCCC	-------	-------	-------	-------
GBF3	CCCCCCC	CCCLZLZ	LZLZLZL	ZLZLZLZ	LZLZLZL	ZLZLZLZ	LZLZCCC	-------	-------	-------	-------
bZIP16	CCCCCCC	CCCLZLZ	LZLZLZL	ZLZLZLZ	LZLZLZL	ZLZLZLZ	LZLZCCC	-------	-------	-------	-------
bZIP68	CCCCCCC	CCCLZLZ	LZLZLZL	ZLZLZLZ	LZLZLZL	ZLZLZLZ	LZLZCCC	-------	-------	-------	-------
Hy5	CCCCCCC	CCCLZLZ	LZLZLZL	ZLZLZLZ	LZLZLZL	ZLZLCCC	CCCCCCC	-------	-------		
HyH	CCCCCCC	CCCLZLZ	LZLZLZL	ZLZLZLZ	LZLZLZL	ZLZLCCC	-------	-----			

Figure 56. Summary of the 2ZIP predictions of the coiled coil (CC, blue) and LZ (LZ, red) motifs for the theoretical LZ sequences of the 16 bZIP proteins. The heptads are numbered based on previous numbering (Deppmann et al., 2004). From Llorca et al., 2015.

3.4.2 Sequence analysis

Then, to try to understand the particularities of the coiled coils in the C- and S1-bZIPs, I took a closer look at their amino acid sequences discovering revealing aspects in the sequences of those bZIPs. First, several of the **d** positions are not occupied by a leucine residue, which is the most stabilizing amino acid in that position and hallmark of the LZ motif (Moitra et al., 1997). Specifically, the third and fourth heptads of all C- and S1-bZIPs, as well as the second heptad of the S1-bZIPs, do not feature a leucine in their **d** positions (Figure 57). Instead, they carry amino acids with low stabilizing properties or even destabilizing, such as the β-branching valine and isoleucine, threonine or alanine (Moitra et al., 1997; Tripet et al., 2000; Reinke et al., 2013).

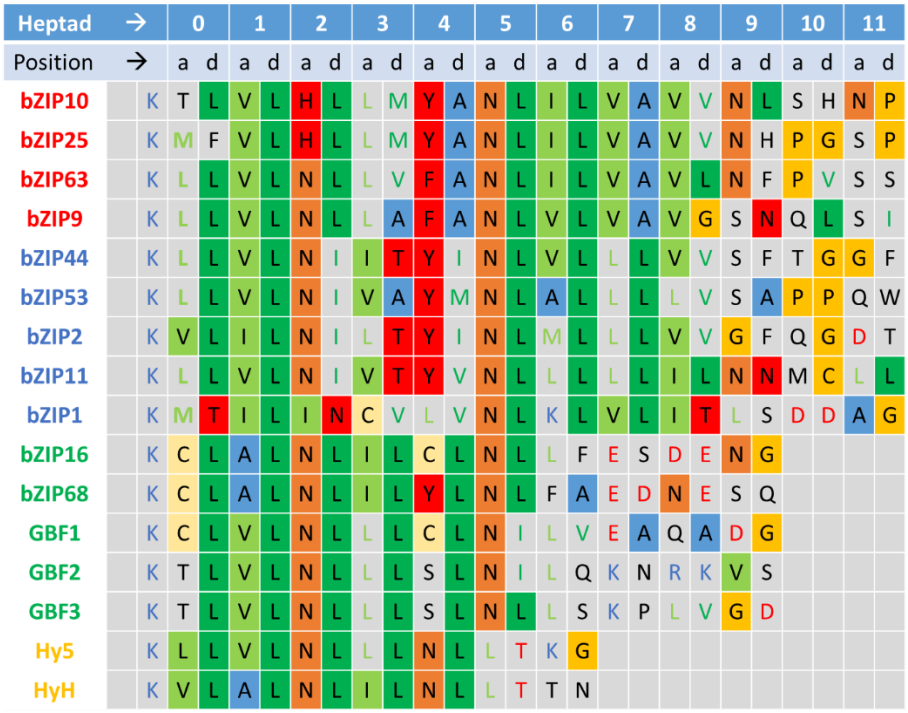

Heptad →		0		1		2		3		4		5		6		7		8		9		10		11	
Position →		a	d	a	d	a	d	a	d	a	d	a	d	a	d	a	d	a	d	a	d	a	d	a	d
bZIP10	K	T	L	V	L	H	L	L	M	Y	A	N	L	I	L	V	A	V	V	N	L	S	H	N	P
bZIP25	K	M	F	V	L	H	L	L	M	Y	A	N	L	I	L	V	A	V	V	N	H	P	G	S	P
bZIP63	K	L	L	V	L	N	L	L	V	F	A	N	L	I	L	V	A	V	L	N	F	P	V	S	S
bZIP9	K	L	L	V	L	N	L	L	A	F	A	N	L	V	L	V	A	V	G	S	N	Q	L	S	I
bZIP44	K	L	L	V	L	N	I	I	T	Y	I	N	L	V	L	L	L	V	V	S	F	T	G	G	F
bZIP53	K	L	L	V	L	N	I	V	A	Y	M	N	L	A	L	L	L	L	V	S	A	P	P	Q	W
bZIP2	K	V	L	I	L	N	I	L	T	Y	I	N	L	M	L	L	L	V	V	G	F	Q	G	D	T
bZIP11	K	L	L	V	L	N	I	V	T	Y	V	N	L	L	L	L	L	I	L	N	N	M	C	L	L
bZIP1	K	M	T	I	L	I	N	C	V	L	V	N	L	K	L	V	L	I	T	L	S	D	D	A	G
bZIP16	K	C	L	A	L	N	L	I	L	C	L	N	L	L	F	E	S	D	E	N	G				
bZIP68	K	C	L	A	L	N	L	I	L	Y	L	N	L	F	A	E	D	N	E	S	Q				
GBF1	K	C	L	V	L	N	L	L	L	C	L	N	I	L	V	E	A	Q	A	D	G				
GBF2	K	T	L	V	L	N	L	L	L	S	L	N	I	L	Q	K	N	R	K	V	S				
GBF3	K	T	L	V	L	N	L	L	L	S	L	N	L	L	S	K	P	L	V	G	D				
Hy5	K	L	L	V	L	N	L	L	L	N	L	L	T	K	G										
HyH	K	V	L	A	L	N	L	I	L	N	L	L	T	T	N										

Figure 57. Amino acid composition of the buried hydrophobic positions **a** and **d**. Color code: green background indicates optimal positioning of the hydrophobic residues, whereby a distinction is made between the β-branched isoleucine and valine in **a** positions (light green) and the Leucine in **d** positions (dark green). Congruently, the green letters indicate suboptimal, but still hydrophobic residues, in the **d** position Met, Ile, and Val (in decreasing order of stability), and in the **a** positions Met and Leu. Asn in **a** positions are colored in orange background: paired to other asparagine results stabilizing, otherwise destabilizing. Alanine induces a significant decrease in the stability in comparison to the optimal amino acids either in the **a** or in the **d** positions, but it is in blue background as it is used as a base for determining the relative variations in the stability of the other amino acids. Residues in red background indicate residues that they are destabilizing respect the alanine. Besides, amino acids colored in red and blue are negatively and positively charged residues respectively, in light yellow background are Cys and in dark yellow background are Gly and Pro, α-helix disruptors. From Llorca et al., 2015.

Furthermore, the majority of the **a** positions in those very same heptads do not bear the most stabilizing amino acids, which in this position would be β-branching (Acharya et al., 2002; Acharya et al., 2006). Contrarily, the **a** position of the fourth heptad in all the C- and S1-bZIPs except for bZIP1, is occupied by tyrosine or phenylalanine, two bulky aromatic amino acids which are rarely found in that position and could produce inter-helical clashes inducing local structural disturbances in the supercoil structure (Wagschal et al., 1999; Shin et al., 2006). Besides, bZIP1, bZIP10, and bZIP25 lack the asparagine residue in the **a** position of the second heptad. Asparagine residues in **a** positions are stabilizing when they are paired with another asparagine in the equivalent position of the opposing helix, but they are destabilizing with other residues (Arndt et al., 2000; Acharya et al., 2002). Therefore, these bZIPs would be favored to dimerize between themselves, rather than the other C- and S1-bZIPs. However, the second heptad of bZIP10 and bZIP25 carries an histidine residue which is highly destabilizing (Wagschal et al., 1999), so dimers between these two bZIPs would also be disfavored.

On the contrary, the sequences of the G- and H-bZIPs follow the canonical composition of the LZ with all **d** positions held by leucines, and the **a** positions filled with β-branched amino acids or cysteines that can form disulfide bridges (Wagschal et al., 1999; Tripet et al., 2000; Acharya et al., 2002; Acharya et al., 2006; Shaikhali et al., 2012). In agreement, all the G- and H-bZIPs were predicted above to form LZ motifs all along the entire theoretical LZ sequence.

In addition, some of the solvent-exposed **b**, **c**, and **f** positions along the six first heptads of the C- and S1-bZIPs are occupied by highly hydrophobic amino acids such as leucine, isoleucine and valine, which are likely to

hamper the hydrophobic force driving the coiled coil interaction (Figure 58). In fact, clusters of hydrophobic amino acid in those positions can induce a transition from the coiled coil to a β-helix secondary structure, and Thr, Val, and Ile -the three amino acids with highest β-helix propensity- abound in those positions (Regan, 1994; Ciani et al., 2002; Dong and Hartgerink, 2007). Conversely, almost none of the β-helix favoring residues are present in the heptads corresponding to the LZ of the G- and H-bZIPs. Altogether, the sequences of the third and fourth heptads of the C- and S1-bZIPs suggested that they were likely to weaken the hydrophobic force and induce a packing defect.

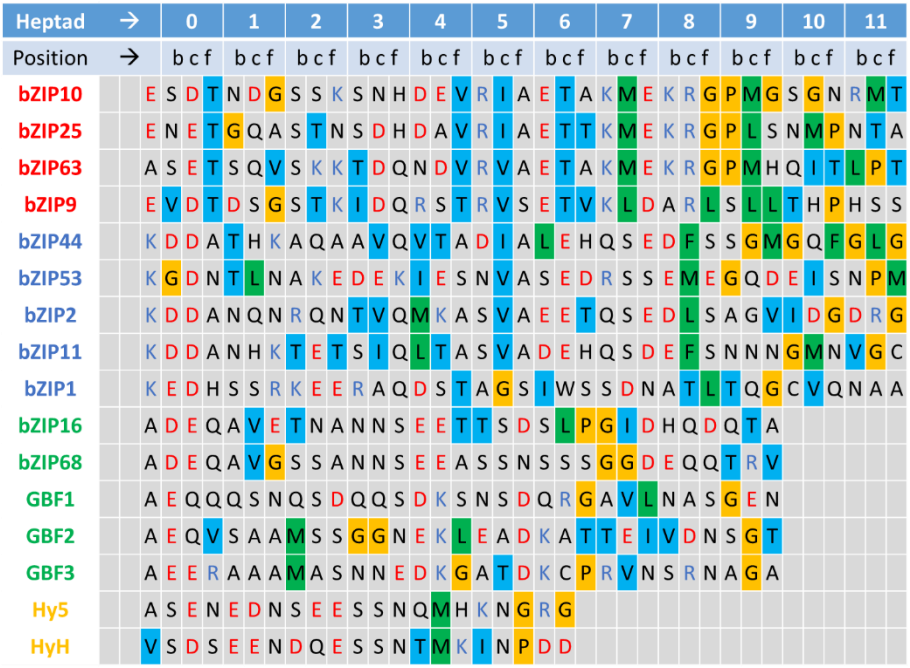

Figure 58. Amino acids in the exposed **b**, **c**, and **f** positions. In blue background are amino acids with a high β-helix propensity, other residues with a positive hydrophaty index Leu, Phe, and Met are in green background (Kyte and Doolittle, 1982). Colored letters are charged residues are red (negatives) and blue (positives), and residues with yellow backgrounds are Gly and Pro, α-helix disruptors.

The composition of the **e** and **g** positions also revealed meaningful differences between the C- and S1-bZIPs and the G- and H-bZIPs (Figure 59). As explained in the introduction, these positions often feature charged amino acids, so that they result in attractive or repulsive forces between the two interacting helices, thus determining the dimer stability. In the C- and S1-bZIPs, the second and third heptad lack almost completely of charged residues, supporting the notion of weaker dimers between these bZIPs. Conversely, in the G- and H-bZIPs there are abundant charged amino acids in those positions which could establish several stabilizing interactions, or discriminate interactions with other monomers.

Heptad →	0		1		2		3		4		5		6		7		8		9		10		11	
Position →	e	g	e	g	e	g	e	g	e	g	e	g	e	g	e	g	e	g	e	g	e	g	e	g
bZIP10	Q	E	Q	K	E	L	Q	N	K	A	G	K	D	R	K	E	T	T	M	L	R	N	N	I	G
bZIP25	Q	D	Q	R	E	I	R	N	K	A	D	R	D	R	K	E	T	T	V	W	R	I	F	S	S
bZIP63	H	E	Q	R	E	M	G	T	T	S	E	K	N	R	K	E	T	T	F	H	M	S	V	E	S
bZIP9	Y	E	Q	K	D	Y	Q	T	Q	G	N	K	D	R	K	E	L	S	T	Q	L	S	P	S	L
bZIP44	H	T	Q	R	E	V	G	T	H	E	E	R	Q	N	R	N	I	E	S	G	E	L	D	D	V
bZIP53	Q	I	E	K	D	T	Q	S	K	E	K	R	Q	T	R	N	V	E	I	L	I	E	M	Q	P
bZIP2	H	T	Q	S	D	L	S	S	L	Q	E	T	Q	S	R	N	I	Q	N	G	D	C	F	V	I
bZIP11	L	T	Q	K	E	V	S	T	H	E	E	R	Q	N	R	N	I	D	S	N	N	S	P	E	D
bZIP1	L	I	E	E	R	S	R	K	R	E	E	R	E	S	Y	E	M	S	T	G	G	D	N	I	V
bZIP16	E	A	R	N	E	R	E	K	Q	T	E	K	Q	P	L	M	N	P	T	A					
bZIP68	E	A	R	N	E	R	E	K	Q	L	E	K	K	P	L	L	K	P	R	D					
GBF1	E	Q	R	S	E	R	E	S	E	K	E	Q	E	L	A	N	E	G	K	T					
GBF2	E	S	K	V	E	R	K	N	E	R	E	L	Q	A	G	L	S	N	S	K					
GBF3	E	A	K	T	E	R	E	N	K	R	A	L	K	E	E	A	M	K	S	K					
Hy5	Y	E	R	E	K	E	R	Q	E	R	I	T	N	G											
HyH	Y	E	R	Q	N	E	K	T	E	R	M	R	K	H											

Figure 59. Composition of the positions **e** and **g**. Amino acids in red and blue backgrounds are negatively and positively charged residues, respectively, in green background are hydrophobic residues, and in yellow background are Gly and Pro, α-helix disruptors. His residues are highlighted with blue letters, as they can adopt a positive charge with lower pH values. From Llorca et al., 2015.

To further explore the role of the **e**-**g** pairs in the stabilization of the bZIP dimers, I calculated the electrostatic interactions between **e** and **g** positions along their coiled coil motifs (Figure 60). Within each one of the three networks, all possible dimer combinations were predicted to form several stabilizing salt bridges, ranging from zero to six salt bridges, and with no distinctive increase in the G and H networks which led to the higher BiFC scores. Thus, their stronger interactions could not be explained by a greater absolute number of salt bridges.

	HyH	Hy5	bZIP68	bZIP16	GBF3	GBF2	GBF1	bZIP63	bZIP25	bZIP10	bZIP9	bZIP53	bZIP44	bZIP11	bZIP2	bZIP1
bZIP1	2-3	2-4	4-2	4-2	3-2	2-4	3(+1)-3	3(+2)-0	4(+3)-1	3(+3)-0	2(+3)-0	4(+1)-2	4(+1)-0	4(+1)-0	1(+1)-0	4(+2)-4
bZIP2	0-1	0-1	2-0	2-0	1-0	1-0	1(+1)-0	2-0	2-0	2-0	1(+1)-0	1-0	1-0	1-0	0-0	
bZIP11	0-3	0-3	3-1	3-1	2-1	2-2	2(+1)-2	3-0	4-0	3-0	1(+1)-0	3-1	2-0	2-0		
bZIP44	0-3	0-3	3-1	2-1	2-1	2-2	2-2	3-0	4-0	2(+1)-0	1(+1)-0	3-1	2-0			
bZIP53	0-4	0-5	2-2	2-2	2-2	2-3	2-3	3-1	4-1	3-1	1(+1)-1	4-2				
bZIP9	0-2	0-2	1(+1)-2	1(+1)-2	1-2	1(+1)-2	1(+2)-2	1(+3)-0	1(+4)-0	0(+4)-0	0(+4)-0					
bZIP10	0-3	0-3	2-2	2-2	1-3	2-3	3-3	4-0	5-0	4-0						
bZIP25	0-3	0-3	3-3	3-3	1-3	2-3	3-3	5-0	6-0							
bZIP63	0-2	0-2	3-2	3-2	1-2	2-2	3(+1)-2	4-0								
GBF1	2-2	3(+1)-3	4-0	4-0	3-1	4-0	4-0									
GBF2	2-2	3-3	3-1	3-1	3-1	4-0										
GBF3	1-3	2-4	3-0	3-0	2-2											
bZIP16	0-3	1-4	6-0	6-0												
bZIP68	0-3	1-4	6-0													
Hy5	4-0	6-0														
HyH	2-0															

Figure 60. Electrostatic interactions calculated between pairs of bZIPs. The numbers indicate the attractive – repulsive interactions between **e**-**g** positions. Interactions that lay outside of the predicted coiled coil region in at least one of the monomers are indicated in parenthesis. Combinations with a positive balance between attractive and repulsive electrostatic interactions are indicated in blue numbers, negative in red, and neutrally balanced in black. The background is colored according to the different bZIP networks. The number of interactions was calculated with DrawCoil 1.0 (www.grigoryanlab.org/drawcoil). From Llorca et al., 2015.

On the other hand, some of those intra-network dimers were predicted to form repulsive **e**-**g** pairs, which is proposed to be the major excluding force in the partner selection among human bZIPs (Vinson et al., 2002), yet for most of them only one repulsive pair amidst several attractive pairs were predicted, so that it could not be excluded that the attractive forces overcame the repulsive ones. As before, there was no apparent correlation between the number of predicted destabilizing **e**-**g** pairs and the measured BiFC scores, so they did not explain *per se* the differences in the dimerization strengths (Figure 61). For instance, homotypic dimers between C-bZIPs resulted in no repulsive forces despite their low BiFC scores, whereas 10 % of the electrostatic interactions between dimers from the G network resulted repulsive in spite of their strong BiFC scores.

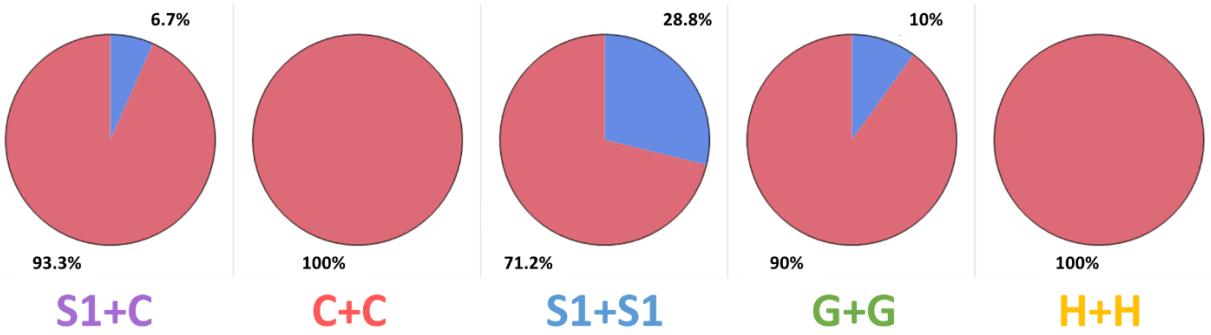

Figure 61. Composition of the resulting electrostatic interactions by group of bZIP dimers. The red fraction are the attractive **e**-**g** pairs, and the blue fraction are the repulsive ones.

Nevertheless, attending to the differences in length of their coiled coil motifs, the dimers in the G and H networks were predicted to form about twice as many salt bridges relative to their number of heptads compared to the C- and S1-bZIPs, which might substantially improve the dimer stability (Table 11). For example, for each salt bridge formed between two S1-bZIPs, four would be formed between two H-bZIPs, if both had the same number of heptad repeats.

Dimer	Rel. e-g
C+S1	2.2
C+C	2
S1+S1	1
G+G	3
H+H	4.2

Table 11. Attractive **e**-**g** pairs for each group of bZIPs on average. Indicated are only the group defining letters, and values are expressed normalized with respect to the total number of heptads and relative to the S1 homotypic dimers, which form the less salt bridges.

Moreover, the calculated electrostatic interactions were not homogeneously distributed all along the coiled coil motif in the C/S1 network dimers, but instead they accumulated distinctly in the different bZIP groups (Figure 62). In the G and H networks, the salt bridges were located towards the beginning of their LZs, and they covered most of their extension. Conversely, in the C/S1 network, the attractive **e**-**g** pairs were calculated to be only in the central heptads, leaving the first and the last part of their coiled coils without the support of the salt bridge formation. Remarkably, the homotypic S1-bZIP dimers accumulated their attractive interactions in the fourth heptad, while the homotypic C-bZIPs did it in their sixth heptad; but in the C/S1 heterodimers

they were more equally distributed between those heptads, what could account to their preferential formation.

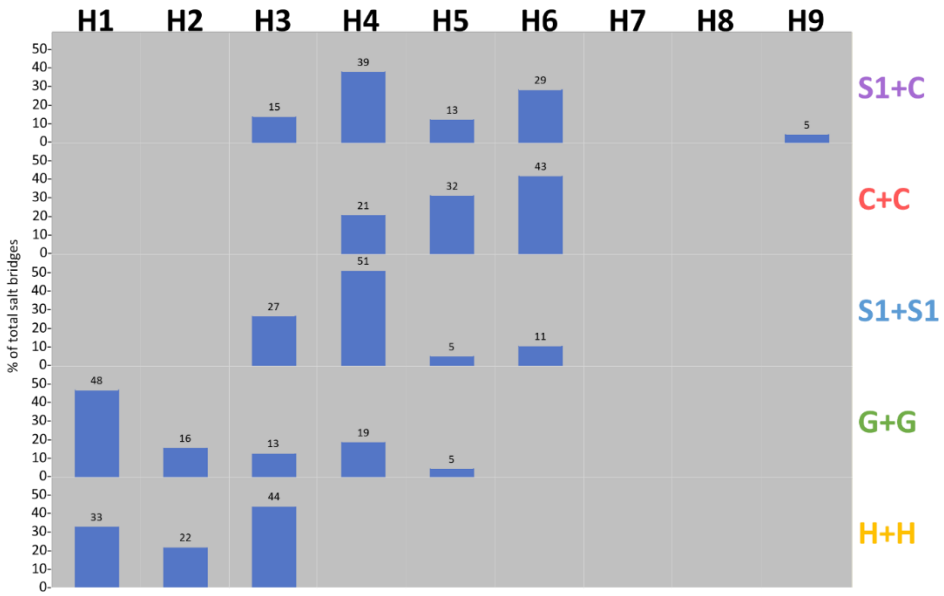

Figure 62. Distribution of the salt bridges along the coiled coil regions. Values are averaged by groups of bZIPs and expressed in percentage with respect to the total number of salt bridges per group. Heptads correspond to the **g** positions, so the salt bridges are formed with the amino acid in the **e** position of the following heptad.

3.4.3 Estimation of the helical content

The finding the hydrophobic patches at the hydrophilic sides along with the β-sheet promoting amino acids, prompted me to investigate the helicity of the coiled coils of the 16 bZIPs, for the helical tendency of coiled coils is an important factor determining their stability (Lee et al., 2001). The helical content of the coiled coil sequences was estimated with the AGADIR algorithm (Lacroix et al., 1998), resulting in distinctly distributed helicity among the different bZIPs groups (Figure 63). The C-bZIPs were predicted to possess a high helix content in heptads 5 and 6, but null content in the rest of their coiled coils. For bZIP25, the estimations were much moderate. Except for bZIP1, the S1-bZIPs exhibited a similar profile, although their helix content was lower, especially for bZIP2. In addition, bZIP2 and bZIP53 also showed helical content in their third heptads. In contrast, bZIP1 resulted in completely different profile, with the maximum helicity accumulated exclusively in the first three heptads.

The G- and H-bZIPs displayed much modest helical tendencies, and shifted towards the beginning of the sequences. GBF1, bZIP16, and bZIP68 displayed the highest helical tendency around the second and third heptads, GBF4 at the fourth heptad, and GBF3 at heptad zero. Regarding the H-bZIPs, both featured a peak of helix content at the first heptad, and Hy5 also around the third heptad. Thus, the distribution of the heptads with the maximum helical content was opposed for the C- and S1-bZIPs compared to the C- and H-bZIPs.

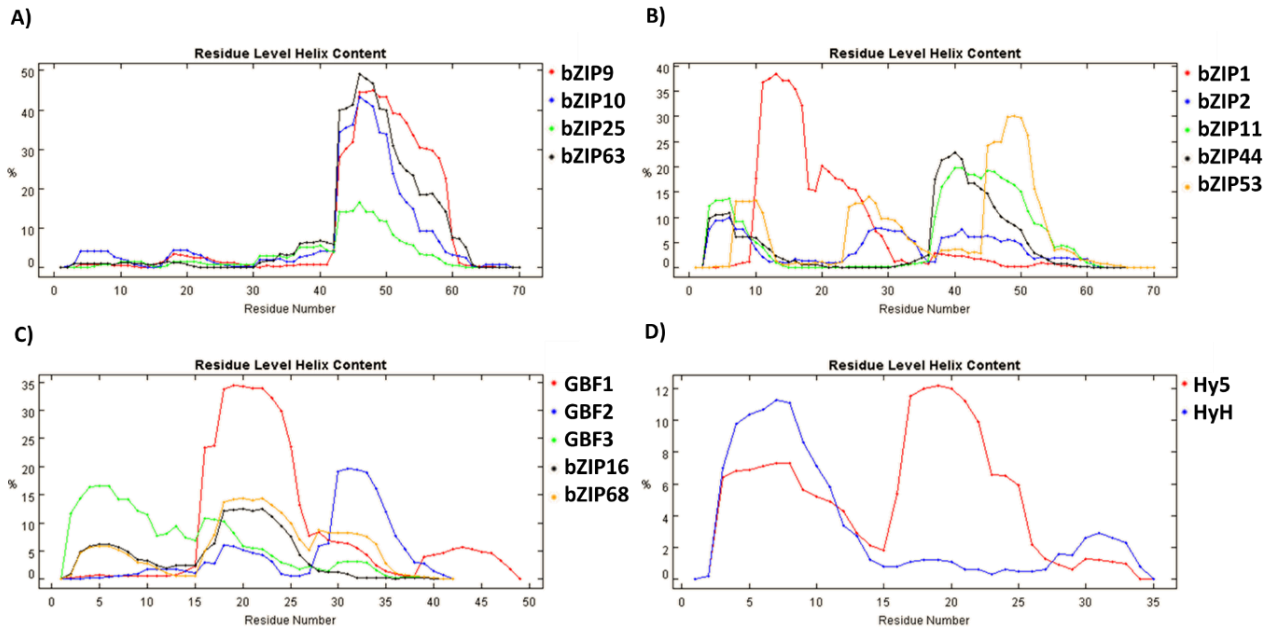

Figure 63. Helical content of the coiled coil sequences estimated starting from heptad 0 and assuming 278 °K, pH 7, and 0.2 M ionic strength. Notice that the scales in the X axes are different, as the bZIPs analyzed feature different numbers of heptad repetitions. A) Results for the C-bZIPs along the 10 heptads. B) S1-bZIP along 10 heptads. C) G-bZIPs along 6 heptads and 7 heptads for GBF1. D) H-bZIPs along 5 heptads. From Llorca et al., 2015.

3.4.4 Protein disorder prediction

Another aspect reported to affect the dimerization dynamics of the bZIPs is the existence of unstructured sections in their LZs. Since the bZIP dimerization is assumed to be coupled to the folding in a two-state transition model from unfolded monomers to the dimeric coiled coil (Mason and Arndt, 2004), the presence of ordered regions such as preformed secondary structures would reduce the entropic cost of the folding process, lowering the transition state free energy and, thus, facilitating the conversion between the different thermodynamic states (Zitzewitz et al., 2000; Moreau et al., 2004; Yoon et al., 2006). Therefore, I analyzed whether the members of the different bZIP networks featured distinctive degrees of disorder.

First, the full length sequences of all the bZIPs were analyzed using the PONDR VL-XT predictor (Romero et al., 2001). According to that method, a disorder value ranging from 0 (order) to 1 (disorder) is attributed to each residue, and a threshold is set at 0.5. Extended intrinsically disordered regions (IDR) were predicted for all bZIPs, yet relevant differences were noticed (Figure 64). In the C- and S1-bZIPs IDRs alternated with large ordered regions, while the C- and H-bZIPs were predicted to be mostly unstructured throughout, so that they could be considered as intrinsically disordered proteins (IDP). Among the latter, only GBF2 and GBF3 exhibited important ordered regions, similarly to the C- or S1-bZIPs.

In general for all bZIPs, significant IDRs were predicted in their BRs, just before their coiled coil motifs. Then, in the C- and S1-bZIPs the coiled coil sequences resulted rather ordered, and in any case but bZIP1, prominent downward spikes indicating ordered regions were predicted at the beginning of their coiled coil, approximately spanning the second, third, and fourth heptads. Conversely, in the G- and H-bZIPs the LZs sequences were calculated as mostly disordered, and only for bZIP68 a significant ordered zone was predicted at the end of its LZ.

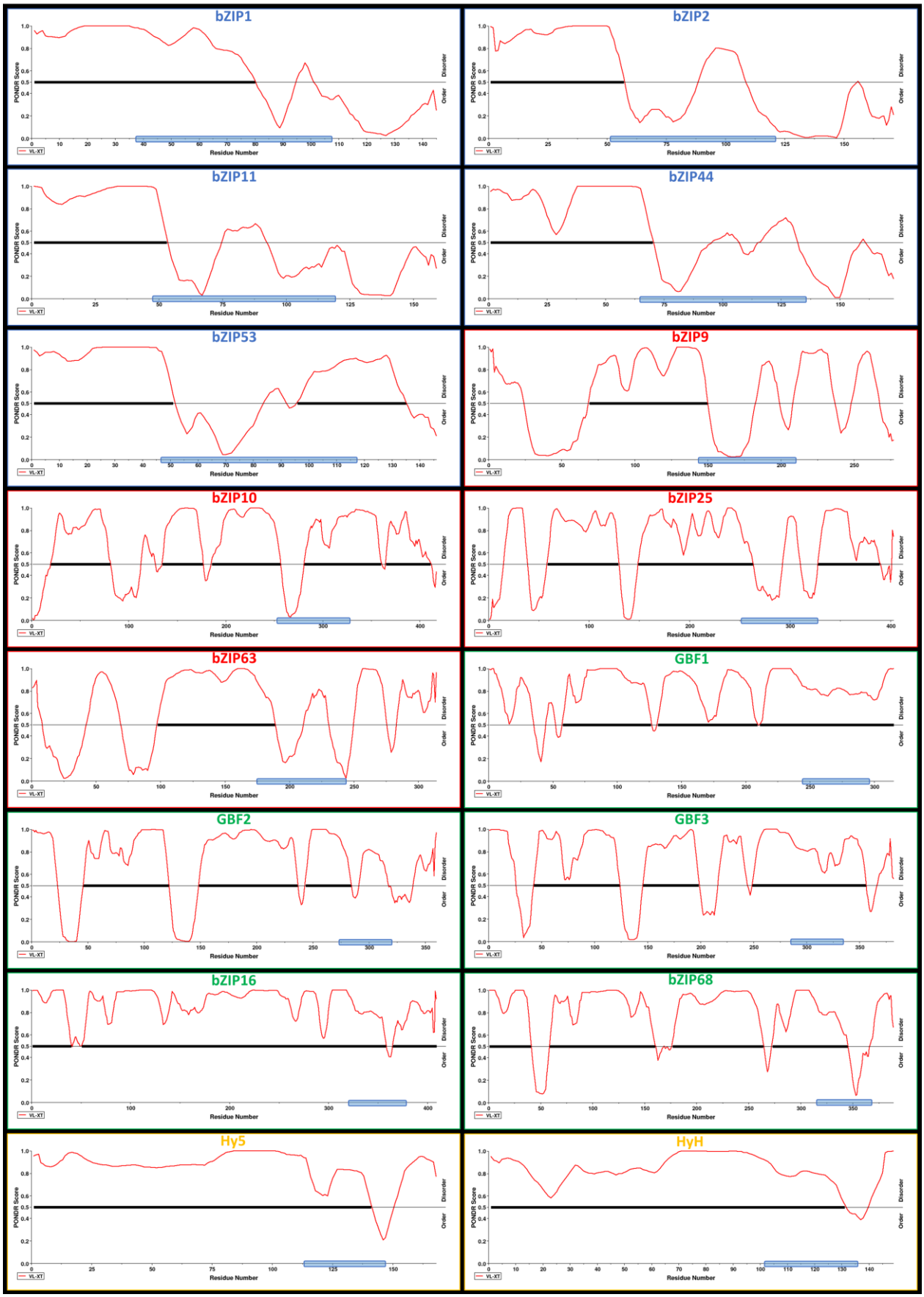

Figure 64. PONDR predictions of disorder for the full length bZIPs using the VL-XT algorithm. Values range between 1 (disorder) and 0 (order) and a threshold represented by the horizontal black line is set to 0.5. From Llorca et al., 2015, modified.

Next, in order to clarify the role of the disorder on the bZIP dimerization, the analyzed region was narrowed down to the dimerization motif and their disorder was assessed in a binary manner. Two different classification methods, the cumulative distribution function (CDF) based on the PONDR VL-TX predictions and the charge-hydropathy plot (CH-plot), were used to categorize the coiled coils of the 16 bZIPs as ordered or disordered (Uversky et al., 2000; Xue et al., 2009). The CDF compiles the PONDR VL-TX predictions for each residue by plotting the predicted PONDR scores against their cumulative frequency, indicating the fraction of residues whose PONDR score is below a given value. Following that approach, the coiled coil sequences of the C- and S1-bZIPs were classified as ordered, again with the exception of bZIP1 (Figure 65). Among those, bZIP1 and bZIP63, with 50 % of their residues predicted with a PONDR score above the 0.5 threshold, exhibited the highest degrees of disorder. In contrast, the LZs of the G- and H-bZIPs were categorized as disordered, and GBF2 displayed the lowest degree of disorder, with only 60 % of their residues predicted with a PONDR score above the 0.5 threshold.

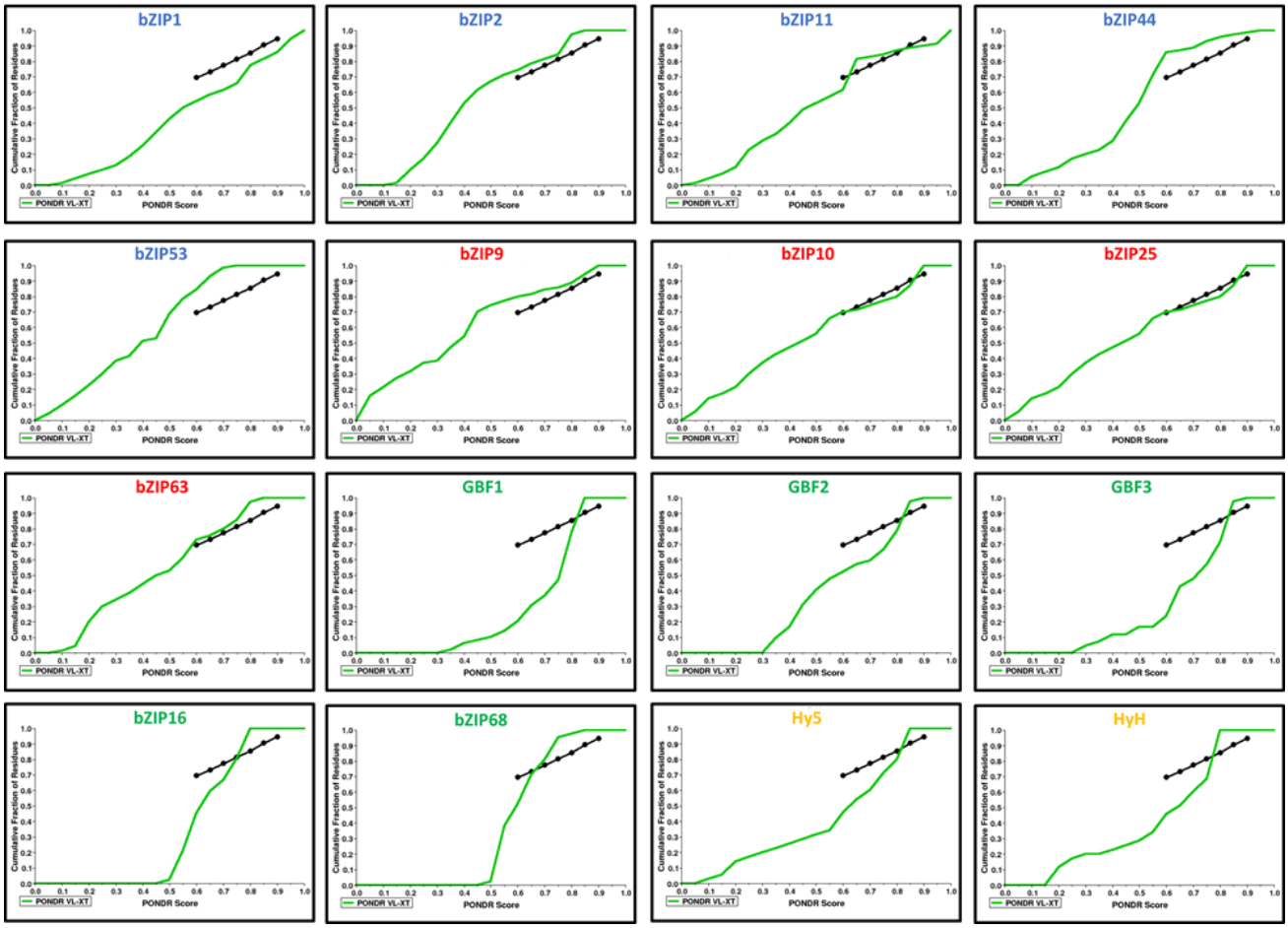

Figure 65. CDFs on the PONDR VL-XT algorithm calculated for the 16 bZIPs. The dotted line represents the boundary between order (above) and disorder (below). The sequences analyzed span from heptad 0 to heptad 5 in H-bZIPs, to heptad 7 in G-bZIPs, and to heptad 10 in C- and S1-bZIPs.

The CH-plot method differentiate ordered and disordered proteins depending on their net charge and hydropathy, for unfolded proteins used to feature low overall hydrophobicity and large net charge. The CH-plot delivered similar results to the CDF (Figure 66). The LZs of the G- and H-bZIPs were plotted predominantly above the threshold line, in the disorder zone, and only GBF2 (No. 12) was clearly in the ordered zone. In contrast, the C- and S1-bZIPs were located mainly below the threshold, and only bZIP11 (No. 5) appeared as

disordered. Therefore, based on the disorder predictions, it was concluded that the coiled coils of the 16 bZIPs presented distinct degrees of ordering, being the bZIPs belonging to the C/S1 network ordered and the G- and H-bZIPs disordered.

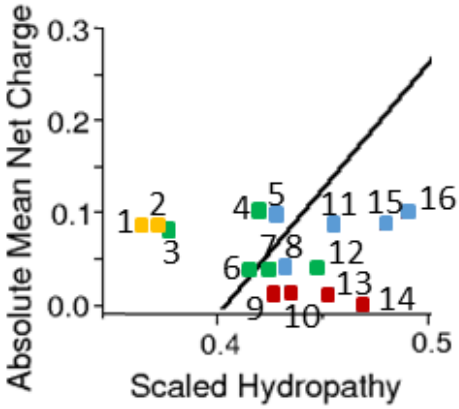

1- Hy5	5- bZIP11	9- bZIP25	13- bZIP63
2- HyH	6- GBF3	10- bZIP10	14- bZIP9
3 – GBF1	7- bZIP68	11-bZIP53	15-bZIP2
4- bZIP16	8- bZIP1	12- GBF2	16-bZIP44

Figure 66. CH-plot for the 16 bZIPs. The black line represents the boundary between disorder (above) and order (below). The identity of the bZIPs is indicated in the adjacent table. The sequences analyzed span from heptad 0 to heptad 5 in H-bZIPs, to heptad 7 in G-bZIPs, and to heptad 10 in C- and S1-bZIPs.

3.5 Analysis of the transactivation activity

Recall, dimerization is assumed to be a central mechanism regulating the bZIP activity, since the combination of different monomers is hypothesized to generate dimers with unique properties as to their DNA-binding and their transactivation potential. To get more insight into this assumption, the transactivation potential of different bZIP dimers was systematically analyzed on five selected promoters previously reported to be directly targeted by some of the 16 bZIPs: *PROLINE DEHYDROGENASE* (*PDH*), *ASPARAGINE SYNTHETASE 1* (*ASN1*), *CATALASE2* (*CAT2*), *RUBISCO SMALL SUBUNIT 1a* (*RBCS1a),* and *LIGHT-HARVESTING CHLOROPHYLL B-BINDING 2* (*LHCB2.4*) genes (Schindler et al., 1992a; Satoh et al., 2004; Alonso et al., 2009; Smykowski et al., 2010; Shaikhali et al., 2012; Veerabagu et al., 2014). For that purpose, the corresponding sequences comprising 1.5 kbp upstream of the gene start, and including the 5'UTR, were cloned into the pBGWFS7 vector to control the expression of a GUS reporter gene (Karimi et al., 2002).

A high-throughput protocol was set up to transform the protoplasts on a small-scale, in 96 well plates and with a Liquidator 96 Manual Pipetting system, and the GUS assay was adapted in consonance. Accordingly, the GUS activity was continuously monitored as previously described (Fior et al., 2009) and the results were calculated as the quotient of the slope in the GUS assay by the measured light in the luciferase assay. This system allowed the processing of multiple samples at once and in an identical manner, so I included three biological replicates in each 96 well plate instead of the doing technical replicates. For each sample, protoplasts were transformed with 2 µg of the GUS construct, 0.1 µg of the 35S::Luciferase construct, and 2 µg of each construct coding for the bZIP protein effectors. When only one bZIP was assayed, 2 µg of the uncloned pUC 35S::c-myc vector were included to keep the transformed total DNA amount constant. The day after the transformation, protoplasts were lysed and protein extracts were assayed for GUS activity in 96 well plates with continuous fluorescence monitoring as described above. Subsequent data processing was performed in collaboration with Dr. Waqas Ahmed Malik and Dr. Hans-Peter Piepho from the University of Hohenheim.

During the initial experiments I could observe that the *ASN1* and *LHCB2.4* promoters did not lead to basally detectable amounts of GUS activity under our conditions (Figure 67). However, while the expression of *ASN1* could be induced by certain bZIP combinations, the *LHCB2.4* promoter resulted in no GUS expression even in the presence of G-bZIPs, which were described to activate the expression of that gene (Shaikhali et al., 2012). For that reason no further work with that promoter was performed. Among the other promoters, judging by the slopes of their fluorescent measurements, the one of *PDH* resulted in a very strong background expression, the one of *CAT2* in middle expression, and the one of *RBCS1a* in weak expression.

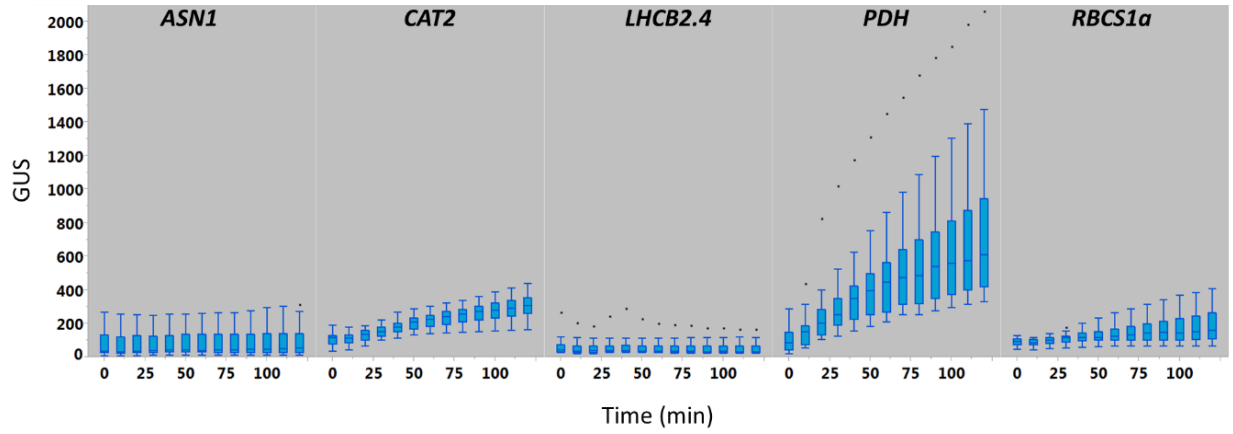

Figure 67. Basal expression of the five promoters studied. Values are only GUS measurements without luciferase normalization. n≥21.

The GUS assays were carried out using the 16 bZIP effectors individually or combined with a second bZIP, considering all the G and H network dimers and the heterotypic dimers from the C/S1 network, as those exhibited the strongest interactions within that network. The results were analyzed for each promoter separately using the calculated mixed model explained in the methods sections. The hypothesis tests were conducted between each bZIPs combination and the reference control (R), which in that case corresponded to 4 µg of the empty effector protein expression vector (pUC 35S::c-myc). The result of the statistical test indicated whether the measured GUS activity in a given bZIP combination was significantly different to the background level of the corresponding promoter.

The interpretation of the results for the single effectors was made straightforward since for each bZIP (A) there were only two possible outcomes: significant (A≠R) or non-significant (A=R). However for the combinations of two effectors (A and B) up to three dimer populations could arise (AA, AB, and BB) and they could interplay differently with the multiple cis-elements present in the promoter, hence it was not distinguishable whether the measured GUS activity resulted from the separate action of the two homodimers, the formation of heterodimers, or a mixture of both situations. The result of the test was, therefore, interpreted comparing the effects of the two single effectors (A and B) with their mixture (M), and focusing only on whether there was a significant change or not. Other possible outcomes such as additive or subtractive effects were not contemplated.

Based on that, I could recognize four different outcomes in the assay (Figure 68): i) **no change of state** when the single effectors produced the same outcome as their mixture (A=B=M), ii) **synergy** when there was a significant change in the measured GUS activity the mixture, but not in any of the bZIPs as single effectors (A=B=R≠M), iii) **dominance** when the single effectors led to different outcomes (one resulted in a significant change, but not the other), so that one of them prevailed over the other in the mixture. In that case, I referred it as **effective dominance** when the bZIP mixture resulted in a significant change (A=R and B,M≠R; or B=R and A,M≠R), and **idle dominance** when there was no significant change in the mixture, yet a change was detected

for one single effector (A≠R and B,M=R; or B≠R and A,M=R). Significantly, there were no combinations in which both single effectors resulted in significant changes in opposing directions, one increasing the expression and the other decreasing it.

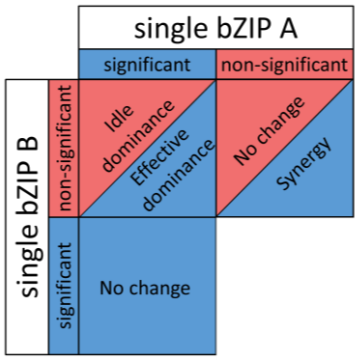

Figure 68. Diagram of the possible outcomes for the bZIP mixtures. The background color of the squares indicates the result of the comparison test for the bZIP mixtures, blue are significant, red are non-significant. From Llorca et al., 2015.

The *ASN1* promoter is known to be activated by the S1-bZIPs (Hanson et al., 2008; Dietrich et al., 2011) and, in agreement, its expression was stimulated in my experiments by bZIP1, bZIP11, bZIP44, and bZIP53 as single effectors (Figure 69). Conversely, none of the other bZIPs induced a significant change as homodimers. As a general trend, among the combinations of two bZIPs effective dominance of the S1-bZIPs over the C-bZIPs was observed, as their co-transformation resulted in significant changes, similarly to the S1-bZIPs alone. In the case of bZIP2, synergy was observed because it did not induce a significant change as single effector but it did so when combined with C-bZIPs. It must also be considered that the lack of basal expression for that promoter could have masked any repressing effects for those bZIPs which did not result in enhanced expression.

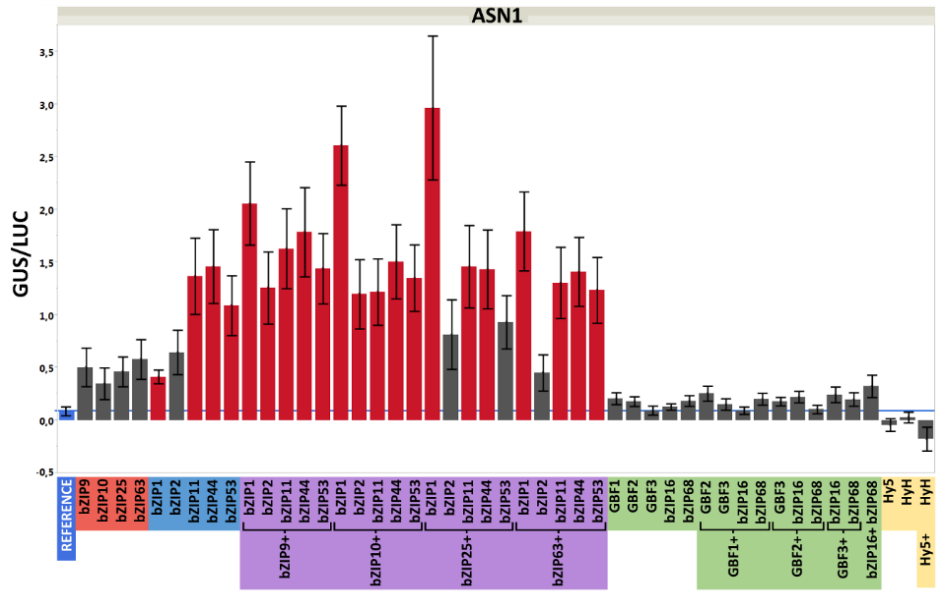

Figure 69. GUS assay on the *ASN1* promoter. The bars indicate the adjusted mean with the standard error. Red bars are significant increases in the measured GUS activity and grey bars are non-significant changes. The blue bar is the control sample. All values represent the means of at least 9 biological replicates. Notice that negative values have no physiological significance, but are artifact products due to the detection limit of the device. From Llorca et al., 2015.

The *CAT2* promoter was reported to be down-regulated by GBF1 (Smykowski et al., 2010), while the effect for the other bZIPs have been analyzed so far. In that assay (Figure 70), GBF1 did not result in a significant reduction of *CAT2* expression, consistent with the previous assays presented in this work. Among the other G-bZIPs, only GBF2 and GBF3 were able to significantly reduce the expression of this promoter. Combinations involving GBF2 resulted in effective dominance over the other G-bZIPs and, conversely, with GBF3 led to idle

dominance. Regarding the C/S1 network, all S1-bZIPs and bZIP25 could reduce the GUS expression, but not the rest of the C-bZIPs; and again, effective dominance of the S1-bZIPs over the C-bZIPs was observed, with the exception of bZIP63 in combination with bZIP1 and bZIP11. Lastly, H-bZIPs also down-regulated the *CAT2* promoter, yet there was no change of state in their combination.

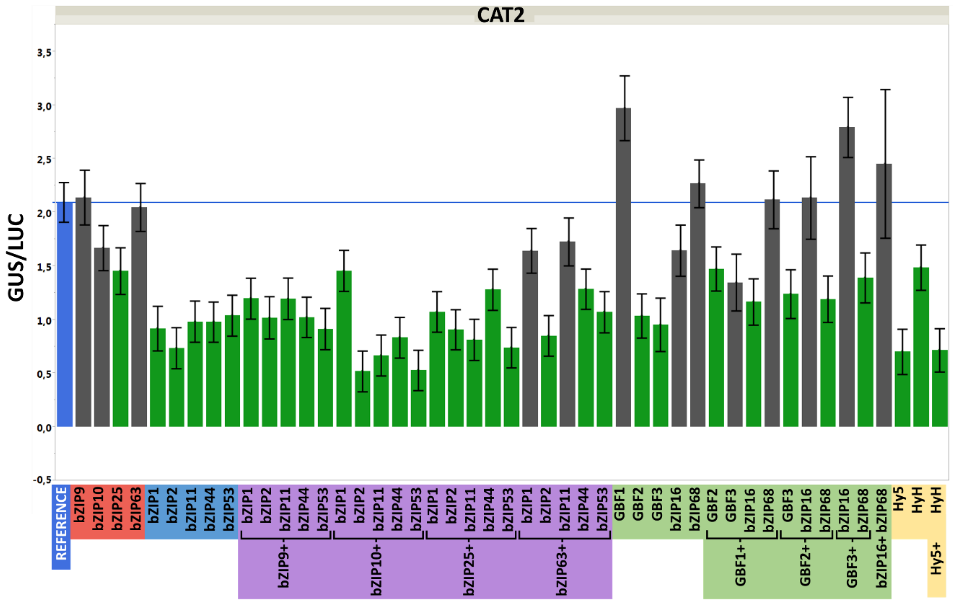

Figure 70. GUS assay on the *CAT2* promoter. The bars indicate the adjusted mean with the standard error. Green bars are significant decreases in the measured GUS activity and grey bars are non-significant changes. The blue bar is the control sample. All values represent the means of at least 9 biological replicates. From Llorca et al., 2015.

The *RBCS1a* promoter carries G-box sequences that are bound by G- and H-bZIPs (Schindler et al., 1992a; Lee et al., 2007; Singh et al., 2012). In my experiments, the H-bZIPs induced no significant changes, whereas among the G-bZIPs only GBF1 and bZIP16 were able to stimulate the transcription (Figure 71), in conflict with the previously reported roles of GBF1 and Hy5 as repressor and activator of that gene, respectively (Singh et al., 2012). Besides that, in the G-bZIPs combinations there was effective dominance of bZIP16 over GBF2 and GBF3, but idle dominance of GBF2 and GBF3 over GBF1. Among the C- and S1-bZIPs, only bZIP11 and bZIP44 activated the expression as single effectors, and they exhibited effective dominance over most of the C-bZIPs. In addition, there was synergy between bZIP2 and all the C-bZIPs except bZIP10, which in turn was the only C-bZIP that showed synergy with bZIP1.

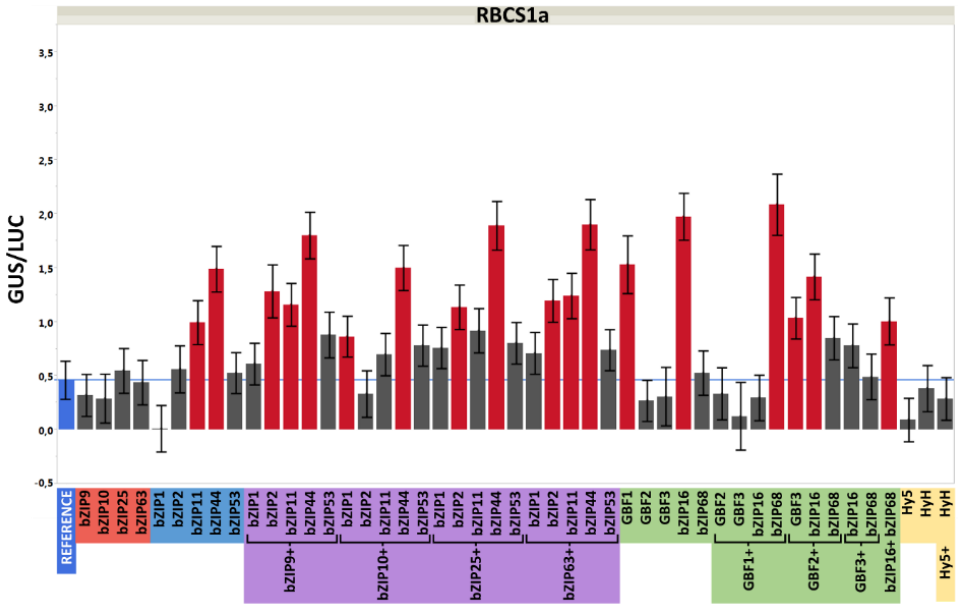

Figure 71. GUS assay on the *RBCS1a* promoter. The bars indicate the adjusted mean with the standard error. Red bars are significant increases in the measured GUS activity and grey bars are non-significant changes. The blue bar is the control sample. All values represent the means of at least 9 biological replicates. From Llorca et al., 2015.

The *PDH* promoter is activated by the S1-bZIPs via an ACTCAT motif present in its sequence, and the effect of the several C/S1 heterodimers has already been addressed systematically. There are though important contradictions regarding which of the S1-bZIPs induce the expression and which do not (Satoh et al., 2004; Weltmeier et al., 2006; Hanson et al., 2008; Dietrich et al., 2011). In my assays, there was a significant activation of this promoter by bZIP2, bZIP11, and bZIP44 as single effectors (Figure 72); and they showed again effective dominance over the C-bZIPs. Significantly, GBF2 and GBF3 resulted in a significant down-regulation, thus displaying an opposite role to the S1-bZIPs. Both G-bZIPs resulted in effective dominance over GBF1, and GBF3 also over bZIP16. The H-bZIPs displayed no effect.

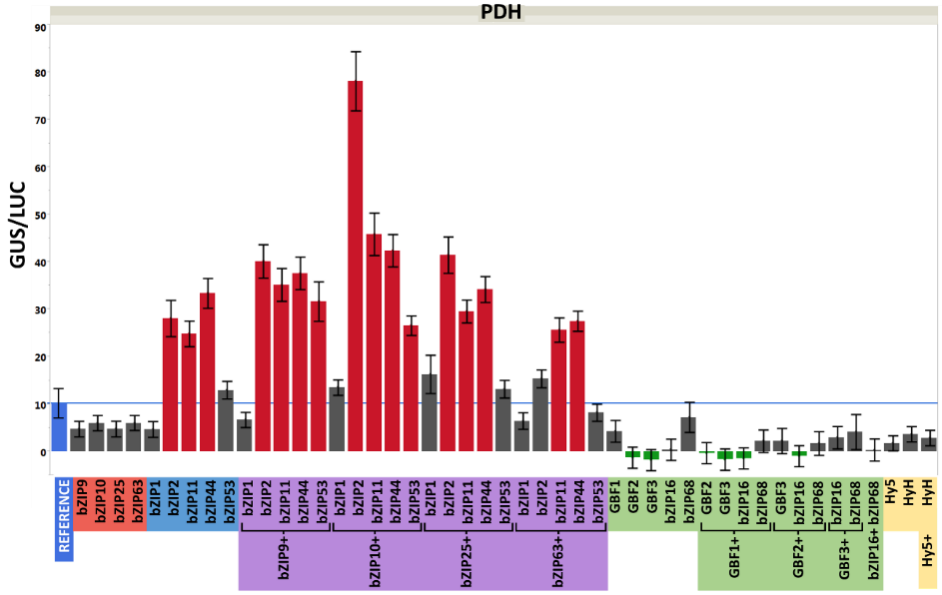

Figure 72. GUS assay on the PDH promoter. The bars indicate the adjusted mean with the standard error. Red bars are significant increases in the GUS activity, green bars are significant decreases, and grey bars are non-significant changes. The blue bar is the control sample. All values represent the means of at least 9 biological replicates. Notice that negative values have no physiological significance, but are due to the detection limit of the device. From Llorca et al., 2015.

To sum up and provide an overview of the results, all comparisons were compiled together (Figure 73). A trend towards a functional consistency among the members of the same network was recognizable. On the one hand, those bZIPs which induced significant changes did so in the same direction (increasing or decreasing). In other words, no coexistence of activating and repressing functions in the same network was observed for a given promoter. On the other hand, the functional relationships between bZIP monomers were also consistent within the same network: the bZIP function within the C/S1 network was mainly determined by active dominance of the S1-bZIPs, which effectively modified the expression of the four promoters tested; while more complex relationships arose in the G network, defined evenly by active and inactive dominance relationships, and a much more selective activation of those bZIPs. The fact that not all the members of a network resulted in significant changes, suggested that the different bZIPs had differentiated functional requirements. Indeed, such conditional activation seems to be a core feature in bZIP function, which is often mediated by further activating factors or certain conditions such as osmolarity or light conditions (Tamai et al., 2002; Satoh et al., 2004; Lee et al., 2007; Dietrich et al., 2011; Babu Rajendra Prasad et al., 2012).

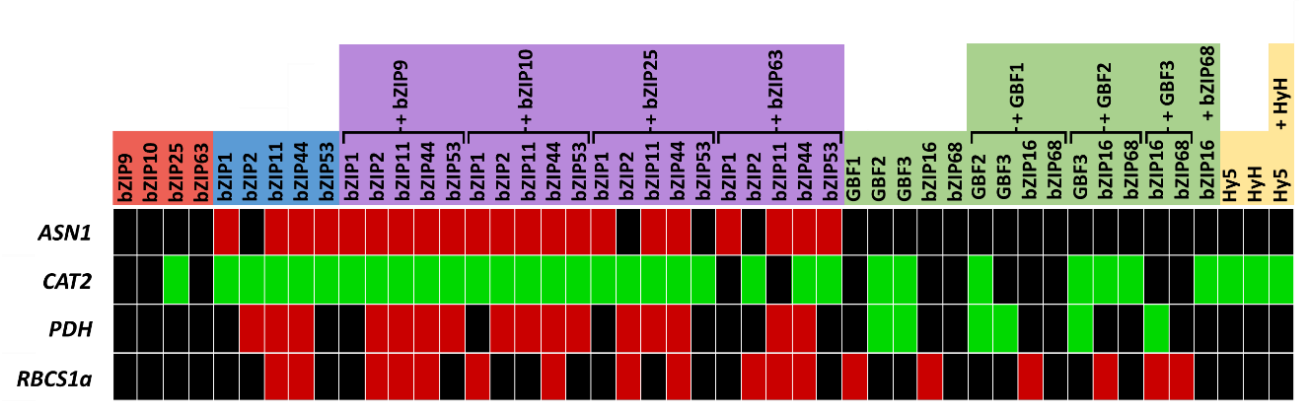

Figure 73. Summary of the results of the hypothesis tests. Red squares indicate significant increase, while green ones represent significant decrease. Black squares indicate no significant change. From Llorca et al., 2015, modified.

3.6 Subcellular localization of the 16 bZIPs

Finally, in order to provide a thorough investigation of the organization of the bZIP networks, it was of interest to establish whether the members of the same network are co-expressed together *in planta* as a prerequisite for their interaction. Additionally, determining the relative expression levels of the 16 bZIPs was also of relevance, for it has been proposed that variations in the expression of specific bZIPs might play a regulatory role altering the balance among the dimer populations and, thus, their function (Weltmeier et al., 2008).

3.6.1 Gene expression

Previous studies established the G-bZIPs as constitutively expressed (Schindler et al., 1992a; Shen et al., 2007), whereas the expression of the C- and S1-bZIPs was reported to be tissue specific in different studies, although with contradictory results (Lara et al., 2003; Lee et al., 2006; Weltmeier et al., 2009). In any case, the expression of the 16 bZIPs has not been addressed as a whole, therefore, I analyzed their transcript levels in order to provide comparable measurements.

The expression of the 16 bZIPs was analyzed in different plant organs - namely, seeds, roots, rosette leaves, cauline leaves, stem, flowers, and siliques - by qPCR. The results showed the presence of the 16 bZIPs in all the plant parts tested. In general, the G- and H-bZIPs exhibited lower levels than the C- and S1-bZIPs, and the S1-bZIPs presented differentiated levels of expression in the different plant parts, while the rest of bZIPs were more homogeneously expressed (Figure 74). Besides, bZIPs within the same network displayed similar levels of expression. All bZIPs presented relatively low levels of expression, which were approximately one to two orders of magnitude below *ACTIN2* levels. In seeds, however, all bZIPs levels were closer to *ACTIN2* due to decreased expression of that gene in that part of the plant.

The most homogeneous measurements were the high levels of bZIP2, in agreement with its reported ubiquitous expression (Lee et al., 2006), and the low levels of GBF3 and bZIP1. In some cases, there were noticeable variations in the expression levels of some bZIPs among the different tissues. For instance, bZIP11 and bZIP44 displayed very low levels in rosette and cauline leaves, in agreement with previous reports (Weltmeier et al., 2008), while bZIP10, bZIP53, GBF2, and GBF3 resulted especially increased in seeds.

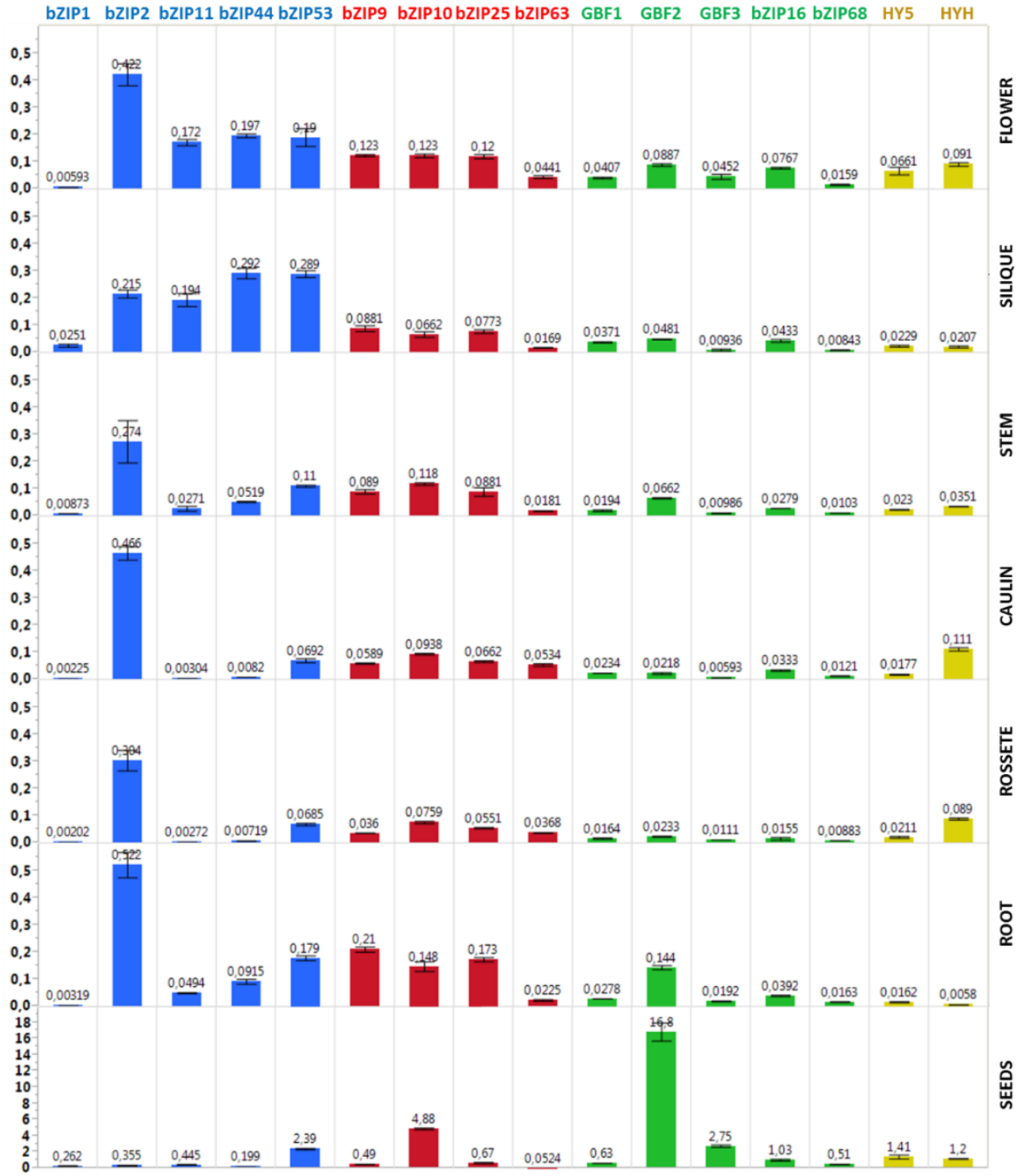

Figure 74. Expression analysis of the 16 bZIPs in a 6 week-old plant. Represented are fold differences in the expression in regard to *ACTIN2*, calculated as 2^ΔCt. Values are averages of three technical replicates, and error bars are standard errors. Note that commas are used here as decimal marks.

Then, in order to validate those results I contrasted them with data from public microarray repositories gathered in the Genevestigator database, which delivered similar relative expression levels (Figure 75). The C- and S1-bZIPs were placed less than one order of magnitude below the level of the *ACTIN2*, while the G- and H-bZIPs resulted in lower levels, between one and two orders of magnitude below *ACTIN2*. Furthermore, the analysis of the expression in the different stages of development indicated that the levels of the all bZIPs are fairly stable along the plant life, with only remarkable variations at the senescence stage. Therewith, data from Genevestigator suggested that all bZIPs are ubiquitously expressed. However, Genevestigator data presented huge dispersions that advise for a cautionary reading (APPENDIX A).

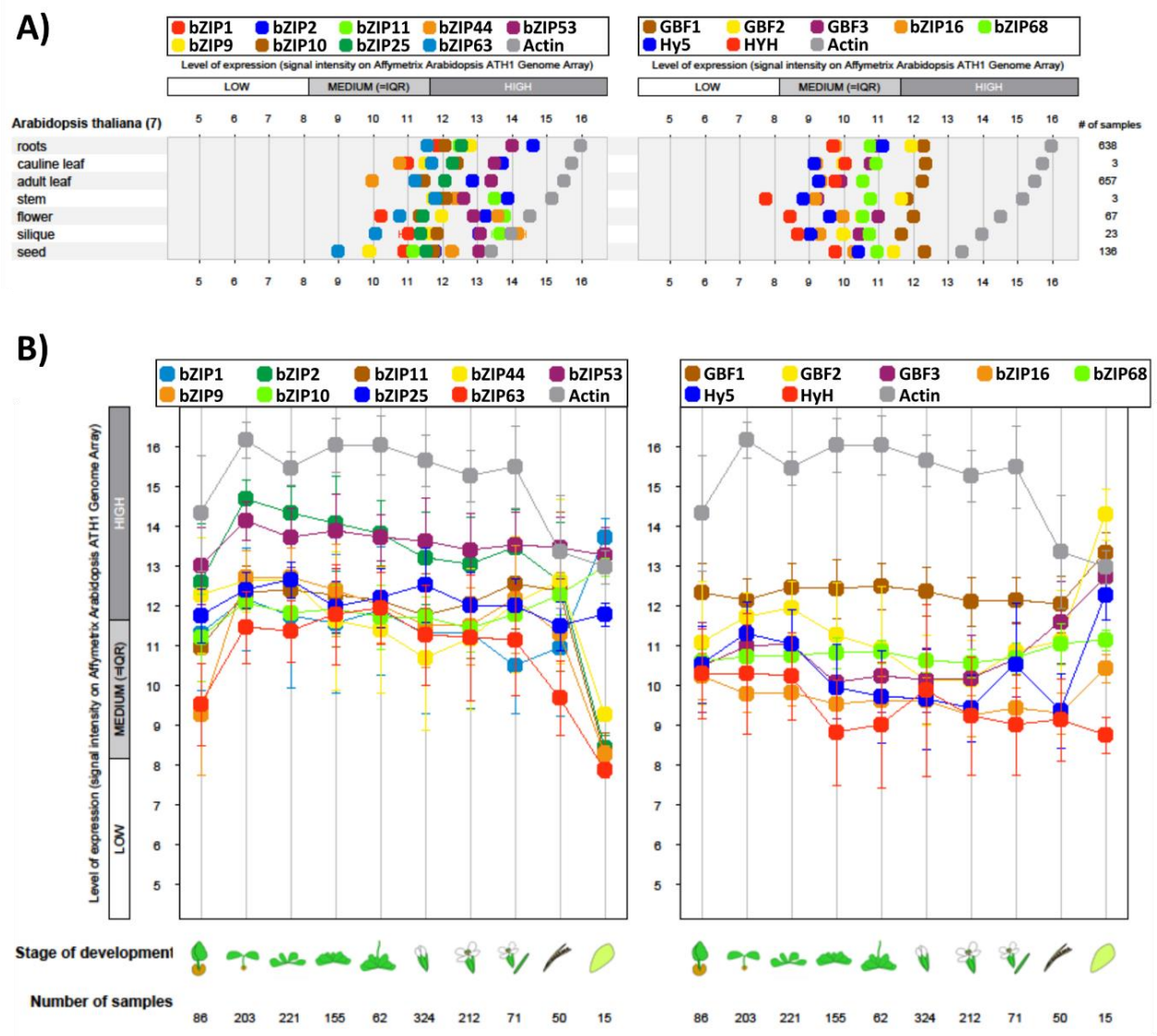

Figure 75. Averaged transcript levels of the bZIP genes estimated from the Genevestigator databases. In all cases the expression levels are represented in Log2 scale. A) Across the different plant parts. B) Along different developmental stages. From Llorca et al., 2015.

3.6.2 Subcellular localization of the 16 bZIPs

Another important aspect considered was whether or not the bZIPs are localized to the nucleus in order to be able to exert their function as transcription factors. The bZIP domain itself features a NLS, hence all bZIPs are expected to be nuclear localized, but for some bZIPs alternative localizations have been reported (Terzaghi et al., 1997; Kaminaka et al., 2006; Iwata et al., 2008; Liu et al., 2008). Therefore, I determined the subcellular localization of the 16 bZIPs by expressing them as GFP fusion proteins in protoplasts.

As expected all bZIPs were found in the nucleus, although a double localization, in the nucleus and in the cytoplasm, was observed for bZIP68, as well as for bZIP10 (Figure 76), congruent to a previous report (Kaminaka et al., 2006). In addition, GBF1 and HyH formed nuclear speckles, a phenomenon associated in plants with light signaling.

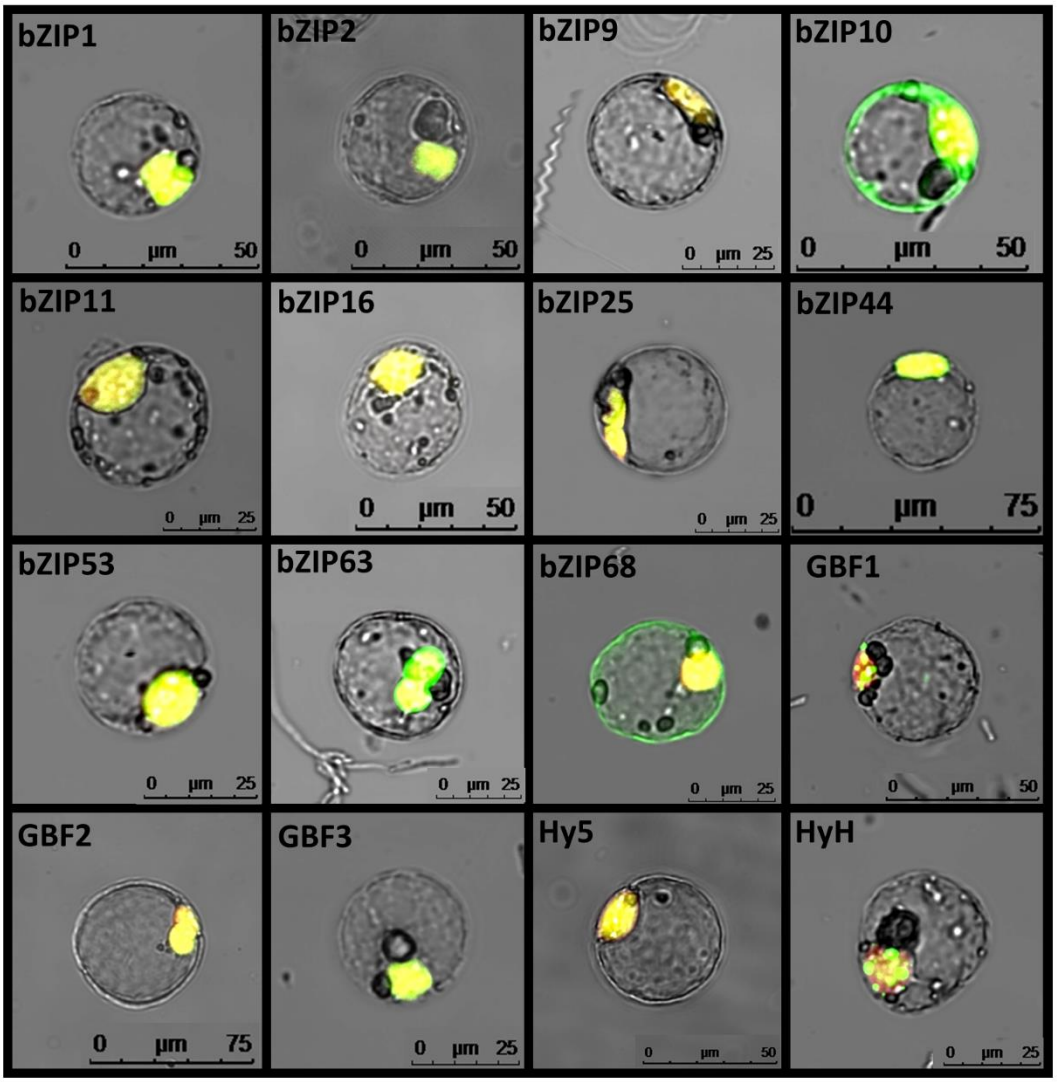

Figure 76. Subcellular localization of the 16 bZIPs in transformed protoplasts. The bZIPs were expressed as GFP fusions (green) along with a plasmid carrying a mCherry gene fused to a NLS for nuclear staining (red). Represented are the merged pictures. From Llorca et al., 2015.

4. Discussion

The present work arose from the observation that plant stress responses and leaf senescence resemble each other in numerous aspects, as it has been introduced above. Both processes are undoubtedly interrelated -plant stress is long known to induce senescence-, but the manner in which they are connected still remains obscure. Bringing insight into that crosstalk was the initial objective of this thesis.

The bZIP family of transcription factors are known to be involved in the regulation of stress responses. Specifically, bZIPs from the C/S1 network are involved in the LES, which appears to be a core feature of all stress responses (Baena-González et al., 2007; Weltmeier et al., 2009; Tomé et al., 2014). Former research in our lab identified another bZIP transcription factor, namely GBF1, as a regulator of the onset of developmental leaf senescence (Smykowski et al., 2010) therewith one allowing to hypothesize about a bZIP-mediated link between stress responses and leaf senescence.

This thesis could not support that hypothesis, as it is discussed below. However, the experience and observations gathered during this project allowed the formulation of new research questions, opening the additional line of research presented in the second part of the Results section, which has been published in PLOS one (Llorca et al., 2015). That second investigation represents the largest integrated study about bZIP dimerization and function in Arabidopsis so far performed, delivering a unique viewpoint to confidently infer in the organization and function of the Arabidopsis bZIP network.

4.1 The GBF1/bZIP63 heterodimer

Dimerization between GFB1 and bZIPs from the C/S1 network was analyzed in order to identify a link between LES and senescence. Among the candidate bZIPs tested, only bZIP63 emerged as a GBF1 interactor in the BiFC assay, but that interaction resulted in pronounced differences between the results obtained with the two alternative orientations of the split YFP fragments (SPC and SPN), which shed doubts on its certainty (Figure 22).

It is known that the fluorescent signal can vary in the BiFC assay depending on the arrangement of the fluorescent protein fragments (Bracha-Drori et al., 2004). In general, false positives and negatives can arise in PFCAs, the former due to the split fragments associating without the interaction of the proteins analyzed, and the latter due to topological constrains precluding the reconstitution of the split reporter when the proteins analyzed actually interact (Kerppola, 2008). Ideally, discriminating those errors would require to test all possible combinations between two fusion-proteins of interest, each one cloned as N- and C- terminal fusions to each split fragment (Horstman et al., 2014), but that would require eight different constructs and 64 combinations to be analyzed per each pair of proteins tested, therefore making it impractical. A common approach is to test only one or two combinations and then verify the interactions with an alternative method, usually Co-immunoprecipitation (Co-IP). However, also Co-IP can result in false positive results, especially when dealing with transcription factors and proteins with hydrophobic domains (Nguyen and Goodrich, 2006; Avila et al., 2015). Hence, any identified protein-protein interaction entails a certain degree of uncertainty.

In this work, in order to understand the disparate results of the GBF1/bZIP63 interaction, truncated versions of GBF1 were tested for interaction with the full-length bZIP63 protein. As illustrated in Figure 24, fluorescence production was not dependent on the presence of the LZ in GBF1 -as it would be expected for a bZIP dimer-, but on the fusion conformation of bZIP63: bZIP63-SPC resulted in no signal, while bZIP63-SPN led to strong

fluorescent emission in combination with both GBF1 truncated versions (with and without LZ). Because of that, and considering the distinct value of the bZIP63-SPN marginal mean in the interaction matrix showed in the second part of this work (Table 8), it can be reasonably concluded that bZIP63-SPN either induced the self-assembly of split YFP or enhanced the fluorescence production. Therefore, measurements generated with the bZIP63-SPN fusion protein cannot serve as evidence for the GBF1/bZIP63 interaction.

As for bZIP63-SPC, it resulted in weak fluorescence production in combination with GBF1-SPN. That would support the GBF1/bZIP63 heterodimer formation, in agreement with the weak interaction between those two bZIPs predicted *in silico* (Deppmann et al., 2006). Still, that possibility was not verified by alternative methods, since this aspect of the research project was aborted. On the other hand, in view of the dimerization rules introduced above, both homodimers would feature a greater number of optimal hydrophobic pairings and salt bridges (Figure 77), whereas the heterodimer would result in a weaker hydrophobic core and the formation of a repulsive **e**-**g** pair. Assessing which of the three possible dimer species will be formed from the combination of two monomers is something that has to be specifically addressed (Carrillo et al., 2010). Nevertheless in this case both homodimers can be predicted to dimerize stronger than the heterodimer, it is disputable if the establishment of an eventual GBF1/bZIP63 heterodimer could compete with the formation of the homodimer under physiological conditions, as it is further discussed below.

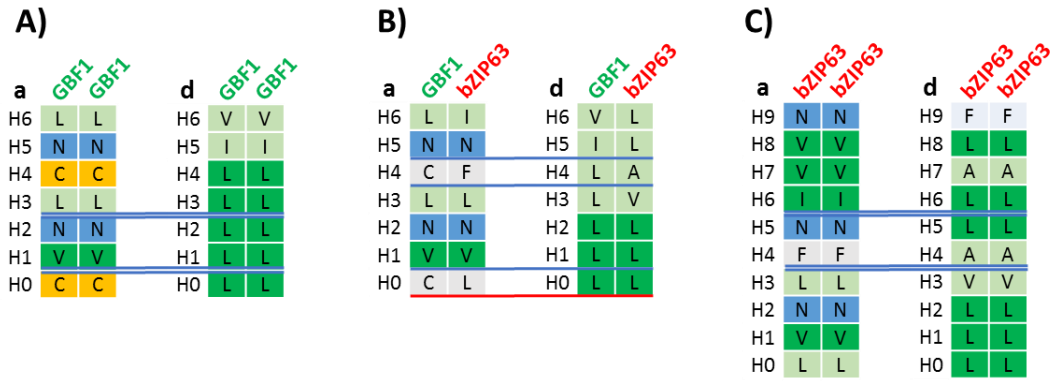

Figure 77. Stabilizing forces in A) the GBF1 homodimer, B) the GBF1/bZIP63 heterodimer, and C) the bZIP63 heterodimer along the predicted coiled coil sequence. Squares indicate the residues occupying the **a** (left) and **d** (right) positions of each heptad (H + number). Dark green background indicates optimal pairs, light green are suboptimal but still nonpolar pairs. Blue are asparagine pairs and yellow are cysteine pairs. Blue lines are salt bridges, and the red line is a repulsive **e**-**g** pair.

In spite of not having provided robust evidence to confirm the GBF1/bZIP63 interaction, further experiments were performed to functionally characterize the GBF1/bZIP63 heterodimer. That was due to the fact that those experiments were not performed stepwise, but in parallel to the BiFC assays, in order to make the most of the research time, and on the basis of previous data that already indicated the possibility of that interaction. Even so, those studies revealed new and unexpected aspects about both bZIPs, GBF1 and bZIP63, as well as methodological issues which are worth discussing here.

4.1.1 Analyzing the DNA binding by DPI-ELISA

To assess whether an eventual GBF1/bZIP63 heterodimer determined differentiated DNA binding properties in regard to the homodimers, the DNA binding specificity of the latter had to be first defined. That was addressed by DPI-ELISA, but conclusive results were not obtained since the bZIP63 protein extracts delivered inconsistent data. However, the variability of the results generated with the bZIP63 protein extract was in sharp contrast with the robustness of the results obtained with the GBF1 ones (which consistently arose in a

concentration dependent manner). Thus, those results pointed at the bZIP63 protein extract as the source of variability.

An important difference between the GBF1 and the bZIP63 protein extracts came from the misuse of the pDEST42 vector to express the recombinant proteins, which lacks a ribosome binding sequence (RBS) (Appendix B). As a result, it can be reasonably conjectured that translation of bZIP63 recombinant protein was initiated from alternative RBSs within the CDS, and so, expressed with a significant truncation of its N-terminus. Although that truncation was unlikely to affect the bZIP domain, it could have disturbed the folding in an unpredictable manner, resulting in non-functional proteins or in protein aggregation. Moreover, it cannot be ruled out that translation was initiated from various alternative methionine residues resulting in a crude extract containing a population of different truncates, or alternatively, in the different expression attempts producing different truncated forms. Since the alternative truncations could affect the protein function differently, both scenarios would account as sources of variability. Likewise bZIP63, GBF1 was expressed in pDEST42 and, hence, it was also likely to be truncated at its N-terminus. However, GBF1 has potential alternative RBS at the beginning of its CDS (Appendix B), so the truncation happened, presumably, to a lesser extent.

An additional cause for the observed variability can be sought in the different composition of the crude extracts assayed. It was already demonstrated that the G-box binding affinity of purified *Zea mays* GBF1 determined by EMSA was enhanced by the mere addition of BSA to the reaction (Sehnke et al., 2005), so that the possibility of the DNA-protein interaction being affected by foreign elements has to be considered, especially when crude extracts are assayed. In that regard, the outcomes of the DPI-ELISA assays seem to be sensitive to the particular conditions assayed, judging by the inconsistent results regularly obtained by different members of our research group when using this method. Indeed, in some of my experiments, the outcomes of the assays could be altered simply by varying the dilution of the bacterial lysates (Appendix C). In those experiments (which were performed with recombinant proteins expressed from the pDEST17 vector, which does carry a RBS), I observed that recombinant proteins with stronger expression resulted more consistent, suggesting that the proportion between the recombinant protein and the bacterial components has a main impact on the result of the assay.

The GBF1 and bZIP63 protein extracts featured disparate proportions between the recombinant protein and the bacterial components, since GBF1 was well expressed, whereas bZIP63 expression was much weaker. Consequently, the induction conditions for bZIP63 were adjusted in order to increase the amount of recombinant protein in the lysate, including the use of larger culture volumes, longer incubation times, and lower temperatures. As a result, the bZIP63 crude extracts contained a greater concentration and fraction of bacterial components in comparison to the GBF1 ones. Those differences could eventually modified the thermodynamics and kinetics of the two bZIPs in a distinct manner, resulting in an additional source of variability.

Because of the foregoing, it was not possible to determine if the occasional binding of bZIP63 was a false positive or, conversely, the absence of binding was a false negative. Literature did not help either in that issue, since other researchers identified bZIP63 as a C-box binder (Kaminaka et al., 2006; Kirchler et al., 2010), but bZIP10 and bZIP25 (also C-bZIPs) can bind to C- and G-boxes indistinctly (Lara et al., 2003; Kaminaka et al., 2006). Thus, it is not possible a priori to negate the possibility that bZIP63 bound G-boxes too. bZIP63 binding to the same *CAT2* G-box was already assayed in our laboratory, and it resulted in no binding signal (Smykowski et al., 2010); but that experiment was performed with the same DPI-ELISA method and with the same bZIP63 pDEST42 clone, so the same doubts apply.

The ambiguity surrounding the bZIP63 binding of the G-box, added to the uncertainty of the GBF1/bZIP63 interaction itself, complicated the interpretation of the DPI-ELISA results for the GBF1/bZIP63 heterodimer. It

is true that increasing amounts of the bZIP63 extract reduced the GBF1 binding in some experiments (Figure 33), but again those results were not robust, and the use of protein extracts from untransformed BL21 cells also reduced the GBF1 binding signal at high concentrations, so it cannot be ruled out that the decrease in the GBF1 signal were due to the mere addition of bacterial lysate instead of the presence of bZIP63.

According to the exposed, the only conclusion that could be drawn from the DPI-ELISA experiments was that GBF1 effectively bound both G-boxes, while the G-box binding by bZIP63 and the eventual GBF1/bZIP63 heterodimer remained inconclusive. Finally, and in consideration of the above, performing the DPI-ELISA assay with full-length purified recombinant proteins should resolve these issues.

4.1.2 The bZIP63 overexpressors are delayed in development

Beyond the study of DNA binding, the investigation of a possible regulation of the GBF1 function by dimerization with bZIP63 also covered the senescence-specific phenotypic analysis of transgenic lines with altered levels of bZIP63 expression. Initially, phenotypic determination based on single time points suggested that the bZIP63 overexpressing lines were delayed in senescence (Figure 36), however I observed that the bZIP63 overexpressing lines exhibited lower rates of germination and a delay in germination, in agreement with a previous report (Veerabagu et al., 2014). Therefore, I established an alternative phenotypic method in order to reflect the growth rate and the general development in order to contextualize the data obtained from the single time point measurements (Figure 38). Those results showed that the bZIP63 overexpressing lines were delayed in development, as well as in senescence progression, but not specifically in the timing of the onset, thus raising the question whether bZIP63 actually plays a role in regulating leaf senescence.

Nutrient remobilization is the hallmark of senescence, so that interfering in the ability of the plants to distribute resources would not be unexpected to result in alterations in the senescence progression. As mentioned in the introduction, bZIPs from the C/S1 network are related to the allocation of energy resources, and congruently they have been implicated in processes that require intensive remobilization of reserves such as seed germination, stress responses, and the maintenance of the energy homeostasis during diurnal changes (Baena-González et al., 2007; Alonso et al., 2009; Weltmeier et al., 2009; Dietrich et al., 2011). Thus, interfering in the function of those bZIPs could be anticipated to impact the progression of senescence, yet that would not directly imply playing a specific role in senescence regulation. Such a side effect is commonly observed in mutants for hormone signaling or biosynthesis genes, which often result in altered senescence phenotypes due to the involvement of the phytohormones in that process, not because the mutated genes played a specific role in senescence (Breeze et al., 2011). Following that argumentation, it seems reasonable to conclude that the delayed senescence progression of the bZIP63 overexpressors actually reflected an alteration in the regulation of nutrient relocation. In agreement, bZIP63 overexpressing lines have been recently reported to exhibit decreased levels of free amino acids in comparison to the wild type, what supports the notion of an overall diminished remobilization capability (Mair et al., 2015). Furthermore, an impaired remobilization capability would also provide an explanation for the delay in the development observed in the bZIP63 overexpressing lines, since it could diminish the efficiency of the plant to overcome fluctuations in the energy availability during the diurnal cycle in a similar manner to the delayed development phenotype observed for starch mutants (Streb and Zeeman, 2012).

Congruently with a delayed-development phenotype, the mostly contributing variables in the PCA were related to the development of the plants (time for silique emergence and flower opening, and IP for height, green leaves emergence, and diameter increase), while variables related to senescence (leaf yellowing, RY50 and RY100 values) were relegated to secondary loading positions. It is, however, needed to bear in mind that

most of the variables (12 out of 18) were derived from fitted curves and those did not resulted accurate in all cases, which could be a source of additional random error. Besides, as it is explained in the Results sections, the annotation of the days in which buds emerged and flowers opened was imprecise. As a result, the PCA output could have been influenced by those aspects. Still, it is remarkable that the bZIP63 overexpressors were localized oppositely to the *bzip63* mutant along the PC1 axis, reasonably depicting that the effect on development correlates with the level of bZIP63.

The PCA also uncovered another distinctive trait of the bZIP63 overexpressing lines that was initially overlooked in the graphical representation. That was the apparent interruption of the rosette expansion between 22 and 25 DAS which occurred in the WT, *gbf1*, and *bzip63* lines, but not in the bZIP63 overexpressors. The cause for that arrest is uncertain, but because it coincided with the emergence of the first yellowing signs it can be attributed to the accidental drought stress period which occurred at the beginning of the experiment, for growth stalling is an early stress response in plants (Mlynárová et al., 2007; Tomé et al., 2014). Accordingly, the unaffected rate of rosette expansion in the bZIP63 overexpressing lines would suggest an enhanced stress tolerance in those lines, congruently with their lesser number of initial yellowing leaves. Still, it has to be mentioned that this conjecture has not been specifically tested in this thesis, and a recent publication reported that bZIP63 overexpressing lines are instead more sensitive to dark extension treatments (Mair et al., 2015). That contradiction cannot be straightforwardly explained, but preliminary stress treatment trials I performed (Appendix D) can bring insight into it. Those assays could not show any difference in the extended dark response between the wild type and any of the lines with altered bZIP63 levels, but they revealed that the survival rate after the experiment was lower when the dark treatment was initiated at 21 DAS than when it started at 28 DAS. Thus, they highlighted that the physiological conditions of the plants at the beginning of the stress treatment strongly affected the outcome, and that could be the cause for the contradictory observations, especially since the bZIP63 overexpressing lines exhibit growth alterations.

4.2 Regulation of GBF1 by phosphorylation

The possibility that the GBF1 function was regulated by phosphorylation was also addressed in this thesis. GBF1 phosphorylation by KIN10 was assayed and resulted negative, although that was not unexpected since GBF1 does not bear the SnRK1 consensus target sequence (Huang and Huber, 2001). Still, previous studies established that GBF1 contains two or three CKII phosphorylation sites (Klimczak et al., 1992), so the regulation of the GBF1 function by phosphorylation was further explored by using phosphorylation-mimicry mutants.

Previous studies highlighted the importance of the three conserved serine residues in the BR for the DNA binding of different bZIPs (Meshi et al., 1998; Kirchler et al., 2010), thus the corresponding serines in GBF1 were likewise studied. Substitutions of those three residues to aspartates decreased the DNA binding as it could be anticipated, since the BR contacts the DNA phosphate backbone and the presence of aspartates would result in repulsive electrostatic interactions with the negative charges of the phosphates. However, substitutions to alanine also reduced the binding, indicating that those serines were important for the DNA binding (Figure 46). In agreement, crystal structures of bZIPs bound to DNA revealed that serines of the BR of bZIPs directly participate in the DNA recognition by forming van der Waals contacts between their hydroxyl group and the methyl group of the thymidine (Glover and Harrison, 1995; Miller et al., 2003). Therefore, it could not be established to what extent the decrease in the DNA binding could be attributed to the presence of the aspartate residues, or to the absence of the serines.

Concerning those results, it has to be taken into consideration that they were obtained with the DPI-ELISA method, which has some limitations when trying to compare results obtained from different samples. That

problem was already noticed by the authors who established the DPI-ELISA protocol followed in this thesis (Brand et al., 2010). They explained that important differences in the absorbance measured can result from variations in the concentration of the epitope tagged protein within different crude extracts or from promiscuous binding to degenerated consensus sequences. Therefore, although the different GBF1 proteins tested (the wild type and the two different triple serine mutants) could be expressed adequately and exhibited similar levels on the western blot (Figure 46), it cannot be excluded the possibility that the absence of binding signal in the mutant carrying the three alanine substitutions were due to some of the factors indicated by Brand et al. or above in the text. Moreover, those factors can also be the reason for the contradictory results obtained by different studies analyzing the effect on the DNA binding of diverse single, double, and triple mutants for the three serines in the BR of GBF1. For instance, the absence of DNA binding in the triple alanine mutant presented here is contradicted in a recent report (Smykowski et al., 2015); and that same report contradicts the results presented in a previous thesis from our laboratory, which showed that certain aspartate substitutions enhanced the DNA binding (Smykowski, 2010). Thus, those discrepancies question the adequacy of the DPI-ELISA method for comparison purposes, when crude extracts are used.

Finally, although the three conserved residues are located outside of the dimerization domain, it was also analyzed whether they impacted the formation of the GBF1 homodimer, since dimerization of other bZIPs has already been reported to be influenced by conformational changes triggered by phosphorylation of residues outside of their dimerization domains (Kim et al., 2007; Liu et al., 2010; Mair et al., 2015). Aspartate but not alanine substitutions resulted in decreased fluorescence levels, indicating that the presence of the negative charges interfered the GBF1 homodimerization.

4.3 The role of GBF1 in senescence

The investigation of a possible modulation of the GBF1 function by bZIP63 required the determination of the GBF1 function alone –that is without bZIP63- in order to be contrasted. However, by doing that, most of the experiments resulted in conflict with the previous studies performed in our laboratory characterizing the function of that bZIP. GBF1 binding to the G-box containing DNA probes could be confirmed by DPI-ELISA, as mentioned above, but not other aspects. Since the results from the GBF1 experiments were regarded as positive controls, failing to reproduce those prompted further experimental repetitions, eventually gathering enough evidences to consider the possibility that the senescence-regulatory function of GBF1 was missing under the experimental conditions assayed. Having reconfirmed the identity of the *gbf1* line and the abolishment of the *GBF1* expression in that line (Figure 43 and Figure 44), I reviewed the data available in order to bring insight into that unexpected outcome.

There are several evidences that oppose to the delayed senescence phenotype described for the *gbf1* line. First, the *gbf1* mutant was previously characterized as an early flowering phenotype (Mallappa et al., 2006; Mallappa et al., 2008). It is known that plants that bolt earlier usually senesce earlier (Levey and Wingler, 2005), and there is an overwhelming number of mutants in which alterations in senescence and flowering are positively correlated (Kim et al., 2004; Miao et al., 2004; Wu et al., 2008; Wingler et al., 2010; Wang et al., 2015). Therefore, the delayed senescence and the early flowering phenotypes are virtually incompatible. Second, the senescence specific phenotype of the *gbf1* mutant line was already studied in our laboratory by a former PhD candidate during her thesis (Petra Zimmermann, 2004), who did not find any difference with respect to the wild type. Those results, thus, agree with the data presented in this thesis, and have therefore contradicted the work performed later in our same laboratory identifying GBF1 as a senescence regulator. Third, during this thesis, the *gbf1* mutant line consistently failed to reproduce the delay senescence phenotype, even when the phenotypic characterization was independently performed by other laboratory

members (Figure 42). This controversy about the delayed senescence phenotype of the *gbf1* line is complicated to explain, since most of those data come from our same research group. Altogether it seems that more evidences oppose the role of GBF1 in regulating senescence, therefore, it might be considered the possibility that the delayed senescence phenotype of the *gbf1* line could have arisen, in one singular case, due to the involvement of other factors which cannot be explained here.

4.3.1 GBF1 has contradictory functions in regulating photomorphogenesis

At the transcriptional level the transcription factor GBF1 was described to be a negative regulator of the *CAT2* and *RBCS1a* expression (Mallappa et al., 2006; Smykowski et al., 2010; Singh et al., 2012), but none of those effects could be replicated in this work. Concerning the *CAT2* promoter, in my experiments GBF1 could not induce any change on the transcription driven by that promoter, and that result was consistent in the GUS assays performed in the first (Figure 34) and in the second part of this work (Figure 70), despite using different methodological approaches. As before, that contradiction is of difficult explanation, since the conflicting results were generated in our same laboratory. Therefore, I can only attribute the cause of those differences to the effect of factors which cannot be explained here.

As for the *RBCS1a* promoter, the results I obtained showed that GBF1 increased the expression of that promoter, instead of decreasing it; and this is an appealing disagreement to discuss. To begin with, it is somewhat unexpected that GBF1 could act as a negative regulator of any gene, since GBF1 features a PRD that functions as a transcriptional activator, not only in plants but also in mammalian cells (Schindler et al., 1992b; Sprenger-Haussels and Weisshaar, 2000; Smykowski et al., 2010), and in agreement, GBF1 activates the expression of *CHLOROPHYLL A/B BINDING PROTEIN 1* (*CAB1*) (Mallappa et al., 2006). In spite of that, GBF1 has been described as a dual-function transcription factor differentially regulating two light-responsive genes, *RBCS1a* and *CAB1* (Mallappa et al., 2006; Mallappa et al., 2008; Singh et al., 2012; Gangappa et al., 2013); yet it has to be taken into account that all those reports were originated from the same research group. Although such antagonistic regulation is not surprising *per se* -it is known that the function of transcription factors can be distinctly regulated depending on the gene context (Boyle and Després, 2010)-, that particular case seems counterintuitive given that the *RBCS1a* and *CAB1* genes are regulated in a coordinated manner: both are induced in response to different kind of lights (Cao et al., 2000; Yadav et al., 2005) and to cytokinins (Cortleven and Schmülling, 2015), repressed by the negative regulator of photomorphogenic growth transcription factor MYC2 (Yadav et al., 2005), and require for their optimal activity a functional ELONGATED HYPOCOTYL 1 (HY1) protein (Babu Rajendra Prasad et al., 2012). So, how could GBF1 act repressing *RBCS1a* and at the same time activating *CAB1*?

A possible explanation for such dichotomy can be found in the work of Feldbrügge et al. characterizing the function of light-responsive bZIPs in parsley. Those authors found that COMMON PLANT REGULATORY FACTOR 1 (CPRF1) activated gene transcription via ACTG-Elements (ACE), but its overexpression reduced the gene expression driven by ACE-containing promoters, presumably by squelching (Feldbrügge et al., 1994). In other words, the excess of CPRF1 bound and depleted protein components required for the activation of the gene induction, resulting in the opposite effect to which it actually promotes. In the case of GBF1, a similar scenario can be speculated since this bZIP is known to function in concert with other transcriptional activators (Tamai et al., 2002; Babu Rajendra Prasad et al., 2012), therefore, assaying the function of GBF1 by gene-transactivation assays could result in a collateral repression of the gene expression by squelching.

In addition to the gene transactivation assays, the *RBCS1a* expression level was reported to be increased in the *gbf1* mutant, thus presenting GBF1 as a negative regulator of that gene (Mallappa et al., 2006; Mallappa

et al., 2008). However, the *gbf1* mutant displays phenotypic traits that appear to be contradictory, suggesting that some of those features could actually represent pleiotropic effects, advising for cautionary interpretations. Specifically, *gbf1* was reported to exhibit shorter hypocotyls and, at the same time, smaller cotyledons than the wild type under blue light (Mallappa et al., 2006), but such description is surprising given that light signals inhibiting hypocotyl elongation also promote cotyledon expansion (Von Arnim and Deng, 1996). Indeed, photomorphogenic mutants exhibit misregulation of hypocotyl length, cotyledon expansion and expression of light regulated-genes in a coordinated manner (Leivar and Quail; Eckardt, 2001). Therefore, it is controversial that the same transcription factor and under the same conditions could promote opposite effects on features which are evenly regulated. Because GBF1 was reported to accumulate in light and degrade in the dark by the 26S proteasome system (Mallappa et al., 2008), and it functions antagonistically to MYC2 which is a known negative regulator of the blue light-mediated photomorphogenesis (Yadav et al., 2005), one would logically consider GBF1 as a positive regulator of light-mediated plant growth, and thus, as an activator of the *RBCS1a* expression. In this situation, deciphering the reason for the increased *RBCS1a* expression in the *gbf1* mutant is complicated, but I believe that precisely because the transcriptional activity of GBF1 seems to strongly depend on further components, lesioning that bZIP does not necessarily have to reflect its lack of function. Previous functional descriptions of the Arabidopsis Hy5 and the tobacco bZI-4 (Lee et al., 2007; Iven et al., 2010) offer a scenario compatible with an increase in the *RBCS1a* expression in the *gbf1* mutant. Accordingly, GBF1 could bind to the *RBCS1a* promoter stably and wait for third parties which regulated its activity, and by doing that, GBF1 would retain the occupancy of the cis-elements preventing the binding of other transcription factors. In that manner, the mutation in *GBF1* would leave free way for other transcription factors to bind to that G-box, eventually promoting the *RBCS1a* expression.

4.4 About the specificity of the bZIP dimerization

Not being able to confirm a senescence-related function for GBF1, the initial aim of this thesis -the search for a link between stress and senescence via GBF1- was left without purpose, and consequently, I decided to stop that project. I conceived a spin-off research plan to systematically analyze the relationship between dimerization and function in Arabidopsis bZIPs, whose major findings are now discussed.

The establishment of the forces defining the specificity of the bZIP interactions allows predicting whether or not two bZIP interact (Fong et al., 2004; Grigoryan et al., 2009; Potapov et al., 2015). However, while predictions proved to be reliable for human bZIPs (Grigoryan and Keating, 2006), they failed to describe dimerization in plants. Arabidopsis bZIPs were predicted to form almost exclusively homodimers (Deppmann et al., 2006), but experimental results showed that homotypic dimers between C- or S1-bZIPs were formed with low affinity and they tended, instead, to heterodimerize (Ehlert et al., 2006; Kang et al., 2010). The analysis of the interaction between the 16 bZIPs in the second part of this thesis also delivered some results not predicted by Deppmann. While it is true that some contradictory results can always happen when dealing with large datasets, in that case it was suspicious that most of the disagreeing results arose clustered in two groups dealing with the same kind of interactions (Figure 78). The first one was the absence of homotypic dimerization between S1-bZIPs already noticed by other studies (Ehlert et al., 2006; Kang et al., 2010), and the second one was the lack of interactions between G- and S1-bZIPs, in spite of most of those combinations being predicted to form only attractive **e**-**g** pairs. Thus, the fact that the unpredicted results appeared in a consistent manner indicated that they were not random, and hinted at the involvement of so far unknown determinants of the dimer specificity. Particularly, they pointed at features of the G- and S1-bZIPs acting in that process.

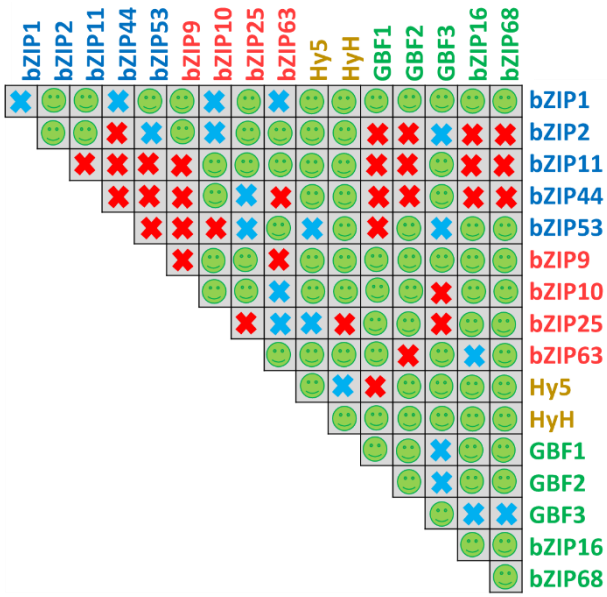

Figure 78. Comparison between the experimental results generated in this work and the theoretical predictions by Deppmann. Green smileys indicate agreement, red crosses are interactions predicted to occur but not observed experimentally, and blue crosses are observed interactions which were predicted to not dimerize.

The examination of the coiled coil motifs of those bZIPs disclosed particularities of their compositions that could account for the distinct dimerization patterns. The G- and S1-bZIPs exhibited distinctive distributions of their salt bridges, hydrophobic pairings, and helical contents. Those stabilizing forces accumulated towards the second part of the coiled coil motif in the S1-bZIPs, but on the initial heptads of the G-bZIPs. Remarkably, that differential distribution of the stabilizing forces seems to be a feature of each interacting network, since similar patterns are repeated in the C- and the H-bZIPs, respectively. So, those observations suggested that certain heptads within the same coiled coil motif are of higher relevance than others in regard to the dimerization process, pointing to a novel mechanism defining the dimerization specificity based on the differential positioning of those heptads which play more prominent roles.

Particularly, the accumulation of the stabilizing forces at the end of the coiled coil motifs of the C- and S1-bZIPs suggests that those heptads could act as trigger heptads. It is known that coiled coil interactions are often initiated from certain heptads with autonomous helical folding which act as trigger units (Kammerer et al., 1998; Steinmetz et al., 1998; Lupas and Gruber, 2005; Ngo et al., 2013). The sequence of the trigger heptads varies among different proteins so that there is no consensus sequence, and no trigger heptads have yet been defined for the bZIPs here studied. However, the fact that the coiled coil motifs of the C- and S1-bZIPs are longer and feature weak heptads which are likely to hinder the establishment of a coiled coil interaction, hints at their requirement for such trigger units. From those stronger heptads dimerization could be initiated and then transmitted to the initial weaker heptads.

How the existence of trigger heptads can define the specificity of the bZIP dimerization is clearly illustrated by the lack of interactions between G- and S1-bZIPs, in spite of their potential formation of several stabilizing salt bridges. In those bZIPs, the stabilizing forces are concentrated in an opposite fashion; so the stronger heptads in the S1-bZIPs are beyond the reach of the shorter LZs of the G-bZIPs. Accordingly, for the formation of eventual G/S1 dimers, the trigger heptads of the S1-bZIPs would miss their counterpart elements to interact with, being unable to initiate the interaction. Moreover, the LZs of the G-bZIPs match just the weak heptads from the S1-bZIPs, resulting in a decreased hydrophobic potential, which is the main force driving the interaction. Conversely, dimers with compatible distributions of stabilizing forces juxtapose their coiled coil motifs so that their stronger heptads match together, maximizing the stability of the interaction (Figure 79). In that manner, the control of the initiation of the dimerization can act as an additional mechanism defining the dimer specificity, discriminating those interactions between monomers without a complementary distribution of forces.

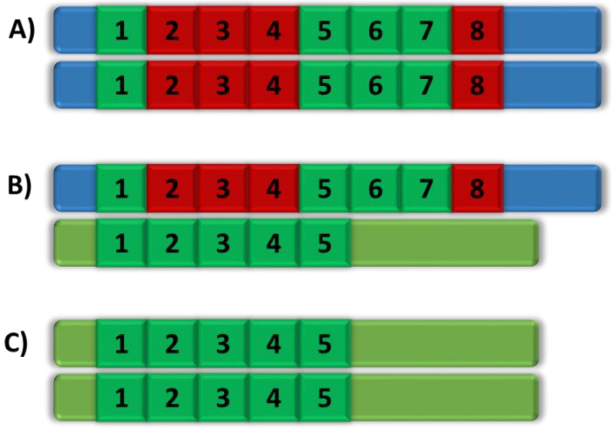

Figure 79. Discrimination of the heterodimers between S1- and G-bZIPs based on the distribution of their stabilizing forces. Depicted are schematic coiled coil motifs. Green squares are strong heptads and red squares are weak heptads. Dimerization can occur when the strong heptads match together between A) S1-bZIPs or C) G-bZIPs, but not when they are mismatched in the heterotypic heterodimers, B).

This hypothesis also allows to speculate about the causes of the preferential formation of the C/S1 heterotypic heterodimers. As indicated in the Results section, the formation of the C/S1 heterotypic heterodimers is not associated with an increase in the number of salt bridges in regard to the respective homotypic dimers; indeed, there is a decrease compared to many of the homotypic heterodimers between C-bZIPs (Figure 60 and Table 11). However, the distribution of the salt bridges does significantly change in the heterotypic heterodimers: while most of the attractive **e**-**g** pairs involve the third and fourth heptads of the S1-bZIPs dimers and the fifth and sixth heptad of the C-bZIPs dimers, salt bridges formed in the C/S1 heterotypic heterodimers arise with a more homogeneous distribution, mainly in the fourth and sixth heptads (Figure 62). In other words, the patterns of salt bridges of the C- and S1-bZIPs, which are biased in opposing directions, complement each other in the C/S1 heterodimers, so achieving a larger coverage of heptads. In addition, the distribution of the helical content along the coiled coil also evokes the notion of complementarity between the C- and S1-bZIPs: the C-bZIPs display a high helix content restricted to the sixth and seven heptads, while the helix content of the S1-bZIPs is more moderate and shifted forwards, to the fifth and sixth heptads (Figure 63). Moreover, the S1-bZIPs also exhibit helix content in some of the first heptads, namely the third, the fourth, and the heptad zero. Therefore, it seems that the preferential formation of C/S1 heterotypic dimers functions by putting together the complementary dimerization-driving properties of the C- and the S1-bZIPs. In that manner, the high helix content in the last heptads of the C-bZIPs could act triggering the dimerization with the S1-bZIPs, and in exchange the moderate helix content of the first heptads in the S1-bZIPs could stabilize the null helicity of the corresponding heptads in the C-bZIPs. Additionally, the heterodimers would better stabilized by the broader distribution of the salt bridges.

There are, however, aspects of the C/S1 network which still remain ambiguous. For instance, bZIP10 and bZIP25 carry a histidine residue in the **a** position of their second heptads, which is highly destabilizing configuration (Wagschal et al., 1999), and despite that, both bZIPs can dimerize with other members of the C/S1 network. Also puzzling is the formation of heterodimers with bZIP1, because this bZIP features many unfavorable elements for the dimerization such as the misalignment of the asparagines, a lysine residue in the **a** position of the sixth heptad (Zeng et al., 1997; Wagschal et al., 1999; Arndt et al., 2000; Tripet et al., 2000; Acharya et al., 2006) or the localization of the helical content opposed to the rest of the C/S1 network bZIPs. In fact, *in silico* dimerization predictions for bZIP1 resulted in a totally distinct dimerization pattern, away from the rest of C- or S1-bZIPs, and with almost no interaction with other bZIPs (Deppmann et al., 2006). Therefore, it cannot be excluded that further, so far unknown mechanisms are involved in defining the interaction specificity.

4.4.1 The bZIP network in Arabidopsis

Predictions by Deppmann et al. of bZIP dimerization across different species concluded that plants and human bZIPs follow different strategies to achieve network complexity (Deppmann et al., 2006). Plant bZIPs were predicted to be organized in many small isolated groups of non-selectively interacting bZIPs, whereas human bZIP would form few large groups amply interconnected. The former would represent a collection of independent networks, the latter a meta-network structure. However, the predicted network structure for Arabidopsis has not been confirmed experimentally, mainly because bZIP research usually deals with few monomers, and combinations not predicted to interact are rarely tested.

The analysis of the interaction of the 16 bZIPs presented in this work proposes that these bZIPs are organized in three interacting networks, so that each network remains defined by the practically indiscriminate interaction of its members. Besides, additional interactions were identified between monomers involved in different networks, although some aspects surrounding the formation of those inter-network dimers are ambiguous and weaken the confidence of their identification. For instance, the three identified inter-network dimers involving H-bZIPs (i.e. Hy5/bZIP25, Hy5/bZIP53, and HyH/GBF3) result in three or more repulsive **e**-**g** pairs and a double mispairing of asparagines in **a** positions which is highly discriminating (Arndt et al., 2000), therefore they are very unlikely to happen according to the current knowledge on the bZIP dimerization. On the other hand, dimers connecting the G and C/S1 networks resulted in an unexplainable degree of specificity, allowing the interaction between just selected bZIP pairs but not others. For instance, dimers between bZIP2 and bZIP16 or bZIP68 are not formed in spite of having an additional salt bridge compared to the dimer bZIP2-GBF3 which does interact. So all in all, there is a big contradistinction between the abundant and unselective intra-network dimer formation and the few and extremely selective inter-network dimers (Figure 80). Put it another way, given the similarity of the coiled coil features among the members of the same network and the high intra-network dimerization promiscuity, the fact that only few inter-network dimers arise is counterintuitive.

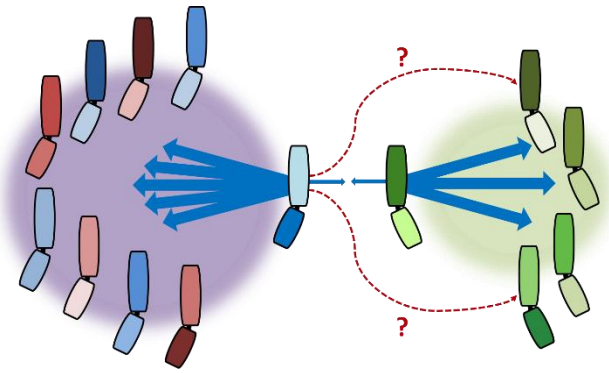

Figure 80. Doubts on the inter-network bZIP dimers. Interactions (blue arrows) within the same network are more stable and abundant, so inter-network dimers formation are in disadvantage. Given the intra-network promiscuity, it is striking that other interactions do not occur (red, dashed lines).

The quantitative double-way BiFC assay performed along with the statistical treatment brought enough confidence on the identification of those inter-network dimers under the conditions tested, so the question revolves around whether they actually occur under physiological conditions. In view of the high intra-network promiscuity, it can be argued that the formation of inter-network dimers would be in unfavorable competition with the intra-network ones, as the latter are expected to form preferentially according to the established rules defining the dimerization specificity. Therefore, I consider that the formation of inter-network dimers under physiological conditions, if any, will be rather limited; thereby supporting the bZIP organization proposed by Deppmann et al. in small independent networks (Deppmann et al., 2004). In any case, as only four of the ten bZIP groups were investigated here, further systematic *in vivo* studies are necessary to conclude about the precise architecture of the Arabidopsis bZIP network.

Alternatively, I also contemplate that the overexpression conditions of the assay could have forced transient formation of disfavored dimers. For instance, increasing peptide concentrations can enhance the helical propensity of coiled coil proteins and their self-assembly (Hicks et al., 1997; Tsang et al., 2011; Pähler et al., 2012); so disfavored dimers could have formed transiently and remained trapped in the form of BiFC complexes due to the irreversibility of the split YFP re-assembly. While this possibility cannot be excluded, it has to be kept in mind that a blanketed overexpression effect was not recognizable – the BIFC scores involving particular bZIPs were varied and not correlated with their protein levels-.

Be that as it may, since no protein-protein interaction detection method is infallible, those data will inevitably contain false positives and false negatives, so their reproducibility by independent studies would be of great value for their authentication. In that regard, among the 16 bZIPs studied, the formation of inter-network dimers has only been addressed in two studies, both dealing with dimers between H- and G-bZIPs. One of them indicated, in agreement with the results presented in this thesis, that Hy5 did not interact with bZIP16 or bZIP68 (Shen et al., 2008), while the other one reported, in opposition to the results obtained in this work, that GBF1 interacted with both H-bZIPs (Singh et al., 2012). The possibility of establishing G/H heterodimers is surprising since H-bZIPs do not feature the asparagine residue in the **a** position of the fifth heptads as the G-bZIPs do, but in the fourth heptad, therewith missing the alignment of asparagines in the **a** positions, which is an important determinant for the dimerization (Zeng et al., 1997; Arndt et al., 2000; Acharya et al., 2006). Thus, formation of heterodimers between GBF1 and the H-bZIPs would be in disadvantageous competition with the other, more stable dimers of their respective networks (Figure 81), in that manner undermining the confidence of the heterodimer formation under physiological conditions likewise it has been discussed above for the GBF1/bZIP63 heterodimer. Curiously, the report identifying the GBF1/HY5 dimer also indicated that truncated versions of Hy5 and HyH consisting of only the BR and the LZ did not interact with the full length GBF1 (Singh et al., 2012), evoking the ambiguity surrounding the identification of the GBF1/bZIP63 heterodimer discussed above.

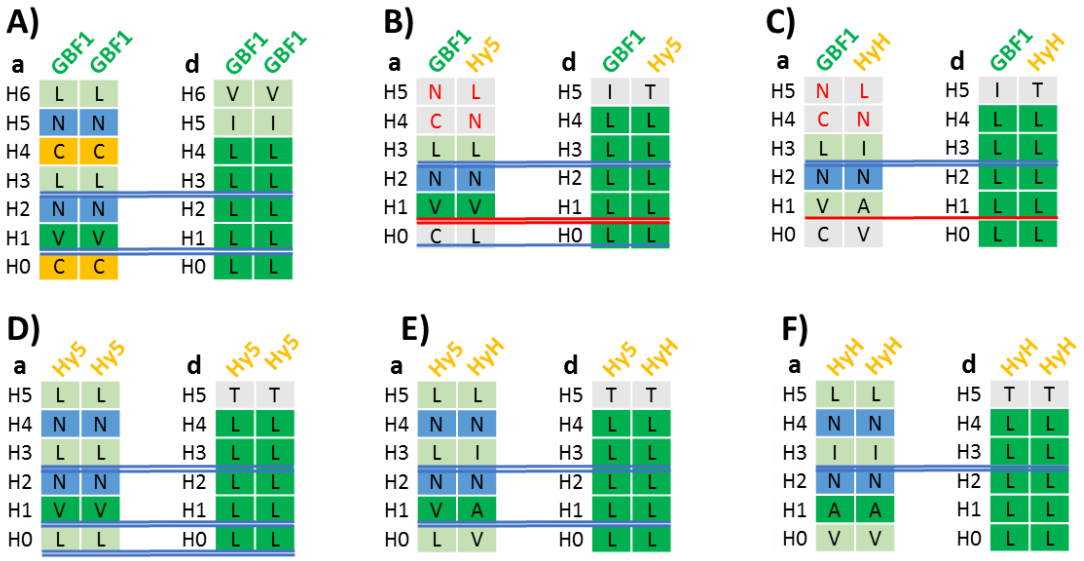

Figure 81. Stabilizing forces in homodimers for A) GBF1, D) Hy5, and F) HyH, as well as in the heterodimers between B) GBF1 and Hy5, C) GBF1 and HyH, and E) Hy5 and HyH. The formation of dimers in B) and C) would compete with all the rest and with the heterodimers between GBF1 and the other G-bZIPs. Squares indicate the residues occupying the **a** (left) and **d** (right) positions of each heptad (H + number). Dark green background indicates optimal pairs, light green are suboptimal but still nonpolar pairs. Blue are asparagine pairs and yellow are cysteine pairs. Mispaired asparagines pairs are indicated in red letters. Blue lines are salt bridges, and red lines are a repulsive **e**-**g** pairs.

As for the intra-network dimers, the interactions within the G and H networks identified in this thesis were consistent with previous reports (Schindler et al., 1992a; Holm et al., 2002; Shen et al., 2008; Shaikhali et al., 2012). On the contrary, the identified dimers within the C/S1 network were not consistent with other studies. To begin with, because results delivered by previous studies already disagreed among themselves (Walter et al., 2004; Ehlert et al., 2006; Kaminaka et al., 2006; Kang et al., 2010); this is to say that there was not a unique dimer arrangement to be compared with. Available studies fail to replicate the precise bZIP combinations that take place within the C/S1 network, although remarkably, the preferential heterodimerization between C- and S1-bZIPs is commonly verified (Figure 82).

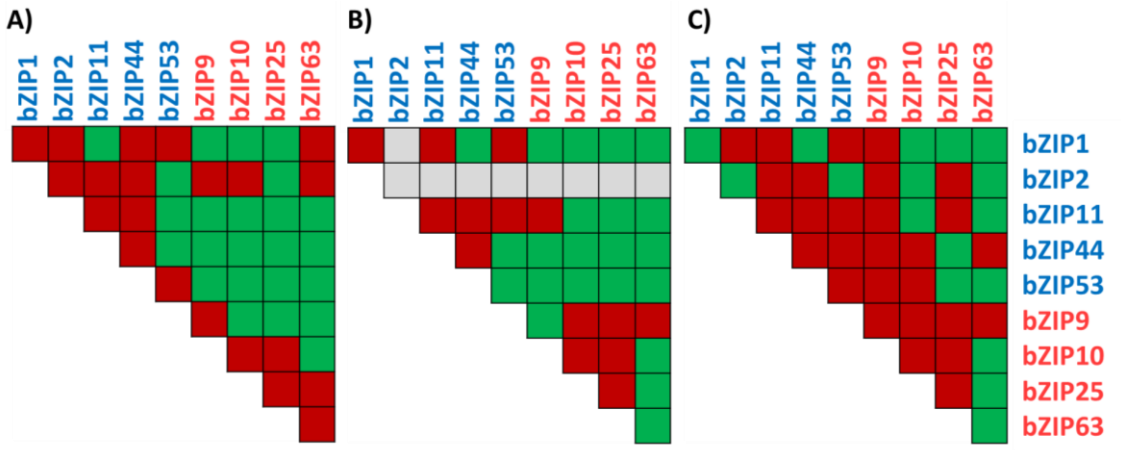

Figure 82. Alternative C/S1 networks experimentally defined by A) Ehlert et at. based on P2H method, B) Kang et al., and C) this work. Green squares are identified interacting dimers, red squares are non-interacting bZIPs, and grey squares are combinations not tested. In addition, Kaminaka et al. identified a bZIP10 homodimer not present in any of the three networks here depicted.

The most conspicuous difference among the three C/S1 networks so far reported are the lesser interactions identified in this study, and particularly the lack of bZIP9 interactors. As mentioned before, these differences probably arise from the less strict criteria followed by the other studies, in which the reciprocity between the two fusion conformations was not considered, and positive interactions were defined by only one positive observation. It is known that alternative methods for the identification of protein-protein interactions can result in different outcomes; without going any further, the P2H approach in Figure 30 could not identified any of the known GBF1 interactors, and the two articles above mentioned studying the C/S1 network found meaningful differences between the results obtained in yeast and in protoplasts. However, the variability of results involving the C/S1 network is outstanding, especially when they are contrasted with the robustness of results described for the G- and H-networks. This suggests that detection of interactions within the C/S1 network is more susceptible to the experimental conditions or the method applied. A possible explanation for that is provided by the different dimerization strengths above highlighted. Accordingly, the looseness of the interactions between C- and S1-bZIPs makes their formation more dependent on the context in which they are analyzed; while the stronger interactions between G- or H-bZIPs lead to the regular formation of those dimers independently of the conditions. Thus, the strength of the dimerization can be contemplated as a feature of each network.

4.5 The bZIP function

The transactivation assay performed with the 16 bZIPs highlighted that the function of a given bZIP is not fixed, but can vary importantly. Depending on the promoter tested, bZIPs could modify or not the expression and they acted distinctively as activators or repressors of the gene expression. In agreement with those

observations, other studies also showed that the bZIP function is strongly dependent on the conditions assayed. For instance, bZIP2 and bZIP44 were found to induce the *PDH* expression only under hypo-osmolarity conditions (Satoh et al., 2004), bZIP53 enhanced the *ASN1* expression only in the dark (Dietrich et al., 2011), and GBF1, bZIP16, and bZIP68 binding to the *LHCB2.4* promoter was dependent on the redox conditions (Shaikhali et al., 2012). Particularly, the function of the G- and H-bZIPs appears to be extensively modulated by further interacting proteins, and indeed, those bZIPs have been several times reported to be insufficient to exert any transactivation function by themselves, without the appropriate conditions (Tamai et al., 2002; Sehnke et al., 2005; Babu Rajendra Prasad et al., 2012). Anyhow, given that the 16 bZIPs analyzed are related to light signaling and environmental responses, their function is indeed not unexpected to be dependent on the cellular conditions.

Nevertheless, it is important to notice that such conditional function greatly complicates the study of the gene transactivation properties of the bZIPs, and it can be the cause for contradictory results found in the literature. For instance regarding whether the *PDH* promoter is activated (or not) by bZIP11 or bZIP53 (Satoh et al., 2004; Weltmeier et al., 2006; Hanson et al., 2008; Dietrich et al., 2011), and the RBCS1a expression is activated (or not) by Hy5 (Lee et al., 2007; Singh et al., 2012). Similarly, the lack of activation of the *LHCB2.4* expression observed in this thesis, even in combination with G-bZIPs which are inductors of that gene (Shaikhali et al., 2012), could be due to the inadequacy of the conditions tested. In this case, a sensible explanation for such inactivity is provided by the nuclear repositioning described for light-regulated genes (Feng et al., 2014). Those authors found that the activation of light-inducible genes such as *RBCS1a* and various *LHCB* family members required a separate regulatory step consisting in the repositioning of the light-induced loci from the nuclear interior to the periphery. In this thesis, the GUS assays were performed with dark-grown protoplasts, so the light-induced repositioning of the assayed promoters could not occur, eventually hampering the activation capability of the *LCHB2.4* and *RBCS1a* promoters.

Overall, the results of the GUS assay revealed that bZIPs belonging to the same interaction network share an important degree of functional consistency. On the one hand, the C/S1 network bZIPs regularly led to significant changes in the expression, while the transactivation effect of the G- and H- bZIPs was more selective; and on the other hand, those bZIPs which did induce significant changes in the expression, did it in the same direction (activating or repressing) and to a similar extent. Therefore, those data indicated that the transactivation properties of interacting bZIPs are partly redundant, an observation that is in agreement with previous reports (Lara et al., 2003; Weltmeier et al., 2006; Baena-González et al., 2007; Shen et al., 2008; Dietrich et al., 2011).

In addition, the gene transactivation experiments unveiled different functional relationships among the bZIPs of each network. In the C/S1 network prevailed a unidirectional interplay, so S1-bZIPs were sufficient to modify the transcription and had a dominant effect on the C-bZIPs, which were insufficient to alter the gene expression by themselves. Differently, the G-bZIPs resulted in intricate relationships based on active and inactive dominance, and exhibited an important degree of context-dependency. Finally, both H-bZIPs performed uniformly in all promoters. However, it has to be kept in mind that, since G- and H-bZIPs are related to light signaling, the fact that experiments were performed with dark-grown protoplasts could have failed to fulfil their activation requirements, what could be a source of additional experimental error. By any means, it is apparent that the bZIP function is distinctly and coordinately regulated in the different networks, what conveys the idea that each network acts as a functional unit.

4.5.1 The balance of the bZIP dimers

In addition to the interplay with other factors, the bZIP function has been proposed to be modulated by the regulation of the abundance of specific bZIPs in order to shift the equilibrium among the different dimers towards certain combinations, and that could be achieved by specific gene transcription regulation and subcellular compartmentalization (Kaminaka et al., 2006; Weltmeier et al., 2009). That presumption was also explored in this thesis. Data gathered indicated that the 16 bZIPs are located in the nucleus (at least partially) and most of them appear to be ubiquitously expressed, although there are differences in their expression levels among different parts of the plant.

While it is apparent that the transcript levels of some bZIPs show some degree of tissue specificity, interpreting that differential expression can be tricky since bZIP expression levels appear to change dynamically, judging from the important contradictory results found in the literature. For instance, according to one study the expression of the C- and S1-bZIPs was detected in sink, but not in source organs (Weltmeier et al., 2008), but other researchers found transcripts for the four C-bZIPs in adult leaves, a source organ (Lara et al., 2003), and a third study indicated that bZIP2 is ubiquitously expressed and bZIP11 is absent in young leaves, a sink organ (Lee et al., 2006). These discrepancies raise the doubt whether the differences measured in the bZIPs transcript levels reflect actual physiological states or are caused by the particularities of the experimental conditions, thereby entangling their interpretation.

Similarly, the localization of the 16 bZIPs as fluorescent fusion proteins by confocal microscopy also pointed in some cases to specific regulation of their localization, but again contradictory reports made it difficult to draw clear conclusions. On the one hand, there is the speckle formation observed for GBF1 and HyH. Regarding GBF1, speckle formation appears to be a robust trait of this bZIP because it could also be observed in Arabidopsis plants overexpressing a GBF1::GFP fusion protein (Appendix F). However, the speckle formation cannot be observed in similar pictures obtained by other researchers (Singh et al., 2012; Maurya et al., 2015). Still, it cannot be excluded that high laser intensities or out-of-focus blur resulted in fuzzy signals masking the punctuate structures. As for HyH, it was previously described to form speckles (Datta et al., 2006) in agreement with my observations, but that report also described speckles formation by Hy5, which I could not observe. Further, other studies could not detect speckle formation by any of these two bZIPs (Chattopadhyay et al., 1998; Shi et al., 2011; Singh et al., 2012). Therefore, how to interpret the speckle formation is also uncertain. On the other hand, confocal microscopy observations presented in this work show that bZIP10 and bZIP68 have a double localization, in the nucleus and in the cytoplasm. The extra-nuclear localization of bZIP10 has been already observed in agreement (Kaminaka et al., 2006), although in contradiction with other observations in which bZIP10 was exclusively nuclear localized (Weltmeier et al., 2006; Pomeranz et al., 2010). For bZIP68, the only report available showed exclusive nuclear localization (Shen et al., 2008), in disagreement with my observations. In addition, I found GBF1 and GBF2 only in the nucleus in agreement with other report (Singh et al., 2012), but in conflict with other description according to which both bZIPs were reported to be mostly cytoplasmic (Terzaghi et al., 1997). So again, the variability of the observations published obscures their assessment.

Altogether, while there are evidences that the localization and expression of certain bZIPs is distinctly adjusted, the inconsistency of the observations complicates the understanding of how they are regulated, and casts doubts on whether all of those disparate results are actually due to specific regulation of the monomer abundance or are experimentally induced. As for the possibility of those variations acting as a regulatory mechanism, it is arguable that changes in the amounts of particular bZIPs could contribute to modify the bZIP function. Considering that interacting bZIPs are functionally redundant and that there is a high intra-network dimerization promiscuity, it can be reasonably assumed that variations in the abundance of individual bZIPs will be balanced by the other members of the network. In fact, a proposed purpose for protein networks is to

bring functional robustness to their activity by, precisely, compensating variations in the activity of singular components (Schrum and Gil, 2012). Besides, that would provide an explanation for the fact that interacting bZIPs are often described to be functionally redundant (Lara et al., 2003; Weltmeier et al., 2006; Baena-González et al., 2007; Shen et al., 2008; Dietrich et al., 2011).

4.6 The combinatorial mechanism of the bZIP function

Inspired by the somatic recombination of immunoglobulins, the observation that many eukaryotic transcription factors form homo- and heterodimers was soon assumed to be a combinatorial mechanism generating a diversified repertoire of functions from a restricted set of regulatory elements (Lamb and McKnight, 1991). This notion has been applied especially to the bZIPs, given that they are obligated dimers and that different bZIP monomers have been reported to possess distinctive DNA-binding affinities and transactivation capabilities. However, that assumption depends on the capability of the bZIPs to form diversified dimers, so that in a scenario in which dimerization is highly restricted – as it was predicted for Arabidopsis bZIPs-, such a combinatorial mechanism would be rather limited.

The integrated view of the bZIP dimerization and function presented in this thesis brings new insights in the manner in which Arabidopsis bZIPs operate. To recapitulate, the main findings presented here are: I) bZIPs are organized in small, rather independent networks, within which bZIPs dimerize promiscuously between themselves. II) In a given network, bZIPs share similar interaction strengths and their coiled coil motifs have common structural features. III) Members of the same network are consistent in regard to their transcriptional effect and functional relationships. IV) These dimerization and functional features are distinctive for each network.

An important consequence of these considerations is that the possibility to generate dimers with new and unique qualities through heterodimerization is strongly limited, since bZIPs that can dimerize already share a high degree of functional redundancy. Thus, no fundamental changes in the bZIP function are expected directly due to intra-network heterodimerization. Instead, that redundancy prompts the notion that the bZIP networks operate as functional units. According to that, variations in the transcript levels, in the localization, or in the transactivation activities among the bZIPs of the same network would serve as varied input possibilities, and heterodimerization would function integrating the multiple inputs in order to maintain a robust output function, rather than generating dimers with specific functions as currently accepted (Figure 83). Besides, since each network seems to be functionally independent, the function of the network-units is likely to be regulated as a whole by alternative mechanisms, such as the repression of the translation of the S1-bZIPs by sucrose (Rahmani et al., 2009).

In addition, the structural particularities of the coiled coil motifs of members of each network together with the differences in the dimerization strength allows to speculate about the existence of alternative dimerization dynamics within each network. Accordingly, the dimerization-folding process within the G and H networks is likely to be more costly since those bZIPs are extensively disordered, but at the same time those dimers remain secured once established due to their optimized LZ motifs. Indeed, three of the G-bZIPs carry cysteine residues in their **a** positions, allowing the formation of intermolecular disulfide bridges which should strongly stabilize the dimer (Shaikhali et al., 2012). Following this argument, dimers belonging to the G and H networks are predicted to be very stable and hard to break apart. Conversely, the C- and S1-bZIPs are less disordered so that their folding has less energetic requirements, and they contain heptads with high helical tendency that can act as triggers facilitating their dimerization. However, these dimers feature fewer stabilizing forces, resulting in weaker interactions that can be easily separated back into monomers. Thus, in such dimers, the transition between the dimer-folded and the monomer-unfolded states entails lower energetic penalties,

facilitating the transition between states in a similar manner to the proposed folding mechanism for the Opaque-2 bZIP in *Coix* plants (Moreau et al., 2004).

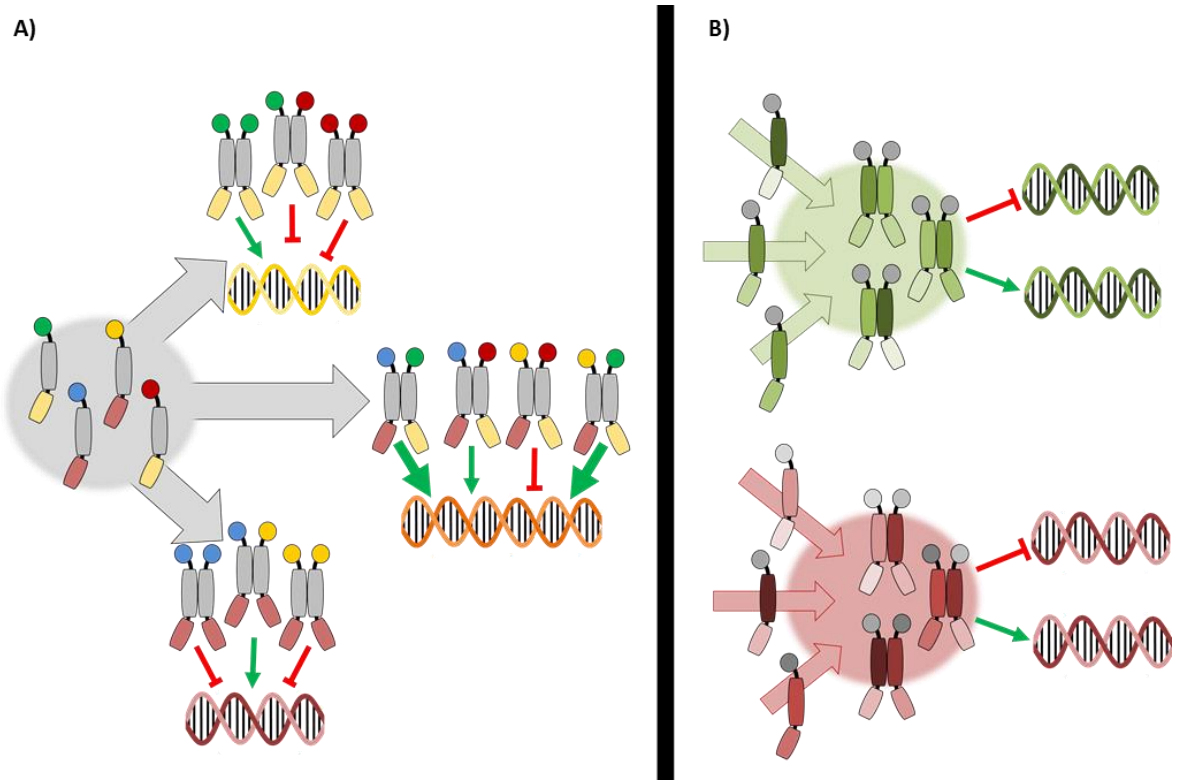

Figure 83. Diagram in which bZIP monomers are depicted highlighting the three main elements defining their function: the DNA binding (bottom part), the dimerization (middle part), and the transactivation (upper circle). A) Classical view of the bZIP dimerization according to which the function lies on the bZIP dimer. Interacting monomers have varied properties regarding transactivation and DNA binding, so that the heterodimerization generates diverse functions. B) Proposed model of bZIP networks as functional units. In this case the function is a property of the network itself, since the monomers already share similar transactivation and DNA binding properties. The role of the heterodimerization here is to integrate the different inputs which impinge on the expression of certain bZIPs or regulate their function. From Llorca et al., 2015.

Because bZIP dimerization defines the function, these different dimerization dynamics imply alternative modes of action for the different networks. The C/S1 network can be regarded as a steady exchange of monomers, with the C-bZIPs triggering the dimerization and the S1-bZIPs providing the transactivation capability. Recently, bZIP1 was described to follow a “hit-and-run” mode of action, according to which bZIP1 binds to a large set of cis elements in a transient manner (Para et al., 2014), a model compatible with a dynamic exchange of monomers. Conversely, the mode of action for the G and H networks involves the establishment of long lasting dimers which stably bind to their *cis*-element targets, while their transactivation activity is regulated by other factors. Indeed, the speckle formation observed in those bZIPs reinforces this idea, as they evidence the interplay of various components and they have been described to be relatively stable structures, independently whether their function in protein degradation or in active transcription processes, what is still under debate (Reddy et al., 2012; Van Buskirk et al., 2012).

5. Final considerations and outlook

This thesis initially dealt with the research project titled “Role of GBF1 in the crosstalk between LES and natural senescence”. That project relied on the role of GBF1 as a regulator of the onset of senescence, but data obtained in this work consistently failed to validate that aspect of GBF1. Understandably, one cannot search for a link connecting two elements when one of them is absent; thus, that project became empty of purpose, and so I set up an alternative research topic, which eventually resulted in the publication of the article titled “The elucidation of the interactome of 16 Arabidopsis bZIP factors reveals three independent functional networks”.

Although the work performed under the initial project could not support the proposed hypothesis -GBF1 acting as a connection between the stress response and senescence-, it contributed to update and broaden the knowledge about GBF1, and to a less extent also about bZIP63. I found apparent contradictions regarding the GBF1 function and localization which have been overlooked in several publications, so I find it appropriate to review them here to offer a hindsight about that bZIP. For instance, the nuclear-cytosolic shift described for GBF1 (Terzaghi et al., 1997) is cited by innumerable research articles about bZIPs, affecting the conclusions reached in many of them, despite the fact that all other studies available about GBF1 show it always and only in the nucleus. Being aware of such inconsistencies is important to determine the manner in which the available data about GBF1 are interpreted, and therefore, affecting the conclusions to take.

The first part of this thesis also dealt with some methodological issues which should be considered by other researchers when they design and carry out their experiments. I realized that the senescence-specific phenotypic characterization of plants entails an important subjective component: selecting which plants are to be analyzed at each time point and classifying their leaves according to the senescence state are aspects that can be strongly influenced by our expectations; if we know the identity of the plants. Therefore, I consider the improvement of performing those experiments as blind assays an essential condition to avoid incurring in selection bias. On the other hand, this work exposed troublesome aspects of the DPI-ELISA method when crude extracts are used, especially when it is intended to follow a quantitative approach. Protein expression conditions can greatly modify the outcome of that assay, therefore making the comparison of the binding signals produced by different samples unreliable; and that is an important drawback of the method that has to be taken into account. Finally, I honestly faced the mistake in the cloning into the pDEST42 vector, which is important to be disclosed in order to prevent other scientists repeating the same mistake. We normally assume that all Gateway vectors are compatible with each other, and do not pay attention to the specific requirements of the different destination vectors. But that is not so, and the cloning procedures have to be specifically designed accordingly.

Since the initial project mostly delivered negative results, reflecting about which steps could follow that work is not something straightforward. I guess it would be important to identify the reasons for the incongruence of the results obtained. Irreproducibility can happen due to a myriad of different causes, but because most of the discrepant results come from our same research group, reviewing the original data from the conflicting experiments seems the logical way to get started.

In the second part of this thesis, the investigation carried on deciphered the dimerization patterns of 16 bZIPs (one fifth of the Arabidopsis bZIP family) and analyzed their gene transactivating function on four different gene promoters. That wide perspective on the relationship between bZIP dimerization and function questioned the current viewpoint of the bZIP heterodimerization as a combinatorial mechanism to generate diversity in Arabidopsis, because heterodimers are usually formed between bZIPs with similar functional properties. In fact, that is what one can find in the literature about Arabidopsis bZIPs: many reports point to functional redundancy among bZIPs that can heterodimerize, and there is a meaningful lack of publications

supporting the premise that heterodimers feature distinctive properties compared to the corresponding homodimers, what is astonishing considering that that assumption is proposed to be a central mechanism defining the bZIP function.

Here, the purpose of the heterodimerization between Arabidopsis bZIPs was interpreted in an alternative manner. I proposed a model in which the inter-network heterodimerization allows the integration of multitude of simultaneously incoming signals, so the different bZIP networks act as functional units. That model was developed through inductive reasoning on the basis of the data I gathered. That is, I generalized the function of the Arabidopsis bZIPs networks from the study of specific cases; and that can be a weakness of this work even having analyzed a reasonably proportion of bZIPs. I have in mind here the fact that the bZIP function is strongly defined by the cellular context, so the methods or the conditions I used could have influenced the experimental outcomes for different bZIPs in distinctive manners; and thus, the conclusions reached subsequently. For instance, performing the GUS assays with dark-grown protoplasts could have specifically interfered with the function of the G- and H-bZIPs (which are light-signaling related) but not with the function of the C- and S1-bZIPs, therefore resulting in a biased representation of their transactivation properties. That is, however, an unavoidable problem inherent to any research decision taken, since there is not a right method or conditions to be chosen. In this case, if the protoplasts experiments would have been performed with green light-incubated protoplasts, it would probably have hampered the activation capability of the *ASN1* promoter, which was reported to be active only in the dark. Therefore, the model I proposed is an early step in the understanding of the bZIP function, which still has to be validated through the formulation and testing of predictions; and maybe adjusted again accordingly, in an iterative interplay between inductive and deductive inference processes.

An unexpected outcome of this work was the finding of the differential distribution of the forces driving the dimerization and defining its specificity along the coiled coil motifs of bZIPs from different networks. That novel mechanism regulating the dimer formation appears to be exclusive of plants, since plant bZIPs have the particularity of featuring coiled coil motifs variable in length, in opposition to other organisms in which bZIPs have comparable coiled coil lengths. This suggests the captivating possibility that bZIPs from plants and other organisms undergone divergent evolutionary processes, which could have even modified the function of the heterodimerization itself, explaining why animal bZIPs form few and extensively interconnected networks in which monomers featuring distinctive properties do can dimerize between them. Understanding the relevance of this mechanism in the function of Arabidopsis bZIPs and the distinctive purposes of the bZIP networks from different organisms are appealing research topics which can be conveniently addressed by bioinformatics studies, for most of the required data could be inferred from amino acid sequences.

6. Literature

Abe, M., Kobayashi, Y., Yamamoto, S., Daimon, Y., Yamaguchi, A., Ikeda, Y., Ichinoki, H., Notaguchi, M., Goto, K., and Araki, T. (2005). FD, a bZIP Protein Mediating Signals from the Floral Pathway Integrator FT at the Shoot Apex. Science **309,** 1052-1056.

Acharya, A., Rishi, V., and Vinson, C. (2006). Stability of 100 homo and heterotypic coiled-coil a-a'pairs for ten amino acids (A, L, I, V, N, K, S, T, E, and R). Biochemistry **45,** 11324-11332.

Acharya, A., Ruvinov, S.B., Gal, J., Moll, J.R., and Vinson, C. (2002). A heterodimerizing leucine zipper coiled coil system for examining the specificity of a position interactions: amino acids I, V, L, N, A, and K. Biochemistry **41,** 14122-14131.

Acharya, B.R., and Assmann, S.M. (2009). Hormone interactions in stomatal function. Plant molecular biology **69,** 451-462.

Ahuja, I., de Vos, R.C., Bones, A.M., and Hall, R.D. (2010). Plant molecular stress responses face climate change. Trends in plant science **15,** 664-674.

Akpinar, B.A., Avsar, B., Lucas, S.J., and Budak, H. (2012). Plant abiotic stress signaling. Plant signaling & behavior **7,** 1450-1455.

Alber, T. (1992). Structure of the leucine zipper. Current opinion in genetics & development **2,** 205-210.

Allen, D.J., and Ort, D.R. (2001). Impacts of chilling temperatures on photosynthesis in warm-climate plants. Trends in plant science **6,** 36-42.

Alonso, R., Onate-Sanchez, L., Weltmeier, F., Ehlert, A., Diaz, I., Dietrich, K., Vicente-Carbajosa, J., and Droge-Laser, W. (2009). A Pivotal Role of the Basic Leucine Zipper Transcription Factor bZIP53 in the Regulation of Arabidopsis Seed Maturation Gene Expression Based on Heterodimerization and Protein Complex Formation. The Plant Cell Online **21,** 1747-1761.

Altarejos, J.Y., and Montminy, M. (2011). CREB and the CRTC co-activators: sensors for hormonal and metabolic signals. Nature reviews Molecular cell biology **12,** 141-151.

Alves, M., Dadalto, S., Gonçalves, A., De Souza, G., Barros, V., and Fietto, L. (2013). Plant bZIP Transcription Factors Responsive to Pathogens: A Review. International journal of molecular sciences **14,** 7815-7828.

Andersson, A., Keskitalo, J., Sjodin, A., Bhalerao, R., Sterky, F., Wissel, K., Tandre, K., Aspeborg, H., Moyle, R., and Ohmiya, Y. (2004). A transcriptional timetable of autumn senescence. Genome biology **5,** /2004/2005/2004/R2024-/2004/2005/2004/R2024.

Apel, K., and Hirt, H. (2004). Reactive oxygen species: metabolism, oxidative stress, and signal transduction. Annu. Rev. Plant Biol. **55,** 373-399.

Araújo, W.L., Tohge, T., Ishizaki, K., Leaver, C.J., and Fernie, A.R. (2011). Protein degradation–an alternative respiratory substrate for stressed plants. Trends in plant science **16,** 489-498.

Arndt, K.M., Pelletier, J.N., MuÈller, K.M., Alber, T., Michnick, S.W., and PluÈckthun, A. (2000). A heterodimeric coiled-coil peptide pair selected in vivo from a designed library-versus-library ensemble. Journal of molecular biology **295,** 627-639.

Ashraf, M., and Harris, P. (2013). Photosynthesis under stressful environments: an overview. Photosynthetica **51,** 163-190.

Avila-Ospina, L., Moison, M., Yoshimoto, K., and Masclaux-Daubresse, C. (2014). Autophagy, plant senescence, and nutrient recycling. Journal of experimental botany**,** eru039.

Avila, J.R., Lee, J.S., and Torii, K.U. (2015). Co-Immunoprecipitation of Membrane-Bound Receptors. The Arabidopsis book/American Society of Plant Biologists **13**.

Avin-Wittenberg, T., Tzin, V., Angelovici, R., and Galili, G. (2012). Deciphering energy-associated gene networks operating in the response of Arabidopsis plants to stress and nutritional cues. The Plant Journal **70,** 954-966.

Babu Rajendra Prasad, V., Gupta, N., Nandi, A., and Chattopadhyay, S. (2012). HY1 genetically interacts with GBF1 and regulates the activity of the Z-box containing promoters in light signaling pathways in Arabidopsis thaliana. Mechanisms of development **129,** 298-307.

Baena-González, E., and Sheen, J. (2008). Convergent energy and stress signaling. Trends in plant science **13,** 474-482.

Baena-González, E., Rolland, F., Thevelein, J.M., and Sheen, J. (2007). A central integrator of transcription networks in plant stress and energy signalling. Nature **448,** 938-942.

Balazadeh, S., Riaño-Pachón, D., and Mueller-Roeber, B. (2008). Transcription factors regulating leaf senescence in Arabidopsis thaliana. Plant Biology **10,** 63-75.

Balazadeh, S., Kwasniewski, M., Caldana, C., Mehrnia, M., Zanor, M.I., Xue, G.-P., and Mueller-Roeber, B. (2011). ORS1, an H 2 O 2-responsive NAC transcription factor, controls senescence in Arabidopsis thaliana. Molecular plant **4,** 346-360.

Banerjee, A., and Roychoudhury, A. (2015). WRKY Proteins: Signaling and Regulation of Expression during Abiotic Stress Responses. The Scientific World Journal **2015**.

Baron, K.N., Schroeder, D.F., and Stasolla, C. (2012). Transcriptional response of abscisic acid (ABA) metabolism and transport to cold and heat stress applied at the reproductive stage of development in Arabidopsis thaliana. Plant Science **188,** 48-59.

Baxter, A., Mittler, R., and Suzuki, N. (2014). ROS as key players in plant stress signalling. Journal of experimental botany **65,** 1229-1240.

Berendzen, K.W., Böhmer, M., Wallmeroth, N., Peter, S., Vesić, M., Zhou, Y., Tiesler, F.K., Schleifenbaum, F., and Harter, K. (2012). Screening for in planta protein-protein interactions combining bimolecular fluorescence complementation with flow cytometry. Plant Methods **8,** 25.

Besseau, S., Li, J., and Palva, E.T. (2012). WRKY54 and WRKY70 co-operate as negative regulators of leaf senescence in Arabidopsis thaliana. Journal of experimental botany**,** err450.

Bieker, S., Riester, L., Stahl, M., Franzaring, J., and Zentgraf, U. (2012). Senescence-specific Alteration of Hydrogen Peroxide Levels in Arabidopsis thaliana and Oilseed Rape Spring Variety Brassica napus L. cv. MozartF. Journal of integrative plant biology **54,** 540-554.

Bläsing, O.E., Gibon, Y., Günther, M., Höhne, M., Morcuende, R., Osuna, D., Thimm, O., Usadel, B., Scheible, W.-R., and Stitt, M. (2005). Sugars and circadian regulation make major contributions to the global regulation of diurnal gene expression in Arabidopsis. The Plant Cell Online **17,** 3257-3281.

Bokszczanin, K.L., Network, S.P.T.I.T., and Consortium, S.F. (2013). Perspectives on deciphering mechanisms underlying plant heat stress response and thermotolerance. Frontiers in plant science **4**.

Bondos, S.E., and Bicknell, A. (2003). Detection and prevention of protein aggregation before, during, and after purification. Analytical biochemistry **316,** 223-231.

Bornberg-Bauer, E., Rivals, E., and Vingron, M. (1998). Computational approaches to identify leucine zippers. Nucleic acids research **26,** 2740-2746.

Boyle, P., and Després, C. (2010). Dual-function transcription factors and their entourage: Unique and unifying themes governing two pathogenesis-related genes. Plant signaling & behavior **5,** 629-634.

Bracha-Drori, K., Shichrur, K., Katz, A., Oliva, M., Angelovici, R., Yalovsky, S., and Ohad, N. (2004). Detection of protein–protein interactions in plants using bimolecular fluorescence complementation. The Plant Journal **40,** 419-427.

Brand, L.H., Kirchler, T., Hummel, S., Chaban, C., and Wanke, D. (2010). DPI-ELISA: a fast and versatile method to specify the binding of plant transcription factors to DNA in vitro. Plant Methods **6,** 25.

Breeze, E., Harrison, E., McHattie, S., Hughes, L., Hickman, R., Hill, C., Kiddle, S., Kim, Y.-s., Penfold, C.A., and Jenkins, D. (2011). High-resolution temporal profiling of transcripts during Arabidopsis leaf senescence reveals a distinct chronology of processes and regulation. The Plant Cell Online **23,** 873-894.

Broadley, M., Escobar-Gutierrez, A., Burns, A., and Burns, I. (2000). What are the effects of nitrogen deficiency on growth components of lettuce? New Phytologist **147,** 519-526.

Buchanan-Wollaston, V. (1997). The molecular biology of leaf senescence. Journal of experimental botany **48,** 181-199.

Buchanan-Wollaston, V., Earl, S., Harrison, E., Mathas, E., Navabpour, S., Page, T., and Pink, D. (2003). The molecular analysis of leaf senescence–a genomics approach. Plant Biotechnology Journal **1,** 3-22.

Buchanan-Wollaston, V., Page, T., Harrison, E., Breeze, E., Lim, P.O., Nam, H.G., Lin, J.F., Wu, S.H., Swidzinski, J., and Ishizaki, K. (2005). Comparative transcriptome analysis reveals significant differences in gene expression and signalling pathways between developmental and dark/starvation-induced senescence in Arabidopsis. The Plant Journal **42,** 567-585.

Bueso, E., Alejandro, S., Carbonell, P., Perez-Amador, M.A., Fayos, J., Bellés, J.M., Rodriguez, P.L., and Serrano, R. (2007). The lithium tolerance of the Arabidopsis cat2 mutant reveals a cross-talk between oxidative stress and ethylene. The Plant Journal **52,** 1052-1065.

Caldana, C., Li, Y., Leisse, A., Zhang, Y., Bartholomaeus, L., Fernie, A.R., Willmitzer, L., and Giavalisco, P. (2013). Systemic analysis of inducible target of rapamycin mutants reveal a general metabolic switch controlling growth in Arabidopsis thaliana. The Plant Journal **73,** 897-909.

Cao, D., Lin, Y., and Cheng, C.-L. (2000). Genetic Interactions between the Chlorate-Resistant Mutant cr88 and the Photomorphogenic Mutants cop1 and hy5. The Plant cell **12,** 199-210.

Carrillo, R.J., Dragan, A.I., and Privalov, P.L. (2010). Stability and DNA-binding ability of the bZIP dimers formed by the ATF-2 and c-Jun transcription factors. Journal of molecular biology **396,** 431-440.

Chattopadhyay, S., Ang, L.-H., Puente, P., Deng, X.-W., and Wei, N. (1998). Arabidopsis bZIP protein HY5 directly interacts with light-responsive promoters in mediating light control of gene expression. The Plant Cell Online **10,** 673-683.

Chen, G.-H., Liu, C.-P., Chen, S.-C.G., and Wang, L.-C. (2011). Role of ARABIDOPSIS A-FIFTEEN in regulating leaf senescence involves response to reactive oxygen species and is dependent on ETHYLENE INSENSITIVE2. Journal of experimental botany**,** err278.

Chen, M., Maodzeka, A., Zhou, L., Ali, E., Wang, Z., and Jiang, L. (2014). Removal of DELLA repression promotes leaf senescence in Arabidopsis. Plant Science **219,** 26-34.

Choi, H.i., Hong, J., Ha, J., Kang, J., and Kim, S.Y. (2000). ABFs, a Family of ABA-responsive Element Binding Factors. Journal of Biological Chemistry **275,** 1723-1730.

Choudhury, S., Panda, P., Sahoo, L., and Panda, S.K. (2013). Reactive oxygen species signaling in plants under abiotic stress. Plant signaling & behavior **8**.

Chundawat, S.P., Beckham, G.T., Himmel, M.E., and Dale, B.E. (2011). Deconstruction of lignocellulosic biomass to fuels and chemicals. Annual review of chemical and biomolecular engineering **2,** 121-145.

Chung, B.-C., Lee, S.Y., Oh, S.A., Rhew, T.H., Nam, H.G., and Lee, C.-H. (1997). The promoter activity of sen 1, a senescence-associated gene of Arabidopsis, is repressed by sugars. Journal of plant physiology **151,** 339-345.

Ciani, B., Hutchinson, E.G., Sessions, R.B., and Woolfson, D.N. (2002). A designed system for assessing how sequence affects α to β conformational transitions in proteins. Journal of Biological Chemistry **277,** 10150-10155.

Clough, S.J., and Bent, A.F. (1998). Floral dip: a simplified method forAgrobacterium-mediated transformation ofArabidopsis thaliana. The plant journal **16,** 735-743.

Conklin, P., and Barth, C. (2004). Ascorbic acid, a familiar small molecule intertwined in the response of plants to ozone, pathogens, and the onset of senescence. Plant, Cell & Environment **27,** 959-970.

Contento, A.L., Kim, S.-J., and Bassham, D.C. (2004). Transcriptome profiling of the response of Arabidopsis suspension culture cells to Suc starvation. Plant physiology **135,** 2330-2347.

Cortleven, A., and Schmülling, T. (2015). Regulation of chloroplast development and function by cytokinin. Journal of experimental botany**,** erv132.

Crick, F.H. (1953). The packing of-helices: simple coiled-coils. Acta crystallographica **6,** 689-697.

Crozet, P., Jammes, F., Valot, B., Ambard-Bretteville, F., Nessler, S., Hodges, M., Vidal, J., and Thomas, M. (2010). Cross-phosphorylation between Arabidopsis thaliana sucrose nonfermenting 1-related protein kinase 1 (AtSnRK1) and its activating kinase (AtSnAK) determines their catalytic activities. Journal of Biological Chemistry **285,** 12071-12077.

Crozet, P., Margalha, L., Confraria, A., Rodrigues, A., Martinho, C., Adamo, M., Elias, C.A., and Baena-González, E. (2014). Mechanisms of regulation of SNF1/AMPK/SnRK1 protein kinases. Frontiers in plant science **5**.

Cui, M.H., Ok, S.H., Yoo, K.S., Jung, K.W., Yoo, S.D., and Shin, J.S. (2013). An Arabidopsis cell growth defect factor-related protein, CRS, promotes plant senescence by increasing the production of hydrogen peroxide. Plant and Cell Physiology **54,** 155-167.

Danquah, A., de Zelicourt, A., Colcombet, J., and Hirt, H. (2014). The role of ABA and MAPK signaling pathways in plant abiotic stress responses. Biotechnology advances **32,** 40-52.

Daszkowska-Golec, A., and Szarejko, I. (2013). Open or close the gate–stomata action under the control of phytohormones in drought stress conditions. Frontiers in plant science **4**.

Datta, S., Hettiarachchi, G., Deng, X.-W., and Holm, M. (2006). Arabidopsis CONSTANS-LIKE3 is a positive regulator of red light signaling and root growth. The Plant Cell Online **18,** 70-84.

del Río, L.A., Pastori, G.M., Palma, J.M., Sandalio, L.M., Sevilla, F., Corpas, F.J., Jiménez, A., López-Huertas, E., and Hernández, J.A. (1998). The activated oxygen role of peroxisomes in senescence. Plant physiology **116,** 1195-1200.

Delatte, T.L., Sedijani, P., Kondou, Y., Matsui, M., de Jong, G.J., Somsen, G.W., Wiese-Klinkenberg, A., Primavesi, L.F., Paul, M.J., and Schluepmann, H. (2011). Growth arrest by trehalose-6-phosphate: an astonishing case of primary metabolite control over growth by way of the SnRK1 signaling pathway. Plant physiology **157,** 160-174.

Deppmann, C.D., Alvania, R.S., and Taparowsky, E.J. (2006). Cross-Species Annotation of Basic Leucine Zipper Factor Interactions: Insight into the Evolution of Closed Interaction Networks. Molecular biology and evolution **23,** 1480-1492.

Deppmann, C.D., Acharya, A., Rishi, V., Wobbes, B., Smeekens, S., Taparowsky, E.J., and Vinson, C. (2004). Dimerization specificity of all 67 B-ZIP motifs in Arabidopsis thaliana: a comparison to Homo sapiens B-ZIP motifs. Nucleic acids research **32,** 3435-3445.

Desikan, R., Last, K., Harrett-Williams, R., Tagliavia, C., Harter, K., Hooley, R., Hancock, J.T., and Neill, S.J. (2006). Ethylene-induced stomatal closure in Arabidopsis occurs via AtrbohF-mediated hydrogen peroxide synthesis. The Plant Journal **47,** 907-916.

Diaz, C., Purdy, S., Christ, A., Morot-Gaudry, J.-F., Wingler, A., and Masclaux-Daubresse, C. (2005). Characterization of markers to determine the extent and variability of leaf senescence in Arabidopsis. A metabolic profiling approach. Plant physiology **138,** 898-908.

Dietrich, K., Weltmeier, F., Ehlert, A., Weiste, C., Stahl, M., Harter, K., and Dröge-Laser, W. (2011). Heterodimers of the Arabidopsis transcription factors bZIP1 and bZIP53 reprogram amino acid metabolism during low energy stress. The Plant Cell Online **23,** 381-395.

Djamei, A., Pitzschke, A., Nakagami, H., Rajh, I., and Hirt, H. (2007). Trojan horse strategy in Agrobacterium transformation: abusing MAPK defense signaling. Science **318,** 453-456.

Donahue Jr, R.A., and Bebee, R.L. (1999). BL21-SI™ competent cells for protein expression in E. coli. Protein Expr. Purif **7,** 289.

Dong, H., and Hartgerink, J.D. (2007). Role of hydrophobic clusters in the stability of α-helical coiled coils and their conversion to amyloid-like β-sheets. Biomacromolecules **8,** 617-623.

Dunnett, C.W. (1955). A multiple comparison procedure for comparing several treatments with a control. Journal of the American Statistical Association **50,** 1096-1121.

Duque, A.S., Farinha, A.P., da Silva, A.B., de Almeida, A.M., Santos, D., da Silva, J.M., Fevereiro, P., and de Sousa Araújo, S. (2013). Abiotic stress responses in plants: unraveling the complexity of genes and networks to survive. (INTECH Open Access Publisher).

Echevarría-Zomeño, S., Yángüez, E., Fernández-Bautista, N., Castro-Sanz, A.B., Ferrando, A., and Castellano, M. (2013). Regulation of translation initiation under biotic and abiotic stresses. International journal of molecular sciences **14,** 4670-4683.

Eckardt, N.A. (2001). From Darkness into Light: Factors Controlling Photomorphogenesis. The Plant cell **13,** 219-221.

Edwards, K., Johnstone, C., and Thompson, C. (1991). A simple and rapid method for the preparation of plant genomic DNA for PCR analysis. Nucleic acids research **19,** 1349.

Ehlert, A., Weltmeier, F., Wang, X., Mayer, C.S., Smeekens, S., Vicente-Carbajosa, J., and Droge-Laser, W. (2006). Two-hybrid protein-protein interaction analysis in Arabidopsis protoplasts: establishment of

a heterodimerization map of group C and group S bZIP transcription factors. The Plant journal : for cell and molecular biology **46,** 890-900.

Fariduddin, Q., Yusuf, M., Ahmad, I., and Ahmad, A. (2014). Brassinosteroids and their role in response of plants to abiotic stresses. Biologia Plantarum **58,** 9-17.

Feild, T.S., Lee, D.W., and Holbrook, N.M. (2001). Why leaves turn red in autumn. The role of anthocyanins in senescing leaves of red-osier dogwood. Plant physiology **127,** 566-574.

Feldbrügge, M., Sprenger, M., Dinkelbach, M., Yazaki, K., Harter, K., and Weisshaar, B. (1994). Functional analysis of a light-responsive plant bZIP transcriptional regulator. The Plant cell **6,** 1607-1621.

Feng, C.-M., Qiu, Y., Van Buskirk, E.K., Yang, E.J., and Chen, M. (2014). Light-regulated gene repositioning in Arabidopsis. Nature communications **5**.

Fernandez, O., Vandesteene, L., Feil, R., Baillieul, F., Lunn, J.E., and Clément, C. (2012). Trehalose metabolism is activated upon chilling in grapevine and might participate in Burkholderia phytofirmans induced chilling tolerance. Planta **236,** 355-369.

Ferrante, A., and Francini, A. (2006). Ethylene and leaf senescence. In Ethylene Action in Plants (Springer), pp. 51-67.

Fior, S., Vianelli, A., and Gerola, P.D. (2009). A novel method for fluorometric continuous measurement of β-glucuronidase (GUS) activity using 4-methyl-umbelliferyl-β-d-glucuronide (MUG) as substrate. Plant Science **176,** 130-135.

Flingquist, S., Shinedling, S., Barrickfi, D., and Gold, L. (1992). Translation initiation in Escherichia coli: sequences within the ribosome-binding site. Molecular microbiology **6,** 1219-1229.

Fong, J., Keating, A., and Singh, M. (2004). Predicting specificity in bZIP coiled-coil protein interactions. Genome Biology **5,** R11.

Foster, R., Izawa, T., and Chua, N.-H. (1994). Plant bZIP proteins gather at ACGT elements. The FASEB Journal **8,** 192-200.

Foyer, C.H., and Noctor, G. (2005). Redox homeostasis and antioxidant signaling: a metabolic interface between stress perception and physiological responses. The Plant Cell Online **17,** 1866-1875.

Foyer, C.H., and Noctor, G. (2009). Redox regulation in photosynthetic organisms: signaling, acclimation, and practical implications. Antioxidants & redox signaling **11,** 861-905.

Friedman, J.S., Khanna, H., Swain, P.K., DeNicola, R., Cheng, H., Mitton, K.P., Weber, C.H., Hicks, D., and Swaroop, A. (2004). The minimal transactivation domain of the basic motif-leucine zipper transcription factor NRL interacts with TATA-binding protein. Journal of Biological Chemistry **279,** 47233-47241.

Fujii, Y., Shimizu, T., Toda, T., Yanagida, M., and Hakoshima, T. (2000). Structural basis for the diversity of DNA recognition by bZIP transcription factors. Nature Structural Biology **7,** 889-893.

Fujiki, Y., Yoshikawa, Y., Sato, T., Inada, N., Ito, M., Nishida, I., and Watanabe, A. (2001). Dark-inducible genes from Arabidopsisthaliana are associated with leaf senescence and repressed by sugars. Physiologia Plantarum **111,** 345-352.

Fujita, Y., Fujita, M., Satoh, R., Maruyama, K., Parvez, M.M., Seki, M., Hiratsu, K., Ohme-Takagi, M., Shinozaki, K., and Yamaguchi-Shinozaki, K. (2005). AREB1 Is a Transcription Activator of Novel ABRE-Dependent ABA Signaling That Enhances Drought Stress Tolerance in Arabidopsis. The Plant Cell Online **17,** 3470-3488.

Gan, S., and Amasino, R.M. (1995). Inhibition of leaf senescence by autoregulated production of cytokinin. Science **270,** 1986-1988.

Gan, S., and Amasino, R.M. (1997). Making sense of senescence (molecular genetic regulation and manipulation of leaf senescence). Plant physiology **113,** 313.

Gangappa, S.N., Srivastava, A.K., Maurya, J.P., Ram, H., and Chattopadhyay, S. (2013). Z-box binding transcription factors (ZBFs): a new class of transcription factors in Arabidopsis seedling development. Molecular plant **6,** 1758-1768.

Garnett, T.P., and Graham, R.D. (2005). Distribution and remobilization of iron and copper in wheat. Annals of Botany **95,** 817-826.

Gaufichon, L., Reisdorf-Cren, M., Rothstein, S.J., Chardon, F., and Suzuki, A. (2010). Biological functions of asparagine synthetase in plants. Plant Science **179,** 141-153.

Gechev, T.S., Van Breusegem, F., Stone, J.M., Denev, I., and Laloi, C. (2006). Reactive oxygen species as signals that modulate plant stress responses and programmed cell death. Bioessays **28,** 1091-1101.

Gehl, C., Kaufholdt, D., Hamisch, D., Bikker, R., Kudla, J., Mendel, R.R., and Hänsch, R. (2011). Quantitative analysis of dynamic protein–protein interactions in planta by a floated-leaf luciferase complementation imaging (FLuCI) assay using binary Gateway vectors. The Plant Journal **67,** 542-553.

Gepstein, S., and Glick, B.R. (2013). Strategies to ameliorate abiotic stress-induced plant senescence. Plant molecular biology **82,** 623-633.

Gill, S.S., and Tuteja, N. (2010). Reactive oxygen species and antioxidant machinery in abiotic stress tolerance in crop plants. Plant Physiology and Biochemistry **48,** 909-930.

Glover, J.N.M., and Harrison, S.C. (1995). Crystal structure of the heterodimeric bZIP transcription factor c-Fos-c-Jun bound to DNA. Nature **373,** 257-261.

Grigoryan, G., and Keating, A.E. (2006). Structure-based prediction of bZIP partnering specificity. Journal of molecular biology **355,** 1125-1142.

Grigoryan, G., Reinke, A.W., and Keating, A.E. (2009). Design of protein-interaction specificity gives selective bZIP-binding peptides. Nature **458,** 859-864.

Guiboileau, A., Sormani, R., Meyer, C., and Masclaux-Daubresse, C. (2010). Senescence and death of plant organs: nutrient recycling and developmental regulation. Comptes rendus biologies **333,** 382-391.

Guo, Y., and Gan, S. (2006). AtNAP, a NAC family transcription factor, has an important role in leaf senescence. The Plant Journal **46,** 601-612.

Guo, Y., Cai, Z., and Gan, S. (2004). Transcriptome of Arabidopsis leaf senescence. Plant, Cell & Environment **27,** 521-549.

Gupta, B., and Huang, B. (2014). Mechanism of salinity tolerance in plants: physiological, biochemical, and molecular characterization. International journal of genomics **2014**.

Hadfield, K.A., and Bennett, A.B. (1997). Programmed senescence of plant organs. Cell death and differentiation **4,** 662-670.

Halford, N., and Hey, S. (2009). Snf1-related protein kinases (SnRKs) act within an intricate network that links metabolic and stress signalling in plants. Biochem. J **419,** 247-259.

Han, M., Kim, C.-Y., Lee, J., Lee, S.-K., and Jeon, J.-S. (2014). OsWRKY42 Represses OsMT1d and Induces Reactive Oxygen Species and Leaf Senescence in Rice. Molecules and cells **37,** 532.

Hanson, J., Hanssen, M., Wiese, A., Hendriks, M.M., and Smeekens, S. (2008). The sucrose regulated transcription factor bZIP11 affects amino acid metabolism by regulating the expression of ASPARAGINE SYNTHETASE1 and PROLINE DEHYDROGENASE2. The Plant Journal **53,** 935-949.

Harbury, P.B., Zhang, T., Kim, P.S., and Alber, T. (1993). A switch between two-, three-, and four-stranded coiled coils in GCN4 leucine zipper mutants. Science **262,** 1401-1407.

Harter, K., Kircher, S., Frohnmeyer, H., Krenz, M., Nagy, F., and Schäfer, E. (1994). Light-regulated modification and nuclear translocation of cytosolic G-box binding factors in parsley. The Plant cell **6,** 545-559.

He, Y., and Gan, S. (2002). A gene encoding an acyl hydrolase is involved in leaf senescence in Arabidopsis. The Plant Cell Online **14,** 805-815.

He, Y., Fukushige, H., Hildebrand, D.F., and Gan, S. (2002). Evidence supporting a role of jasmonic acid in Arabidopsis leaf senescence. Plant physiology **128,** 876-884.

Hedbacker, K., and Carlson, M. (2008). SNF1/AMPK pathways in yeast. Frontiers in bioscience: a journal and virtual library **13,** 2408.

Heinekamp, T., Kuhlmann, M., Lenk, A., Strathmann, A., and Dröge-Laser, W. (2002). The tobacco bZIP transcription factor BZI-1 binds to G-box elements in the promoters of phenylpropanoid pathway genes in vitro, but it is not involved in their regulation in vivo. Molecular Genetics and Genomics **267,** 16-26.

Hey, S.J., Byrne, E., and Halford, N.G. (2010). The interface between metabolic and stress signalling. Annals of Botany **105,** 197-203.

Hicks, M.R., Holberton, D.V., Kowalczyk, C., and Woolfson, D.N. (1997). Coiled-coil assembly by peptides with non-heptad sequence motifs. Folding and Design **2,** 149-158.

Himelblau, E., and Amasino, R.M. (2001). Nutrients mobilized from leaves of Arabidopsis thaliana during leaf senescence. Journal of Plant Physiology **158,** 1317-1323.

Hinderhofer, K., and Zentgraf, U. (2001). Identification of a transcription factor specifically expressed at the onset of leaf senescence. Planta **213,** 469-473.

Holm, M., Ma, L.-G., Qu, L.-J., and Deng, X.-W. (2002). Two interacting bZIP proteins are direct targets of COP1-mediated control of light-dependent gene expression in Arabidopsis. Genes & Development **16,** 1247-1259.

Horstman, A., Tonaco, I.A., Boutilier, K., and Immink, R.G. (2014). A cautionary note on the use of split-YFP/BiFC in plant protein-protein interaction studies. International journal of molecular sciences **15,** 9628-9643.

Hörtensteiner, S. (2006). CHLOROPHYLL DEGRADATION DURING SENESCENCE*. Annu. Rev. Plant Biol. **57,** 55-77.

Hörtensteiner, S. (2013). Update on the biochemistry of chlorophyll breakdown. Plant molecular biology **82,** 505-517.

Hörtensteiner, S., and Kräutler, B. (2011). Chlorophyll breakdown in higher plants. Biochimica et Biophysica Acta (BBA)-Bioenergetics **1807,** 977-988.

Hossain, M.A., Piyatida, P., da Silva, J.A.T., and Fujita, M. (2012). Molecular mechanism of heavy metal toxicity and tolerance in plants: central role of glutathione in detoxification of reactive oxygen species and methylglyoxal and in heavy metal chelation. Journal of Botany **2012**.

Hou, K., Wu, W., and Gan, S.-S. (2013). SAUR36, a small auxin up RNA gene, is involved in the promotion of leaf senescence in Arabidopsis. Plant physiology **161,** 1002-1009.

Hsieh, W.P., Hsieh, H.L., and Wu, S.H. (2012). Arabidopsis bZIP16 transcription factor integrates light and hormone signaling pathways to regulate early seedling development. The Plant cell **24,** 3997-4011.

Huang, J.-Z., and Huber, S.C. (2001). Phosphorylation of synthetic peptides by a CDPK and plant SNF1-related protein kinase. Influence of proline and basic amino acid residues at selected positions. Plant and Cell Physiology **42,** 1079-1087.

Iglesias-Fernandez, R., Wozny, D., Iriondo-de Hond, M., Onate-Sanchez, L., Carbonero, P., and Barrero-Sicilia, C. (2014). The AtCathB3 gene, encoding a cathepsin B-like protease, is expressed during germination of Arabidopsis thaliana and transcriptionally repressed by the basic leucine zipper protein GBF1. Journal of experimental botany **65,** 2009-2021.

Im Kim, J., Murphy, A.S., Baek, D., Lee, S.-W., Yun, D.-J., Bressan, R.A., and Narasimhan, M.L. (2011). YUCCA6 over-expression demonstrates auxin function in delaying leaf senescence in Arabidopsis thaliana. Journal of experimental botany**,** err094.

Ishida, H., Izumi, M., Wada, S., and Makino, A. (2014). Roles of autophagy in chloroplast recycling. Biochimica et Biophysica Acta (BBA)-Bioenergetics **1837,** 512-521.

Iven, T., Strathmann, A., Böttner, S., Zwafink, T., Heinekamp, T., Guivarc'h, A., Roitsch, T., and Dröge-Laser, W. (2010). Homo-and heterodimers of tobacco bZIP proteins counteract as positive or negative regulators of transcription during pollen development. The Plant Journal **63,** 155-166.

Iwata, Y., Fedoroff, N.V., and Koizumi, N. (2008). Arabidopsis bZIP60 Is a Proteolysis-Activated Transcription Factor Involved in the Endoplasmic Reticulum Stress Response. The Plant Cell Online **20,** 3107-3121.

Jakoby, M., Weisshaar, B., Dröge-Laser, W., Vicente-Carbajosa, J., Tiedemann, J., Kroj, T., and Parcy, F. (2002). bZIP transcription factors in Arabidopsis. Trends in Plant Science **7,** 106-111.

Janda, M., and Ruelland, E. (2014). Magical mystery tour: salicylic acid signalling. Environmental and Experimental Botany.

Jefferson, R.A. (1987). Assaying chimeric genes in plants: the GUS gene fusion system. Plant molecular biology reporter **5,** 387-405.

Jensen, M., Kjaersgaard, T., Nielsen, M., Galberg, P., Petersen, K., O'shea, C., and Skriver, K. (2010). The Arabidopsis thaliana NAC transcription factor family: structure-function relationships and determinants of ANAC019 stress signalling. Biochem. J **426,** 183-196.

Ji, X., Wang, L., Nie, X., He, L., Zang, D., Liu, Y., Zhang, B., and Wang, Y. (2014). A novel method to identify the DNA motifs recognized by a defined transcription factor. Plant molecular biology **86,** 367-380.

Jiao, Y., Lau, O.S., and Deng, X.W. (2007). Light-regulated transcriptional networks in higher plants. Nature Reviews Genetics **8,** 217-230.

Jibran, R., Hunter, D.A., and Dijkwel, P.P. (2013). Hormonal regulation of leaf senescence through integration of developmental and stress signals. Plant molecular biology **82,** 547-561.

Jing, H.-C., Schippers, J.H., Hille, J., and Dijkwel, P.P. (2005). Ethylene-induced leaf senescence depends on age-related changes and OLD genes in Arabidopsis. Journal of experimental botany **56,** 2915-2923.

Jing, H.C., Hebeler, R., Oeljeklaus, S., Sitek, B., Stühler, K., Meyer, H., Sturre, M., Hille, J., Warscheid, B., and Dijkwel, P. (2008). Early leaf senescence is associated with an altered cellular redox balance in Arabidopsis cpr5/old1 mutants. Plant Biology **10,** 85-98.

Jongebloed, U., Szederkényi, J., Hartig, K., Schobert, C., and Komor, E. (2004). Sequence of morphological and physiological events during natural ageing and senescence of a castor bean leaf: sieve tube occlusion and carbohydrate back-up precede chlorophyll degradation. Physiologia Plantarum **120,** 338-346.

Jung, C., Lyou, S.H., Yeu, S., Kim, M.A., Rhee, S., Kim, M., Lee, J.S., Do Choi, Y., and Cheong, J.-J. (2007). Microarray-based screening of jasmonate-responsive genes in Arabidopsis thaliana. Plant cell reports **26,** 1053-1063.

Kaminaka, H., Näke, C., Epple, P., Dittgen, J., Schütze, K., Chaban, C., Holt, B.F., Merkle, T., Schäfer, E., and Harter, K. (2006). bZIP10-LSD1 antagonism modulates basal defense and cell death in Arabidopsis following infection. The EMBO journal **25,** 4400-4411.

Kammerer, R.A., Schulthess, T., Landwehr, R., Lustig, A., Engel, J., Aebi, U., and Steinmetz, M.O. (1998). An autonomous folding unit mediates the assembly of two-stranded coiled coils. Proceedings of the National Academy of Sciences **95,** 13419-13424.

Kang, S.G., Price, J., Lin, P.C., Hong, J.C., and Jang, J.C. (2010). The arabidopsis bZIP1 transcription factor is involved in sugar signaling, protein networking, and DNA binding. Molecular plant **3,** 361-373.

Karimi, M., Inzé, D., and Depicker, A. (2002). GATEWAY™ vectors for Agrobacterium-mediated plant transformation. Trends in plant science **7,** 193-195.

Kaup, M.T., Froese, C.D., and Thompson, J.E. (2002). A role for diacylglycerol acyltransferase during leaf senescence. Plant physiology **129,** 1616-1626.

Kawamoto, N., Sasabe, M., Endo, M., Machida, Y., and Araki, T. (2015). Calcium-dependent protein kinases responsible for the phosphorylation of a bZIP transcription factor FD crucial for the florigen complex formation. Scientific reports **5**.

Keech, O., Pesquet, E., Ahad, A., Askne, A., Nordvall, D., Vodnala, S.M., Tuominen, H., Hurry, V., Dizengremel, P., and Gardestroem, P. (2007). The different fates of mitochondria and chloroplasts during dark-induced senescence in Arabidopsis leaves. Plant, cell & environment **30,** 1523-1534.

Keil, R.M. (2004). Coping and stress: a conceptual analysis. Journal of advanced nursing **45,** 659-665.

Kerppola, T.K. (2008). Bimolecular fluorescence complementation (BiFC) analysis as a probe of protein interactions in living cells. Annual review of biophysics **37,** 465-487.

Keskitalo, J., Bergquist, G., Gardeström, P., and Jansson, S. (2005). A cellular timetable of autumn senescence. Plant physiology **139,** 1635-1648.

Khan, M., Rozhon, W., and Poppenberger, B. (2013). The role of hormones in the aging of plants-a mini-review. Gerontology **60,** 49-55.

Khanna-Chopra, R. (2012). Leaf senescence and abiotic stresses share reactive oxygen species-mediated chloroplast degradation. Protoplasma **249,** 469-481.

Kim, J.-w., Tang, Q.-Q., Li, X., and Lane, M.D. (2007). Effect of phosphorylation and S–S bond-induced dimerization on DNA binding and transcriptional activation by C/EBPβ. Proceedings of the National Academy of Sciences **104,** 1800-1804.

Kim, J.H., Durrett, T.P., Last, R.L., and Jander, G. (2004). Characterization of the Arabidopsis TU8 glucosinolate mutation, an allele of TERMINAL FLOWER2. Plant molecular biology **54,** 671-682.

Kim, J.H., Woo, H.R., Kim, J., Lim, P.O., Lee, I.C., Choi, S.H., Hwang, D., and Nam, H.G. (2009). Trifurcate feed-forward regulation of age-dependent cell death involving miR164 in Arabidopsis. Science **323,** 1053-1057.

Kim, Y.-H., Khan, A.L., Kim, D.-H., Lee, S.-Y., Kim, K.-M., Waqas, M., Jung, H.-Y., Shin, J.-H., Kim, J.-G., and Lee, I.-J. (2014). Silicon mitigates heavy metal stress by regulating P-type heavy metal ATPases, Oryza sativa low silicon genes, and endogenous phytohormones. BMC plant biology **14,** 13.

Kircher, S., Wellmer, F., Nick, P., Rügner, A., Schäfer, E., and Harter, K. (1999). Nuclear import of the parsley bZIP transcription factor CPRF2 is regulated by phytochrome photoreceptors. The Journal of cell biology **144,** 201-211.

Kirchler, T., Briesemeister, S., Singer, M., Schütze, K., Keinath, M., Kohlbacher, O., Vicente-Carbajosa, J., Teige, M., Harter, K., and Chaban, C. (2010). The role of phosphorylatable serine residues in the DNA-binding domain of Arabidopsis bZIP transcription factors. European journal of cell biology **89,** 175-183.

Kitsios, G., and Doonan, J.H. (2011). Cyclin dependent protein kinases and stress responses in plants. Plant signaling & behavior **6,** 204-209.

Kleinow, T., Himbert, S., Krenz, B., Jeske, H., and Koncz, C. (2009). NAC domain transcription factor ATAF1 interacts with SNF1-related kinases and silencing of its subfamily causes severe developmental defects in Arabidopsis. Plant Science **177,** 360-370.

Klimczak, L.J., Schindler, U., and Cashmore, A.R. (1992). DNA binding activity of the Arabidopsis G-box binding factor GBF1 is stimulated by phosphorylation by casein kinase II from broccoli. The Plant cell **4,** 87-98.

Kohli, A., Sreenivasulu, N., Lakshmanan, P., and Kumar, P.P. (2013). The phytohormone crosstalk paradigm takes center stage in understanding how plants respond to abiotic stresses. Plant cell reports **32,** 945-957.

Kollist, H., Nuhkat, M., and Roelfsema, M.R.G. (2014). Closing gaps: linking elements that control stomatal movement. New Phytologist **203,** 44-62.

Komaki, S., and Sugimoto, K. (2012). Control of the plant cell cycle by developmental and environmental cues. Plant and Cell Physiology **53,** 953-964.

Koncz, C., and Schell, J. (1986). The promoter of TL-DNA gene 5 controls the tissue-specific expression of chimaeric genes carried by a novel type of Agrobacterium binary vector. Molecular and General Genetics MGG **204,** 383-396.

Kotak, S., Larkindale, J., Lee, U., von Koskull-Döring, P., Vierling, E., and Scharf, K.-D. (2007). Complexity of the heat stress response in plants. Current opinion in plant biology **10,** 310-316.

Kranner, I., Minibayeva, F.V., Beckett, R.P., and Seal, C.E. (2010). What is stress? Concepts, definitions and applications in seed science. New Phytologist **188,** 655-673.

Krylov, D., Mikhailenko, I., and Vinson, C. (1994). A thermodynamic scale for leucine zipper stability and dimerization specificity: e and g interhelical interactions. The EMBO Journal **13,** 2849–2861.

Kulik, A., Wawer, I., Krzywińska, E., Bucholc, M., and Dobrowolska, G. (2011). SnRK2 protein kinases—key regulators of plant response to abiotic stresses. Omics: a journal of integrative biology **15,** 859-872.

Kültz, D. (2005). Molecular and evolutionary basis of the cellular stress response. Annu. Rev. Physiol. **67,** 225-257.

Kuo, M.-H., vom Baur, E., Struhl, K., and Allis, C.D. (2000). Gcn4 Activator Targets Gcn5 Histone Acetyltransferase to Specific Promoters Independently of Transcription. Molecular Cell **6,** 1309-1320.

Kyte, J., and Doolittle, R.F. (1982). A simple method for displaying the hydropathic character of a protein. Journal of molecular biology **157,** 105-132.

Lacroix, E., Viguera, A.R., and Serrano, L. (1998). Elucidating the folding problem of α-helices: local motifs, long-range electrostatics, ionic-strength dependence and prediction of NMR parameters. Journal of molecular biology **284,** 173-191.

Lamb, P., and McKnight, S.L. (1991). Diversity and specificity in transcriptional regulation: the benefits of heterotypic dimerization. Trends in biochemical sciences **16,** 417-422.

Lara, M.E.B., Garcia, M.-C.G., Fatima, T., Ehneß, R., Lee, T.K., Proels, R., Tanner, W., and Roitsch, T. (2004). Extracellular invertase is an essential component of cytokinin-mediated delay of senescence. The Plant Cell Online **16,** 1276-1287.

Lara, P., Onate-Sanchez, L., Abraham, Z., Ferrandiz, C., Diaz, I., Carbonero, P., and Vicente-Carbajosa, J. (2003). Synergistic activation of seed storage protein gene expression in Arabidopsis by ABI3 and two bZIPs related to OPAQUE2. The Journal of biological chemistry **278,** 21003-21011.

Larkindale, J., Hall, J.D., Knight, M.R., and Vierling, E. (2005). Heat stress phenotypes of Arabidopsis mutants implicate multiple signaling pathways in the acquisition of thermotolerance. Plant physiology **138,** 882-897.

Lastdrager, J., Hanson, J., and Smeekens, S. (2014). Sugar signals and the control of plant growth and development. Journal of experimental botany **65,** 799-807.

Lee, D.L., Lavigne, P., and Hodges, R.S. (2001). Are trigger sequences essential in the folding of two-stranded α-helical coiled-coils? Journal of molecular biology **306,** 539-553.

Lee, I.C., Hong, S.W., Whang, S.S., Lim, P.O., Nam, H.G., and Koo, J.C. (2011). Age-dependent action of an ABA-inducible receptor kinase, RPK1, as a positive regulator of senescence in Arabidopsis leaves. Plant and cell physiology **52,** 651-662.

Lee, J., He, K., Stolc, V., Lee, H., Figueroa, P., Gao, Y., Tongprasit, W., Zhao, H., Lee, I., and Deng, X.W. (2007). Analysis of transcription factor HY5 genomic binding sites revealed its hierarchical role in light regulation of development. The Plant Cell Online **19,** 731-749.

Lee, S., Seo, P.J., Lee, H.J., and Park, C.M. (2012). A NAC transcription factor NTL4 promotes reactive oxygen species production during drought-induced leaf senescence in Arabidopsis. The Plant Journal **70,** 831-844.

Lee, S.S., Yang, S.H., Berberich, T., Miyazaki, A., and Kusano, T. (2006). Characterization of AtbZIP2, AtbZIP11 and AtbZIP53 from the group S basic region-leucine zipper family in Arabidopsis thaliana. Plant Biotechnology **23,** 249-258.

Lee, T.A., Wetering, S.W.V., and Brusslan, J.A. (2013). Stromal protein degradation is incomplete in Arabidopsis thaliana autophagy mutants undergoing natural senescence. BMC research notes **6,** 17.

Leivar, P., and Quail, P.H. PIFs: pivotal components in a cellular signaling hub. Trends in Plant Science **16,** 19-28.

Levey, S., and Wingler, A. (2005). Natural variation in the regulation of leaf senescence and relation to other traits in Arabidopsis. Plant, Cell & Environment **28,** 223-231.

Li, J.-F., Bush, J., Xiong, Y., Li, L., and McCormack, M. (2011). Large-scale protein-protein interaction analysis in Arabidopsis mesophyll protoplasts by split firefly luciferase complementation. PloS one **6,** e27364-e27364.

Li, M., Berendzen, K.W., and Schöffl, F. (2010a). Promoter specificity and interactions between early and late Arabidopsis heat shock factors. Plant molecular biology **73,** 559-567.

Li, M., Doll, J., Weckermann, K., Oecking, C., Berendzen, K.W., and Schöffl, F. (2010b). Detection of in vivo interactions between Arabidopsis class A-HSFs, using a novel BiFC fragment, and identification of novel class B-HSF interacting proteins. European journal of cell biology **89,** 126-132.

Li, Z., Peng, J., Wen, X., and Guo, H. (2013). Ethylene-insensitive3 is a senescence-associated gene that accelerates age-dependent leaf senescence by directly repressing miR164 transcription in Arabidopsis. The Plant cell **25,** 3311-3328.

Liang, L., Lai, Z., Ma, W., Zhang, Y., and Xue, Y. (2002). AhSL28, a senescence-and phosphate starvation-induced S-like RNase gene in Antirrhinum. Biochimica et Biophysica Acta (BBA)-Gene Structure and Expression **1579,** 64-71.

Liao, W., Tang, Y., Lin, S.-F., Kung, H.-J., and Giam, C.-Z. (2003). K-bZIP of Kaposi's sarcoma-associated herpesvirus/human herpesvirus 8 (KSHV/HHV-8) binds KSHV/HHV-8 Rta and represses Rta-mediated transactivation. Journal of virology **77,** 3809-3815.

Lim, P.O., Kim, H.J., and Gil Nam, H. (2007). Leaf senescence. Annu. Rev. Plant Biol. **58,** 115-136.

Liu, G., Ji, Y., Bhuiyan, N.H., Pilot, G., Selvaraj, G., Zou, J., and Wei, Y. (2010). Amino acid homeostasis modulates salicylic acid–associated redox status and defense responses in Arabidopsis. The Plant Cell Online **22,** 3845-3863.

Liu, J.X., Srivastava, R., and Howell, S.H. (2008). Stress-induced expression of an activated form of AtbZIP17 provides protection from salt stress in Arabidopsis. Plant, cell & environment **31,** 1735-1743.

Liu, W., Li, R.-J., Han, T.-T., Cai, W., Fu, Z.-W., and Lu, Y.-T. (2015). Salt stress reduces root meristem size by nitric oxide-mediated modulation of auxin accumulation and signaling in Arabidopsis. Plant physiology **168,** 343-356.

Liu, Y., and Bassham, D.C. (2012). Autophagy: pathways for self-eating in plant cells. Annual review of plant biology **63,** 215-237.

Liu, Z.-B., Hagen, G., and Guilfoyle, T.J. (1997). A G-box-binding protein from soybean binds to the E1 auxin-response element in the soybean GH3 promoter and contains a proline-rich repression domain. Plant physiology **115,** 397-407.

Llorca, C.M., Potschin, M., and Zentgraf, U. (2014). bZIPs and WRKYs: two large transcription factor families executing two different functional strategies. Frontiers in plant science **5**.

Llorca, C.M., Berendzen, K.W., Malik, W.A., Mahn, S., Piepho, H.-P., and Zentgraf, U. (2015). The Elucidation of the Interactome of 16 <italic>Arabidopsis</italic> bZIP Factors Reveals Three Independent Functional Networks. PLoS ONE **10,** e0139884.

Lockshin, R.A., and Zakeri, Z. (2004). Apoptosis, autophagy, and more. The international journal of biochemistry & cell biology **36,** 2405-2419.

Luis, A., Sandalio, L.M., Corpas, F.J., Palma, J.M., and Barroso, J.B. (2006). Reactive oxygen species and reactive nitrogen species in peroxisomes. Production, scavenging, and role in cell signaling. Plant physiology **141,** 330-335.

Lundquist, P.K., Poliakov, A., Bhuiyan, N.H., Zybailov, B., Sun, Q., and van Wijk, K.J. (2012). The functional network of the Arabidopsis plastoglobule proteome based on quantitative proteomics and genome-wide coexpression analysis. Plant physiology **158,** 1172-1192.

Lupas, A., Van Dyke, M., and Stock, J. (1991). Predicting coiled coils from protein sequences. Science **252,** 1162-1164.

Lupas, A.N., and Gruber, M. (2005). The structure of α-helical coiled coils. Advances in protein chemistry **70,** 37-38.

Lyzenga, W.J., and Stone, S.L. (2011). Abiotic stress tolerance mediated by protein ubiquitination. Journal of experimental botany**,** err310.

Ma, J., Hanssen, M., Lundgren, K., Hernández, L., Delatte, T., Ehlert, A., Liu, C.M., Schluepmann, H., Dröge-Laser, W., and Moritz, T. (2011). The sucrose-regulated Arabidopsis transcription factor bZIP11 reprograms metabolism and regulates trehalose metabolism. New Phytologist **191,** 733-745.

Macková, H., Hronková, M., Dobrá, J., Turečková, V., Novák, O., Lubovská, Z., Motyka, V., Haisel, D., Hájek, T., and Prášil, I.T. (2013). Enhanced drought and heat stress tolerance of tobacco plants with ectopically enhanced cytokinin oxidase/dehydrogenase gene expression. Journal of experimental botany **64,** 2805-2815.

Maharjan, S., Oku, M., Tsuda, M., Hoseki, J., and Sakai, Y. (2014). Mitochondrial impairment triggers cytosolic oxidative stress and cell death following proteasome inhibition. Scientific reports **4**.

Mahfouz, M.M., Kim, S., Delauney, A.J., and Verma, D.P.S. (2006). Arabidopsis TARGET OF RAPAMYCIN interacts with RAPTOR, which regulates the activity of S6 kinase in response to osmotic stress signals. The Plant Cell Online **18,** 477-490.

Maillard, A., Diquélou, S., Billard, V., Lainé, P., Garnica, M., Prudent, M., Garcia-Mina, J., Yvin, J., and Ourry, A. (2015). Leaf mineral nutrient remobilization during leaf senescence and modulation by nutrient deficiency. Name: Frontiers in Plant Science **6,** 317.

Mair, A., Pedrotti, L., Wurzinger, B., Anrather, D., Simeunovic, A., Weiste, C., Valerio, C., Dietrich, K., Kirchler, T., and Nägele, T. (2015). SnRK1-triggered switch of bZIP63 dimerization mediates the low-energy response in plants. eLife**,** e05828.

Mallappa, C., Yadav, V., Negi, P., and Chattopadhyay, S. (2006). A basic leucine zipper transcription factor, G-box-binding factor 1, regulates blue light-mediated photomorphogenic growth in Arabidopsis. Journal of Biological Chemistry **281,** 22190-22199.

Mallappa, C., Singh, A., Ram, H., and Chattopadhyay, S. (2008). GBF1, a transcription factor of blue light signaling in Arabidopsis, is degraded in the dark by a proteasome-mediated pathway independent of COP1 and SPA1. The Journal of biological chemistry **283,** 35772-35782.

Malys, N. (2012). Shine-Dalgarno sequence of bacteriophage T4: GAGG prevails in early genes. Molecular biology reports **39,** 33-39.

Martínez, D.E., Bartoli, C.G., Grbic, V., and Guiamet, J.J. (2007). Vacuolar cysteine proteases of wheat (Triticum aestivum L.) are common to leaf senescence induced by different factors. Journal of experimental botany **58,** 1099-1107.

Masclaux-Daubresse, C., Valadier, M.H., Carrayol, E., Reisdorf-Cren, M., and Hirel, B. (2002). Diurnal changes in the expressionof glutamate dehydrogenase and nitrate reductase are involved in the C/N balance of tobacco source leaves. Plant, Cell & Environment **25,** 1451-1462.

Masclaux, C., Valadier, M.-H., Brugière, N., Morot-Gaudry, J.-F., and Hirel, B. (2000). Characterization of the sink/source transition in tobacco (Nicotiana tabacum L.) shoots in relation to nitrogen management and leaf senescence. Planta **211,** 510-518.

Mason, J.M., and Arndt, K.M. (2004). Coiled coil domains: stability, specificity, and biological implications. ChemBioChem **5,** 170-176.

Matiolli, C.C., Tomaz, J.P., Duarte, G.T., Prado, F.M., Del Bem, L.E., Silveira, A.B., Gauer, L., Correa, L.G., Drumond, R.D., Viana, A.J., Di Mascio, P., Meyer, C., and Vincentz, M. (2011). The Arabidopsis bZIP gene AtbZIP63 is a sensitive integrator of transient abscisic acid and glucose signals. Plant physiology **157,** 692-705.

Matsuo, H., Kajihara, M., Tomizawa, D., Watanabe, T., Saito, A., Fujimoto, J., Horibe, K., Kodama, K., Tokumasu, M., and Itoh, H. (2014). Prognostic implications of CEBPA mutations in pediatric acute myeloid leukemia: a report from the Japanese Pediatric Leukemia/Lymphoma Study Group. Blood cancer journal **4,** e226.

Maurya, J.P., Sethi, V., Gangappa, S.N., Gupta, N., and Chattopadhyay, S. (2015). Interaction of MYC2 and GBF1 results in functional antagonism in blue light-mediated Arabidopsis seedling development. The Plant Journal **83,** 439-450.

McCullagh, P., and Nelder, J.A. (1989). Generalized linear models. (Chapman and Hall London).

Melotto, M., Underwood, W., and He, S.Y. (2008). Role of stomata in plant innate immunity and foliar bacterial diseases. Annual review of phytopathology **46,** 101.

Menkens, A.E., Schindler, U., and Cashmore, A.R. (1995). The G-box: a ubiquitous regulatory DNA element in plants bound by the GBF family of bZIP proteins. Trends in biochemical sciences **20,** 506-510.

Mermod, N., O'Neill, E.A., Kelly, T.J., and Tjian, R. (1989). The proline-rich transcriptional activator of CTF/NF-I is distinct from the replication and DNA binding domain. Cell **58,** 741-753.

Meshi, T., Moda, I., Minami, M., Okanami, M., and Iwabuchi, M. (1998). Conserved Ser residues in the basic region of the bZIP-type transcription factor HBP-1a (17): importance in DNA binding and possible targets for phosphorylation. Plant molecular biology **36,** 125-136.

Miao, Y., Laun, T., Zimmermann, P., and Zentgraf, U. (2004). Targets of the WRKY53 transcription factor and its role during leaf senescence in Arabidopsis. Plant molecular biology **55,** 853-867.

Miller, M., Shuman, J.D., Sebastian, T., Dauter, Z., and Johnson, P.F. (2003). Structural Basis for DNA Recognition by the Basic Region Leucine Zipper Transcription Factor CCAAT/Enhancer-binding Protein alpha. Journal of Biological Chemistry **278,** 15178-15184.

Miotto, B., and Struhl, K. (2006). Differential Gene Regulation by Selective Association of Transcriptional Coactivators and bZIP DNA-Binding Domains. Molecular and Cellular Biology **26,** 5969-5982.

Mittler, R. (2002). Oxidative stress, antioxidants and stress tolerance. Trends in plant science **7,** 405-410.

Mittler, R. (2006). Abiotic stress, the field environment and stress combination. Trends in plant science **11,** 15-19.

Mittler, R., and Blumwald, E. (2015). The Roles of ROS and ABA in Systemic Acquired Acclimation. The Plant Cell Online**,** tpc. 114.133090.

Mlynárová, L., Nap, J.P., and Bisseling, T. (2007). The SWI/SNF chromatin-remodeling gene AtCHR12 mediates temporary growth arrest in Arabidopsis thaliana upon perceiving environmental stress. The Plant Journal **51,** 874-885.

Moitra, J., Szilák, L., Krylov, D., and Vinson, C. (1997). Leucine is the most stabilizing aliphatic amino acid in the d position of a dimeric leucine zipper coiled coil. Biochemistry **36,** 12567-12573.

Moore, B., Zhou, L., Rolland, F., Hall, Q., Cheng, W.-H., Liu, Y.-X., Hwang, I., Jones, T., and Sheen, J. (2003). Role of the Arabidopsis glucose sensor HXK1 in nutrient, light, and hormonal signaling. Science **300,** 332-336.

Moreau, V.H., da Silva, A.C., Siloto, R.M., Valente, A.P., Leite, A., and Almeida, F.C. (2004). The bZIP region of the plant transcription factor opaque-2 forms stable homodimers in solution and retains its helical structure upon subunit dissociation. Biochemistry **43,** 4862-4868.

Morell, M., Espargaro, A., Aviles, F.X., and Ventura, S. (2008). Study and selection of in vivo protein interactions by coupling bimolecular fluorescence complementation and flow cytometry. Nature protocols **3,** 22-33.

Morris, K., Mackerness, S.A.H., Page, T., John, C.F., Murphy, A.M., Carr, J.P., and Buchanan-Wollaston, V. (2000). Salicylic acid has a role in regulating gene expression during leaf senescence. The Plant Journal **23,** 677-685.

Muller, B., Pantin, F., Génard, M., Turc, O., Freixes, S., Piques, M., and Gibon, Y. (2011). Water deficits uncouple growth from photosynthesis, increase C content, and modify the relationships between C and growth in sink organs. Journal of experimental botany **62,** 1715-1729.

Munné-Bosch, S., and Alegre, L. (2002). Plant aging increases oxidative stress in chloroplasts. Planta **214,** 608-615.

Munoz, A., and Castellano, M. (2012). Regulation of translation initiation under abiotic stress conditions in plants: is it a conserved or not so conserved process among eukaryotes? Comparative and functional genomics **2012**.

Müntz, K. (2007). Protein dynamics and proteolysis in plant vacuoles. Journal of experimental botany **58,** 2391-2407.

Murata, N., Takahashi, S., Nishiyama, Y., and Allakhverdiev, S.I. (2007). Photoinhibition of photosystem II under environmental stress. Biochimica et Biophysica Acta (BBA)-Bioenergetics **1767,** 414-421.

Navabpour, S., Morris, K., Allen, R., Harrison, E., Soheila, A., and Buchanan-Wollaston, V. (2003). Expression of senescence-enhanced genes in response to oxidative stress. Journal of experimental botany **54,** 2285-2292.

Ngo, B., Hu, C.-M., Guo, X.E., Ngo, B., Wei, R., Zhu, J., and Lee, W.-H. (2013). Complementary Interhelical Interactions between Three Buried Glu-Lys Pairs within Three Heptad Repeats Are Essential for Hec1-Nuf2 Heterodimerization and Mitotic Progression. Journal of Biological Chemistry **288,** 34403-34413.

Nguyen, T.N., and Goodrich, J.A. (2006). Protein-protein interaction assays: eliminating false positive interactions. Nature methods **3,** 135-139.

Nishiyama, R., Watanabe, Y., Fujita, Y., Le, D.T., Kojima, M., Werner, T., Vankova, R., Yamaguchi-Shinozaki, K., Shinozaki, K., and Kakimoto, T. (2011). Analysis of cytokinin mutants and regulation of cytokinin metabolic genes reveals important regulatory roles of cytokinins in drought, salt and abscisic acid responses, and abscisic acid biosynthesis. The Plant Cell Online **23,** 2169-2183.

Nishizawa, M., Fu, S.-L., Kataoka, K., and Vogt, P.K. (2003). Artificial oncoproteins: modified versions of the yeast bZip protein GCN4 induce cellular transformation. Oncogene **22,** 7931-7941.

Noh, Y.-S., and Amasino, R.M. (1999). Identification of a promoter region responsible for the senescence-specific expression of SAG12. Plant molecular biology **41,** 181-194.

Noodén, L.D., and Penney, J.P. (2001). Correlative controls of senescence and plant death in Arabidopsis thaliana (Brassicaceae). Journal of experimental botany **52,** 2151-2159.

Norris, S.R., Meyer, S.E., and Callis, J. (1993). The intron of Arabidopsis thaliana polyubiquitin genes is conserved in location and is a quantitative determinant of chimeric gene expression. Plant molecular biology **21,** 895-906.

Nouet, C., Motte, P., and Hanikenne, M. (2011). Chloroplastic and mitochondrial metal homeostasis. Trends in plant science **16,** 395-404.

Obata, T., and Fernie, A.R. (2012). The use of metabolomics to dissect plant responses to abiotic stresses. Cellular and Molecular Life Sciences **69,** 3225-3243.

Oh, S.A., Park, J.H., Lee, G.I., Paek, K.H., Park, S.K., and Nam, H.G. (1997). Identification of three genetic loci controlling leaf senescence in Arabidopsis thaliana. The Plant Journal **12,** 527-535.

Oliphant, A.R., Brandl, C.J., and Struhl, K. (1989). Defining the sequence specificity of DNA-binding proteins by selecting binding sites from random-sequence oligonucleotides: analysis of yeast GCN4 protein. Molecular and Cellular Biology **9,** 2944-2949.

Oñate-Sánchez, L., and Vicente-Carbajosa, J. (2008). DNA-free RNA isolation protocols for Arabidopsis thaliana, including seeds and siliques. BMC Research Notes **1,** 93.

Osuna, D., Usadel, B., Morcuende, R., Gibon, Y., Bläsing, O.E., Höhne, M., Günter, M., Kamlage, B., Trethewey, R., and Scheible, W.R. (2007). Temporal responses of transcripts, enzyme activities and metabolites after adding sucrose to carbon-deprived Arabidopsis seedlings. The Plant Journal **49,** 463-491.

Otegui, M.S., Noh, Y.S., Martínez, D.E., Vila Petroff, M.G., Andrew Staehelin, L., Amasino, R.M., and Guiamet, J.J. (2005). Senescence-associated vacuoles with intense proteolytic activity develop in leaves of Arabidopsis and soybean. The Plant Journal **41,** 831-844.

Pähler, G., Panse, C., Diederichsen, U., and Janshoff, A. (2012). Coiled-Coil Formation on Lipid Bilayers—Implications for Docking and Fusion Efficiency. Biophysical journal **103,** 2295-2303.

Palma, J.M., Corpas, F.J., and del Río, L.A. (2009). Proteome of plant peroxisomes: new perspectives on the role of these organelles in cell biology. Proteomics **9,** 2301-2312.

Para, A., Li, Y., Marshall-Colón, A., Varala, K., Francoeur, N.J., Moran, T.M., Edwards, M.B., Hackley, C., Bargmann, B.O., and Birnbaum, K.D. (2014). Hit-and-run transcriptional control by bZIP1 mediates rapid nutrient signaling in Arabidopsis. Proceedings of the National Academy of Sciences **111,** 10371-10376.

Park, J.-H., Oh, S.A., Kim, Y.H., Woo, H.R., and Nam, H.G. (1998). Differential expression of senescence-associated mRNAs during leaf senescence induced by different senescence-inducing factors in Arabidopsis. Plant molecular biology **37,** 445-454.

Parthier, B. (1988). Gerontoplasts-the yellow end in the ontogenesis of chloroplasts. Endocytobiosis and Cell Research **5,** 163-190.

Paul, M.J., Primavesi, L.F., Jhurreea, D., and Zhang, Y. (2008). Trehalose metabolism and signaling. Annu. Rev. Plant Biol. **59,** 417-441.

Peleg, Z., and Blumwald, E. (2011). Hormone balance and abiotic stress tolerance in crop plants. Current opinion in plant biology **14,** 290-295.

Penfold, C.A., and Buchanan-Wollaston, V. (2014). Modelling transcriptional networks in leaf senescence. Journal of experimental botany **65,** 3859-3873.

Phillips, A.R., Suttangkakul, A., and Vierstra, R.D. (2008). The ATG12-conjugating enzyme ATG10 is essential for autophagic vesicle formation in Arabidopsis thaliana. Genetics **178,** 1339-1353.

Pomeranz, M.C., Hah, C., Lin, P.-C., Kang, S.G., Finer, J.J., Blackshear, P.J., and Jang, J.-C. (2010). The Arabidopsis tandem zinc finger protein AtTZF1 traffics between the nucleus and cytoplasmic foci and binds both DNA and RNA. Plant physiology **152,** 151-165.

Ponnu, J., Wahl, V., and Schmid, M. (2011). Trehalose-6-phosphate: connecting plant metabolism and development. Frontiers in plant science **2**.

Potapov, V., Kaplan, J.B., and Keating, A.E. (2015). Data-Driven Prediction and Design of bZIP Coiled-Coil Interactions. PLoS computational biology **11,** e1004046.

Pottier, M., Masclaux-Daubresse, C., Yoshimoto, K., and Thomine, S. (2014). Autophagy as a possible mechanism for micronutrient remobilization from leaves to seeds. Frontiers in plant science **5**.

Pourtau, N., Jennings, R., Pelzer, E., Pallas, J., and Wingler, A. (2006). Effect of sugar-induced senescence on gene expression and implications for the regulation of senescence in Arabidopsis. Planta **224,** 556-568.

Pourtau, N., Marès, M., Purdy, S., Quentin, N., Ruël, A., and Wingler, A. (2004). Interactions of abscisic acid and sugar signalling in the regulation of leaf senescence. Planta **219,** 765-772.

Quirino, B.F., Reiter, W.-D., and Amasino, R.D. (2001). One of two tandem Arabidopsis genes homologous to monosaccharide transporters is senescence-associated. Plant molecular biology **46,** 447-457.

Rahmani, F., Hummel, M., Schuurmans, J., Wiese-Klinkenberg, A., Smeekens, S., and Hanson, J. (2009). Sucrose control of translation mediated by an upstream open reading frame-encoded peptide. Plant physiology **150,** 1356-1367.

Raven, J.A. (2012). Protein turnover and plant RNA and phosphorus requirements in relation to nitrogen fixation. Plant Science **188,** 25-35.

Reape, T.J., Molony, E.M., and McCabe, P.F. (2008). Programmed cell death in plants: distinguishing between different modes. Journal of experimental botany **59,** 435-444.

Reddy, A.S., Day, I.S., Göhring, J., and Barta, A. (2012). Localization and dynamics of nuclear speckles in plants. Plant physiology **158,** 67-77.

Regan, L. (1994). Protein structure: born to be beta. Current Biology **4,** 656-658.

Reinke, A.W., Baek, J., Ashenberg, O., and Keating, A.E. (2013). Networks of bZIP Protein-Protein Interactions Diversified Over a Billion Years of Evolution. Science **340,** 730-734.

Ren, M., Qiu, S., Venglat, P., Xiang, D., Feng, L., Selvaraj, G., and Datla, R. (2011). Target of rapamycin regulates development and ribosomal RNA expression through kinase domain in Arabidopsis. Plant physiology **155,** 1367-1382.

Riechmann, J., Heard, J., Martin, G., Reuber, L., Jiang, C.-Z., Keddie, J., Adam, L., Pineda, O., Ratcliffe, O., and Samaha, R. (2000). Arabidopsis transcription factors: genome-wide comparative analysis among eukaryotes. Science **290,** 2105-2110.

Robaglia, C., Thomas, M., and Meyer, C. (2012). Sensing nutrient and energy status by SnRK1 and TOR kinases. Current opinion in plant biology **15,** 301-307.

Robatzek, S., and Somssich, I.E. (2001). A new member of the Arabidopsis WRKY transcription factor family, AtWRKY6, is associated with both senescence-and defence-related processes. The Plant Journal **28,** 123-133.

Robatzek, S., and Somssich, I.E. (2002). Targets of AtWRKY6 regulation during plant senescence and pathogen defense. Genes & development **16,** 1139-1149.

Roberts, I.N., Caputo, C., Criado, M.V., and Funk, C. (2012). Senescence-associated proteases in plants. Physiologia Plantarum **145,** 130-139.

Rochon, A., Boyle, P., Wignes, T., Fobert, P.R., and Despres, C. (2006). The Coactivator Function of Arabidopsis NPR1 Requires the Core of Its BTB/POZ Domain and the Oxidation of C-Terminal Cysteines. The Plant Cell Online **18,** 3670-3685.

Rodrigues, A., Adamo, M., Crozet, P., Margalha, L., Confraria, A., Martinho, C., Elias, A., Rabissi, A., Lumbreras, V., and González-Guzmán, M. (2013). ABI1 and PP2CA phosphatases are negative regulators of Snf1-related protein kinase1 signaling in Arabidopsis. The Plant Cell Online **25,** 3871-3884.

Rodríguez-Gamir, J., Ancillo, G., González-Mas, M.C., Primo-Millo, E., Iglesias, D.J., and Forner-Giner, M.A. (2011). Root signalling and modulation of stomatal closure in flooded citrus seedlings. Plant Physiology and Biochemistry **49,** 636-645.

Romero, P., Obradovic, Z., Li, X., Garner, E.C., Brown, C.J., and Dunker, A.K. (2001). Sequence complexity of disordered protein. Proteins: Structure, Function, and Bioinformatics **42,** 38-48.

Roy, N., Laskar, S., and Barik, A. (2013). Amino acids through developmental stages of sunflower leaves. Acta Botanica Croatica **72,** 23-33.

Rylott, E., Hooks, M., and Graham, I. (2001). Co-ordinate regulation of genes involved in storage lipid mobilization in Arabidopsis thaliana. Biochemical Society Transactions **29,** 283-286.

Santino, A., Taurino, M., De Domenico, S., Bonsegna, S., Poltronieri, P., Pastor, V., and Flors, V. (2013). Jasmonate signaling in plant development and defense response to multiple (a) biotic stresses. Plant cell reports **32,** 1085-1098.

Satoh, R., Fujita, Y., Nakashima, K., Shinozaki, K., and Yamaguchi-Shinozaki, K. (2004). A novel subgroup of bZIP proteins functions as transcriptional activators in hypoosmolarity-responsive expression of the ProDH gene in Arabidopsis. Plant and Cell Physiology **45,** 309-317.

Sawchuk, M.G., Donner, T.J., Head, P., and Scarpella, E. (2008). Unique and overlapping expression patterns among members of photosynthesis-associated nuclear gene families in Arabidopsis. Plant physiology **148,** 1908-1924.

Scheffe, H. (1953). A method for judging all contrasts in the analysis of variance*. Biometrika **40,** 87-110.

Schenk, P.M., Kazan, K., Rusu, A.G., Manners, J.M., and Maclean, D.J. (2005). The SEN1 gene of Arabidopsis is regulated by signals that link plant defence responses and senescence. Plant Physiology and Biochemistry **43,** 997-1005.

Schindler, U., Menkens, A.E., Beckmann, H., Ecker, J.R., and Cashmore, A.R. (1992a). Heterodimerization between light-regulated and ubiquitously expressed Arabidopsis GBF bZIP proteins. The EMBO journal **11,** 1261.

Schindler, U., Terzaghi, W., Beckmann, H., Kadesch, T., and Cashmore, A.R. (1992b). DNA binding site preferences and transcriptional activation properties of the Arabidopsis transcription factor GBF1. The EMBO Journal **11,** 1275-1289.

Schrum, A.G., and Gil, D. (2012). Robustness and Specificity in Signal Transduction via Physiologic Protein Interaction Networks. Clinical & experimental pharmacology **2,** S3: 001.

Schumacher, M.A., Goodman, R.H., and Brennan, R.G. (2000). The Structure of a CREB bZIPmiddle dotSomatostatin CRE Complex Reveals the Basis for Selective Dimerization and Divalent Cation-enhanced DNA Binding. Journal of Biological Chemistry **275,** 35242-35247.

Sehnke, P.C., Laughner, B.J., Linebarger, C.R.L., Gurley, W.B., and Robert, J.F. (2005). Identification and characterization of GIP1, an Arabidopsis thaliana protein that enhances the DNA binding affinity and reduces the oligomeric state of G-box binding factors. Cell research **15,** 567-575.

Seldeen, K.L., McDonald, C.B., Deegan, B.J., and Farooq, A. (2008). Coupling of folding and DNA-binding in the bZIP domains of Jun–Fos heterodimeric transcription factor. Archives of Biochemistry and Biophysics **473,** 48-60.

Shaikhali, J., Norén, L., de Dios Barajas-López, J., Srivastava, V., König, J., Sauer, U.H., Wingsle, G., Dietz, K.-J., and Strand, Å. (2012). Redox-mediated mechanisms regulate DNA binding activity of the G-group of basic region leucine zipper (bZIP) transcription factors in Arabidopsis. Journal of Biological Chemistry **287,** 27510-27525.

Shane, M.W., Stigter, K., Fedosejevs, E.T., and Plaxton, W.C. (2014). Senescence-inducible cell wall and intracellular purple acid phosphatases: implications for phosphorus remobilization in Hakea prostrata (Proteaceae) and Arabidopsis thaliana (Brassicaceae). Journal of experimental botany **65,** 6097-6106.

Sharma, P., Jha, A.B., Dubey, R.S., and Pessarakli, M. (2012). Reactive oxygen species, oxidative damage, and antioxidative defense mechanism in plants under stressful conditions. Journal of Botany **2012**.

Sheen, J. (2002). A transient expression assay using Arabidopsis mesophyll protoplasts.

Sheen, J. (2014). Master regulators in plant glucose signaling networks. Journal of Plant Biology **57,** 67-79.

Shen, H., Cao, K., and Wang, X. (2007). A conserved proline residue in the leucine zipper region of AtbZIP34 and AtbZIP61 in Arabidopsis thaliana interferes with the formation of homodimer. Biochemical and Biophysical Research Communications **362,** 425-430.

Shen, H., Cao, K., and Wang, X. (2008). AtbZIP16 and AtbZIP68, two new members of GBFs, can interact with other G group bZIPs in Arabidopsis thaliana. BMB Rep **41,** 132-138.

Shi, Q.-M., Yang, X., Song, L., and Xue, H.-W. (2011). Arabidopsis MSBP1 is activated by HY5 and HYH and is involved in photomorphogenesis and brassinosteroid sensitivity regulation. Molecular plant **4,** 1092-1104.

Shin, D.H., Kim, J.S., Yokota, H., Kim, R., and Kim, S.H. (2006). Crystal structure of the DUF16 domain of MPN010 from Mycoplasma pneumoniae. Protein science **15,** 921-928.

Shine, J., and Dalgarno, L. (1974). The 3'-terminal sequence of Escherichia coli 16S ribosomal RNA: complementarity to nonsense triplets and ribosome binding sites. Proceedings of the National Academy of Sciences **71,** 1342-1346.

Shiu, S.H., Shih, M.C., and Li, W.H. (2005). Transcription factor families have much higher expansion rates in plants than in animals. Plant physiology **139,** 18-26.

Simonetti, A., Marzi, S., Jenner, L., Myasnikov, A., Romby, P., Yusupova, G., Klaholz, B., and Yusupov, M. (2009). A structural view of translation initiation in bacteria. Cellular and molecular life sciences **66,** 423-436.

Singh, A., Ram, H., Abbas, N., and Chattopadhyay, S. (2012). Molecular interactions of GBF1 with HY5 and HYH proteins during light-mediated seedling development in Arabidopsis thaliana. The Journal of biological chemistry **287,** 25995-26009.

Sirichandra, C., Davanture, M., Turk, B.E., Zivy, M., Valot, B., Leung, J., and Merlot, S. (2010). The Arabidopsis ABA-activated kinase OST1 phosphorylates the bZIP transcription factor ABF3 and creates a 14-3-3 binding site involved in its turnover. PLoS One **5,** e13935-e13935.

Smeekens, S., Ma, J., Hanson, J., and Rolland, F. (2010). Sugar signals and molecular networks controlling plant growth. Current opinion in plant biology **13,** 273-278.

Smékalová, V., Doskočilová, A., Komis, G., and Šamaj, J. (2014). Crosstalk between secondary messengers, hormones and MAPK modules during abiotic stress signalling in plants. Biotechnology advances **32,** 2-11.

Smykowski, A., Zimmermann, P., and Zentgraf, U. (2010). G-Box binding factor1 reduces CATALASE2 expression and regulates the onset of leaf senescence in Arabidopsis. Plant physiology **153,** 1321-1331.

Smykowski, A., Fischer, S.M., and Zentgraf, U. (2015). Phosphorylation Affects DNA-Binding of the Senescence-Regulating bZIP Transcription Factor GBF1. Plants **4,** 691-709.

Somerville, C., Bauer, S., Brininstool, G., Facette, M., Hamann, T., Milne, J., Osborne, E., Paredez, A., Persson, S., and Raab, T. (2004). Toward a systems approach to understanding plant cell walls. Science **306,** 2206-2211.

Soudry, E., Ulitzur, S., and Gepstein, S. (2005). Accumulation and remobilization of amino acids during senescence of detached and attached leaves: in planta analysis of tryptophan levels by recombinant luminescent bacteria. Journal of experimental botany **56,** 695-702.

Sprenger-Haussels, M., and Weisshaar, B. (2000). Transactivation properties of parsley proline-rich bZIP transcription factors. The Plant Journal **22,** 1-8.

Srivalli, S., and Khanna-Chopra, R. (2009). Delayed wheat flag leaf senescence due to removal of spikelets is associated with increased activities of leaf antioxidant enzymes, reduced glutathione/oxidized glutathione ratio and oxidative damage to mitochondrial proteins. Plant Physiology and Biochemistry **47,** 663-670.

Steinmetz, M.O., Stock, A., Schulthess, T., Landwehr, R., Lustig, A., Faix, J., Gerisch, G., Aebi, U., and Kammerer, R.A. (1998). A distinct 14 residue site triggers coiled-coil formation in cortexillin I. The EMBO Journal **17,** 1883-1891.

Steitz, J.A., and Jakes, K. (1975). How ribosomes select initiator regions in mRNA: base pair formation between the 3'terminus of 16S rRNA and the mRNA during initiation of protein synthesis in Escherichia coli. Proceedings of the National Academy of Sciences **72,** 4734-4738.

Strack, D. (1997). 10 Phenolic Metabolism. Plant biochemistry**,** 387.

Streb, S., and Zeeman, S.C. (2012). Starch metabolism in Arabidopsis. The Arabidopsis book/American Society of Plant Biologists **10**.

Sulmon, C., Van Baaren, J., Cabello-Hurtado, F., Gouesbet, G., Hennion, F., Mony, C., Renault, D., Bormans, M., El Amrani, A., and Wiegand, C. (2015). Abiotic stressors and stress responses: What commonalities appear between species across biological organization levels? Environmental Pollution **202,** 66-77.

Suttle, J.C., Lulai, E.C., Huckle, L.L., and Neubauer, J.D. (2013). Wounding of potato tubers induces increases in ABA biosynthesis and catabolism and alters expression of ABA metabolic genes. Journal of plant physiology **170,** 560-566.

Tamai, H., Iwabuchi, M., and Meshi, T. (2002). Arabidopsis GARP transcriptional activators interact with the Pro-rich activation domain shared by G-box-binding bZIP factors. Plant and cell physiology **43,** 99-107.

Tang, N., Zhang, H., Li, X., Xiao, J., and Xiong, L. (2012). Constitutive activation of transcription factor OsbZIP46 improves drought tolerance in rice. Plant physiology **158,** 1755-1768.

Tarkowská, D., Novák, O., Floková, K., Tarkowski, P., Turečková, V., Grúz, J., Rolčík, J., and Strnad, M. (2014). Quo vadis plant hormone analysis? Planta **240,** 55-76.

Taylor, N.L., Heazlewood, J.L., Day, D.A., and Millar, A.H. (2004). Lipoic acid-dependent oxidative catabolism of α-keto acids in mitochondria provides evidence for branched-chain amino acid catabolism in Arabidopsis. Plant physiology **134,** 838-848.

Taylor, R.G., Walker, D.C., and McInnes, R. (1993). E. coli host strains significantly affect the quality of small scale plasmid DNA preparations used for sequencing. Nucleic acids research **21,** 1677.

Terzaghi, W.B., Bertekap, R.L., and Cashmore, A.R. (1997). Intracellular localization of GBF proteins and blue light-induced import of GBF2 fusion proteins into the nucleus of cultured Arabidopsis and soybean cells. The Plant Journal **11,** 967-982.

Thomas, H. (2013). Senescence, ageing and death of the whole plant. New Phytologist **197,** 696-711.

Thomas, H., Ougham, H.J., Wagstaff, C., and Stead, A.D. (2003). Defining senescence and death. Journal of experimental botany **54,** 1127-1132.

Tomé, F., Nägele, T., Adamo, M., Garg, A., Marco-llorca, C., Nukarinen, E., Pedrotti, L., Peviani, A., Simeunovic, A., and Tatkiewicz, A. (2014). The low energy signaling network. Frontiers in plant science **5**.

Tripet, B., Wagschal, K., Lavigne, P., Mant, C.T., and Hodges, R.S. (2000). Effects of side-chain characteristics on stability and oligomerization state of a de novo-designed model coiled-coil: 20 amino acid substitutions in position "d". Journal of molecular biology **300,** 377-402.

Troncoso-Ponce, M.A., Cao, X., Yang, Z., and Ohlrogge, J.B. (2013). Lipid turnover during senescence. Plant Science **205,** 13-19.

Tsang, B.P., Bretscher, H.S., Kokona, B., Manning, R.S., and Fairman, R. (2011). Thermodynamic Analysis of Self-Assembly in Coiled-Coil Biomaterials. Biochemistry **50,** 8548-8558.

Tuteja, N. (2007). Abscisic acid and abiotic stress signaling. Plant signaling & behavior **2,** 135-138.

Uauy, C., Distelfeld, A., Fahima, T., Blechl, A., and Dubcovsky, J. (2006). A NAC gene regulating senescence improves grain protein, zinc, and iron content in wheat. Science **314,** 1298-1301.

Ülker, B., Mukhtar, M.S., and Somssich, I.E. (2007). The WRKY70 transcription factor of Arabidopsis influences both the plant senescence and defense signaling pathways. Planta **226,** 125-137.

Uversky, V.N., Gillespie, J.R., and Fink, A.L. (2000). Why are "natively unfolded" proteins unstructured under physiologic conditions? Proteins: Structure, Function, and Bioinformatics **41,** 415-427.

Van Buskirk, E.K., Decker, P.V., and Chen, M. (2012). Photobodies in light signaling. Plant physiology **158,** 52-60.

van der Graaff, E., Schwacke, R., Schneider, A., Desimone, M., Flügge, U.-I., and Kunze, R. (2006). Transcription analysis of Arabidopsis membrane transporters and hormone pathways during developmental and induced leaf senescence. Plant physiology **141,** 776-792.

van Doorn, W.G. (2008). Is the onset of senescence in leaf cells of intact plants due to low or high sugar levels? Journal of experimental botany **59,** 1963-1972.

van Doorn, W.G., and Woltering, E.J. (2004). Senescence and programmed cell death: substance or semantics? Journal of experimental botany **55,** 2147-2153.

Vandenbussche, F., Vaseva, I., Vissenberg, K., and Van Der Straeten, D. (2012). Ethylene in vegetative development: a tale with a riddle. New Phytologist **194,** 895-909.

Vass, I. (2012). Molecular mechanisms of photodamage in the Photosystem II complex. Biochimica et Biophysica Acta (BBA)-Bioenergetics **1817,** 209-217.

Veerabagu, M., Kirchler, T., Elgass, K., Stadelhofer, B., Stahl, M., Harter, K., Mira-Rodado, V., and Chaban, C. (2014). The interaction of the arabidopsis response regulator arr18 with bzip63 mediates the regulation of PROLINE DEHYDROGENASE expression. Molecular plant **7,** 1560-1577.

Veneklaas, E.J., Lambers, H., Bragg, J., Finnegan, P.M., Lovelock, C.E., Plaxton, W.C., Price, C.A., Scheible, W.R., Shane, M.W., and White, P.J. (2012). Opportunities for improving phosphorus-use efficiency in crop plants. New Phytologist **195,** 306-320.

Vinson, C., Myakishev, M., Acharya, A., Mir, A.A., Moll, J.R., and Bonovich, M. (2002). Classification of Human B-ZIP Proteins Based on Dimerization Properties. Molecular and Cellular Biology **22,** 6321-6335.

Vlot, A.C., Dempsey, D.M.A., and Klessig, D.F. (2009). Salicylic acid, a multifaceted hormone to combat disease. Annual review of phytopathology **47,** 177-206.

Von Arnim, A., and Deng, X.-W. (1996). Light control of seedling development. Annual review of plant biology **47,** 215-243.

Wada, S., Ishida, H., Izumi, M., Yoshimoto, K., Ohsumi, Y., Mae, T., and Makino, A. (2009). Autophagy plays a role in chloroplast degradation during senescence in individually darkened leaves. Plant physiology **149,** 885-893.

Wagschal, K., Tripet, B., Lavigne, P., Mant, C., and Hodges, R.S. (1999). The role of position a in determining the stability and oligomerization state of [alpha]-helical coiled coils: 20 amino acid stability coefficients in the hydrophobic core of proteins. Protein Science **8,** 2312-2329.

Walter, M., Chaban, C., Schütze, K., Batistic, O., Weckermann, K., Näke, C., Blazevic, D., Grefen, C., Schumacher, K., and Oecking, C. (2004). Visualization of protein interactions in living plant cells using bimolecular fluorescence complementation. The Plant Journal **40,** 428-438.

Wang, J., Leister, D., and Bolle, C. (2015). Photosynthetic lesions can trigger accelerated senescence in Arabidopsis thaliana. Journal of experimental botany**,** erv393.

Wang, L., and Carnegie, G.K. (2013). Flow Cytometric Analysis of Bimolecular Fluorescence Complementation: A High Throughput Quantitative Method to Study Protein-protein Interaction**,** e50529.

Wasternack, C., and Kombrink, E. (2009). Jasmonates: structural requirements for lipid-derived signals active in plant stress responses and development.

Watanabe, M., Balazadeh, S., Tohge, T., Erban, A., Giavalisco, P., Kopka, J., Mueller-Roeber, B., Fernie, A.R., and Hoefgen, R. (2013). Comprehensive dissection of spatiotemporal metabolic shifts in primary, secondary, and lipid metabolism during developmental senescence in Arabidopsis. Plant physiology **162,** 1290-1310.

Waters, B.M., Uauy, C., Dubcovsky, J., and Grusak, M.A. (2009). Wheat (Triticum aestivum) NAM proteins regulate the translocation of iron, zinc, and nitrogen compounds from vegetative tissues to grain. Journal of experimental botany **60,** 4263-4274.

Weaver, L.M., and Amasino, R.M. (2001). Senescence is induced in individually darkened Arabidopsis leaves, but inhibited in whole darkened plants. Plant physiology **127,** 876-886.

Wehner, N., Hartmann, L., Ehlert, A., Böttner, S., Oñate-Sánchez, L., and Dröge-Laser, W. (2011). High-throughput protoplast transactivation (PTA) system for the analysis of Arabidopsis transcription factor function. The Plant Journal **68,** 560-569.

Wei, K., Chen, J., Wang, Y., Chen, Y., Chen, S., Lin, Y., Pan, S., Zhong, X., and Xie, D. (2012). Genome-Wide Analysis of bZIP-Encoding Genes in Maize. DNA Research **19,** 463-476.

Weltmeier, F., Ehlert, A., Mayer, C.S., Dietrich, K., Wang, X., Schutze, K., Alonso, R., Harter, K., Vicente-Carbajosa, J., and Droge-Laser, W. (2006). Combinatorial control of Arabidopsis proline dehydrogenase transcription by specific heterodimerisation of bZIP transcription factors. EMBO J **25,** 3133-3143.

Weltmeier, F., Rahmani, F., Ehlert, A., Dietrich, K., Schütze, K., Wang, X., Chaban, C., Hanson, J., Teige, M., Harter, K., Vicente-Carbajosa, J., Smeekens, S., and Dröge-Laser, W. (2008). Expression patterns within the Arabidopsis C/S1 bZIP transcription factor network: availability of heterodimerization

partners controls gene expression during stress response and development. Plant molecular biology **69,** 107-119.

Weltmeier, F., Rahmani, F., Ehlert, A., Dietrich, K., Schutze, K., Wang, X., Chaban, C., Hanson, J., Teige, M., Harter, K., Vicente-Carbajosa, J., Smeekens, S., and Droge-Laser, W. (2009). Expression patterns within the Arabidopsis C/S1 bZIP transcription factor network: availability of heterodimerization partners controls gene expression during stress response and development. Plant molecular biology **69,** 107-119.

Wiese, A., Elzinga, N., Wobbes, B., and Smeekens, S. (2005). Sucrose-induced translational repression of plant bZIP-type transcription factors. Biochemical Society Transactions **33,** 272-275.

Wingler, A., and Roitsch, T. (2008). Metabolic regulation of leaf senescence: interactions of sugar signalling with biotic and abiotic stress responses. Plant Biology **10,** 50-62.

Wingler, A., Marès, M., and Pourtau, N. (2004). Spatial patterns and metabolic regulation of photosynthetic parameters during leaf senescence. New Phytologist **161,** 781-789.

Wingler, A., Masclaux-Daubresse, C., and Fischer, A.M. (2009). Sugars, senescence, and ageing in plants and heterotrophic organisms. Journal of experimental botany **60,** 1063-1066.

Wingler, A., Purdy, S.J., Edwards, S.A., Chardon, F., and Masclaux-Daubresse, C. (2010). QTL analysis for sugar-regulated leaf senescence supports flowering-dependent and-independent senescence pathways. New Phytologist **185,** 420-433.

Wingler, A., Delatte, T.L., O'Hara, L.E., Primavesi, L.F., Jhurreea, D., Paul, M.J., and Schluepmann, H. (2012). Trehalose 6-phosphate is required for the onset of leaf senescence associated with high carbon availability. Plant physiology **158,** 1241-1251.

Woo, H.R., Kim, J.H., Nam, H.G., and Lim, P.O. (2004). The delayed leaf senescence mutants of Arabidopsis, ore1, ore3, and ore9 are tolerant to oxidative stress. Plant and Cell Physiology **45,** 923-932.

Woo, H.R., Kim, H.J., Nam, H.G., and Lim, P.O. (2013). Plant leaf senescence and death–regulation by multiple layers of control and implications for aging in general. Journal of cell science **126,** 4823-4833.

Woo, H.R., Chung, K.M., Park, J.-H., Oh, S.A., Ahn, T., Hong, S.H., Jang, S.K., and Nam, H.G. (2001). ORE9, an F-box protein that regulates leaf senescence in Arabidopsis. The Plant Cell Online **13,** 1779-1790.

Wu, A., Allu, A.D., Garapati, P., Siddiqui, H., Dortay, H., Zanor, M.-I., Asensi-Fabado, M.A., Munné-Bosch, S., Antonio, C., and Tohge, T. (2012a). JUNGBRUNNEN1, a reactive oxygen species–responsive NAC transcription factor, regulates longevity in Arabidopsis. The Plant Cell Online **24,** 482-506.

Wu, K., Zhang, L., Zhou, C., Yu, C.-W., and Chaikam, V. (2008). HDA6 is required for jasmonate response, senescence and flowering in Arabidopsis. Journal of experimental botany **59,** 225-234.

Wu, X.Y., Kuai, B.K., Jia, J.Z., and Jing, H.C. (2012b). Regulation of Leaf Senescence and Crop Genetic ImprovementF. Journal of integrative plant biology **54,** 936-952.

Xia, X.-J., Zhou, Y.-H., Shi, K., Zhou, J., Foyer, C.H., and Yu, J.-Q. (2015). Interplay between reactive oxygen species and hormones in the control of plant development and stress tolerance. Journal of experimental botany **66,** 2839-2856.

Xiang, C., Han, P., Lutziger, I., Wang, K., and Oliver, D.J. (1999). A mini binary vector series for plant transformation. Plant molecular biology **40,** 711-717.

Xiao, W., Sheen, J., and Jang, J.-C. (2000). The role of hexokinase in plant sugar signal transduction and growth and development. Plant molecular biology **44,** 451-461.

Xiong, Y., and Sheen, J. (2012). Rapamycin and glucose-target of rapamycin (TOR) protein signaling in plants. Journal of Biological Chemistry **287,** 2836-2842.

Xiong, Y., and Sheen, J. (2014). The Role of Target of Rapamycin Signaling Networks in Plant Growth and Metabolism. Plant physiology **164,** 499-512.

Xiong, Y., McCormack, M., Li, L., Hall, Q., Xiang, C., and Sheen, J. (2013). Glucose-TOR signalling reprograms the transcriptome and activates meristems. Nature **496,** 181-186.

Xu, F., Meng, T., Li, P., Yu, Y., Cui, Y., Wang, Y., Gong, Q., and Wang, N.N. (2011). A soybean dual-specificity kinase, GmSARK, and its Arabidopsis homolog, AtSARK, regulate leaf senescence through synergistic actions of auxin and ethylene. Plant physiology **157,** 2131-2153.

Xue, B., Oldfield, C.J., Dunker, A.K., and Uversky, V.N. (2009). CDF it all: consensus prediction of intrinsically disordered proteins based on various cumulative distribution functions. FEBS letters **583,** 1469-1474.

Yadav, V., Mallappa, C., Gangappa, S.N., Bhatia, S., and Chattopadhyay, S. (2005). A Basic Helix-Loop-Helix Transcription Factor in Arabidopsis, MYC2, Acts as a Repressor of Blue Light–Mediated Photomorphogenic Growth. The Plant cell **17,** 1953-1966.

Yamada, K., Matsushima, R., Nishimura, M., and Hara-Nishimura, I. (2001). A slow maturation of a cysteine protease with a granulin domain in the vacuoles of senescing Arabidopsis leaves. Plant physiology **127,** 1626-1634.

Yang, S.-D., Seo, P.J., Yoon, H.-K., and Park, C.-M. (2011). The Arabidopsis NAC transcription factor VNI2 integrates abscisic acid signals into leaf senescence via the COR/RD genes. The Plant Cell Online **23,** 2155-2168.

Yang, Z., and Ohlrogge, J.B. (2009). Turnover of fatty acids during natural senescence of Arabidopsis, Brachypodium, and switchgrass and in Arabidopsis β-oxidation mutants. Plant physiology **150,** 1981-1989.

Yoon, M.K., Shin, J., Choi, G., and Choi, B.S. (2006). Intrinsically unstructured N-terminal domain of bZIP transcription factor HY5. Proteins **65,** 856-866.

Yoshimoto, K. (2010). Plant autophagy puts the brakes on cell death by controlling salicylic acid signaling. Autophagy **6,** 192-193.

Yoshimoto, K., Jikumaru, Y., Kamiya, Y., Kusano, M., Consonni, C., Panstruga, R., Ohsumi, Y., and Shirasu, K. (2009). Autophagy negatively regulates cell death by controlling NPR1-dependent salicylic acid signaling during senescence and the innate immune response in Arabidopsis. The Plant Cell Online **21,** 2914-2927.

Zavaleta-Mancera, H.A., López-Delgado, H., Loza-Tavera, H., Mora-Herrera, M., Trevilla-García, C., Vargas-Suárez, M., and Ougham, H. (2007). Cytokinin promotes catalase and ascorbate peroxidase activities and preserves the chloroplast integrity during dark-senescence. Journal of plant physiology **164,** 1572-1582.

Zeng, X., Herndon, A.M., and Hu, J.C. (1997). Buried asparagines determine the dimerization specificities of leucine zipper mutants. Proceedings of the National Academy of Sciences **94,** 3673-3678.

Zentgraf, U., and Hemleben, V. (2008). Molecular cell biology: are reactive oxygen species regulators of leaf senescence? In Progress in botany (Springer), pp. 117-138.

Zentgraf, U., Jobst, J., Kolb, D., and Rentsch, D. (2004). Senescence-related gene expression profiles of rosette leaves of Arabidopsis thaliana: Leaf age versus plant age. Plant Biology **6,** 178-183.

Zhang, K., Xia, X., Zhang, Y., and Gan, S.S. (2012). An ABA-regulated and Golgi-localized protein phosphatase controls water loss during leaf senescence in Arabidopsis. The Plant Journal **69,** 667-678.

Zhang, Y., Primavesi, L.F., Jhurreea, D., Andralojc, P.J., Mitchell, R.A., Powers, S.J., Schluepmann, H., Delatte, T., Wingler, A., and Paul, M.J. (2009). Inhibition of SNF1-related protein kinase1 activity and regulation of metabolic pathways by trehalose-6-phosphate. Plant physiology **149,** 1860-1871.

Zhong, H., Guo, Q.-Q., Chen, L., Ren, F., Wang, Q.-Q., Zheng, Y., and Li, X.-B. (2012). Two Brassica napus genes encoding NAC transcription factors are involved in response to high-salinity stress. Plant cell reports **31,** 1991-2003.

Zimmermann, P., and Zentgraf, U. (2005). The correlation between oxidative stress and leaf senescence during plant development. Cellular and Molecular Biology Letters **10,** 515.

Zimmermann, P., Heinlein, C., Orendi, G., and Zentgraf, U. (2006). Senescence-specific regulation of catalases in Arabidopsis thaliana (L.) Heynh. Plant, cell & environment **29,** 1049-1060.

Zitzewitz, J.A., Ibarra-Molero, B., Fishel, D.R., Terry, K.L., and Matthews, C.R. (2000). Preformed secondary structure drives the association reaction of GCN4-p1, a model coiled-coil system. Journal of molecular biology **296,** 1105-1116.

7. List of abbreviations

4MUG	4-Methylumbelliferyl-b-D-glucuronide
ABA	Abscisic acid
APS	Ammonium persulfate
ASN1	ASPARAGINE SYNTHETASE 1
bp	Base pair
BR	Brassinosteroid
BR	Basic region
BSA	Bovin serum albumin
bZIP	Basic region/leucine zipper protein
CaMV	Cauliflower mosaic virus
CAT2	CATALASE 2
CDF	Cumulative distribution function
CDS	Gene coding sequence
cDNA	Complementary DNA
CH	Charge-Hydropathy
Ci	Curie
CK	Citokinin
CKII	Casein kinase II
c-Myc	Cellular *myelocytomatosis* oncogene
Col-0	Columbia-0
DAS	Days after sowing
DEPC	Diethylpyrocarbonate
dNTP	Deoxynucleotide
DTT	Dithiothreitol
ECL	Enhanced chemiluminescence
EDTA	Ethylenediaminetetraacetic acid
ET	Ethylene
ETC	Electron transport chain
GA	Gibberelin
GBF	G-BOX BINDING FACTOR
GFP	Green fluorescent protein
GST	Glutathione S-transferase
GUS	β-glucuronidase
HA	Hemagglutinin
HRP	Horse radish peroxidase
Hy5	ELONGATED HYPOCOTYL 5
HyH	HY5-HOMOLOG
IAA	Indole acetic acid
IDP	Intrinsically disordered protein
IDR	Intrinsically disordered region
IP	Inflexion point
IPTG	Isopropyl-β-D-thiogalactopyranosid
JA	Jasmonic acid
Kbp	Kilo base pair

KDa	Kilo Dalton
Lb	Left border T-DNA primer
LB	Luria Broth
LBA	Luria Broth Agar
Ler	Landsberg erecta
LHCB2.4	LIGHT-HARVESTING CHLOROPHYLL B-BINDING 2
LP	Left genomic primer
LZ	Leucine zipper
MCS	Multiple cloning site
MW	Molecular weight
NLS	Nuclear localization signal
NosT	Nopaline synthase terminator
OD	Optical density
OPD	o-Phenylenediamine dihydrochloride
ORF	Open reading frame
PAGE	Polyacrylamide gel electrophoresis
PCA	Principal component analysis
PCR	Polymerase chain reaction
PDH	PROLINE DEHYDROGENASE
PEG	Polyethylene glycol
PRD	Proline rich domain
PVDF	Polyvinylidene difluoride
qPCR	Quantitative PCR
RBCS1a	RIBULOSE BISPHOSPHATE CARBOXYLASE SMALL CHAIN 1A
RBS	Ribosome binding site
ROS	Reactive oxygen species
RP	Right genomic primer
RT	Room temperature
RT-PCR	Reverse transcription polymerase chain reaction
SA	Salicylic acid
SD	Shine-Dalgarno sequence
SDS	Sodium dodecyl sulfate
SPYCE	Split YFP C-terminal fragment expression
SPYNE	Split YFP N-terminal fragment expression
SSCT	Saline sodium citrate - Tween
TAD	Transactivation domain
TBS	Tris-buffered saline
TBS-T	Tris-buffered saline with tween
TCA	Tricarboxylic acid cycle
TE	Tris EDTA
TEMED	Tetramethylethylenediamine
Tm	Melting temperature
U	Enzyme unit
UTR	Untranslated region
Ws	Wassilewskija
YFP	Yellow fluorescent protein

8. Contributions

Some parts of this work were performed with the cooperation of other researches, whose contributions have been indicated throughout the text where appropriate. In addition to that, the present writing contains extracts (modified to different extents) and figures from the three following publications produced with my co-authorship and whose reproduction is permitted:

1- The elucidation of the interactome of 16 Arabidopsis bZIP factors reveals three independent functional networks (Llorca et al., 2015).

2- The low energy signaling network (Tomé et al., 2014).

3- bZIPs and WRKYs: two large transcription factor families executing two different functional strategies (Llorca et al., 2014).

That affects especially the second part of the Results and the corresponding segments of the Discussion which represent an improved version of the article #1, for which I wrote the most part (other authors contributed to the writing only with corrections and suggestions). Fragments of the articles #2 and #3 can be found in the Introduction.

Figures 1-7, 23, and 31 were designed by or with the help of Milagros Collados Rodriguez.

APPENDIX A

Boxplot representation of Genevestigator data

The Genevestigator platform is often used to contrast experimental gene expression results with repositories of public microarray data. In order to simplify the representations, usually only the averages are displayed in the form of heat-map or scatter graph. However, when data are represented in the form of boxplots, huge variances are apparent. In order to reflect the actual data depicted in Figure 75, the same Genevestigator results are represented here are boxplots.

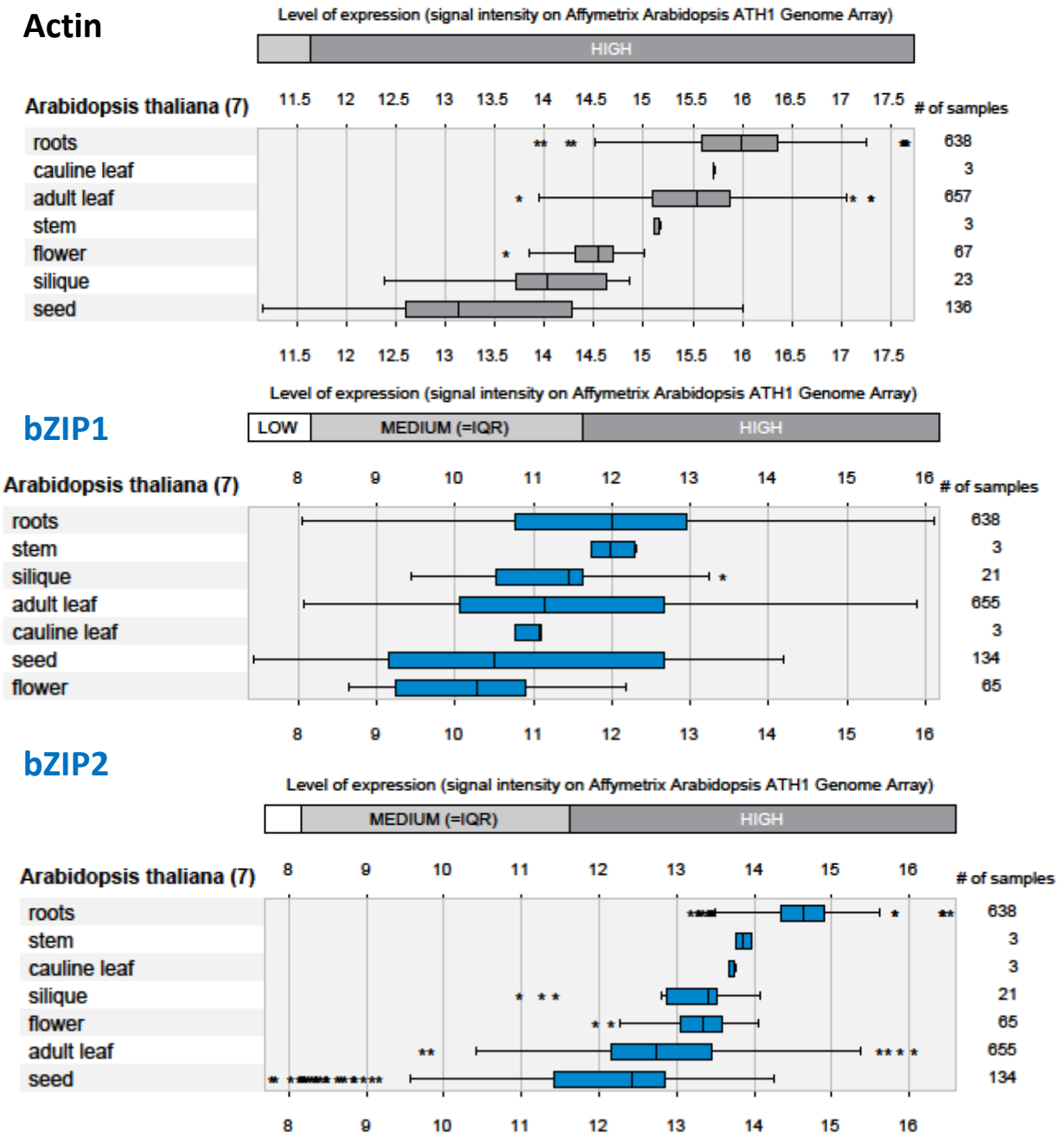

bZIP11

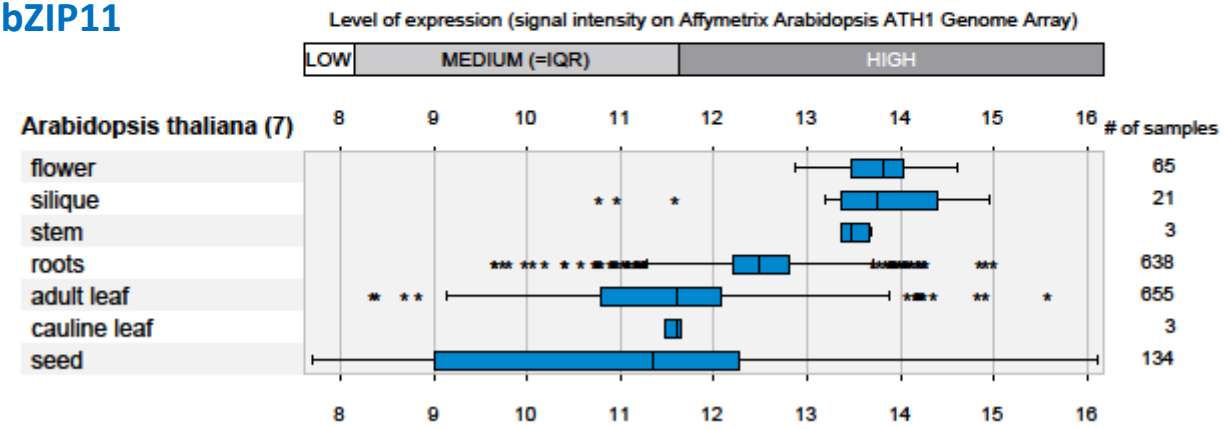

bZIP44

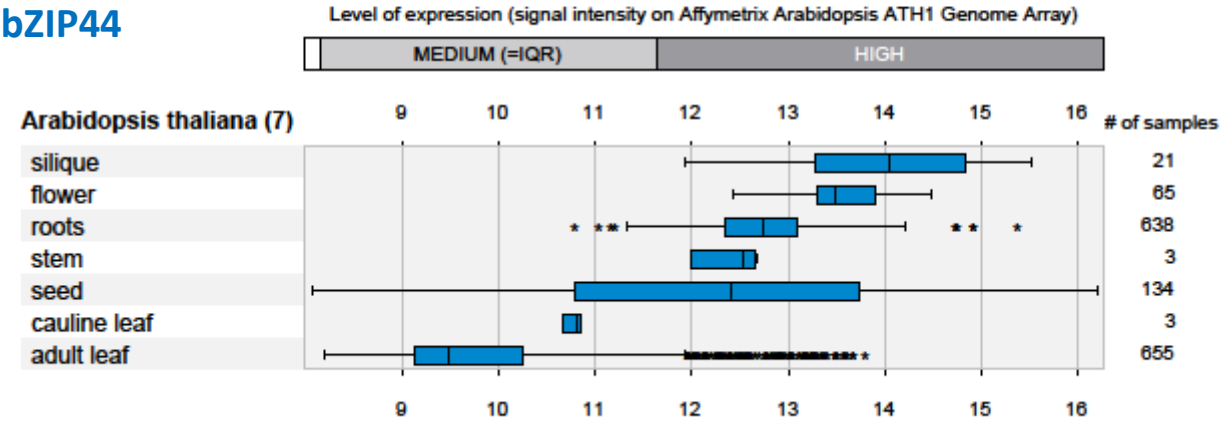

bZIP53

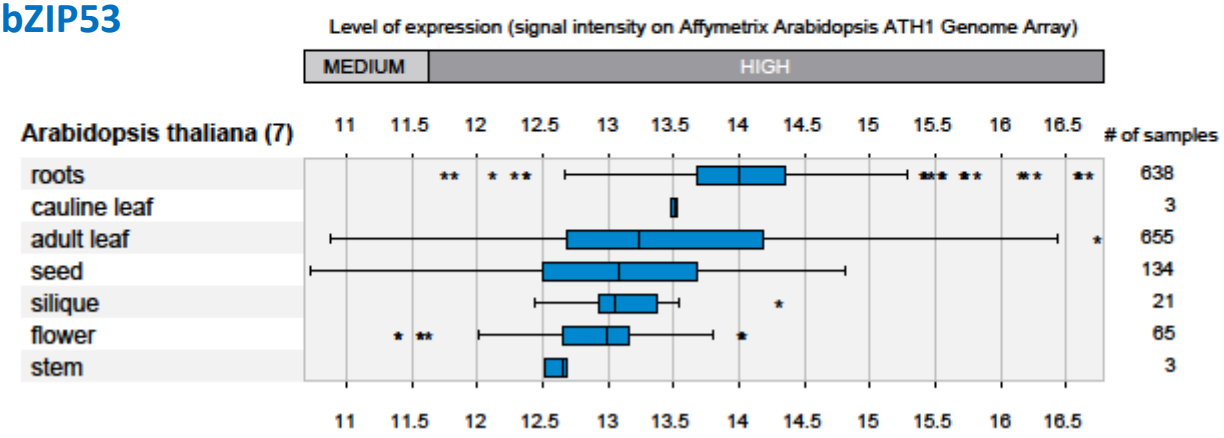

bZIP9

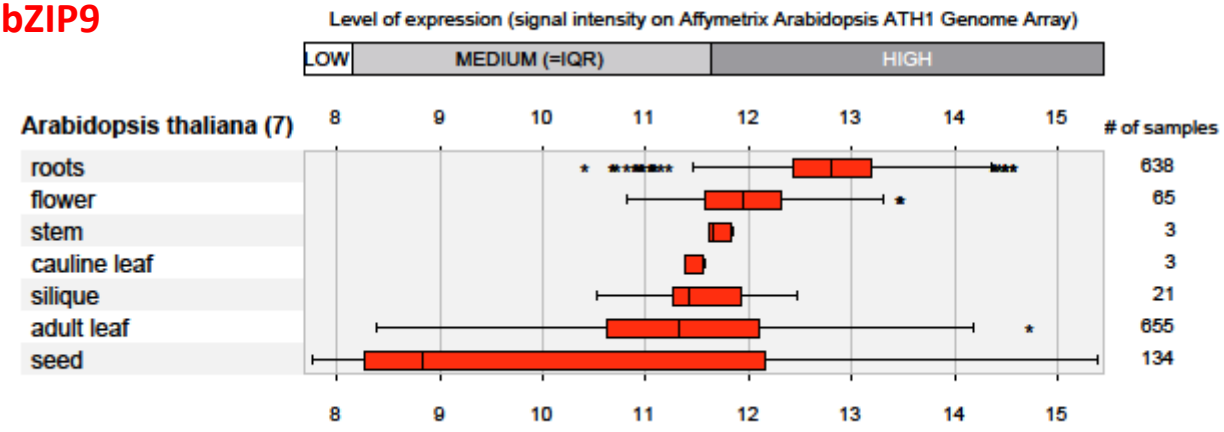

bZIP10

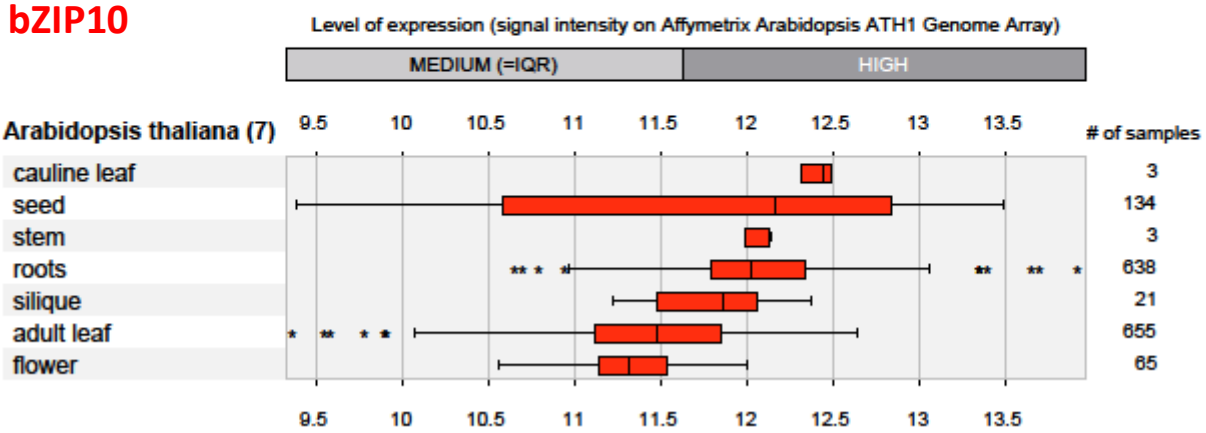

bZIP25

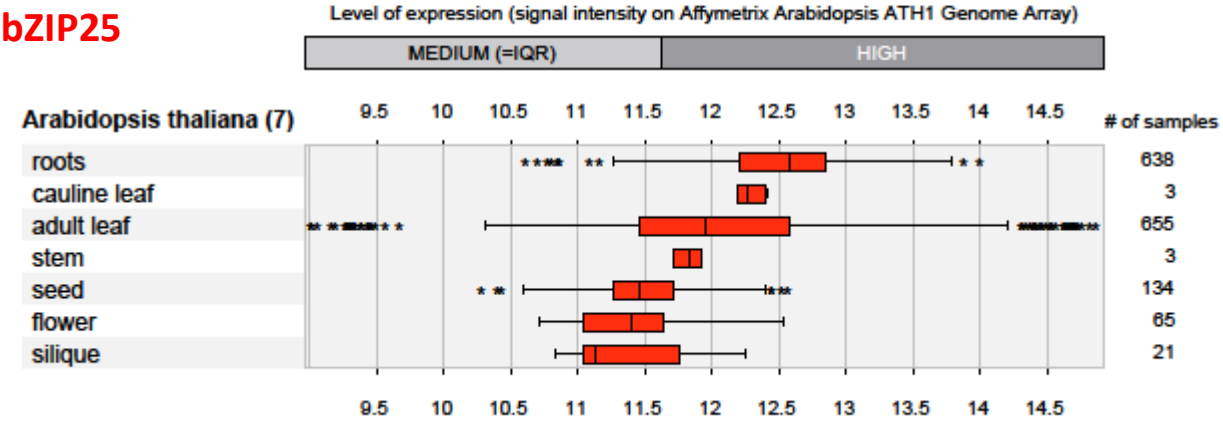

bZIP63

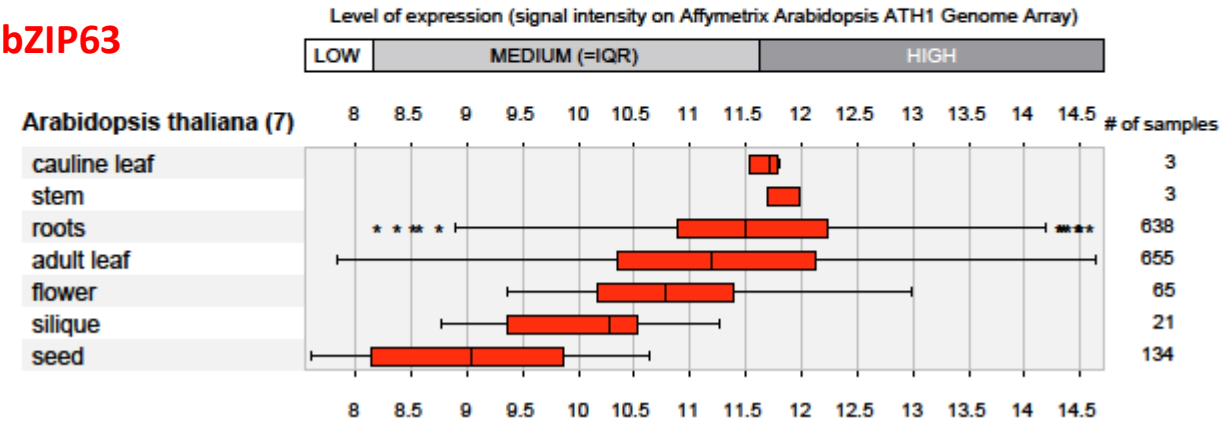

GBF1

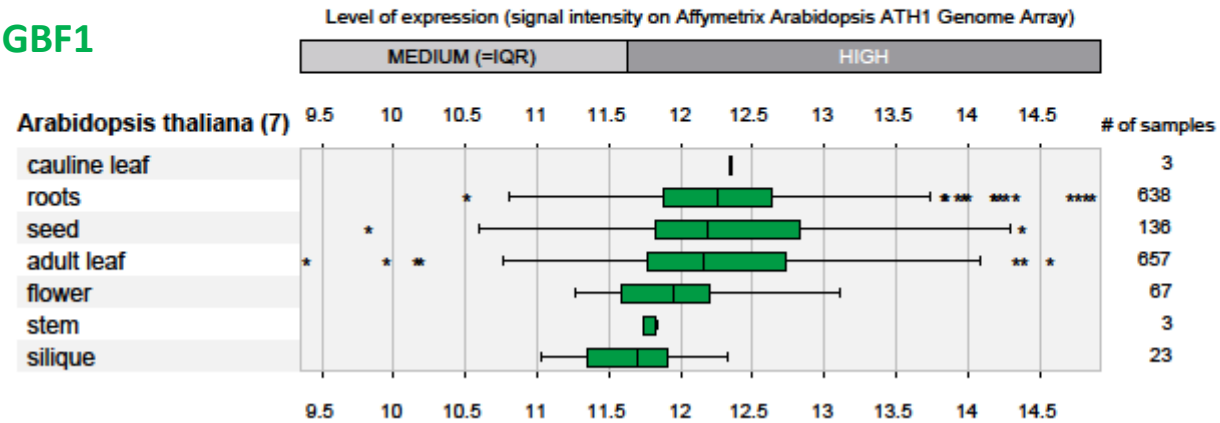

GBF2

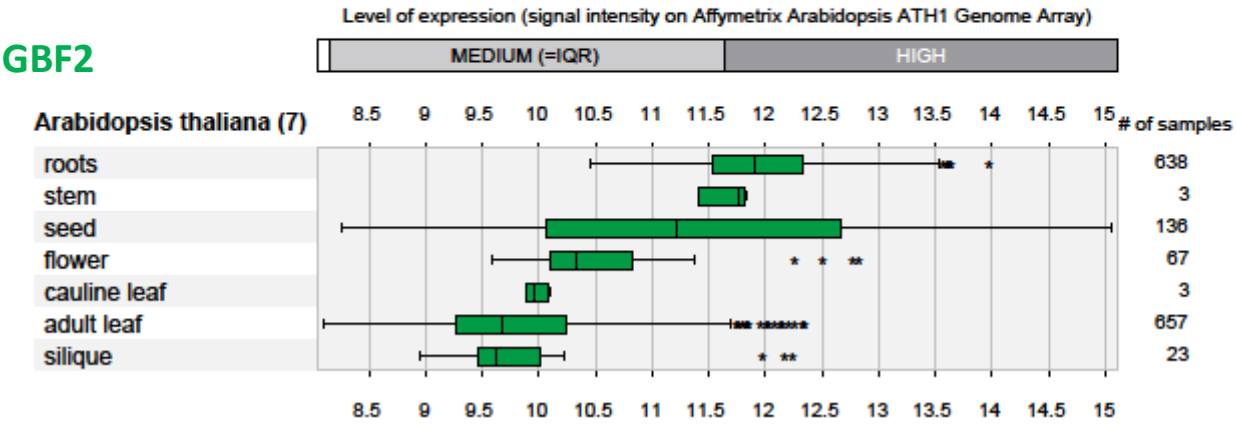

GBF3

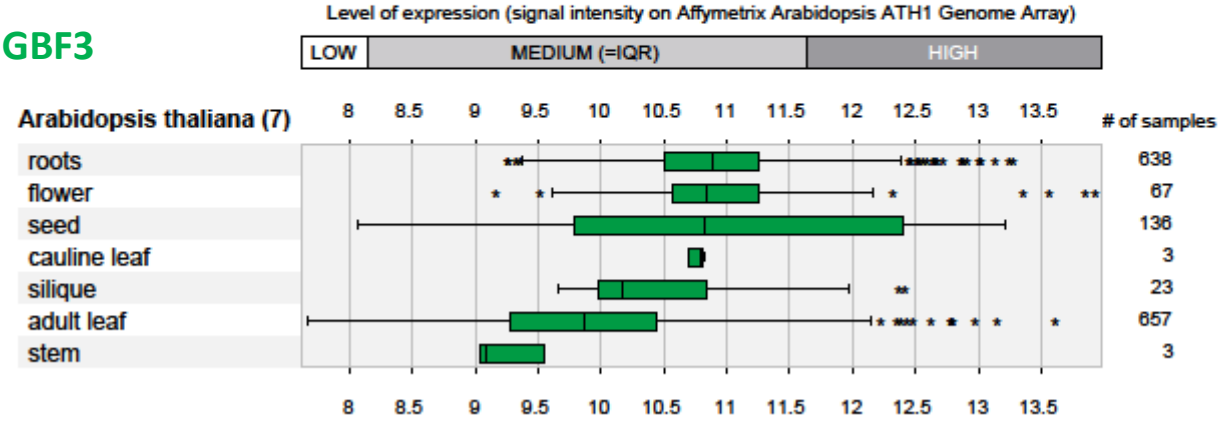

bZIP16

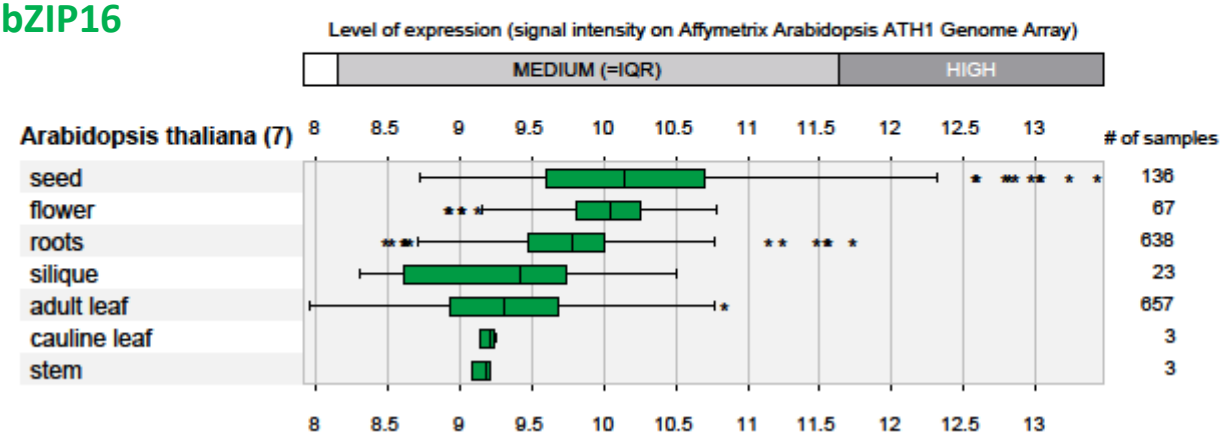

bZIP68

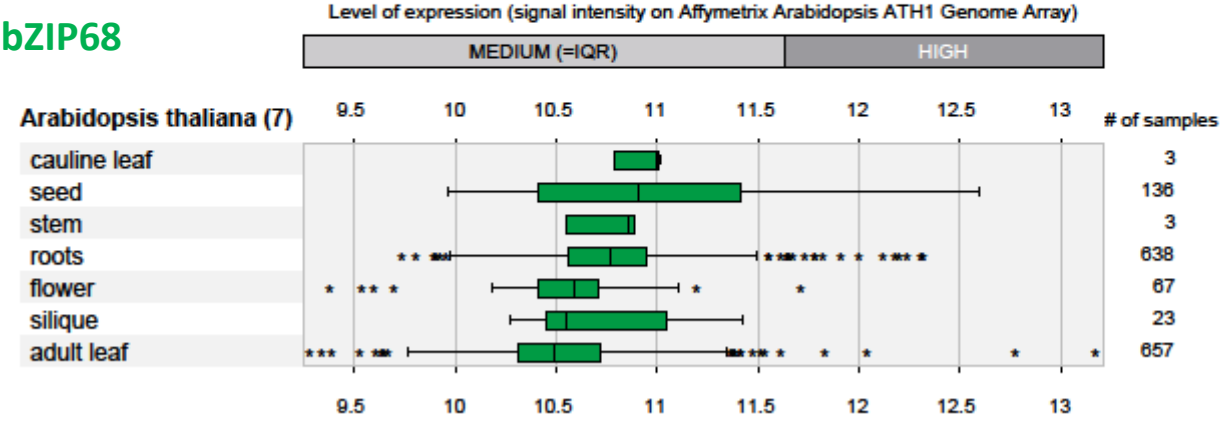

Hy5

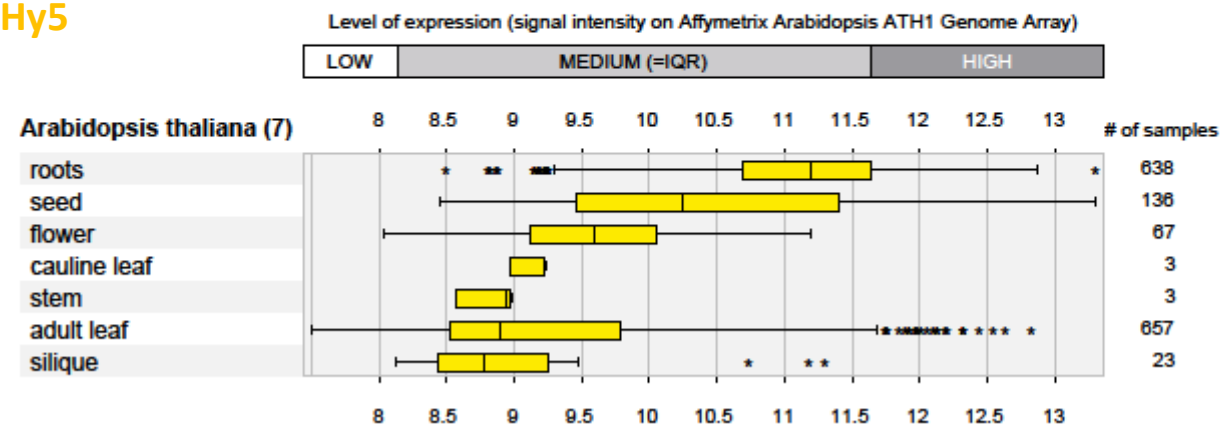
Level of expression (signal intensity on Affymetrix Arabidopsis ATH1 Genome Array)
LOW
MEDIUM (=IQR)
HIGH
Arabidopsis thaliana (7)
8 8.5 9 9.5 10 10.5 11 11.5 12 12.5 13
# of samples
roots 638
seed 136
flower 67
cauline leaf 3
stem 3
adult leaf 657
silique 23

HyH

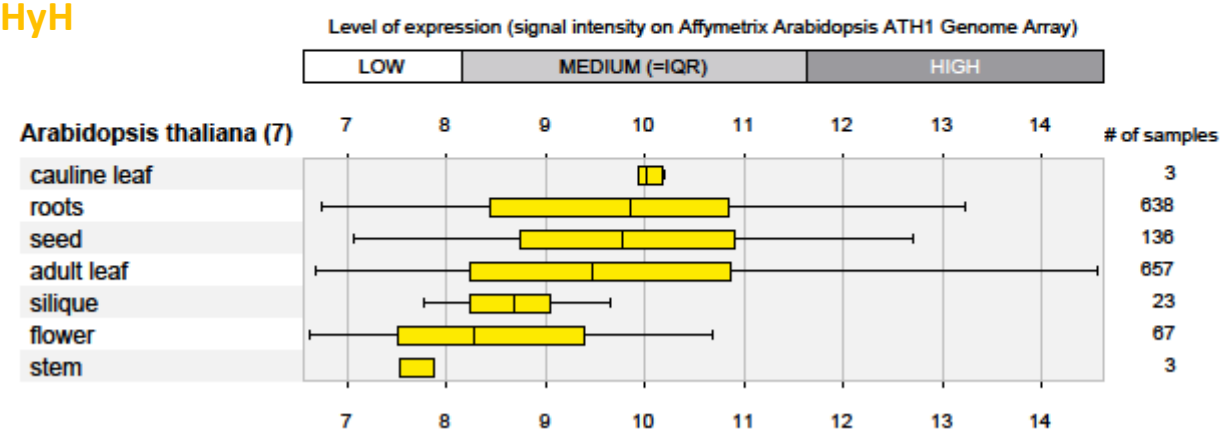
Level of expression (signal intensity on Affymetrix Arabidopsis ATH1 Genome Array)
LOW
MEDIUM (=IQR)
HIGH
Arabidopsis thaliana (7)
7 8 9 10 11 12 13 14
# of samples
cauline leaf 3
roots 638
seed 136
adult leaf 657
silique 23
flower 67
stem 3

APPENDIX B

Protein expression from pDEST42 vector

For the ELISA assays described in the first part of the results, the recombinant proteins assayed were expressed from the pDEST42 vector, which codifies for a C-terminal 6xHis-tag. However, the pDEST42 vector does not carry a ribosome binding site, which is expected to be cloned together with the protein coding sequence as the following verbatim extract from the pDEST42 User Manual (Invitrogen) indicates: "Your insert should contain a ribosome binding site [AGGAG(A/G)] approximately 9-10 base pairs upstream of the ATG initiation codon".

That ribosome binding site sequence is known as the Shine –Dalgarno (SD) sequence, which serves as a docking site for the 30S ribosomal unit, and is of decisive importance for the initiation of prokaryotic translation (Simonetti et al., 2009). The SD is located in the 5'UTR of prokaryotic mRNAs, and is complementary to the 3' end of the 16S rRNA (GAUCACCUCCUUA). The efficiency of the translation is determined by the spacing between the SD and the initial ATG codon, as well as the degree of matching between the SD and the 16S RNA. In *E.coli*, SD sequences are usually located around 8 nucleotides before the translation start site, and matching between the two sequences spans along at least 4 consecutive bases. Binding is more efficient as more G-C pairs match, and G-U pairs establish wobble pairing (Shine and Dalgarno, 1974; Steitz and Jakes, 1975; Flingquist et al., 1992; Malys, 2012).

All pDEST42 constructs used in this study were cloned without the SD sequence, but in spite of that the recombinant proteins could be detected in Western blot using anti His-tag antibodies. However, while GBF1 was well expressed and regularly resulted in a single band with the expected MW, the expression of bZIP63 was weak, and different expression attempts led to distinct patterns of bands. Besides, when a single band pattern could be obtained for bZIP63, it resulted in a markedly lower MW than expected. Therefore, I wondered whether protein translation could start from other in-frame ATG codons using alternative SD sequences in that clone.

The examination of the bZIP63 CDS revealed several sequences matching the SD consensus sequences on 4 or more nucleotides, but they were more than 30 nucleotides away from the following ATG (Figure 84). In contrast, the CDS of GBF1 included various potential SD sites within a reasonable distance to the ensuing in-frame ATG (Figure 85), the first one laying just at the beginning of both coding sequences. Furthermore, GBF1 included a perfect SD sequence -although it was significantly away from the next ATG- and abundant in-frame ATGs at the beginning of the protein that could be used as alternative sites to start translation.

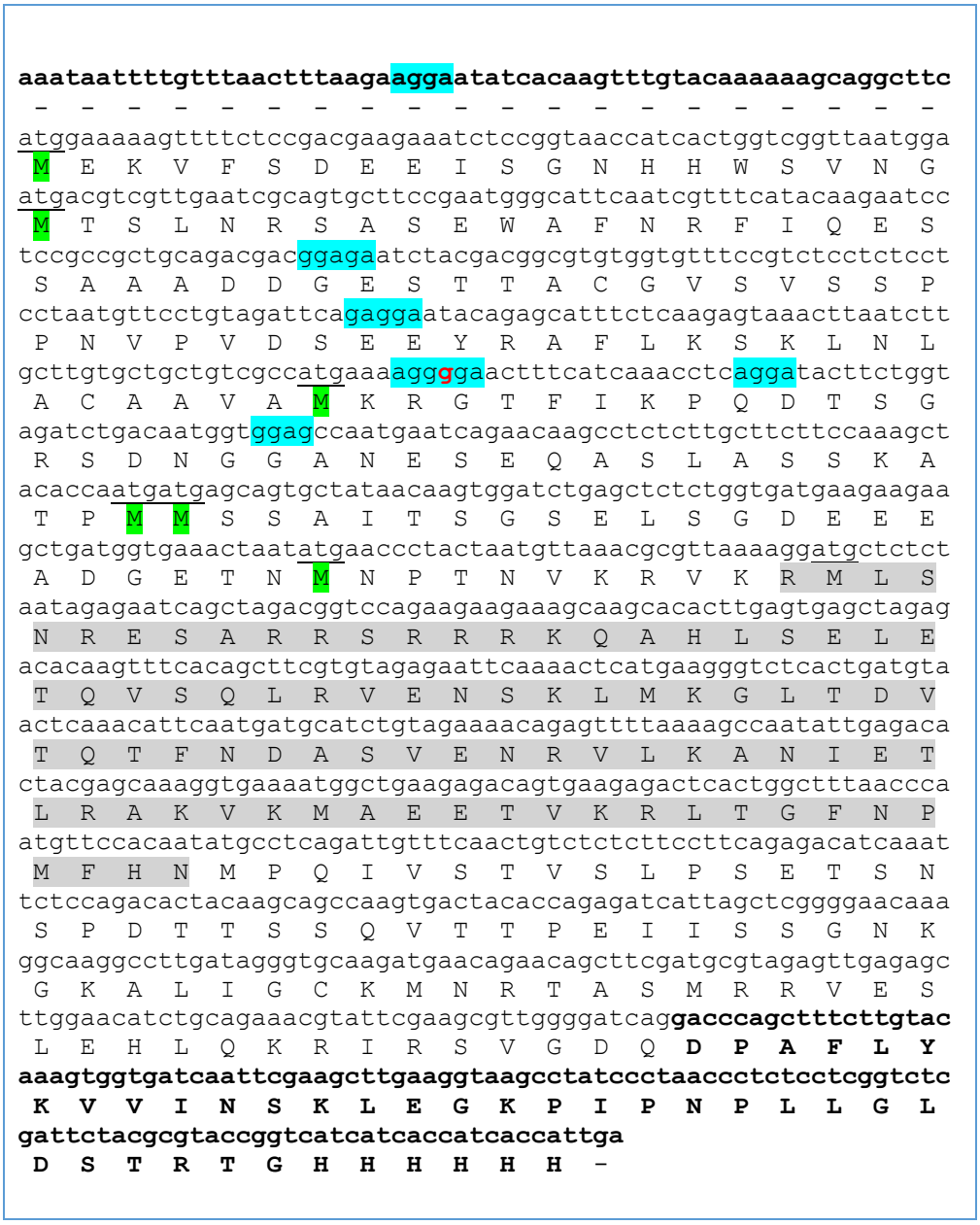

Figure 84. Sequence of the bZIP63 pDEST42 clone. The DNA sequence is indicated in lower case, the protein sequence in upper case. Bold letters indicate vector sequences. In-frame ATG codons are underlined and the corresponding methionines are in green background, possible SD sequences before the bZIP domain in light blue, and the bZIP domain in grey. Wobble U-G pairings within the SD sequence are indicated in bold red letters.

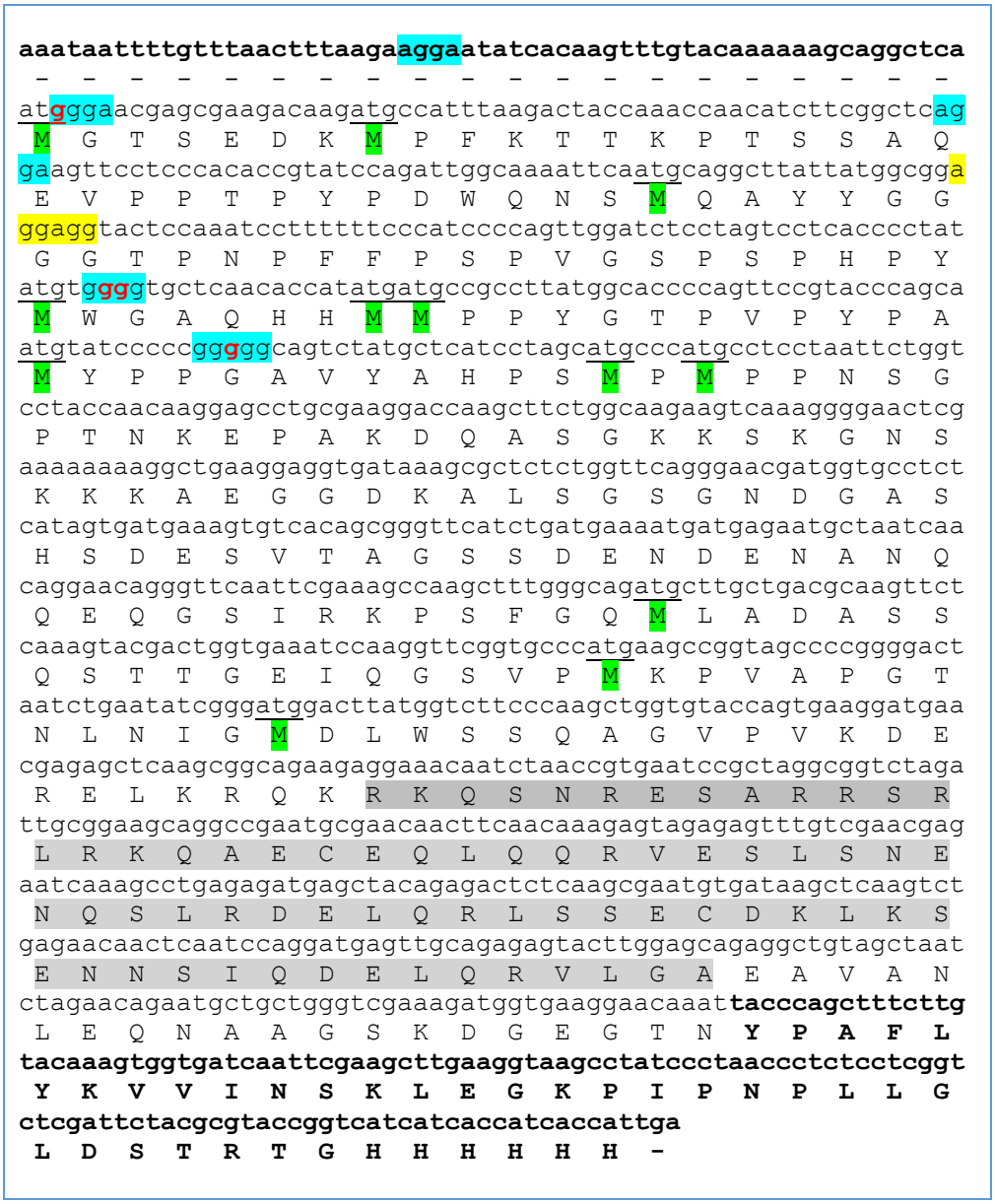

Figure 85. Sequence of the GBF1 pDEST42 clone. The DNA sequence is indicated in lower case, the protein sequence in upper case. Bold letters indicate vector sequences. In-frame ATG codons are underlined and the corresponding methionines are in green background, possible SD sequences before the bZIP domain in light blue, and the bZIP domain in grey. Wobble U-G pairings within the SD sequence are indicated in bold red letters. A perfect SD sequence is indicated in yellow background.

Those observations suggested that translation could be initiated within the CDS from sequences matching the SD site. Regarding GBF1, those alternative ribosome docking sites lay at the beginning of the CDS, so they would result in slight truncations at the N-terminus. Specifically, GBF1 translation could be initiated from methionines in positions 68 or 73, which would result in truncate proteins of 30.0, and 28.2 KDa, respectively. In that manner, the bands in SDS-PAGE corresponded with the theoretically calculated for the full protein, given that bZIPs migrated with a higher apparent molecular weight in SDS-PAGE (Figure 52 and Figure 87).

The bZIP63 clone presented a more difficult scenario, as no alternative SD sites are identifiable within a reasonable distance to the following ATG codon. The bZIP63 CDS comprises three sequences with a significant overlap with the 16S rRNA (five and six nucleotides) and resulting in at least three G-C pairs, thus it could be contemplated that they resulted in sufficiently strong ribosome binding to overcome the large spacing

between them and the following ATG, especially if we consider the context of mRNA overexpression by the T7 promoter. Alternatively, other sequences sharing similarity with the SD site, although not featuring at least 4 consecutive bases, could be used as RBS, again eased by the mRNA overexpression. Anyhow, unlike GBF1, most of the in-frame ATG codons within the bZIP63 CDS were found backwards in the sequence, so that it could be reasonable assumed that the bZIP63 protein expressed from the pDEST42 had a significant truncation of its N-terminus. Concretely, in base of the bZIP63 band size observed in Western blots, it could be speculated that translation started from methionine 123, which would result in a 25.6 KDa protein.

APPENDIX C

Analysis of the DNA binding of the 16 bZIPs

To provide a thorough overview of the bZIP function in the second part of the work, analyses on the DNA binding of the 16 bZIPs were planned. Although they did not finally come to fruition due to time issues, preliminary results can be of use for the interpretation of other data or as source for new scientific questions. Therefore the results of the initial tries are encapsulated in this appendix.

The DNA-binding activity was tested by ELISA as described in the material and methods section with few modifications, which basically were aimed to strictly adjust the protocol to the manufacturer's instructions in an attempt to enhance the reproducibility of the results. An additional step was introduced at the beginning of the protocol to pre-wash the plates 3 times for 5 minutes with 300 µL of 5X SCCT buffer (750 mM NaCl, 75 mM sodium citrate, 0.05% Tween-20, pH 7.0) per well. DNA was then incubated in 5X SSCT buffer for 2 hours at RT, instead of in TBS-T for 30 minutes at 37°C. After blocking the residual binding spots with the Roche blocking buffer, wells were washed with 200 µl of a solution 150mM NaCl with 0.1% Tween. Protein extracts were incubated overnight at 4°C, instead of 1 hour at RT. In addition, all bZIPs were cloned and expressed from the pDEST17 vector, which already contains a RBS.

Raw protein extracts were prepared as stated in material and methods section, and were kept frozen at -20 °C in small aliquots. For each assay, a new aliquot was used and protein master-mixes were prepared in a 96 well 0.3 mL plate according to the diagram in Figure 86. ELISAs were performed with the Liquidator 96, so that the same protein master-mix was tested with various plates containing different DNA-probes.

	1	2	3	4	5	6	7	8	9	10	11	12
A	bZIP1	bZIP53	bZIP63	bZIP16	bZIP9	bZIP9	bZIP9	bZIP9	bZIP9	bZIP63	bZIP63	bZIP63
B					bZIP1	bZIP2	bZIP11	bZIP44	bZIP53	bZIP9	GBF1	bZIP68
C	bZIP2	bZIP9	GBF1	bZIP68	bZIP10	bZIP10	bZIP10	bZIP10	bZIP10	bZIP63	bZIP63	bZIP63
D					bZIP1	bZIP2	bZIP11	bZIP44	bZIP53	bZIP10	GBF2	Hy5
E	bZIP11	bZIP10	GBF2	Hy5	bZIP25	bZIP25	bZIP25	bZIP25	bZIP25	bZIP63	bZIP63	bZIP63
F					bZIP1	bZIP2	bZIP11	bZIP44	bZIP53	bZIP25	GBF3	HyH
G	bZIP44	bZIP25	GBF3	HyH	bZIP63	bZIP63	bZIP63	bZIP63	bZIP63	C1	bZIP63	C2
H					bZIP1	bZIP2	bZIP11	bZIP44	bZIP53		bZIP16	

Figure 86. Diagram of the protein master-mix. Plates were divided in three parts. The first one contained single bZIP protein extracts (background colors according to the bZIP group), the second part were bZIP mixes reproducing the C/S1 heterodimers (purple background), and the third part were bZIP mixes combining bZIP63 and the G- and H-bZIPs (grey background). Besides, two controls were included (white background): control 1 (C1) consisting of the DNA probe without protein extract, and control 2 (C2) with neither DNA, no protein extract.

The main weakness of these experiments -and eventually the reason why they were not concluded- was to achieve similar amounts of the proteins tested in order to produce comparable results. The 16 bZIPs were expressed in separated batches, and for each one the expression of the proteins was confirmed by Western blot. However, when the protein levels were compared all together in the same gel, ostensibly differences arose. Therefore, I tried to individually adjust the dilution of each protein extract in order to obtain comparable

signals. That was done iteratively, so for the first Western blot all protein extracts were diluted 1:50, and after estimating their relative amounts recombinant protein, the dilutions of each protein were adjusted accordingly. The new dilutions were then used for a new Western blot, repeating the process. Eventually, three different tries were performed, which are referred as T1, T2, and T3 (Figure 87).

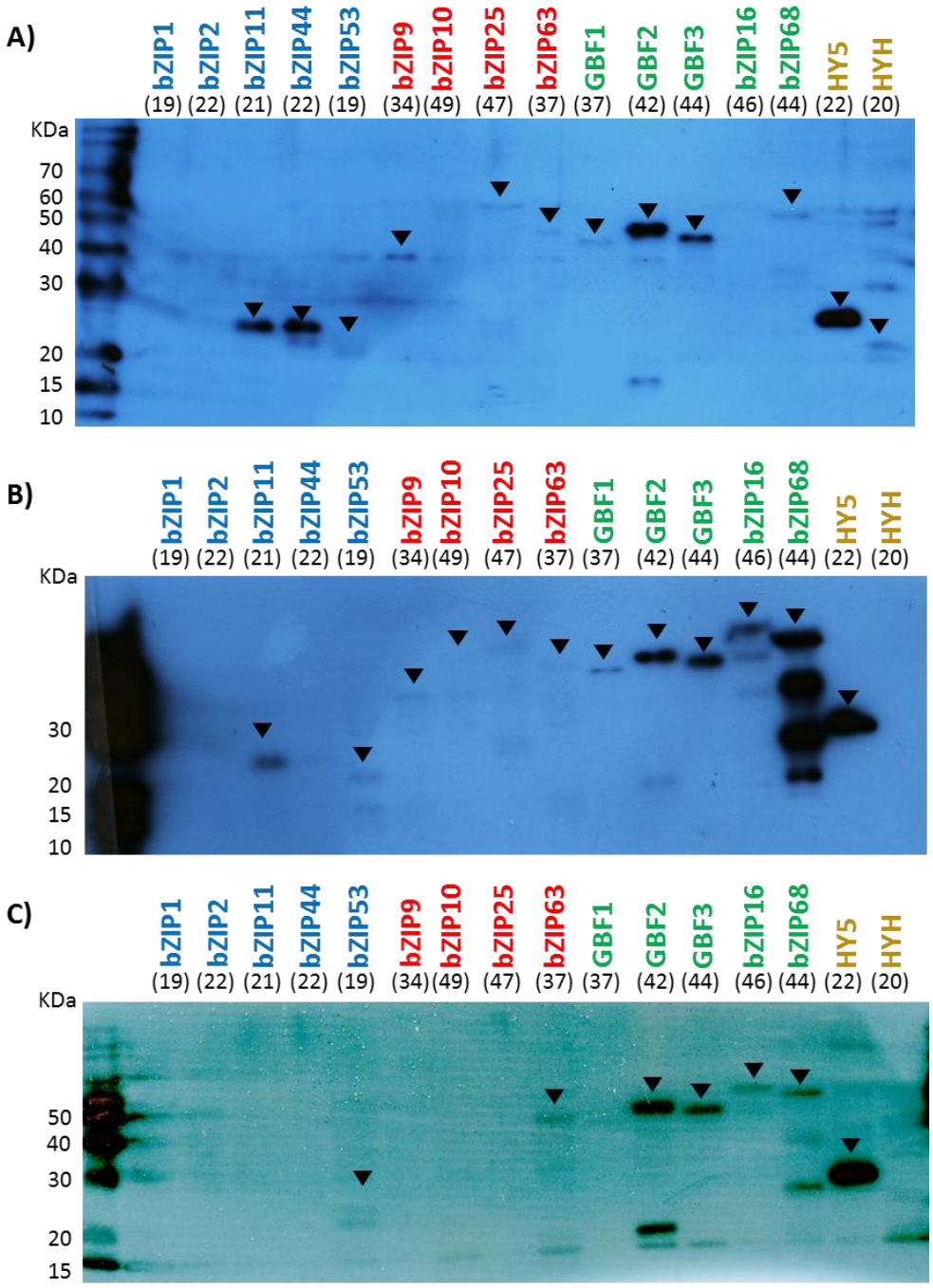

Figure 87. Western blots for the three tries. In brackets are indicated the theoretical MW for each bZIP. A) T1, B) T2, and C) T3. 5 µL of a 6xHis Protein Ladder (Qiagen) was used as standard (on the left). Notice that not all the bands are recognizable in B) and C).

Along with the Western blots, thawed protein aliquots were used to be tested by DPI-ELISA, in that manner generating these preliminary results. In these attempts, three different DNA probes from the CAT2 promoter were analyzed: the G-box tested in the first part of the Results section (No.1), and two other C-boxes (no. 2 and 3). The G-box and the C-box 2 were bound by G- and H-bZIPs, but not the C-box 3 (Figure 88). That outcome was reasonably consistent, while other conclusions were difficult to drawn because of the different protein amounts tested and the absence of sequential dilutions.

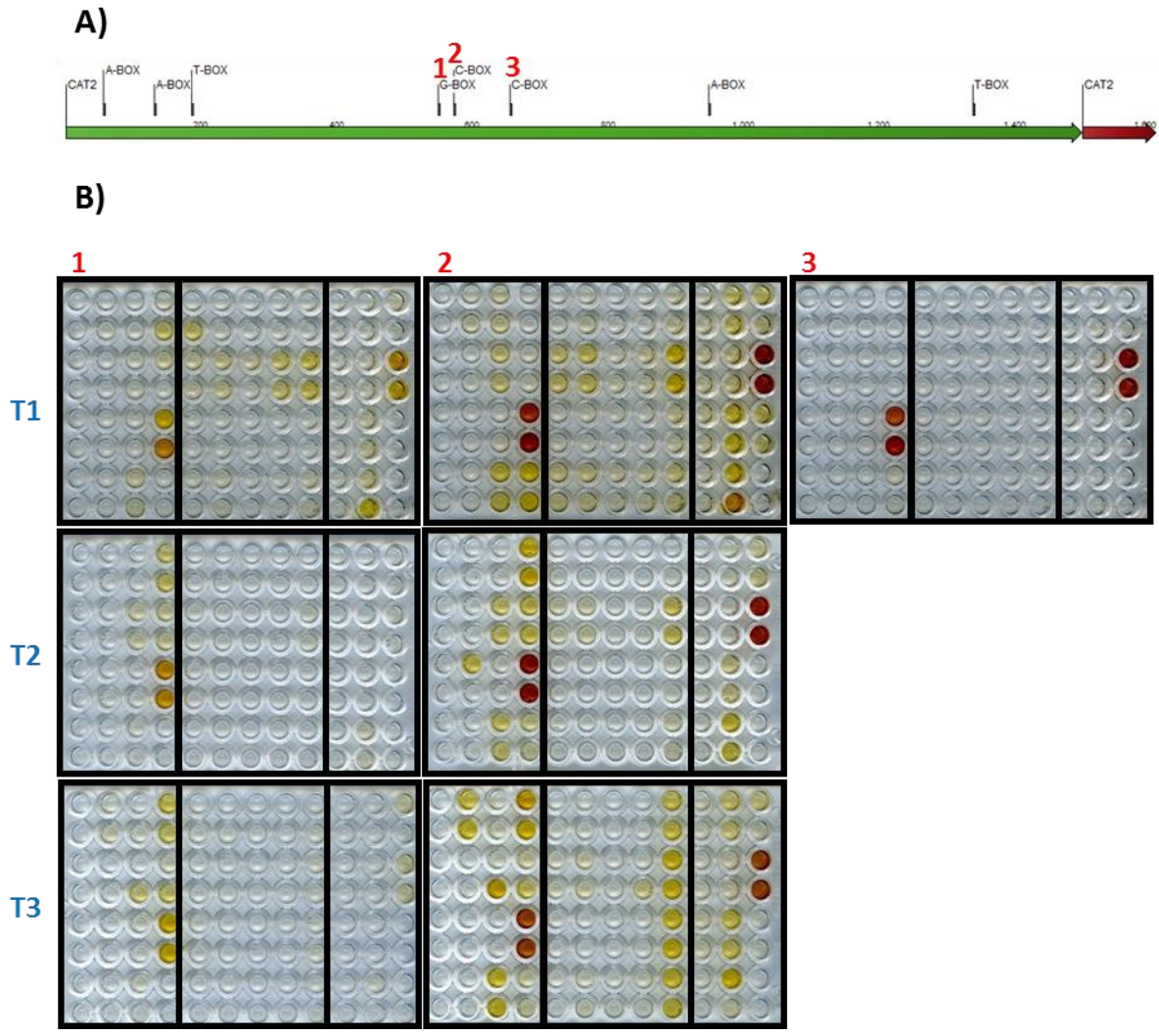

Figure 88. ELISA on the *CAT2* promoter. A) Outline of the *CAT2* promoter indicating the potential cis-elements based on an ACGT core. Green arrow represents 1.5 Kbp upstream of the gene, and red arrow the 5'UTR. Red numbers indicate the three different DNA probes tested: 1 is the DNA probe tested in the first part of the Results, 2 corresponds to the sequence ACAAAGCAGCCACGTCACCCAAGACC, and 3 corresponds to the sequence ACAGCCCAATGACGTCCTCATTTATT. B) Pictures of the ELISA plates after the reaction. The protein master mixes assayed are indicated in blue.

Concerning the *RBCS1a* promoter, two G-boxes were tested (No. 1 and 2), being the G-box No.1 the one tested in the first part of the Results. As before, the only safe inference derivable from those results was that the G-box No.1 was bound by G- an H-bZIPs, but not the G-box No.2 (Figure 89).

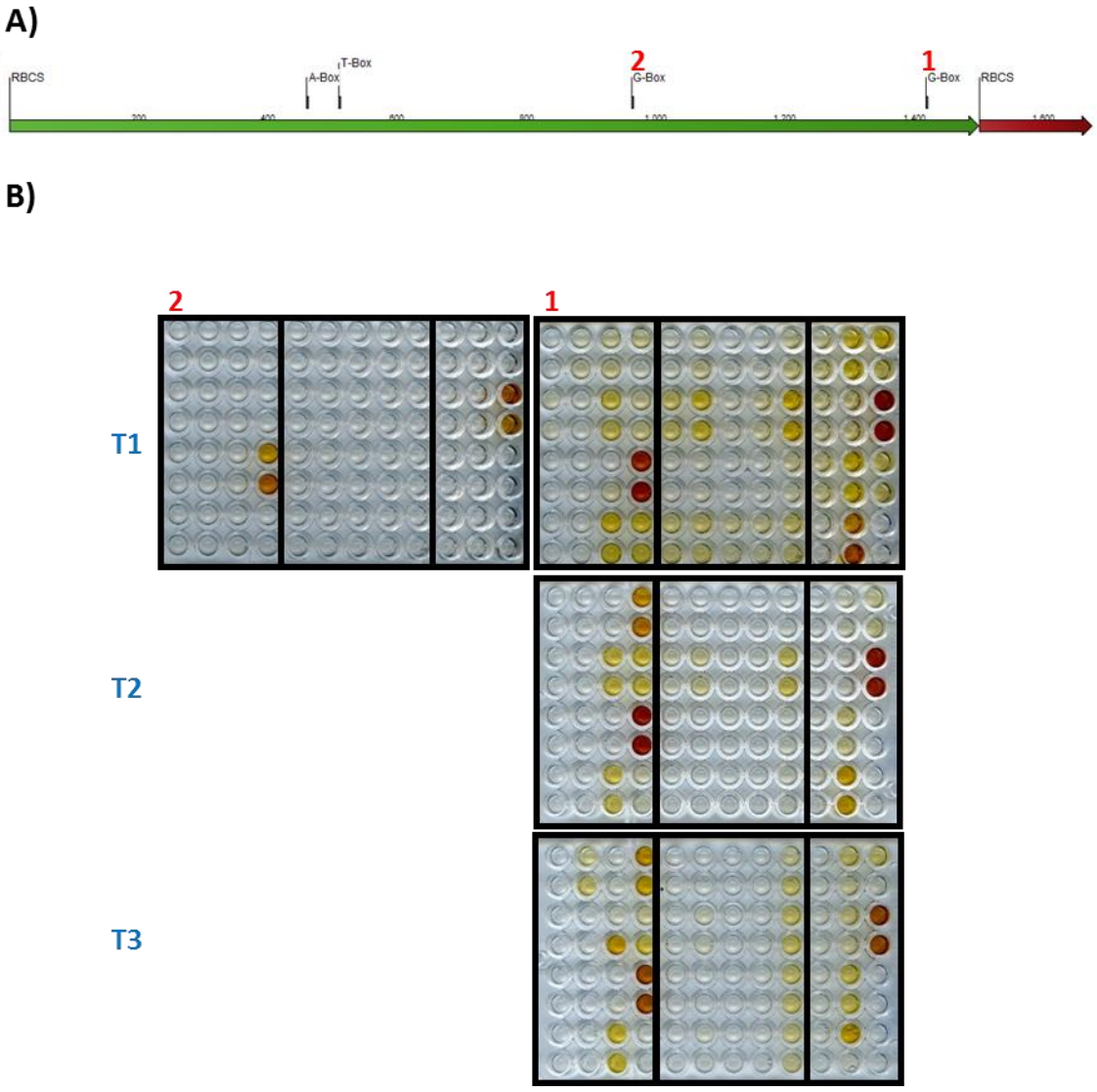

Figure 89. ELISA on the *RBCS1a* promoter. A) Outline of the *RBCS1a* promoter indicating the potential cis-elements based on an ACGT core. Green arrow represents 1.5 Kbp upstream of the gene, and red arrow the 5'UTR. Red numbers indicate the two different DNA probes tested: 1 is the DNA probe tested in the first part of the Results, 2 corresponds to the sequence AGTTTATTTAGACGTGCTAACTTTGT. B) Pictures of the ELISA plates after the reaction. The protein master mixes assayed are indicated in blue

As for the *PDH* promoter, there was no binding from any bZIP but Hy5 (Figure 90). Because most of the G- and H-bZIPs were proved to be functional (they resulted in binding signal with the *RBCS1a* and *CAT2* DNA probes), those results reliably indicated that none of the *PDH* promoter-derived DNA probes was bound by the G- or H-bZIPs.

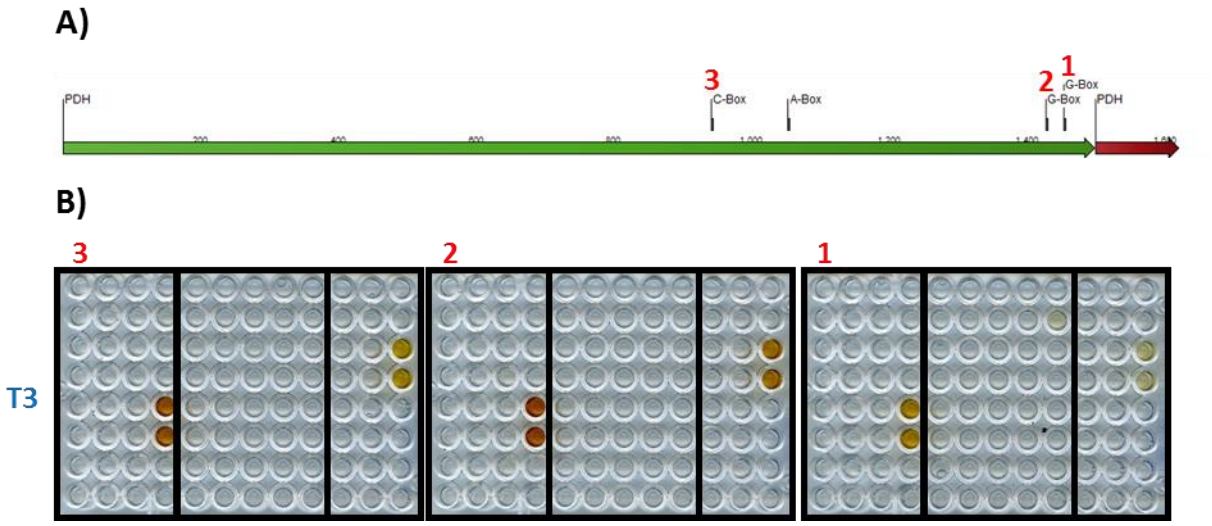

Figure 90. ELISA on the *PDH* promoter. A) Outline of the *PDH* promoter indicating the potential cis-elements based on an ACGT core. Green arrow represents 1.5 Kbp upstream of the gene, and red arrow the 5'UTR. Red numbers indicate the three different DNA probes tested: 1 is CATAAGGTTTTACGTGCTTCTATAAA, 2 is TAACAGGTAAAACGTGTATGTACATG, and 3 is TGCTGTCTCTGACGTCCTTAATTATC. B) Pictures of the ELISA plates after the reaction. These DNA probes were tested only with the T3 protein master-mix.

In contrast to the consistent lack of signal in the C- and S1-bZIPs single extracts -which made them unsuitable to draw any conclusion-, the fact that the G- and H-bZIPs specifically resulted in signal with particular DNA probes opened the way for a further characterization of their DNA-binding specificity. A detailed examination of the sequences of the DNA probes tested revealed a cytosine in position -2 of the three DNA probes resulting in positive signals, and absent in the DNA probes that led to negative results (Figure 91). Thus, those results pointed to the requirement of that cytosine for the specific DNA binding of the G- and H-bZIPs.

RBCS1	AATTATCTTCCACGTGGCATTATTC
RBCS2	AGTTTATTTAGACGTGCTAACTTTGT
CAT1	CTCATCACACGTGGAATCC
CAT2	ACAAAGCAGCCACGTCACCCAAGACC
CAT3	ACAGCCCAATGACGTCCTCATTTATT
PDH3	TGCTGTCTCTGACGTCCTTAATTATC
PDH2	TAACAGGTAAAACGTGTATGTACATG
PDH1	CATAAGGTTTTACGTGCTTCTATAAA

Figure 91. Sequences of the DNA probes tested, containing C- or G-boxes. Probes resulting in binding by G- and H-bZIPs are in green background, and those with no binding are in red background. The ACGT core is indicated in red, and the cysteine in -2 position is

As preliminary results, these data cannot bring much information about the specificity of the DNA binding of the 16 bZIPs, however, they highlighted some aspects of the ELISA method that can help to interpret other results. They exposed a strong effect of the protein dilution on the results. That could be clearly appreciated in the results arisen from C/S1 heterodimers, in which the signal pattern was correlated with the protein master-mix, rather than with the individual bZIP combinations as it would be expected for specific binding. The T1 master-mix led to signals in the bZIP combinations involving bZIP10 and bZIP63, while in the T3 binding signals appeared in the bZIP53 combinations. Because the only difference among those three trials was the different dilutions of the protein extracts, those results suggested that the DPI-ELISA method can be strongly influenced by the composition of the protein dilutions. It seems reasonable to attribute that effect to contaminating bacterial components, so that their relative amount in the protein extract in regard to the recombinant protein, as well as their absolute concentration are likely to be determinant for the assay outcome.

In above results Hy5 bound to all DNA probes assayed, in a completely distinct manner than the closely related HyH and the G-bZIPs, so it could be suspected that that protein extract resulted in unspecific signal production. Of course that possibility could be easily confirmed using mutated DNA probes in an actual experiment, but those experiments were only initial setting up tries. Still, it is interesting to notice that the induced culture for the Hy5 expression resulted in a notably larger bacterial pellet than the cultures for the expression of other bZIPs, and that it was resuspended in the same volume as the others. That means that the concentration of the recombinant protein, as well as bacterial components, was higher in that sample. According to that, it can be speculated that the use of highly concentrated raw protein extracts in the ELISA could induce unspecific signal production. In agreement, undiluted protein extracts assayed in the first part of the results, led in some cases to strong signals while their dilutions resulted negative.

APPENDIX D

Testing of the stress-response of the bZIP63 lines

The continuous phenotypic determination of the *Arabidopsis* lines with altered bZIP63 levels revealed that the bZIP63 overexpressing lines exhibited less initial yellow leaves, presumably due to a drought stress period, suggesting that bZIP63 overexpression enhanced stress tolerance (Figure 41). Indeed, bZIP63 seems to play an important role in different stress response, and it is activated by SNRK1 (Baena-González et al., 2007; Matiolli et al., 2011; Veerabagu et al., 2014), therefore I tested whether a stress-related phenotype could be identified in the lines with altered bZIP63 levels.

The response of the plants to prolonged darkness was investigated, resulting in no apparent difference between the wild type and the transgenic lines in the initial exploratory experiments, therefore the stress response was not further analyzed. Two different experiments were performed as blind assays with the different lines randomly distributed within the tray, for which the different lines were identified with labels according to the color code in Figure 92.

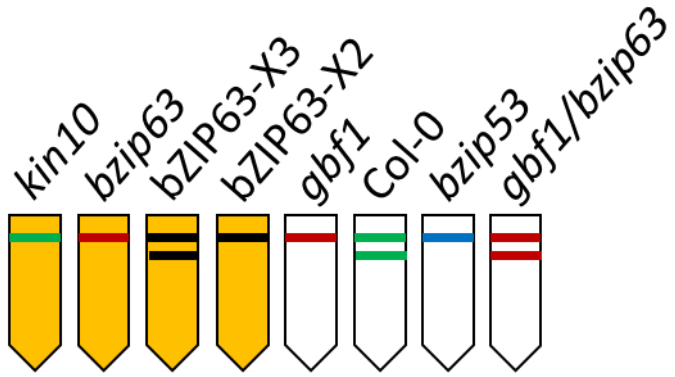

Figure 92. Color code followed for the identification of the lines analyzed.

A first attempt was performed with 28 DAS plants subjected to six days of dark incubation. The effect on the plants was assessed by visual examination of the plants just after the treatment, and again after an additional period of nine days under long day conditions as a recovery time. As it is illustrated in *Figure 93*, just after the incubation in dark all lines showed similar extents of yellowing, but after the recovery time some of the plants were severely affected or dead. Among those there were three of the ten overexpressors plants, and none of the wild type or *bzip63* mutant. Nevertheless, it is important to notice that those three plants were significantly smaller at the beginning of the assay, so they could be more susceptible to darkness. Thus, it could not be stated that any of the bZIP63 lines had differentiated phenotype respect to the wild type. Conversely, the *gbf1* and the *bzip53* lines appeared to be more affected than the wild type.

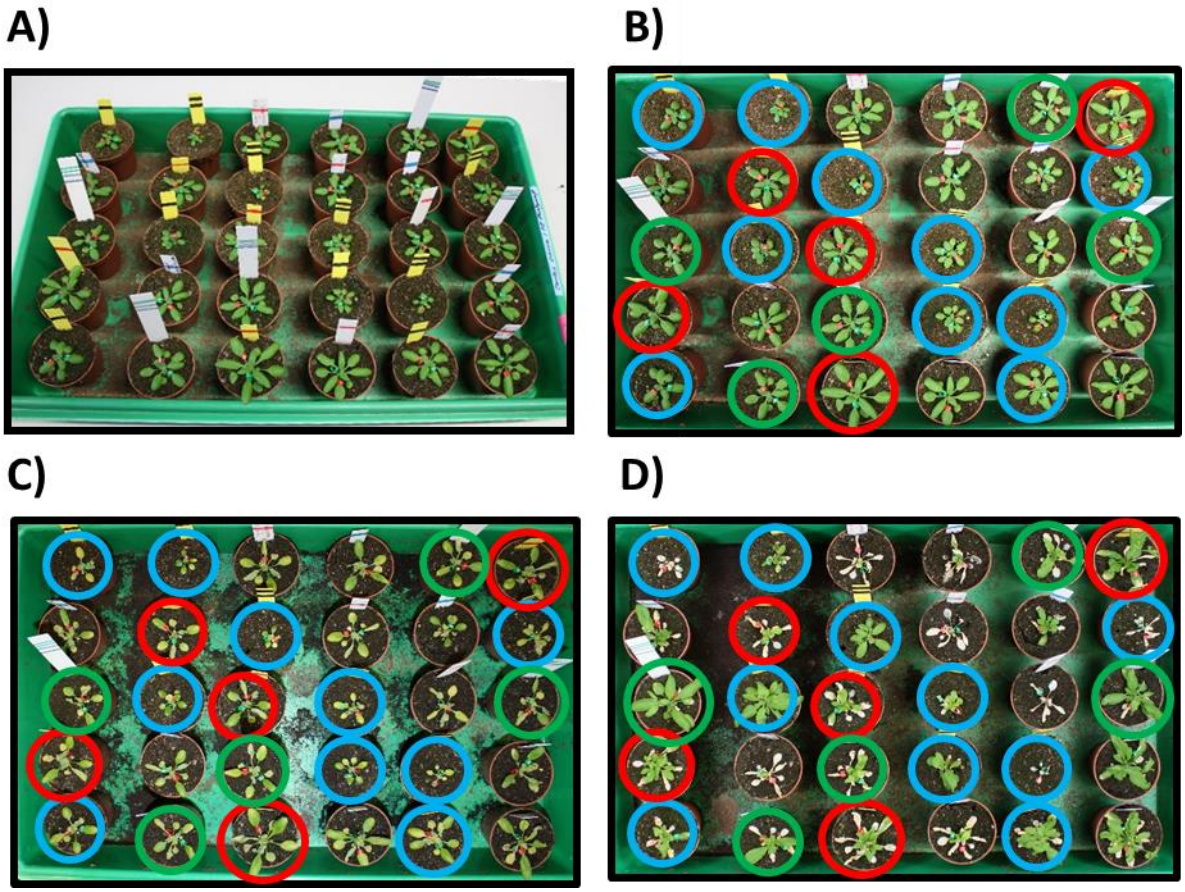

Figure 93. Phenotypic effect of 6 days of dark incubation. A) The tray containing the plants analyzed photographed in perspective to make the labels visible. B) The plants before the dark treatment, C) just after the six days of treatment, and D) after an additional period of nine days of recovery. Green circles are wild type, red circles are *bzip63* mutant, and blue circles are the bZIP63 overexpressors.

The second attempt was performed with 21 DAS plants and various dark incubation times were assayed, namely, 2, 4, and 6 days in darkness. Three different trays were prepared, each one for each incubation period, and they were photographed before and after the recovery time, which was seven days under long light conditions. As in the first attempt, no clear differences were distinguishable among any of the bZIP63 lines and the wild type Figure 94. On the other hand, the survival rate in that experiment was markedly lower than in the first experiment, as after six days in darkness almost all plants were dead. Therefore those results suggested that the particular conditions of the plants at the beginning of the stress treatment have a major impact on the outcome of the experiment.

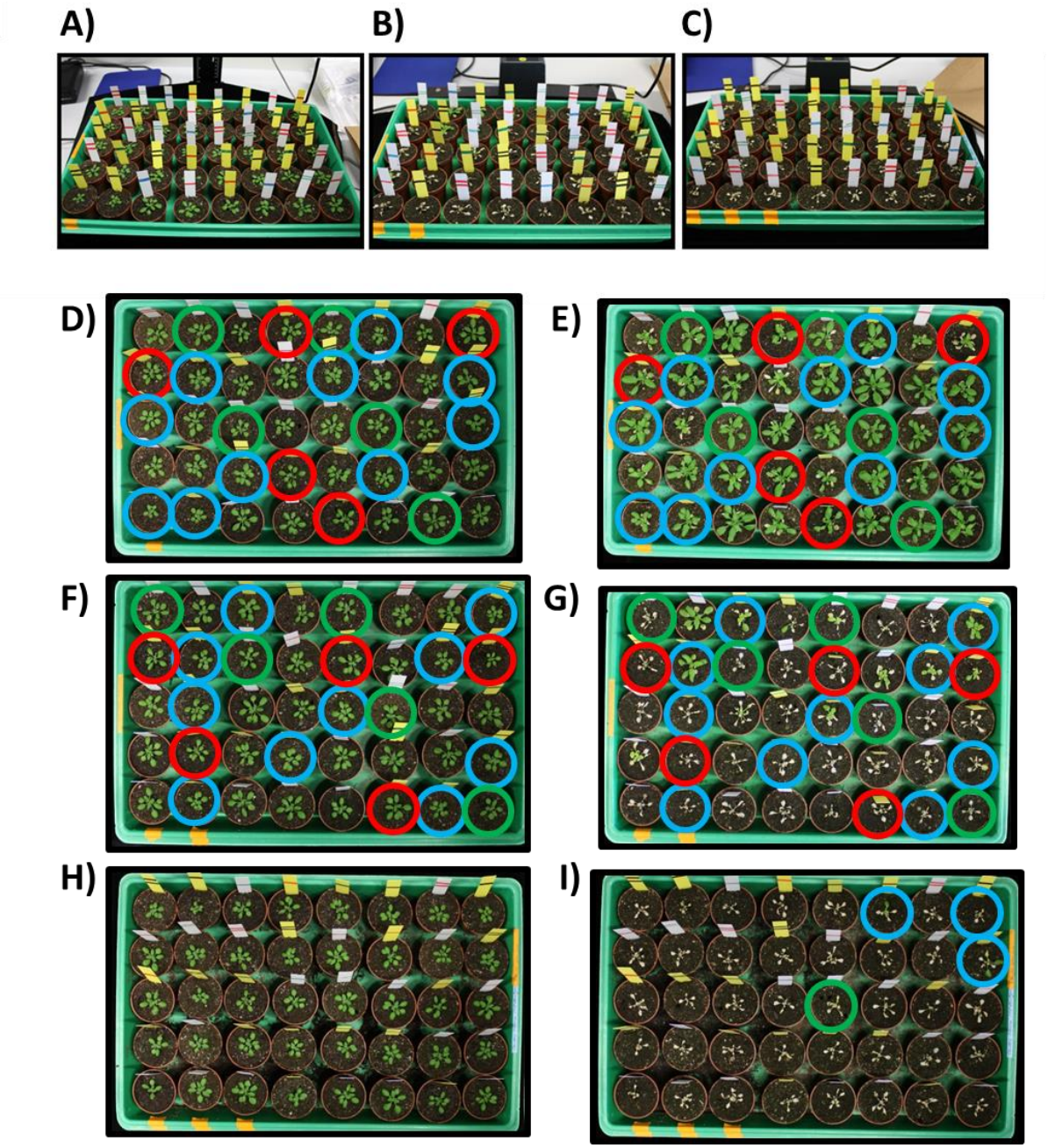

Figure 94. Phenotypic effect darkness incubation. A), B), and C) are pictures of the trays corresponding to the 2, 4, and 6 days of incubation, respectively, in perspective to make the labels visible. Plants before, D), and after, E), two days in darkness; before, F), and after, G), four days in darkness; and before, H), and after, I), six days in darkness. Green circles are wild type, red circles are *bzip63* mutant, and blue circles are the bZIP63 overexpressors.

APPENDIX F

Generation and phenotypic characterization of Arabidopsis plants overexpressing GBF1

For a complete characterization of the GBF1 function, Arabidopsis lines overexpressing that bZIP were constructed in order to determine its phenotypic effect. GBF1 was cloned into a pK7FWG2 vector for its overexpression as a C-terminal GFP fusion driven by a CaMV 35S promoter and then transformed into the *Agrobacterium tumefaciens* strain GV3101 (Koncz and Schell, 1986). Plant transformation was performed by floral dip as previously described (Clough and Bent, 1998) and seeds were plated on kanamycin selective medium. Resistant seedlings were transferred to single pots and growth under long day conditions. Overexpression of GBF1 could be verified by fluorescence microscopy (Figure 95).

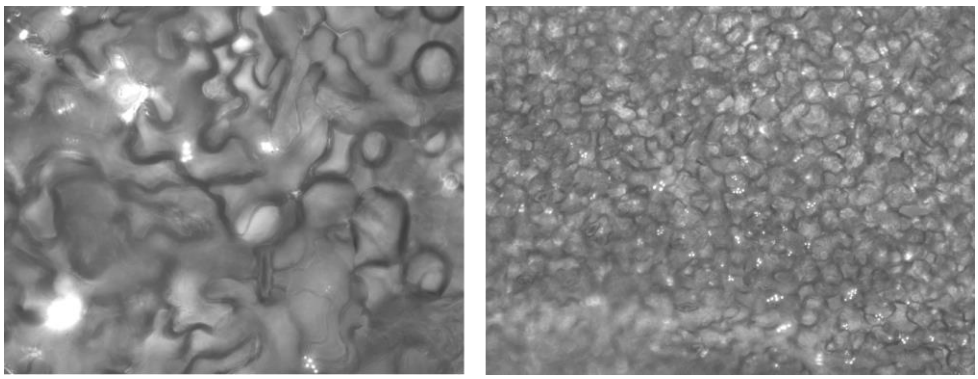

Figure 95. Two examples of grey scale images captured with fluorescence microscope showing the expression of GBF1 fused to GFP in rosette leaves.

Senescence-specific phenotype characterization of two different GBF1 overexpressing lines indicated no apparent differences between those and the wild type (Figure 96). However, although there is no doubt that the GBF1 fusion protein was expressed, it is unknown to which extent it was overexpressed, since transcript levels were not assessed by qPCR.

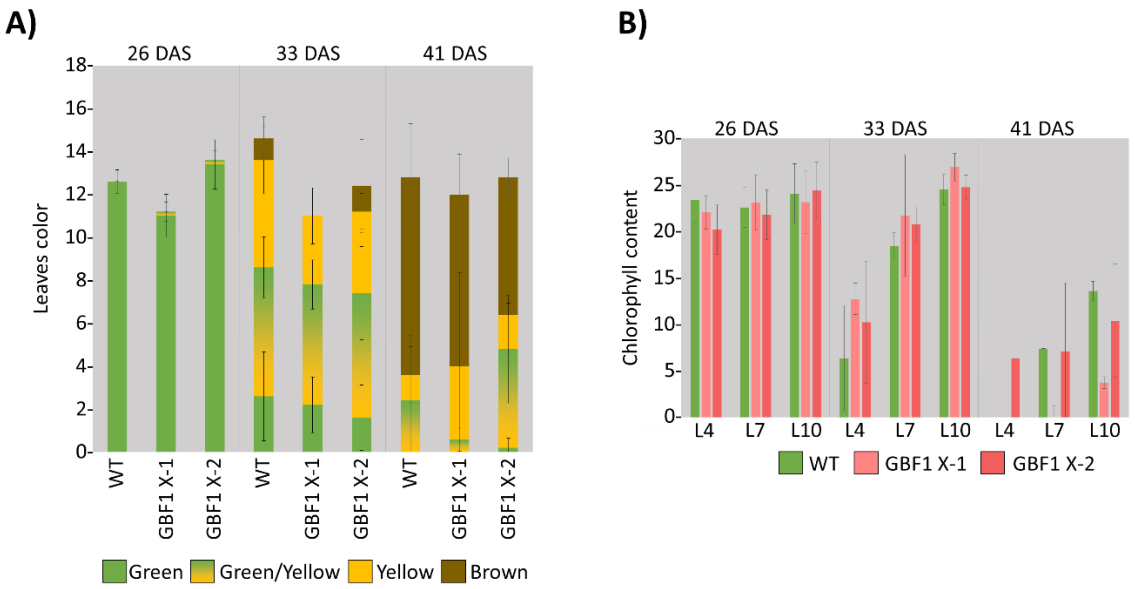

Figure 96. Senescence phenotypes of Arabidopsis lines overexpressing GBF1. WT is the wild type, and GBF1 X-1 and X-2 are the two overexpressing lines tested. Charts represent the average of four plants randomly selected. Error bars are standard deviation. A) Number of leaves categorized by colors. B) Chlorophyll content measured with an atLEAF+ chlorophyll meter (no units). Measurements were performed in leaf Nr.4 (L4), Nr.7 (L7), and Nr.10 (L10).